# KONINKLIJK NEDERLANDS METEOROLOGISCH INSTITUUT

WETENSCHAPPELIJK RAPPORT

SCIENTIFIC REPORT

W.R. 83 - 13

P.J. Rijkoort

A compound Weibull model for the description of surface wind velocity distributions


De Bilt, 1983

Publikatienummer: K.N.M.I. W.R. 83-13 (FM)

Koninklijk Nederlands Meteorologisch Instituut,
Fysisch Meteorologisch Onderzoek,
Postbus 201,
3730 AE De Bilt,
Nederland.

U.D.C.: 551.501.75 :
551.552

# A compound Weibull model for the description of surface wind velocity distributions.

P.J. Rijkoort *)
Royal Netherlands Meteorological Institute, De Bilt

Abstract.

A mathematical model is described, which has been developed to calculate frequency distributions of wind speed for arbitrary locations in the Netherlands, irrespective of the availability of wind measurements at such locations. The principle of the model is the extension of the Weibull frequency distribution function with a stability parameter, and the application of this to a data base divided into meteorologically homogeneous groups, primarily into daytime and nighttime data. The use of wind data which are transformed to standard exposure then allows a regional analysis and a simplification of the model parameter array.

Model parameters have been computed from the surface wind data of 12 basic stations, and then the parameters have been smoothed analytically and graphically. The resulting model has been checked with independent wind data from 15 other stations, and is shown to be reliable within the limits of climatological variability. In particular, the model appears to be very suitable for the estimation of extreme values of average wind speed for long recurrence periods.

## 1. Introduction.

It is practically advantageous to describe observed wind speed frequency distributions by means of an analytical function. Primarily, such a description provides a certain amount of necessary smoothing. Generally the amounts of data in subsequent wind speed classes show irregularities due to limitations in the amount of available data and due to random fluctuations. As a result of this, some classes may contain very much less (or more) data than both the preceding and the next class. Such unrealistic variations are not likely to be due to natural causes, and they can be removed by fitting of an appropriate analytic function.

A second advantage of an analytic description is, that a large amount of numerical data is summarized by a small number of function

*) Retired.

parameters. In this way it becomes easier to compare frequency distributions of different origin (different stations, different azimuths etcetera): the information in the data becomes more manageable. Also it becomes easier to discern the various meteorological causes of the wind phenomenon.

A third advantage of an analytic approach, and the primary purpose of this investigation, is the possibility to estimate wind frequency distributions for locations without wind observations. This purpose can been attained by spatial interpolation of a limited amount of variable distribution parameters.

Finally, by way of an optimal analytic description of a distribution it becomes possible to estimate extreme values, e.g. annual or seasonal wind speed maxima. This is our second purpose.

In the past various attempts have been made to find a suitable analytic description for a wind speed distribution; for a review see e.g. Brooks and Carruthers (1953), ch. 8. These attempts were not really satisfactory, until in the sixties attention was paid to distribution functions of the following type:

$$F(U) = 1 - \exp\left[-\left(\frac{U - U_o}{a}\right)^k\right] \qquad (1.1)$$

This is the cumulative form of the distribution function, i.e. F(U) is the probability that the wind speed is observed not to exceed U.

The formula (1.1) for F(U) has been first used in 1939 by the Swedish scientist Wallodi Weibull for distributions of refraction indices, and therefore is generally called the Weibull distribution formula. In this formula, U is the variable (in this case, wind speed) and a, k and $U_o$ are distribution parameters. The parameter a is called scale parameter, because multiplication of all U-values with some factor implies that description of the distribution of these products requires the multiplication of a with the same factor, while the same value of k remains applicable. The parameter k is called shape parameter : its value determines the degree of peakedness of the function around the mean, the width of the distribution "tails" etcetera. The parameter $U_o$ is a lower limit, which in case of wind speed distributions is zero, so that the cumulative distribution formula (1.1) is reduced to

$$F(U) = 1 - \exp\left[-\left(\frac{U}{a}\right)^{k}\right] \qquad (1.2)$$

The corresponding distributive function f(U) has the form

$$f(U) = \frac{k}{a}\left(\frac{U}{a}\right)^{k-1} \exp\left[-\left(\frac{U}{a}\right)^{k}\right] \qquad (1.3)$$

Here f(U) is the probability that an arbitrary wind speed observation has a value between U and (U+dU). Consequently (1.2) and (1.3) are related by

$$F(U) = \int_{-\infty}^{U} f(U)\, dU$$

Additional information on the statistical techniques for application of the distribution can be found in the appendix. We restrict ourselves here to showing in figure 1, what the shape of the distributive function (1.3) is for various values of the parameter k, using a normalized scale. It appears that increasing k gives a sharper-peaked function with relatively less very large and very small values.

The notation convention used here deserves a brief comment. In the recent literature on the use of Weibull wind distribution functions the most-used notations are that of Hennessey (1977) with a for the scale and c for the shape parameter, and that of Justus et al. (1978) with c for the scale and k for the shape parameter. The use of these alternatives is about evenly divided among researchers in various countries, and confusion and misunderstanding may easily arise, since the two notations attach different meanings to the letter c. In the context of a project towards a joint wind energy atlas for the European Economic Community (see Petersen, 1982) it was therefore decided by the project participants from nine countries in 1983 to introduce as a compromise the Justus-Hennessey-notation used here. This omits the letter c and uses the other letter from both notations, thus a for the scale parameter and k for the shape parameter.

Graphically this distribution function can be handled by using so-called Weibull graph paper, based on a transcription of (1.2) :

$$\ln\left[-\ln(1-F)\right] = k \ln U - k \ln a \qquad (1.4)$$

On Weibull paper a logarithmic scale is used for the wind speed U, and the F-scale is proportional to $\ell n[-\ell n(1-F)]$ . Consequently an observed frequency distribution which conforms to (1.2) will plot as a straight line on such paper.

Below a model is given for description of frequency distributions of wind speed in the Netherlands. This model, based on the Weibull distribution, has been developed for the above-named purposes of geographical interpolation and estimation of extreme values. The result is not pretended to be a definitive and exceedingly accurate description of the Dutch surface wind climate. However, it is shown that the set purposes have been attained to some degree, and that in particular extreme wind speeds can be estimated better than before.

The basic material used in model development consists of hourly averages of observed wind. Due to the fact that such observations are not independent, but have a high degree of short-range persistence of as yet insufficiently known character, it was not considered useful to try application of standard statistical significance tests. However, the model parameters have been determined from data of 12 stations, and for an empirical estimation of the model quality we had data from 15 other stations at our disposal. In this fashion an independent quality check could be obtained.

## 2. Available station data series and their subdivision.

From our archived hourly-averaged wind data a dozen observation series were selected from geographically well-distributed stations, which were all available for the whole 15-year period 1962-1976. The data had been extensively checked and corrected for e.g. calibration errors (Wieringa and Rijkoort, 1983). In addition, the effects of any occurring changes in location or observation height were eliminated by application of exposure corrections (Wieringa 1976, 1980, 1983). This implies, that the corrected data all refer to 10 m height over homogeneous open country with a roughness length $z_o$ = 0.03 m. It was shown that this reduction to uniform exposure was essential to obtain wind data, of which the extreme hourly averages were representative of the region around the station (Rijkoort and Wieringa, 1983).

The twelve 'basic' stations are : Beek (06380), De Bilt (06260), Deelen (06275), Eelde (06280), Eindhoven (06370), Gilze Rijen (06350), Leeuwarden (06270), lightvessel Texel (06220), Schiphol (06240), Soesterberg (06265), Vlissingen (06310) and Zestienhoven (06344). The bracketed figures are their WMO synoptic station numbers. Station locations are shown in figure 2.

It was remarked above in the introduction, that the Weibull function (1.2) is generally used for descriptions of cumulative wind frequency distributions. To what extent is this use justifiable ? Figure 3 shows for example these 'overall' cumulative distributions for the stations Leeuwarden and Beek. The distributions are plotted on Weibull graph paper, designed so as to linearize the graphical representation of (1.2). In figure 3 the curvature of the plotted distribution graphs is quite evident, and only over a limited range (at most between 3 and 15 m/s) the application of (1.2) appears approximately useful for these overall distributions.

In order to obtain more accurate descriptions it stands to reason to subdivide the total material in a fashion appropriate to our wind climate. After all, we know from experience that in our country the winds are generally stronger in autumn than in summer, and that strong winds occur more frequently from southwesterly than from easterly directions. Accordingly the material was split up into seasonal and azimuthal groups.

For seasons we did not use the well-known four seasons of astronomical origin starting on March 21st, because in our country these seasons show pronounced climatological inhomogenuities, particularly in spring and autumn. In accordance with the annual course of the general circulation (see Gaskell and Morris, 1979) preference was given to six seasons of two months each :

| | |
|---|---|
| January - February | : midwinter |
| March - April | : spring |
| May - June | : presummer |
| July - August | : midsummer |
| September - October | : autumn |
| November - December | : prewinter |

For the azimuth groups we used $30^{o}$-sectors denoted by 0, 30, etcetera, where e.g. 0 refers to the sector $345^{o}$-$15^{o}$.

The characterization of meteorological phenomena generally requires

not only an annual course, but also a diurnal course. The winds are generally weaker at night than by day. It is well known that this stems from general differences between the daytime and nighttime stability of the atmospheric boundary layer, and that these differences generally decrease with increasing wind speed level.

As a result, we can expect that frequency distributions consisting exclusively of daytime winds differ from distributions of nighttime wind observations. Indeed such a difference does occur, as shown for example in the figures 4.1 and 4.2. These daytime and nighttime distribution curves approach each other at high wind speeds, and where station wind speeds do exceed 15 m/s they are practically indistinguishable.

In the course of subdividing wind data series by season, by azimuth and also into day and night, we encounter an assignment problem. This is caused by the fact that anemometers have a finite starting speed and therefore are unable to register weak wind speeds below ~ 2 m/s. In such weak-wind situations it is also not possible to measure the wind direction reliably. Therefore climatological tables of wind data subdivided according to azimuth sectors usually contain a separate group "calm and/or variable" (in Dutch: "windstil en/of veranderlijk"). This group contains not only a small amount of real calms but also the weak winds, and generally more nighttime than daytime winds do fall into this category. If in the course of azimuth subdivision the group "calm and/or variable" is omitted, then daytime frequency distributions will contain a number of observations which lack counterpart nighttime observations. This distorts the comparison of both distributions.

A simple way to avoid this problem, which has been used here, is to distribute the "calm" class over the azimuth sectors in proportion to the amount of data in each sector class. An additional argument in favour of applying this procedure is that the final aim is to make a model, which describes distributions of subgroups in a manner which does not distort the overall picture. It should be possible to reconstitute the overall seasonal and annual distributions, including the "calm and/or variable" class originally present. The analytical complexity would be notably increased, if the model had to contain a 'separate and unequal' group for these weak winds.

In all, the data are split up according to three criteria : season, azimuth sector, and day or night. Consequently we have for each station

6 × 12 × 2 = 144 frequency distributions. The separation between day and night hours varies per month according to the following table :

Hours assigned to the daytime per month (GMT):

| | | | |
|---|---|---|---|
| January | 10 - 14 | July | 6 - 18 |
| February | 9 - 15 | August | 6 - 18 |
| March | 8 - 16 | September | 7 - 17 |
| April | 7 - 17 | October | 8 - 16 |
| May | 6 - 18 | November | 9 - 14 |
| June | 5 - 18 | December | 10 - 13 |

The hour figures refer to the previous hour : 4 means 03.00 - 04.00 GMT. The changeover between day and night has been taken at the approximate average hour when the vertical flow of thermal energy at the earth's surface changes sign (Holtslag and Van Ulden, 1983).

In this analytic approach the 'overall' frequency distribution is therefore described as the sum of a number of subset frequency distributions, with separate Weibull distribution parameters for each subset. One should realize the fact that a sum of Weibull distributions is generally not a Weibull distribution itself. As an example, figure 5 shows two simple Weibull distribution representations $b_1$ and $b_2$, having the same shape parameter (taken as k = 2) but different scale parameters ($a_1$ = 4, $a_2$ = 10). The calculated distribution curve of the sum of these two is shown to be an S-shape curve between $b_1$ and $b_2$. In the same way we get, even if for each wind data subset the distribution conforms exactly to (1.2), an overall sum distribution which deviates from the exact Weibull distribution function.

## 3. The compound model.

The basic hypothesis of the distribution model is, that per season-and-azimuth subset the daytime distribution conforms exactly to the Weibull function (1.2).

For the nighttime distribution subsets we introduce a modification of the Weibull function, which approaches to (1.2) at high wind speeds. This can be accomplished by multiplying (U/a) with a factor of the type $(1 + \gamma \exp[\beta U])$ . This factor formula has been empirically determined from preliminary analysis; parameter $\beta$ must be negative. During further

analysis on fitting this formula it proved to be unnecessary to vary $\beta$, and a constant value $\beta = -1/5$ led to very acceptable fits.

Consequently we have now a daytime distribution function $F_d$ and a nighttime distribution function $F_n$, given by the formulas

$$F_d(U) = 1 - \exp\left[-\left(\frac{U}{a}\right)^k\right] \tag{3.1a}$$

$$F_n(U) = 1 - \exp\left[-\left\{\frac{U}{a}\left(1 + \gamma \exp\left(-\frac{U}{5}\right)\right)\right\}^k\right] \tag{3.1b}$$

We will call the parameter $\gamma$ the stability parameter for reasons to be explained below.

Next to the three parameters a, k and $\gamma$ also the numbers of daytime and nighttime observations are required; we will call these numbers d and n. Finally we introduce indices for azimuth and season groups. For the azimuth groups we use i (0, 1, ..., 11), where i = 0 indicates the $0^o$-sector, i = 1 the $30^o$-sector etcetera. For the season group index we use j (0, ..., 5), indicating by j = 0 midwinter, j = 1 spring etcetera.

In all we have per station 12 × 6 × 5 parameters, called the model parameters from now on, namely $a_{ij}$, $k_{ij}$, $\gamma_{ij}$, $d_{ij}$ and $n_{ij}$. For a specified j-value the $d_{ij}$ and $n_{ij}$ constitute the azimuth sector frequency distribution of the daytime, respectively nighttime observations.

Estimates of the 360 parameter values have been obtained for each station by fitting (3.1) to the 72 day-night pairs of frequency distributions. This has been done by way of a maximum likelihood approach (see appendix).

For an individual season-azimuth group the wind distribution is now

$$\frac{d_{ij}F_d + n_{ij}F_n}{d_{ij} + n_{ij}} \tag{3.2}$$

and for a combination of season-azimuth groups we get

$$\frac{\sum(d_{ij}F_d + n_{ij}F_n)}{\sum(d_{ij} + n_{ij})} \tag{3.3}$$

Here i-summation gives seasonal distributions, j-summation leads to azimuthal distributions of wind speed, and summation over both i and j produces the total annual distribution.

## 4. Smoothing of the model-parameters.

Computer analysis of wind observation series in the above fashion produces primarily 360 distribution parameters per station. In order to make this large amount somewhat more manageable, the 12 azimuthal parameters have been subjected to harmonic analysis, as follows :

$$a_{ij} = \tilde{a}_{j0} + \tilde{a}_{j1}\sin(30\ i + \tilde{a}_{j2}) + \tilde{a}_{j3}\sin(60\ i + \tilde{a}_{j4}) \qquad (4.1)$$

and analogously for $k_{ij}$ , $\gamma_{ij}$ , $d_{ij}$ and $n_{ij}$ . Typically a wind rose is bimodal (e.g. figure 12.1) and this is the simplest way to summarize it.

In this fashion the 360 parameters are reduced to 150 parameters $\tilde{a}_{j0}$ , $\tilde{a}_{j1}$ , $\tilde{a}_{j2}$ , $\tilde{a}_{j3}$ , $\tilde{a}_{j4}$ , $\tilde{k}_{j0}$ etcetera. These condensed parameters obtained by harmonic analysis we will call the harmonic parameters. Though this reduction in number is already useful, still a total of 150 parameters varying from station to station is excessive for interpolation purposes : for the 12 stations we have 1800 harmonic parameters !

For further smoothing we aim primarily at reducing to the utmost the number of parameters that varies from station to station. Parameters which are applicable jointly to all stations, but which vary seasonally, can without much trouble be incorporated in a computer program and be applied that way. However, interpolation of station-variable parameters must be done geographically, by way of isoline maps, and the number of such maps ought to be minimal for a manageable model.

As a first step we can note, that the first harmonic parameter (i=0), namely $\tilde{a}_{j0}$ , $\tilde{k}_{j0}$ , $\tilde{\gamma}_{j0}$ , $\tilde{d}_{j0}$ and $\tilde{n}_{j0}$ is nothing but the average of the parameter in question over all directions combined. This average is in the case of of $\tilde{d}_{j0}$ en $\tilde{n}_{j0}$ just one-twelfth of the number of hours in season j , a fixed number which is the same for all stations and is given below :

| | Jan-Febr | March-Apr | May-June | July-Aug | Sept-Oct | Nov-Dec |
|---|---|---|---|---|---|---|
| $\tilde{d}_{j0}$ | 441 | 761 | 1029 | 1008 | 761 | 380 |
| $\tilde{n}_{j0}$ | 1335 | 1069 | 801 | 852 | 1069 | 1450 |

Further steps of simplification and smoothing cannot be attempted without taking a solid look at the actual harmonic parameter values from

the 12 basic stations. These are therefore given graphically in figure 6 in two groups of six stations each. In figures 6.1 - 6.3 the five harmonic parameters of a, k and $\gamma$ are given. In figures 6.4 and 6.5 the normalized amplitudes of the first and second harmonics of d and n are plotted, divided by $\tilde{d}_{j0}$ , respectively $\tilde{n}_{j0}$ ; these quotients will be noted with a star : $\tilde{d}_{j1}/\tilde{d}_{j0} \equiv d^*_{j1}$ , etcetera. The phase angles are given in figures 6.4 and 6.5 without such normalization, of course.

Now we can continue to investigate the first harmonic parameters (i=0) of a, k and $\gamma$ . By averaging $\tilde{a}_{j0}$ , $\tilde{k}_{j0}$ and $\tilde{\gamma}_{j0}$ over season index j we get their annual averages $\bar{a}$ , $\bar{k}$ and $\bar{\gamma}$ , indicating for each station the general level of these parameters. These averages have been mapped in figures 7.1 - 7.3.

Essentially $\bar{a}$ is the overall level of the scale parameter of wind speed, and therefore strongly linked to the local annual average of wind speed as given by Wieringa (1982). Thus $\bar{a}$ varies over the country from large values at the coast (7 to 8 m/s) to much smaller values inland (~ 5 m/s). The average shape parameter $\bar{k}$ also shows variation across the country, but to a lesser degree, from 2.5 to 2.2. The average stability-parameter $\bar{\gamma}$ varies from zero at sea to ~ 0.8 inland, with a very marked gradient of this parameter in the coastal zone.

It will be remarked that the model values of the shape parameter k are ~ 15% larger than the k-values which are obtained by fitting a simple two-parameter Weibull function (1.2). This difference is due to the fact, that the model uses the explicit parameter $\gamma$ to account systematically for stability effects, while two-parameter representations have no explicit stability handling. Consequently, the requirement of representing low nighttime wind speeds decreases the value of the shape parameter in two-parameter Weibull frequency distributions.

Two-parameter Weibull shape parameters for the same Dutch station distributions are found to be in the range $1.7 \leq k \leq 2.2$ (Wieringa and Rijkoort, 1983). When fitting (1.2), it was necessary to restrict the computation to the range 4 - 16 m/s, where the actual distribution does not curve away too badly from (1.2).

Next, the seasonal variation of $\tilde{a}_{j0}$ , $\tilde{k}_{j0}$ and $\tilde{\gamma}_{j0}$ requires our attention. Figures 6.1 - 6.3 show differences between stations in the

curves of these parameters, and the question is whether this is just an average magnitude difference which can be accounted for by the obtained annual averages. Quotients of $\tilde{a}_{j0}$ , $\tilde{k}_{j0}$ and $\tilde{\gamma}_{j0}$ divided by respectively $\bar{a}$, $\bar{k}$ and $\bar{\gamma}$ are plotted in figure 8. In this figure the differences between stations are no longer significant for the normalized first harmonic parameters of shape and stability. Therefore we can conclude that the annual course of these parameters is independent of station location. Averaging $\tilde{k}_{j0}/\bar{k}$ and $\tilde{\gamma}_{j0}/\bar{\gamma}$ over all stations gives two season-dependent variables which we will call $k^*_{j0}$ and $\gamma^*_{j0}$ .

The values of $\tilde{a}_{j0}/\bar{a}$ require a closer inspection. To this purpose we approximate their seasonal variation sinusoidally as follows :

$$\tilde{a}_{j0}/\bar{a} = 1 + c \sin (60\ j + \chi) \qquad (4.2)$$

If we calculate c and $\chi$ for the twelve stations, we find that c varies little, between 0.09 and 0.13; we will take it to be constant, c = 0.11. The parameter $\chi$ shows more variation : at "coastal" stations Vlissingen and Lightvessel Texel we find $\chi > 100^o$ , while inland $\chi$ varies between $38^o$ and $78^o$. The variation of $\chi$ across the country has been mapped in figure 7.4.

Note that for the computation it is necessary to express $\chi$ in degrees. For interpretation purposes we can read $\chi$ in terms of days by assuming a year of 360 days and an origin at February 1st.

Before investigating the behavior of the parameters d and n, we will first look at the remaining harmonic parameters of a, k and $\gamma$ .

The other harmonic parameters of a $(\tilde{a}_{j1}$ , $\tilde{a}_{j2}$ , $\tilde{a}_{j3}$ , $\tilde{a}_{j4})$ show some differences in the station values, but there is no discernible systematic variation across the country. Therefore we restrict ourselves to azimuthal averaging over all basic stations, retaining for the whole country the seasonal variations because these show a marked annual variation -- at least in case of the amplitude and phase of the first harmonic.

With regard to the second harmonic parameters of k and $\gamma$ we find that the amplitudes have very small values and the phase angles have irregular unsystematic variations. However, if the amplitudes are assumed to be not significantly different from zero, then the phase

angle values are irrelevant and can also be taken at zero. For the first harmonic of k and $\gamma$ , the amplitudes and phase angles again do not show any manifest pattern of variation across the country, so that we decide here simply to average the station values.

Finally we investigate the harmonic parameters of the azimuthal frequencies d and n. Primarily the relative amplitudes $d^*_{j1}$ etcetera were averaged over the seasons, using the following notation :

$$\overline{d}^*_1 \equiv \frac{1}{6} \sum_j d^*_{j1} \quad \text{etcetera.}$$

It is then found that a large correlation exists between $\overline{d}^*_1$ and $\overline{d}^*_3$ , and similarly between $\overline{n}^*_1$ and $\overline{n}^*_3$ , namely 0.92 and 0.89 respectively (see figure 9). The linear regression formulas are

$$\overline{d}^*_3 = 3\ \overline{d}^*_1 - 0.96 \quad \text{and} \quad \overline{n}^*_3 = 1.05\ \overline{n}^*_1 \ .$$

On account of these large correlations, the computed relative amplitudes have been substituted by corrected values obtained through projection on the regression lines of the points $(\overline{d}^*_1 , \overline{d}^*_3)$ , respectively $(\overline{n}^*_1 , \overline{n}^*_3)$ . These corrected values are indicated by $\hat{d}^*$ and $(3\ \hat{d}^* - 0.96)$ , respectively $\hat{n}^*$ and $1.05\ \hat{n}^*$. The variation of the relative amplitudes between the stations is given through these parameters $\hat{d}^*$ and $\hat{n}^*$ (see figures 7.5 and 7.6).

Next the seasonal variation of these relative amplitudes has been determined by way of all-station-averaging of the deviations $(d^*_{j1} - d)$ etcetera. The seasonal variations are indicated by $\delta_{j1}$ , $\delta_{j2}$ , $\nu_{j1}$ and $\nu_{j2}$ respectively. It is found that $\nu_{j2}$ can be taken to be zero. Finally the phase angles have simply been averaged over the stations for the separate seasons : this gives four annual courses $d^*_{j2}$ , $d^*_{j4}$ , $n^*_{j2}$ and $n^*_{j4}$ .

In the following table a review is given of the obtained working relations for determination of the harmonic parameters. The first row contains the averages, the second row the amplitude of the first harmonic, the third row the phase of the first harmonic, the fourth row the amplitude of the second harmonic and the fifth row the phase of the

second harmonic in (4.1).

In all, the 150 harmonic parameters per station have been reduced to 19 season-variable parameters (which are everywhere the same) and 6 station-variable parameters. Their values are tabulated in section 7.

Harmonic parameter review

| a | k | γ | d | n |
|---|---|---|---|---|
| $(1+0.11\ \sin(60j+\chi))\bar{a}$ | $k^*_{j0}\bar{k}$ | $\gamma^*_{j0}\bar{\gamma}$ | $\hat{d}_{j0}$ | $\hat{n}_j$ |
| $\tilde{a}_{j1}$ | $\tilde{k}_{j1}$ | $\tilde{\gamma}_{j1}$ | $(d^*+\delta_{j1})\hat{d}_{j0}$ | $(n^*+\nu_{j1})\hat{n}_{j0}$ |
| $\tilde{a}_{j2}$ | $\tilde{k}_{j2}$ | $\tilde{\gamma}_{j2}$ | $d^*_{j2}$ | $n^*_{j2}$ |
| $\tilde{a}_{j3}$ | 0 | 0 | $(3d^*-0.96+\delta_{j2})\hat{d}_{j0}$ | $1.05\ n^*\ \hat{n}_{j0}$ |
| $\tilde{a}_{j4}$ | 0 | 0 | $d^*_{j4}$ | $n^*_{j4}$ |

## 5. Model extension for the calculation of extreme values.

Before we discuss the quality of the model, first we will proceed to the application of the model for determination of so-called extreme values. In this context 'extreme values' denote the expectation value of the largest hourly-averaged wind speed, either for the whole year independent of direction, or for separate seasons and/or azimuth sectors.

Knowledge of these extremes is required towards estimation of wind loading on constructions; construction engineers generally ask this information for specified recurrence periods. Rather, extremes are required for average recurrence periods, in view of the stochastic nature of the occurrence of wind speeds above a specified level, which results in varying time intervals between subsequent exceedances of this level. The most generally requested average recurrence period is 50 years, but also extremes occurring once in 10 000 years on the average

are sometimes asked for. This implies that wind data series, which seldom are much longer than twenty or thirty years, must be extrapolated very far.

For extreme value estimation, the most generally used approach is the so-called Gumbel method. This is based on the fact that, for samples of size N of independent elements out of a homogeneous non-exceedance distribution F(x), the maxima of these samples have a distribution which approaches asymptotically to one out of three extreme value distributions derived by Fisher and Tippett (1928). The conditions for F(x) required for this are not severe but the problem is that, even if the conditions are met, the distance between the exact distribution and the asymptote remains large upon extrapolation, even with large N values. For the case of a Rayleigh distribution, $F(x) = 1 - \exp[-(x/a)^2]$, Cook (1982) has shown that for large x-values even N = 10 000 still gives a noticeable deviation. In case of annual maxima of hourly averages of wind speed we would have $N = 8766 = 24 \times 365\frac{1}{4}$ if the hourly averages were independent, but because of persistence a smaller N value would be applicable. Even when we neglect the lack of homogenuity in the distribution of annual wind speeds, we cannot expect that the Fisher-Tippett distributions are quite reliable towards extrapolation of wind speed distributions.

In addition it must be stated that, even if the complete annual extreme value distribution is asymptotically applicable to annual maxima, this need not be the case for maxima of partial distributions.

In the previous analysis we have seen that the annual distribution of wind speed can be handled as a sum of separate distributions for day, night, azimuth sectors and seasons. Because a model has been developed to describe these subgroup distributions and to construct from this arbitrary combinations of distributions, therefore it makes sense to attempt the derivation of 'extreme value distributions' with the aid of this basic distribution model. If this is done properly, asymptotic approximations would no longer be required.

The exact general formula for a distribution of maxima is

$$G_N(x_m) = \left(F(x)\right)^N$$

Here F(x) is the probability that a "stochastic" variable $\underline{x}$ is smaller than x, and $(F(x))^N$ is the probability that all elements $\underline{x}$ from a sample of size N are smaller than x, so that also the largest element $\underline{x}_m < x$. Then the probability that the maximum exceeds x is $(1 - G_N(x))$.

In the case of the model from section 2 we get for an individual azimuth-season group (i,j):

$$G_{ij} = [F_d(U)]^{d_{ij}} [F_n(U)]^{n_{ij}} \qquad (5.1)$$

This only applies if the $d_{ij}$ , respectively $n_{ij}$ , hourly averages are mutually independent. Because this is not quite the case for wind speeds, it will be necessary to introduce a persistence correction factor $q_{ij}$ in order to reduce the $d_{ij}$ and $n_{ij}$ to numbers of seemingly independent elements, as follows :

$$G_{ij} = [F_d(U)]^{\frac{d_{ij}}{q_{ij}}} [F_n(U)]^{\frac{n_{ij}}{q_{ij}}} \qquad (5.2)$$

It makes little sense to take separate $q_{ij}$-values for day and night, because for extremes we have to do with very large wind speeds, where the day-night difference is secondary. It might even be justified to take simply

$$G_{ij} = [F_d(U)]^{\frac{d_{ij} + n_{ij}}{q_{ij}}}$$

However, we will stick to the formally correct version (5.2).

For the extreme values, belonging respectively to seasons, to azimuth sectors and to the full year, the distributions have the basic form

$$\Pi_i G_{ij} \ , \ \Pi_j G_{ij} \text{ and } \Pi_{ij} G_{ij} \qquad (5.3)$$

However, it is possible that some relative dependence exists between groups -- certainly between neighbouring azimuth sectors, but possibly also between subsequent seasons. In that case additional corrections for persistence might be required.

## 6. Determination of persistence correction factors.

For the 12 basic stations calculations have primarily been made according to (5.1), which actually implies that $q_{ij} = 1$. Some results are shown in figure 10. The observed annual maxima in the appropriate season-azimuth group have been plotted against the plotting position of Benard and Bos-Levenbach (1953). In this case that position is given by

$$(r - 0.3) / (15 + 0.4)$$

since the number of years is 15. The 'theoretical' distribution (5.1) has been indicated by an uninterrupted curve.

In general it is apparent that the data points remain below the model line -- this is the effect of persistence. Moreover it appears that the distance between the data points and the line decreases with increasing wind velocity. This is plausible, since the persistence we are dealing with can be described as the probability, that the occurrence of wind speed within a given interval in a given hour is followed by repetition of the same occurrence in the next hour. Evidently this probability decreases as the speed level becomes more excessive, and we would expect that the data points approach the line $q_{ij} = 1$ asymptotically if $U \to \infty$.

However, in figs. 10.2 and 10.3 the observations are seen to exceed the theoretical distribution for increasing $U_m$. Apparently the model is not quite correct in the upper tail, and for a good fit an empirical 'tail' correction seems required besides the persistence correction.

Towards systematic determination of such a correction the following analysis was done for the annual extremes. For integer values of $U_{max}$ the non-exceedance probabilities $P(U_{max} \leq U)$ were calculated by way of (5.2) and (5.3) with $q_{ij} = 1$, as follows :

$$P(U_{max} \leq U) = \Pi_{i,j} \left(F_d(U)\right)^{d_{ij}} \left(F_n(U)\right)^{n_{ij}} \qquad (6.1)$$

The corresponding probability value $H(U_M)$ for the actual observations was obtained graphically by plotting the observations on Gumbel graph paper and interpolating them linearly. Next q-values were obtained by way of

$$(\Pi_{ij}G_{ij})^{\frac{1}{q}} = H(U_M) \quad , \quad \text{or} \quad q = \frac{\ln \Pi_{ij}G_{ij}(U_M)}{\ln H(U_M)} \tag{6.2}$$

These q-values have been plotted against $U_M$ in figure 11.1. Full correctness of the model would require $q \to 1$ for increasing $u_M$. This is evidently not the case.

Moreover there appears to be quite some variation in the position of q-lines, with as extreme cases Lightvessel Goeree and the airport Beek far inland. This suggests that it might be necessary to take the general station wind speed average into account. Therefore the q-values are plotted against $U_M/a$ in figure 11.2, with the result that now both Goeree and Beek fit nicely into the overall picture.

Finally, values of the persistence correction and the "tail" correction have been determined for the various individual seasonal and azimuth-sector groups. By trial and error a useful relation was found here between $q_{ij}$ and $(U_M/a)_{ij}$ in the following form :

$$\ln q_{ij} = A_{ij} \left(\frac{U_M}{a}\right)^2_{ij} + B_{ij} \tag{6.3}$$

where the $A_{ij}$ are negative.

No definite systematic variation was found between the values of $A_{ij}$ and $B_{ij}$ for different stations, so these parameters were averaged over the twelve basic stations (see Table 3). From these averages and the station values of a we can compute the correction factors $q_{ij}$ , and from there we can determine the extreme value distributions for arbitrary i and j by (5.2).

Next we can determine the distributions for separate seasons, for separate azimuth sectors, and for the overall maxima. In this it proved necessary to introduce mutual persistence dependency. For seasonal calculations, obtained by taking the product $\Pi_i G_{ij}$ , the mutual dependency between azimuth groups was accounted for by a persistence factor 0.5. For sectorial calculations the mutual dependency of seasons required a factor 1/(1.2) = 0.83. Then (5.3) is replaced by

$$(\Pi_i G_{ij})^{0.5}, \ (\Pi_j G_{ij})^{0.83} \text{ and } (\Pi_{ij} G_{ij})^{0.5} \tag{6.4}$$

Primarily overall results, the distribution functions $(\pi_{ij}G_{ij})^{0.5}$ , were submitted to a final check. It appeared that the stations L.S.Texel,

De Bilt, Vlissingen, Gilze Rijen, Eindhoven and Beek showed a really excellent fit, while the fit of other stations was slightly worse. In general it was found that the result was decidedly sensitive to the shape parameter values : small changes in the k-values of the basic modelling calculation (section 2) hardly were discernible in the distributions of U itself, but showed up clearly in the extreme value distribution. Therefore if an optimum fit is required, it makes sense to adjust k-values slightly; this implies essentially that, next to the basic distribution model fit, also the observed extremes are used.

## 7. Numerical values of the model parameters

In the following tables a review is given of the parameter values obtained by the analysis as described above. In Table 1 three k-values have been adjusted slightly; the original values are given in brackets.

Table 1 : Parameters which vary per station.

| | $\overline{a}$ | $\chi$ | $\overline{k}$ | $\overline{\gamma}$ | $d^*$ | $n^*$ |
|---|---|---|---|---|---|---|
| Schiphol | 6.36 | 74° | 2.35 | 0.76 | 0.43 | 0.30 |
| Eelde | 5.52 | 58° | 2.30(2.37) | 0.74 | 0.43 | 0.39 |
| Soesterberg | 5.24 | 38° | 2.26 | 0.87 | 0.44 | 0.36 |
| De Bilt | 5.05 | 58° | 2.28 | 0.79 | 0.42 | 0.34 |
| Deelen | 5.77 | 66° | 2.25(2.18) | 0.82 | 0.44 | 0.35 |
| Vlissingen | 5.86 | 101° | 2.33 | 0.30 | 0.45 | 0.41 |
| Gilze Rijen | 5.58 | 60° | 2.35 | 0.85 | 0.49 | 0.51 |
| Eindhoven | 5.60 | 58° | 2.32 | 0.79 | 0.48 | 0.42 |
| Beek | 4.69 | 75° | 2.25 | 0.45 | 0.52 | 0.52 |
| Leeuwarden | 6.38 | 68° | 2.40(2.48) | 0.70 | 0.42 | 0.30 |
| Texel L.S. | 7.99 | 129° | 2.47 | 0.00 | 0.36 | 0.27 |
| Zestienhoven | 6.21 | 78° | 2.35 | 0.75 | 0.44 | 0.41 |

Table 2 : Parameters which vary by season

| | $\tilde{a}_{j1}$ | $\tilde{a}_{j2}$ | $\tilde{a}_{j3}$ | $\tilde{a}_{j4}$ | $k^*_{j0}$ |
|---|---|---|---|---|---|
| Jan-Febr. | 0.98 | 198° | 0.60 | 312° | 0.941 |
| March-April | 0.90 | 163° | 0.65 | 317° | 1.034 |
| May-June | 0.77 | 165° | 0.60 | 316° | 1.066 |
| July-Aug. | 1.04 | 179° | 0.47 | 318° | 1.089 |
| Sept-Oct | 1.28 | 200° | 0.47 | 313° | 0.956 |
| Nov-Dec | 1.39 | 195° | 0.51 | 298° | 0.915 |

| | $\tilde{k}_{j1}$ | $\tilde{k}_{j2}$ | $\gamma^*_{j0}$ | $\tilde{\gamma}_{j1}$ | $\tilde{\gamma}_{j2}$ |
|---|---|---|---|---|---|
| Jan-Febr. | 0.25 | -19° | 0.566 | 0.12 | 122° |
| March-April | 0.13 | 59° | 1.191 | 0.26 | 138° |
| May-June | 0.20 | 67° | 1.316 | 0.20 | 173° |
| July-Aug | 0.20 | 54° | 1.304 | 0.32 | 169° |
| Sept-Oct | 0.20 | 8° | 1.117 | 0.26 | 143° |
| Nov-Dec | 0.13 | -40° | 0.503 | 0.10 | 149° |

| | $\tilde{d}_{j0}$ | $\tilde{n}_{j0}$ | $\delta_{j1}$ | $\nu_{j1}$ | $\delta_{j2}$ |
|---|---|---|---|---|---|
| Jan-Febr. | 441 | 1335 | +0.10 | +0.05 | -0.05 |
| March-April | 761 | 1069 | -0.21 | -0.23 | -0.03 |
| May-June | 1029 | 801 | -0.05 | -0.18 | -0.04 |
| July-Aug | 1008 | 852 | +0.06 | -0.06 | +0.04 |
| Sept-Oct | 761 | 1069 | +0.05 | +0.16 | +0.01 |
| Nov-Dec | 380 | 1450 | +0.25 | +0.30 | +0.08 |

| | $d^*_{j2}$ | $d^*_{j4}$ | $n^*_{j2}$ | $n^*_{j4}$ |
|---|---|---|---|---|
| Jan-Febr. | 249° | 327° | 258° | -27° |
| March-April | 151° | 335° | 232° | -11° |
| May-June | 170° | 333° | 156° | 1° |
| July-Aug | 174° | 324° | 194° | -2° |
| Sept-Oct | 233° | 350° | 257° | 10° |
| Nov-Dec | 232° | 354° | 255° | -5° |

Table 3

Persistence factors A and tail correction factors B.

| Season → | Jan-Febr | | March-April | | May-June | |
|---|---|---|---|---|---|---|
| Azimuth | A | B | A | B | A | B |
| 0 | -0.368 | 2.55 | -0.635 | 2.72 | -0.677 | 2.87 |
| 30 | -0.412 | 2.86 | -0.571 | 2.83 | -0.630 | 3.16 |
| 60 | -0.587 | 3.20 | -0.695 | 3.24 | -0.602 | 3.28 |
| 90 | -0.613 | 3.49 | -0.834 | 3.76 | -0.604 | 3.05 |
| 120 | -0.638 | 3.50 | -0.842 | 3.27 | -0.698 | 2.80 |
| 150 | -0.511 | 3.08 | -0.560 | 2.30 | -0.518 | 2.32 |
| 180 | -0.585 | 3.19 | -0.532 | 2.49 | -0.422 | 2.56 |
| 210 | -0.536 | 3.45 | -0.446 | 2.60 | -0.475 | 2.90 |
| 240 | -0.374 | 3.25 | -0.480 | 2.92 | -0.584 | 3.18 |
| 270 | -0.381 | 3.28 | -0.761 | 3.65 | -0.590 | 3.20 |
| 300 | -0.423 | 2.88 | -0.925 | 3.75 | -0.824 | 3.48 |
| 330 | -0.466 | 2.28 | -1.131 | 3.77 | -0.952 | 3.40 |

| | July-Aug | | Sept-Oct | | Nov-Dec | |
|---|---|---|---|---|---|---|
| Azimuth | A | B | A | B | A | B |
| 0 | -0.835 | 3.35 | -0.679 | 2.79 | -0.494 | 2.27 |
| 30 | -0.956 | 3.76 | -0.557 | 2.80 | -0.434 | 2.78 |
| 60 | -0.799 | 3.56 | -0.500 | 2.82 | -0.583 | 2.93 |
| 90 | -0.687 | 2.97 | -0.525 | 2.52 | -0.647 | 3.18 |
| 120 | -0.815 | 2.65 | -0.470 | 2.41 | -0.548 | 3.04 |
| 150 | -0.746 | 2.65 | -0.519 | 2.88 | -0.590 | 2.70 |
| 180 | -0.749 | 3.13 | -0.508 | 2.88 | -0.572 | 2.76 |
| 210 | -0.612 | 3.23 | -0.470 | 2.78 | -0.485 | 2.82 |
| 240 | -0.501 | 3.10 | -0.448 | 3.31 | -0.337 | 2.91 |
| 270 | -0.550 | 3.32 | -0.365 | 2.74 | -0.340 | 2.56 |
| 300 | -0.835 | 3.45 | -0.418 | 2.29 | -0.480 | 2.97 |
| 330 | -1.118 | 3.69 | -0.521 | 2.16 | -0.398 | 1.55 |

## 8. Results of parameter smoothing

We present in figures 12.1 - 12.5 for the station Gilze-Rijen the model parameters calculated by way of fitting, as well as the parameter values calculated with the smoothing procedures. The overall agreement looks satisfactory. It is plausible, that in the smoothing approach some not quite realistic fluctuations have disappeared. On the other hand it may be possible that some realistic deviations have been neglected. It is never fully traceable to what extent the latter has occurred.

Support for the realistic effect of smoothing may be found in the figures 13.1 - 13.6 of the station De Bilt. For this station the data have not only been analyzed for the standard period 1962-1976, but also for the ten-year periods 1961/1970 and 1971/1980. We first can deduce from figure 13.1 that the overall distributions of both periods are quite similar. However, figures 13.2 - 13.4 show that between these periods marked differences may occur for individual azimuth-season distributions. In addition, figures 13.5 - 13.6 show the model parameters for the Jan-Febr-season and for the July-August-season, indicating that we find irregularities in the behavior as well as large differences between the two periods. It may be concluded that an estimate of a distribution over some arbitrary period in future can better be obtained from a smoothed description, as given by the model, than from observations taken over a similar period in the past.

## 9. Meteorological meaning of the station-dependent parameters

We have deduced six model parameters of which the values are different from station to station. It seems useful to discuss their climatological meaning.

The average scale parameter $\overline{a}$ represents essentially the local average wind speed. Its value is large over sea and at the coast, going inland it decreases significantly over the first few kilometers behind the coastline, and then decreases at a slower rate as we advance inland.

$\overline{a}$ is not exactly proportional to the average value $\overline{U}$ of the overall distribution : the ratio between the two depends slightly on the values

of k and $\gamma$ . In a simple 2-parameter Weibull distribution (1.2) the relation is $\overline{U} = a \,/\, \Gamma(1 + \frac{1}{k})$ . In this model the relation is more complex, though the geographical distributions of $\overline{a}$ and $\overline{U}$ remain similar.

The shape parameter $\overline{k}$ indicates the concentration of data around the level $\overline{a}$ . Smaller values of k imply relatively more deviations from the average level, more data with large or small values; large k-values indicate a compact peaked distribution. The seasonal variation of the shape parameter shows in particular relatively small k-values in winter seasons. This is due to the fact that in some years the winter season is stormy, with many large wind speeds, while in other years very prolonged periods with stationary freezing weather and weak winds are experienced.

The parameter $\overline{\gamma}$ is related to the stability climate, the average degree of thermal stratification of the boundary layer. This in turn is directly related to the average amplitude of the diurnal wind variation. If we represent this average diurnal course by fitting a sinusoidal curve with amplitude $A_d$ , figure 14 shows the relation of $A_d$ and $\overline{\gamma}$ . Approximately, $\overline{\gamma}$ is 70% of $A_d$.

The parameter $\overline{\chi}$ indicates the variation of the azimuth of the maximum in the "wind rose" representation of the azimuthal wind speed distribution, i.e. whether the predominant winds are more southerly or more westerly (in our country). Here too a significant difference between sea and land is found.

The parameters $d^*$ and $n^*$ are indications for the degree of absolute difference between an azimuthal wind frequency distribution and a uniform distribution. It is generally experienced, that the shape of a wind rose representation is not quite circular and not quite elliptical either. The values of $d^*$ and $n^*$ show the deviation from circularity. The parameters $\delta_{j1}$ , $\delta_{j2}$ and $\nu_{j1}$ determine the seasonal variation of the deviation, while the parameters $d^*_{j2}$ and $n^*_{j2}$ indicate the direction of the primarily predominant winds (southwesterly), and $d^*_{j4}$ and $n^*_{j4}$ determine a second (smaller) peak in northeasterly directions.

## 10. Validity of modelled distributions of hourly averages

In the figures 15 frequency distributions of hourly averaged wind speeds are given both from observations and from the smoothed model. This is done for individual azimuth groups, for season groups, and also for the overall distribution. The results look acceptable, but this proves little because here the model has been applied to data, which also have been used to derive the model formulas.

However, we have also frequency distributions available from fifteen other stations over reasonably long observation periods (see figure 2); only, these observation periods are not exactly 1962/1976. For these stations we made rough estimates of the six station-variable model parameters, using the maps of figures 7.1 - 7.6. The results of this geographical interpolation are tabulated below.

Table 4. Model parameters for interpolated stations

| | Period | $\bar{a}$ | $\bar{k}$ | $\bar{\gamma}$ | $\chi$ | $d^*$ | $n^*$ |
|---|---|---|---|---|---|---|---|
| Den Helder | 1909-1971 | 7.50 | 2.40 | 0.28 | 110° | 0.40 | 0.29 |
| IJmuiden | 1956-1967 | 6.90 | 2.40 | 0.18 | 114° | 0.40 | 0.29 |
| Diepenveen | 1965-1980 | 5.50 | 2.28 | 0.76 | 60° | 0.43 | 0.38 |
| Someren | 1965-1975 | 5.20 | 2.30 | 0.78 | 60° | 0.48 | 0.42 |
| Zierikzee | 1961-1977 | 5.40 | 2.32 | 0.35 | 90° | 0.45 | 0.41 |
| Kornwerderzand | 1962-1980 | 7.00 | 2.48 | 0.10 | 100° | 0.38 | 0.28 |
| Lelystad | 1961-1980 | 6.50 | 2.40 | 0.37 | 70° | 0.42 | 0.30 |
| Urk | 1960-1975 | 7.00 | 2.40 | 0.26 | 70° | 0.42 | 0.30 |
| Valkenburg | 1966-1975 | 6.40 | 2.35 | 0.74 | 80° | 0.42 | 0.35 |
| Terschelling | 1969-1980 | 7.60 | 2.45 | 0.20 | 120° | 0.40 | 0.27 |
| Goeree | 1951-1970 | 8.00 | 2.47 | 0.01 | 110° | 0.40 | 0.30 |
| Hoek v.Holland | 1960-1980 | 6.60 | 2.40 | 0.29 | 110° | 0.40 | 0.30 |
| Herwijnen | 1966-1977 | 5.90 | 2.30 | 0.69 | 60° | 0.45 | 0.40 |
| Lauwersoog | 1969-1980 | 7.00 | 2.40 | 0.36 | 80° | 0.40 | 0.30 |
| Vlieland | 1949-1972 | 7.40 | 2.45 | 0.23 | 120° | 0.40 | 0.27 |

Having determined these parameters, we applied again the model programme to calculate the frequency distributions of hourly averages according to (3.1a) and (3.1b).

The results of these 15 stations are presented in figures 16 in analogy to the figures 15 obtained for the 12 basic stations. Generally the degree of correspondence for the interpolated stations is similar to the agreement obtained at the basic stations.

A summarizing representation of the degree of agreement between model and obervations at basic interpolated stations was obtained as follows. For all stations percentiles were obtained from the frequency distributions by interpolation, representing the average wind speeds having exceedance probabilities of respectively 50%, 20%, 10%, 1% and 0.1%. This was done both for the observed distributions (notation $U_{50\%}$) and for the modelled distributions (notation $\hat{U}_{50\%}$). The differences $\Delta_{50\%} \equiv U_{50\%} - \hat{U}_{50\%}$ were determined, and separately for the groups of 12 basic stations and 15 interpolated stations the group averages and standard deviations of $\Delta$ were calculated for the various percentiles. Figure 17.1 shows the evolution of $\overline{\Delta} \pm 2\ \sigma_\Delta$ for decreasing percentage, i.e. increasing wind speed.

It appears that $\overline{\Delta}$ does not deviate significantly from zero, both for the basic stations and for the interpolated stations. The small systematic departure is practically negligible. Moreover the $\sigma_\Delta$ values are somewhat larger for the interpolated stations than for the basic stations, as could be expected, yet the difference is not large.

The absolute values of $\sigma_\Delta$ increase with decreasing exceedance probability, which is logical because the smaller exceedance probabilities correspond to larger U values. Therefore it is really more appropriate to normalize the deviations through division by U and to investigate the deviations

$$\delta_p \equiv \frac{U_p - \hat{U}_p}{U_p} ,$$

with p referring to the percentiles (50% etc.).

In figure 17.2 these deviations are given for the overall distribution, while figures 17.3 - 17.4 give the corresponding results for the seasonal and azimuthal distributions. Of course the variances for the seasonal distributions are larger than for the overall distributions, and for the azimuthal distributions they are even larger. The latter is due to the fact that in the azimuthal case the total number of observations varies as well, which is not so for the seasons. For the overall distribution the deviations are generally $< 5\%$, which seems acceptable.

Additional illustrations are presented in a distributive fashion for some individual interpolated stations, namely Urk which can be considered the "worst" of the 15 test stations (see the large percentile deviations in figure 17), and Herwijnen which is a very well-behaved test station. Urk, in particular, is a good example of the distortion suffered by a frequency distribution of wind observed with an anemometer which does not work well at low speeds: the lowest speed class is excessively high, and the next-higher speeds are therefore underrepresented.

In figure 18.1 the observed and the modelled distribution are given for both stations; in case of Herwijnen the correspondence is nearly perfect. Even for Urk, though, the correspondence can be considered acceptable because it is of the same order of magnitude as the climatological variation of such distributions at any single location. This is illustrated in figure 18.2, where the distributive frequency distributions of station De Bilt are given for the two 10-year periods 1961/1970 and 1971/1980, with the modelled distribution curve also drawn in. In figure 13.1 it was already shown that the cumulative distributions of both periods are virtually identical, so that an actual climatological difference between the 10-year periods is unlikely -- the surroundings of De Bilt also showed no great changes from 1960 to 1980. Even so, the frequency distributions in figure 18.2 show sizeable differences. Compared to this, the deviations between observations and model in figure 18.1 for Urk and Herwijnen are not significant.

For separate seasonal groups larger deviations are observed, and for azimuthal groups even larger, but even here even the outlying cases can be deemed acceptable. For instance, in figure 18.3 the worst subgroup case is pictured, namely the Kornwerderzand midwinter distribution for seasonal groups, and also another rather deviationist case is given, namely Lauwersoog. As a more satisfactory subgroup example figure 18.4 shows three cases where the deviations in figure 17.3 were $< 10\%$.

In the following table is given for all test station calculations (90 = 15 × 6 for any set of subgroups) how many of these showed respectively 0, 1, 2, 3 or 4 times a deviation $> 10\%$ for any single percentile.

| | none | 1× | 2× | 3× | 4× |
|---|---|---|---|---|---|
| season groups | 61 | 16 | 7 | 5 | 1 |
| azimuth groups | 30 | 28 | 11 | 7 | 5 |

Some other comparisons of observations and model are given in figures 18.5 and 18.6. Here e.g. Hoek van Holland 120° is a case which deviates rather far. Again for comparison in figure 18.7 the same azimuth case and also a season are given for De Bilt for the two ten-year-periods of figure 18.2. In view of the differences seen in figure 18.7, those in figure 18.6 seem to be as reliable as the climate permits.

Summarizing, it can be stated that the model is capable to provide a frequency distribution of potential wind speed for any season or azimuth sector, or for the year, at an arbitrary location in our (not very complex) country. The reliability of these modelled distributions seems to be acceptable within the limits of climatological variability.

## 11. Validity of modelled extreme value distributions.

In figures 19 and 20 the annual maxima, obtained by application of (5.2) and (5.3), have been plotted cumulatively on extreme value graph paper (Gumbel), both for the 12 basic stations and for the 15 interpolated stations. The observations have been entered at the plotting positions of Benard and Bos-Levenbach.

In analogy to our analysis of the reliability of modelled distributions of hourly averages in figure 17, we have given here in figures 21 the relative deviations of the extremes, restricting ourselves to the 50% and the 10% case. Smaller percentiles cannot be analyzed in this fashion because of the small number of observations.

It appears that the majority of deviations is less than ± 10%, which is very good for extreme values. Of course the deviations are larger for the 15 test stations than for the 12 basic stations, but no evident systematic differences between the two groups are found. Because we only have 15 annual maxima for the basic stations (sometimes a few more for test stations) it would make little sense to draw distribution curves, as we did for the average value distributions.

Finally we investigate the quality of the developed procedure for determination of "extreme values" by way of the compound Weibull model, as compared with extreme values obtained by the classical methods given

by Fisher-Tippett and Gumbel.

In section 6 we already stated that classical theory requires that the basic observations are mutually independent. This is certainly not the case for series of wind observations made every hour. Nevertheless the classical method is often applied in literature, and we will do the same. The method requires that on "Gumbel-type" graph paper the extreme values should lie on a straight line, and for fitting this line we use the weighing method of Lieblein (see Thom, 1968).

In this way the 0.1 % extreme values, with an average recurrence period of 1000 years, have been determined for all 27 stations by graphical extrapolation of the Lieblein line on Gumbel graph paper. Next to this, the same extreme values were determined by extrapolation of the Weibull-model curves. The results have been mapped in figures 22.1 and 22.2. We see that the Gumbel extremes show a much more irregular variation across our (not very complex) country than the Weibull-model extremes.

In addition, the 1000-year extremes obtained by the Gumbel method are generally much larger than those obtained from the Weibull-model. The latter is due to the linear extrapolation on the Gumbel graph paper and the neglect of persistence in the Gumbel method. This is shown in figure 23, where for the station Schiphol the 'overall' annual extremes are plotted as well as the annual extremes observed in the 270°-sector. The Lieblein-lines are drawn, and also the Weibull-model curves.

Extrapolating to large recurrence periods in figure 23, we see primarily that the Lieblein lines exceed the Weibull-model curves by an increasing amount. Moreover, the Lieblein line for the 270°-sector crosses the line for the overall extremes and exceeds it at very large recurrence periods -- which is patent nonsense. Evidently overall extremes should always be larger than extremes for seasonal or azimuth sector subgroups for the same recurrence period. The Weibull-model extremes for the 270°-sector always are smaller than the overall extremes, as it should be.

This example shows clearly the unreliability of the Gumbel method for determining extreme wind speeds. On the other hand, the Weibull-model allows the determination of distributions and extreme values which are mutually consistent.

For average recurrence periods of 10, 25, 50, 100, 200 and 500 years maps are given according to the Weibull-model only, in figures 22.3-22.8. In addition, figures 24.1-24.12 give extreme values with a 50 year average recurrence period for the 12 azimuth sectors.

## 12. Applicability of the model at heights above 10 m.

The origin of the wind distribution model described above is an analysis, which was made of a single year of wind data obtained from the 80m-mast at Vlaardingen (Rijkoort et al., 1970). The analysis is given at length in Dutch by Rijkoort (1972), and will be summarized below.

Observations of hourly-averaged wind at 10 m, 40 m and 80 m height, taken in the year March 1967 - April 1968 every four hours, were split up into four season groups (the "official" ones), four azimuth sector groups (N, E, S and W) and day and night -- 96 groups in all. These observation distributions were fitted by two-parameter Weibull distributions. The obtained values of the scale parameter a and the shape parameter k were smoothed graphically, which made it possible to investigate separately the effects due to season, azimuth, day/night and height.

The most significant result was the day-night-difference in the variation of a and k with height, as tabulated below :

| height | $a_{day}$ | $a_{night}$ | $a_{day} - a_{night}$ | $k_{day}$ | $k_{night}$ | $k_{day} - k_{night}$ |
|---|---|---|---|---|---|---|
| 10 m | 5.78 | 4.73 | + 1.05 | 2.68 | 2.14 | + 0.54 |
| 40 m | 7.06 | 6.35 | + 0.71 | 2.74 | 2.50 | + 0.24 |
| 80 m | 8.15 | 8.15 | 0 | 2.69 | 2.73 | - 0.04 |

Both for a and k the difference between daytime and nighttime values decreases with increasing height and approaches zero at the 80 m level. Moreover with increasing height $k_{day}$ varies little and $k_{night}$ increases.

In the present report the compound Weibull model has been developed only for the potential wind speed, referring to the 10 m level. In view of the results of Rijkoort (1972) it can be expected, that the compound model will be applicable over that boundary layer height range in which the wind is well correlated with the wind at 10 m. In fact, a recent analysis of data from the 200 m meteorological mast at Cabauw made by Holtslag (1984) proves, that the actual wind distribution at 10 m can be

reasonably well transformed into the actual distribution at 80 m, when proper corrections for atmospheric stability are applied. Therefore it seems feasible to extend the compound Weibull model in future to the whole "matching layer" (Tennekes, 1973) between ~ 5 m (depending on the terrain roughness) and ~ 80 m.

It will probably be possible to assign a height-independent value to k, while making a and $\gamma$ vary with height in a fashion yet to be investigated. It may be that a increases logarithmically with height, like its counterpart parameter $\overline{U}$ . The stability parameter $\gamma$ is expected to approach zero at a height of 60 to 80 m, where the amplitude of the diurnal course of the wind is minimal. The change in $\gamma$ then replaces the increase of k with height, which has been reported in literature for two-parameter Weibull representations of wind (e.g. Justus et al, 1976). It is expected that the other three location-dependent model parameters, $\chi$ , d and n, will not vary with height to a first approximation because of their large-scale meteorological nature (see section 9). Similarly we do not expect the location-independent parameters to vary with height.

## 13. Conclusion

It has been proved possible to compute frequency distributions of hourly averaged potential wind speed for an arbitrary location in the Netherlands -- both overall annual distributions and distributions for separate two-month seasons or separate $30^{o}$ azimuth sectors. This has been accomplished by way of a mathematical model, of which the parameters were determined from statistical analysis of observed 15-year distributions at 12 stations.

Computing the distributions at any arbitrary location requires the geographical interpolation of six basic model parameters, of which the variation across the country has been determined from the 12 basic station series. The six basic parameters are the location-dependent remnants of a smoothing operation, which also produced a set of other model parameters which do not vary geographically. The parameter smoothing was performed by simple, generally graphical methods taking account of physical properties of the wind climate. In principle it should be possible to systematize the method to greater extent, which

might eliminate some still-present deviations, particularly in the azimuthal variation.

The model results were checked against distributions observed at 15 other independent stations. The agreement is very satisfactory, when compared with the existing climatological fluctuations observed in distributions from the same station over different 10-year periods.

The model has been applied to the estimation of extreme values of average wind speeds with long recurrence periods (Rijkoort and Wieringa, 1983). Using persistence corrections and a secondary tail correction it proves possible to obtain a plausible representation of observed extreme values, not only for annual extremes but also for seasonal and azimuth sector extremes. It is shown that for long recurrence periods the model extremes are much more consistent than the results of Gumbel-type extreme value computations.

The model, which has proved very workable for the Netherlands, should be applicable elsewhere to the modelling of frequency distributions in regions without major orography problems. The basic requirement is the availability of good wind data series of at least 10 years for a sufficient number of stations with known exposure corrections.

In computing the appropriate model parameter array for other regions, the fundamental step is the separation into daytime and nighttime data. The regional wind climate characteristics then determine to what extent subdivision into seasons and azimuth sectors is needed. In non-complex wind climates the number of final parameters could very well be less than we needed in the Netherlands. Moreover, if the model were applied in a few essentially different climate regions, it should be possible to develop generalized relations (like figure 14) for the determination of model parameters from known climate characteristics.

The amount of parameters used in the model seems large, but that is a consequence of the complexity of meteorology. In this computer age such elaboration is more viable than a generation ago. Moreover, the net result proves to be a simplification as soon as distributions for data subsets are required. A description of separate wind distributions for six seasons and for $30^{o}$-sectors would require 144 parameters if we tried to do it with two-parameter Weibull functions (1.2), while the model does the same job better with 114 regional and 6 local parameters.

At present the model has been developed for potential wind speed, referring to 10 m height over open terrain. It seems definitely possible to use the model at heights to ~ 80 m by systematically changing two of the six basic model parameters. Future research (by others than this author) will have to develop this possibility.

## Acknowledgments

The completion of this report was only possible through the collaboration with and cooperation of a large number of (former) collegues at the Royal Netherlands Meteorological Institute (K.N.M.I.). I feel much gratitude towards all of them.

In the first place I wish to mention Jon Wieringa. More than fifteen years of intensive cooperation have been an unforgettable experience. With respect to this report in particular he contributed his work in compiling a wind data set which was reliable, homogenized and exposure-corrected. In addition I thank him for his aid in translating the original text into English and discussing its presentation. With respect to the data compilation, the work of B. Oemraw on the history of the station observations has also been a great help.

Moreover I wish to mention the statistical advice and assistance of S. Kruizinga, T.A. Buishand, G.J. Yperlaan and A. Denkema, who were my collegues at the former KNMI Statistical Bureau. Text discussions with C.A. Velds were very helpful. For extensive and meticulous computer programming assistance I could rely on G.J. Yperlaan and J.M. Koopstra.

The excellent figure drawings by M. Latupeirissa, C. van Stralen and R.J. Meijer are highly appreciated. Mrs. M.L. Collet - van Laere provided the reliable typework for the many reports made during this study, and I thank J.J. Wittebol and C.R.H. Holland for the professional printing work.

## Appendix

The estimates of the parameters of the ordinary and the extended Weibull distributions, used in this report, were obtained by application of the maximum likelihood method in a fashion given below. We will commence by repeating the cumulative distribution formulas :

$$F_d(U) = 1 - \exp\left(-\left(\frac{U}{a}\right)^k\right) \qquad (A.1)$$

and

$$F_n(U) = 1 - \exp\left(-\left\{\frac{U}{a}\left[1 + \gamma \exp\left(-\frac{U}{5}\right)\right]\right\}^k\right) \qquad (A.2)$$

For (A.1) the method to estimate a and k can be found in literature for non-grouped data (e.g. Johnson and Kotz, 1970). In our case, however, the data have been grouped into intervals, and moreover we require estimates which are valid simultaneously for (A.1) and (A.2).

In this case we define the likelihood function L by

$$L \equiv \Pi_r \left(F_d(U_r) - F_d(U_{r-1})\right)^{d_r} \left(F_n(U_r) - F_n(U_{r-1})\right)^{n_r} \qquad (A.3)$$

When the parameters a, k and $\gamma$ vary, so does L. It will be evident that for small values of L we find a, k and $\gamma$ deviating strongly from their "true" values. If we maximize L, we will get estimates of a, k and $\gamma$ which will approach closely their "true" values.

From practical considerations subsequent calculations are done using ln L, and the maximum of L is obtained by requiring

$$\frac{\partial \ln L}{\partial a} = 0 \ , \quad \frac{\partial \ln L}{\partial k} = 0 \ , \quad \frac{\partial \ln L}{\partial \gamma} = 0 \ . \qquad (A.4)$$

Introducing $G_r \equiv 1 - F_d(U_r)$ and $P_r \equiv 1 - F_n(U_r)$ and also $\Delta G \equiv G_{r-1} - G_r$ and $\Delta P_r \equiv P_{r-1} - P_r$, we obtain

$$\ln L = \sum_r d_r \ln \Delta G + \sum_r n_r \ln \Delta P \qquad (A.5)$$

We introduce some auxiliary functions, $T \equiv \ln\left(\frac{U}{a}\right)$ and $H \equiv \left(\frac{U}{a}\right)^k$, where the index r is omitted for easier notation.

This gives $G = \exp[-H]$ and $H = \exp[kT]$. In addition we define

$$Q \equiv \frac{U}{a}\left(1 + \gamma \exp\left(-\frac{U}{5}\right)\right) \text{ and } R \equiv \frac{U}{a} \exp\left(-\frac{1}{5} U\right) ,$$

giving $P = \exp\left(-Q^{k}\right)$ and $Q \equiv \frac{U}{a} + \gamma R$ .

We then find for the various differential quotients :

$$\frac{\partial G}{\partial a} = \frac{k}{a} GH \quad , \quad \frac{\partial G}{\partial k} = - GHT \quad , \quad \frac{\partial G}{\partial \gamma} = 0$$

$$\frac{\partial P}{\partial a} = \frac{k}{a} P Q^{k} \quad , \quad \frac{\partial P}{\partial k} = - P Q^{k} \ln Q \quad , \quad \frac{\partial P}{\partial \gamma} = - k P Q^{k-1} R$$

Using the notation $\Delta GH \equiv G_{r-1} H_{r-1} - G_r H_r$ , etcetera, we then get

$$\frac{\partial \ln L}{\partial a} = \frac{k}{a} \sum d \frac{\Delta GH}{\Delta G} + \frac{k}{a} \sum n \frac{\Delta P Q^{k}}{\Delta P}$$

$$\frac{\partial \ln L}{\partial k} = - \sum d \frac{\Delta GHT}{\Delta G} - \sum n \frac{\Delta P Q^{k} \ln Q}{\Delta P}$$

$$\frac{\partial \ln L}{\partial \gamma} = - k \sum n \frac{\Delta P Q^{k-1} R}{\Delta P}$$

Now the parameters a , k and $\gamma$ can be estimated by way of an iterative computer programme, based on

$$\sum d \frac{\Delta GH}{\Delta G} + \sum n \frac{\Delta P Q^{k}}{\Delta P} = 0$$

$$\sum d \frac{\Delta GHT}{\Delta G} + \sum n \frac{\Delta P Q^{k} \ln Q}{\Delta G} = 0$$

$$\sum n \frac{\Delta P Q^{k-1} R}{\Delta P} = 0$$

The complete formulas are listed in an internal report (Rijkoort 1981).

References :

A. Benard, E.C. Bos-Levenbach (1953): The plotting of observations on probability paper. Statistica 7, 163-173.

C.E.P. Brooks, N. Carruthers (1953): Handbook of statistical methods in meteorology (Met.Off.538). H.M. Stationery Office, London, U.K.

N.J. Cook (1982): Towards better estimation of extreme winds. J. Wind Engin. Industr. Aerodyn. 9, 295-323.

R.A. Fisher, L.H.C. Tippett (1928): Limiting forms of the frequency distribution of the largest or smallest number of a sample. Proc. Cambridge Philos. Soc. 24, 180-190.

T.F. Gaskell, M. Morris (1979): World climate -- the weather, the environment and man. Thames and Hudson, U.K.

J.P. Hennessey (1977): Some aspects of wind power statistics. J. Appl. Meteor. 16, 119-128.

A.A.M. Holtslag, A.P. Van Ulden (1983): A simple scheme for daytime estimates of the surface fluxes from routine weather data. J. Clim. Appl. Meteor. 22, 517-529.

A.A.M. Holtslag (1984): Estimation of diabatic wind speed profiles from routine weather data compared with Cabauw tower observations. Submitted to Boundary-Layer Meteorology.

N.J. Johnson, S. Kotz (1970): Distributions in statistics 1: Continuous univariate distributions. Houghton Mifflin, Boston, U.S.A.

C.G. Justus, W.R. Hargraves, A. Yalcin (1976): Nationwide assessment of potential output from wind-powered generators. J. Appl. Meteor. 15, 673-678.

C.G. Justus, W.R. Hargraves, A. Mikhail, D. Graber (1978): Methods for estimating wind speed frequency distributions. J. Appl. Meteor. 17, 350-353.

E.L. Petersen (1982): Wind atlas for the European Community. In: "Wind energy" (editors W. Palz, W. Schnell), Solar Energy R&D in the E.E.C. (Reidel, Dordrecht) vol. G 1, 70-86.

P.J. Rijkoort, F.H. Schmidt, C.A. Velds, J. Wieringa (1970): A meteorological 80-m tower near Rotterdam. Bound.-Layer Meteor. 1, 5-17.

P.J. Rijkoort (1972): De variatie van de windsnelheidsverdeling volgens waarnemingen op 10, 40 en 80 m hoogte aan de meteorologische meetmast te Vlaardingen. KNMI-Sc.Rep. 72-4.

P.J. Rijkoort (1981): Schattingen van de parameters van de gewone en de gemodificeerde Weibull-verdeling en van hun standaarddeviaties. Internal Rep. Roy. Netherl. Meteor. Inst. KNMI-VSB-80-2.

P.J. Rijkoort, J. Wieringa (1983): Extreme wind speeds by compound Weibull analysis of exposure-corrected data. (6th Internat. Conf. on Wind Engineering, Australia 1983; Prepr.vol.1). To be published in J. Wind Engin. Industr. Aerodyn., vol. 13.

H. Tennekes (1973): The logarithmic wind profile. J. Atmos. Sci. 30, 234-238.

H.C.S. Thom (1968): Some methods of climatological analysis. W.M.O.-Techn. Note 81.

J. Wieringa (1976): An objective exposure correction method for average wind speeds measured at a sheltered location. Quart. J. Roy. Meteor. Soc. 102, 241-253.

J. Wieringa (1980): Representativeness of wind observations at airports. Bull. Am. Meteor. Soc. 61, 962-971.

J. Wieringa (1982): Review of wind climate research in the Netherlands. In: "Wind energy" (editors W. Palz, W. Schnell), Solar Energy R&D in the E.E.C. (Reidel, Dordrecht) vol. G 1, 123-127.

J. Wieringa (1983): Description requirements for assessment of non-ideal wind stations -- for example Aachen. J. Wind Engin. Industr. Aerodyn. 11, 121-131.

J. Wieringa, P.J. Rijkoort (1983): Windklimaat van Nederland. Staatsuitgeverij, Den Haag.

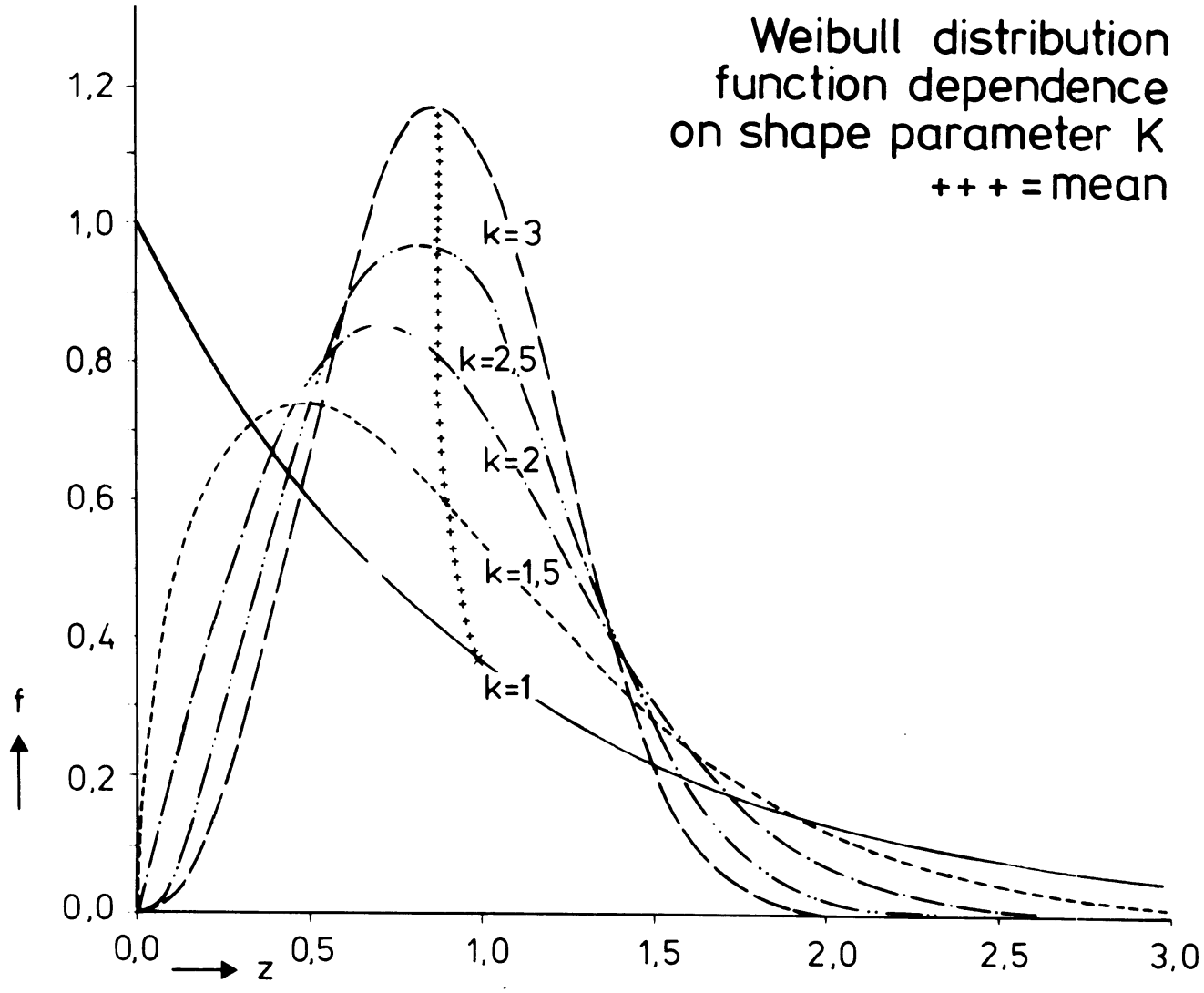


Fig. 1 Variation of the shape of distributive functions depending on the value of the shape parameter k.


Fig. 2 Wind observation stations in the Netherlands used for model construction and for model testing.

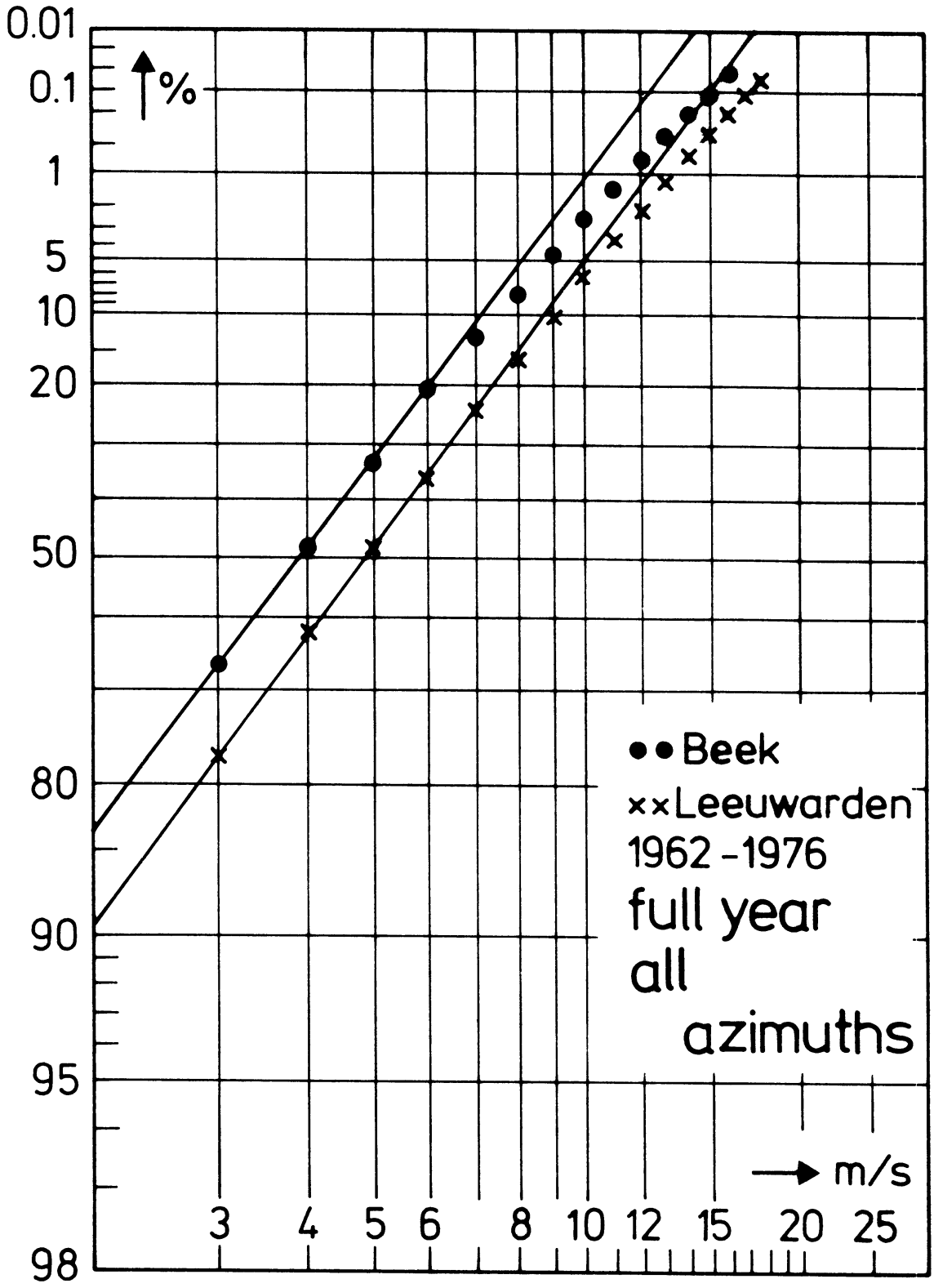


Fig. 3 Deviation from linearity on Weibull-paper of wind speed distributions for the stations Leeuwarden and Beek.

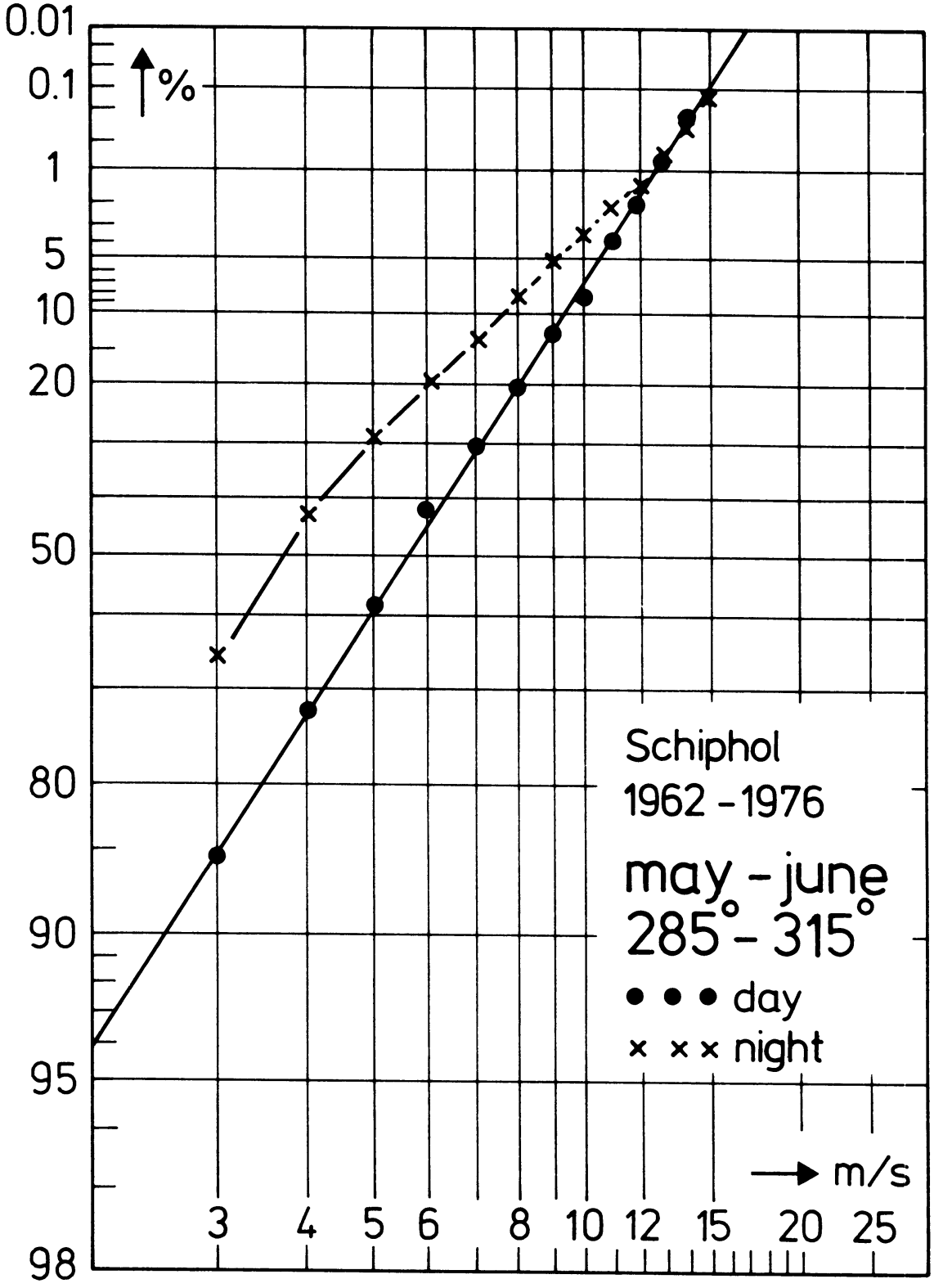


Fig. 4.1 Daytime and nighttime wind distribution for Schiphol.

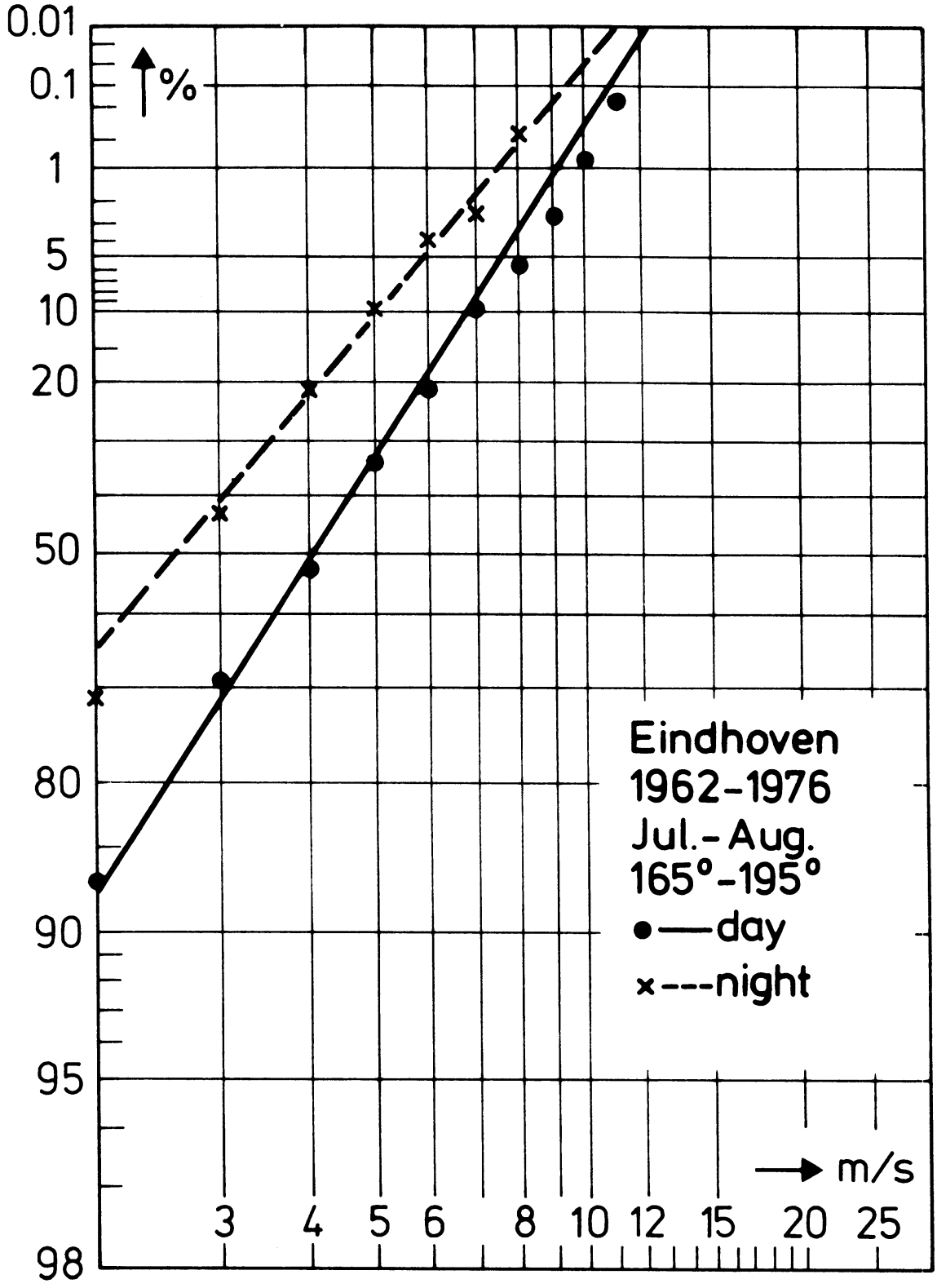


Fig. 4.2 Daytime and nighttime wind distribution for Eindhoven.

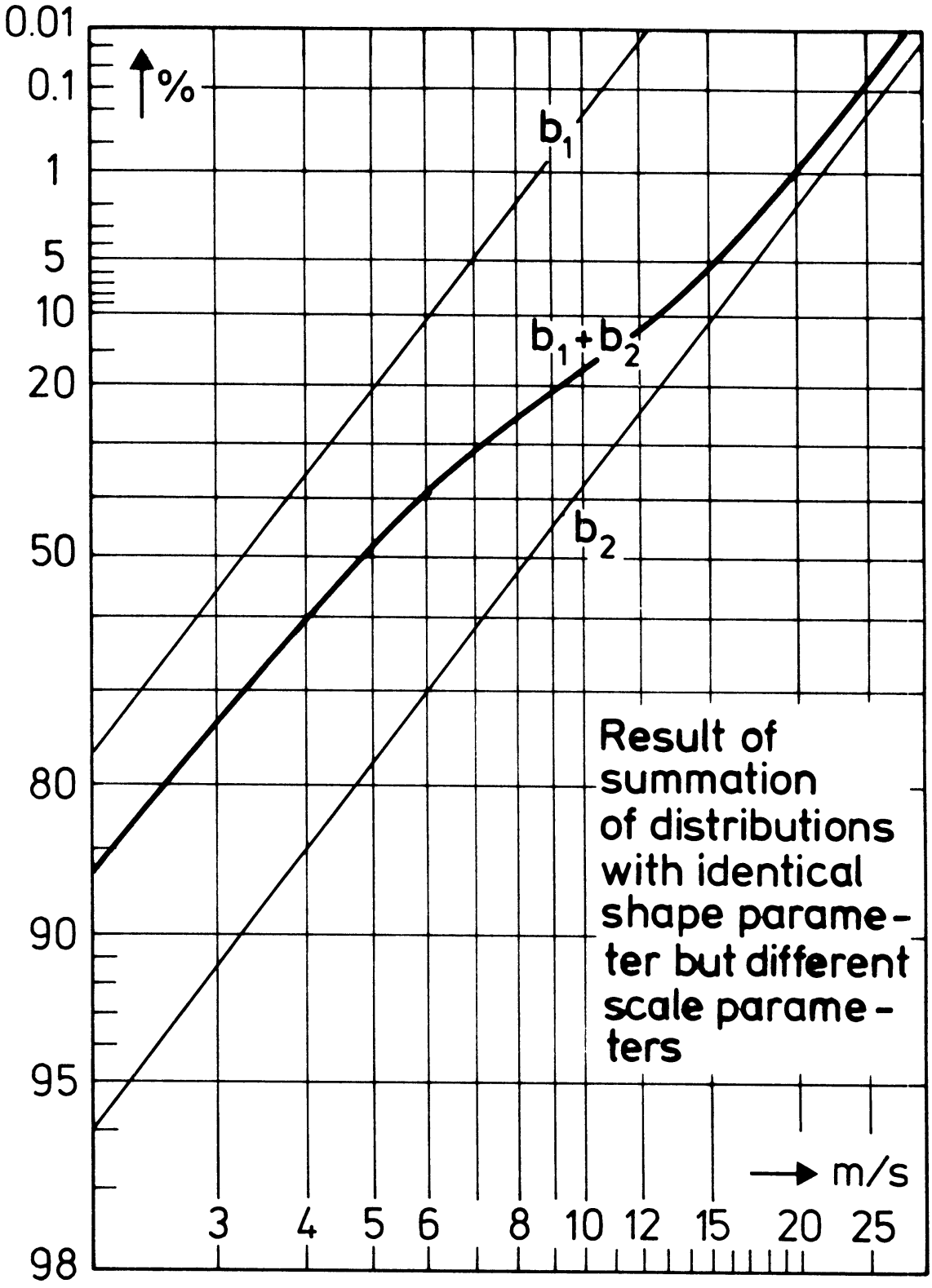


Fig. 5 Result of summation of two data sets $b_1$ and $b_2$ , which are both Weibull-distributed and have identical shape parameters and different scale parameters.

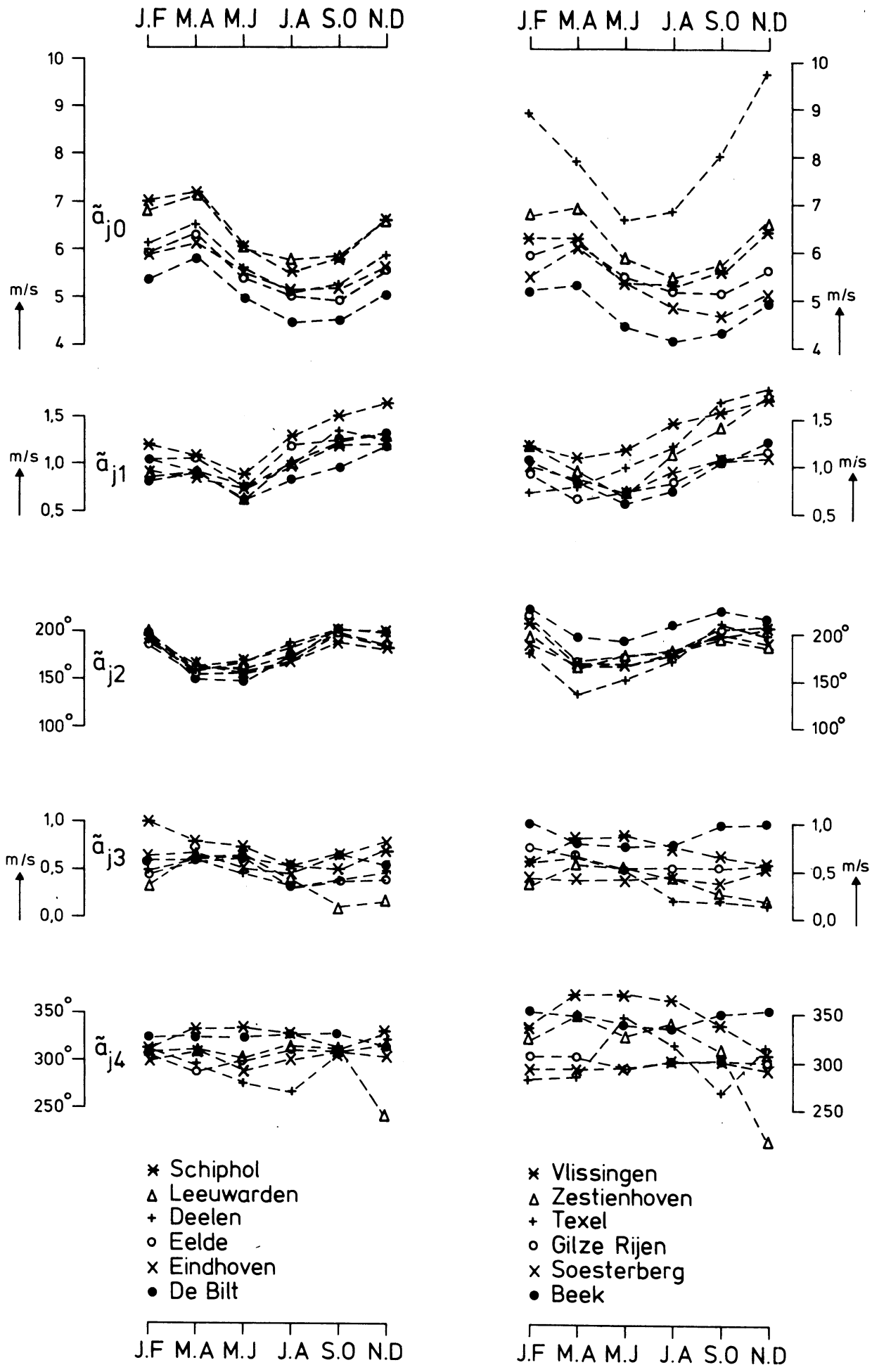


Fig. 6.1 Harmonic analysis parameters for the model parameter a.

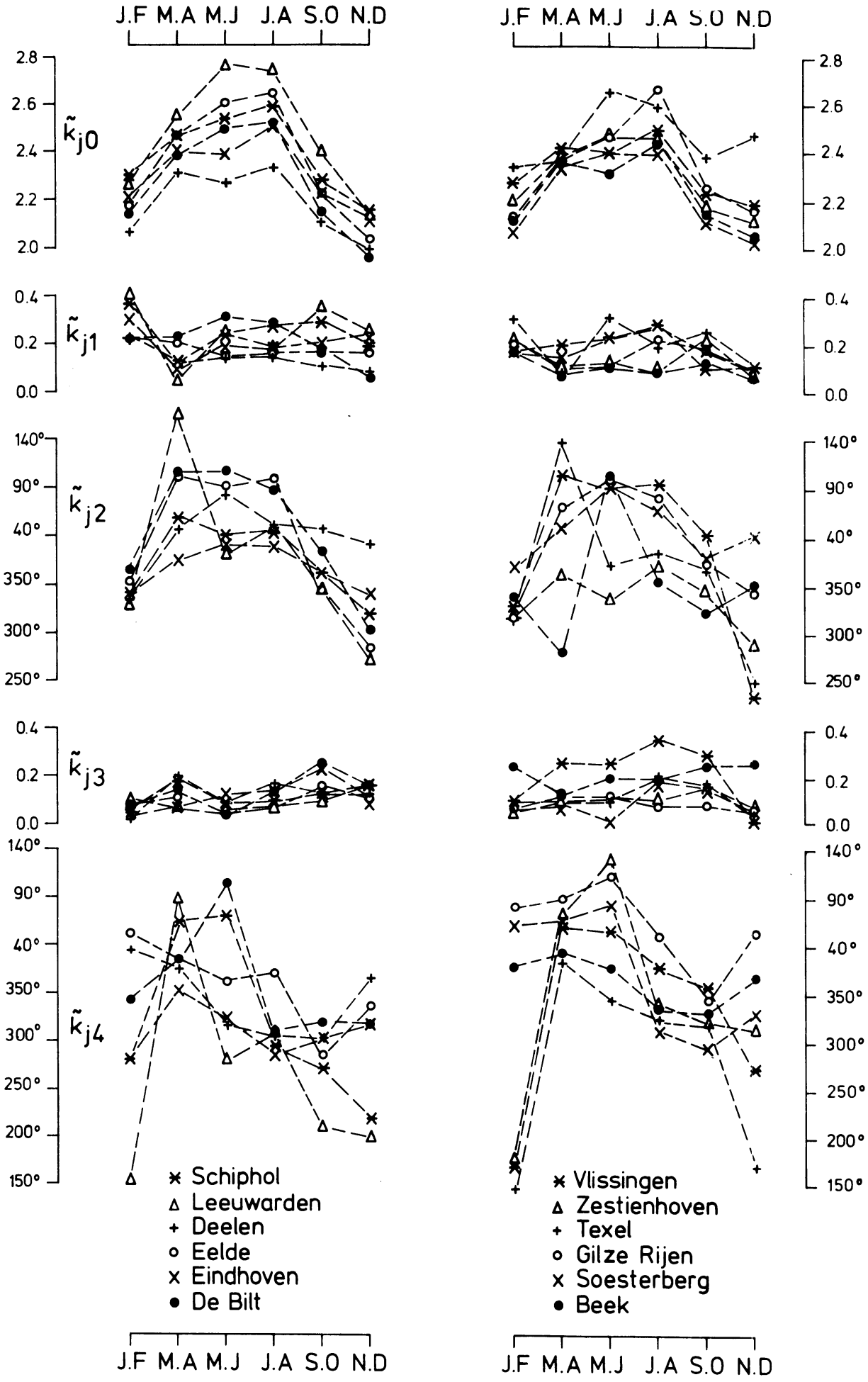


Fig. 6.2 Harmonic analysis parameters for the model parameter k.

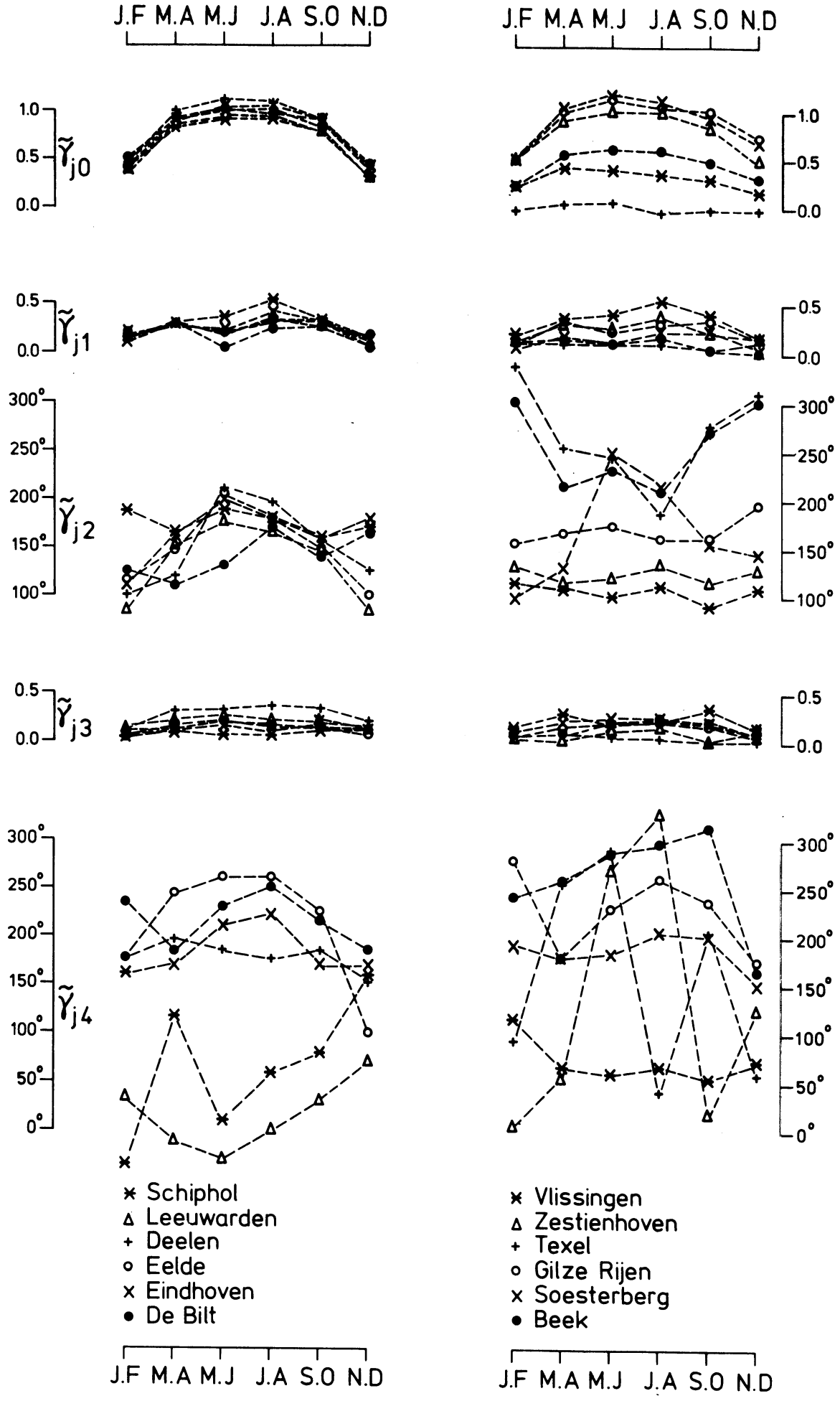


Fig. 6.3 Harmonic analysis parameters for the model parameter $\gamma$ .

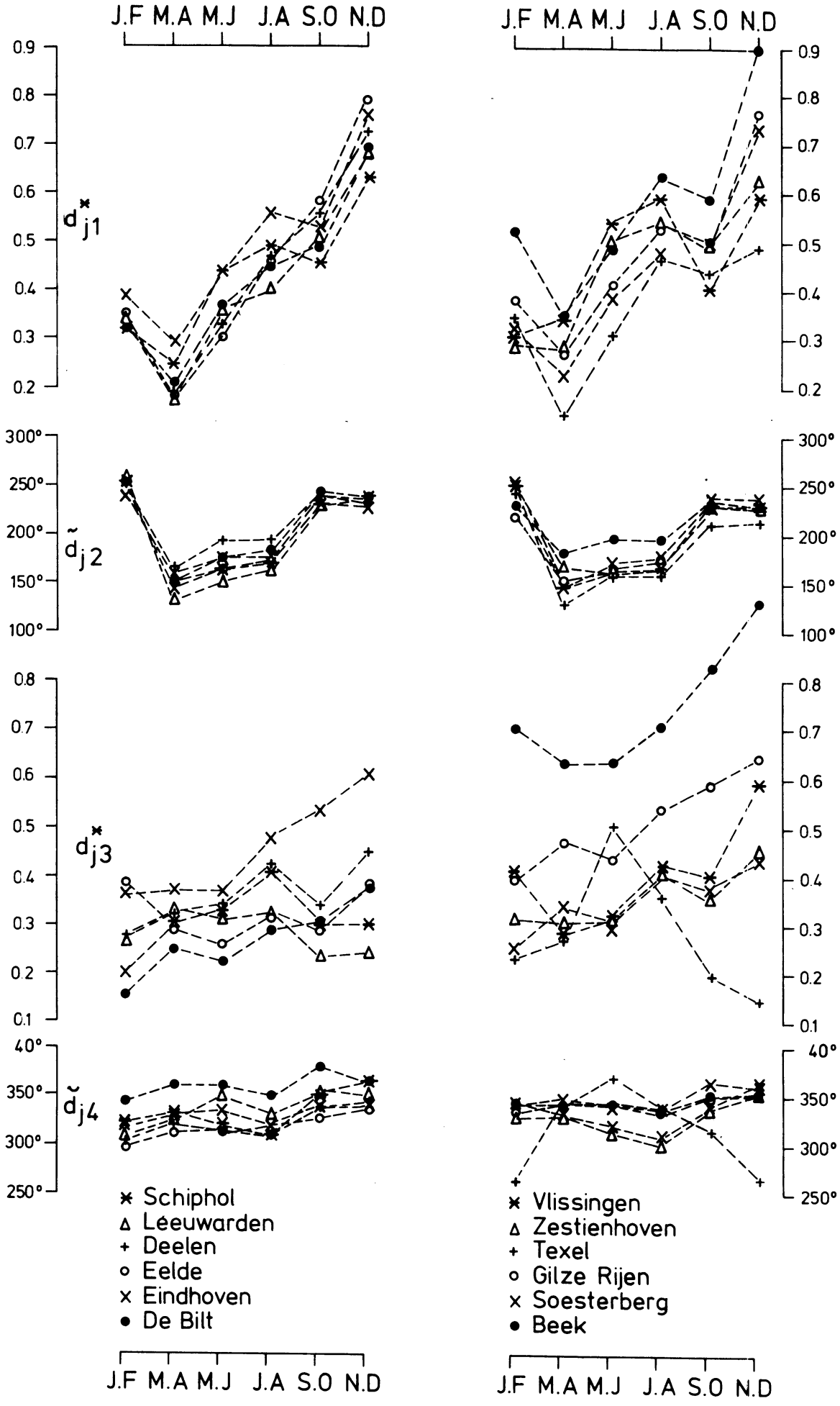


Fig. 6.4 Harmonic analysis parameters for the model parameter d.

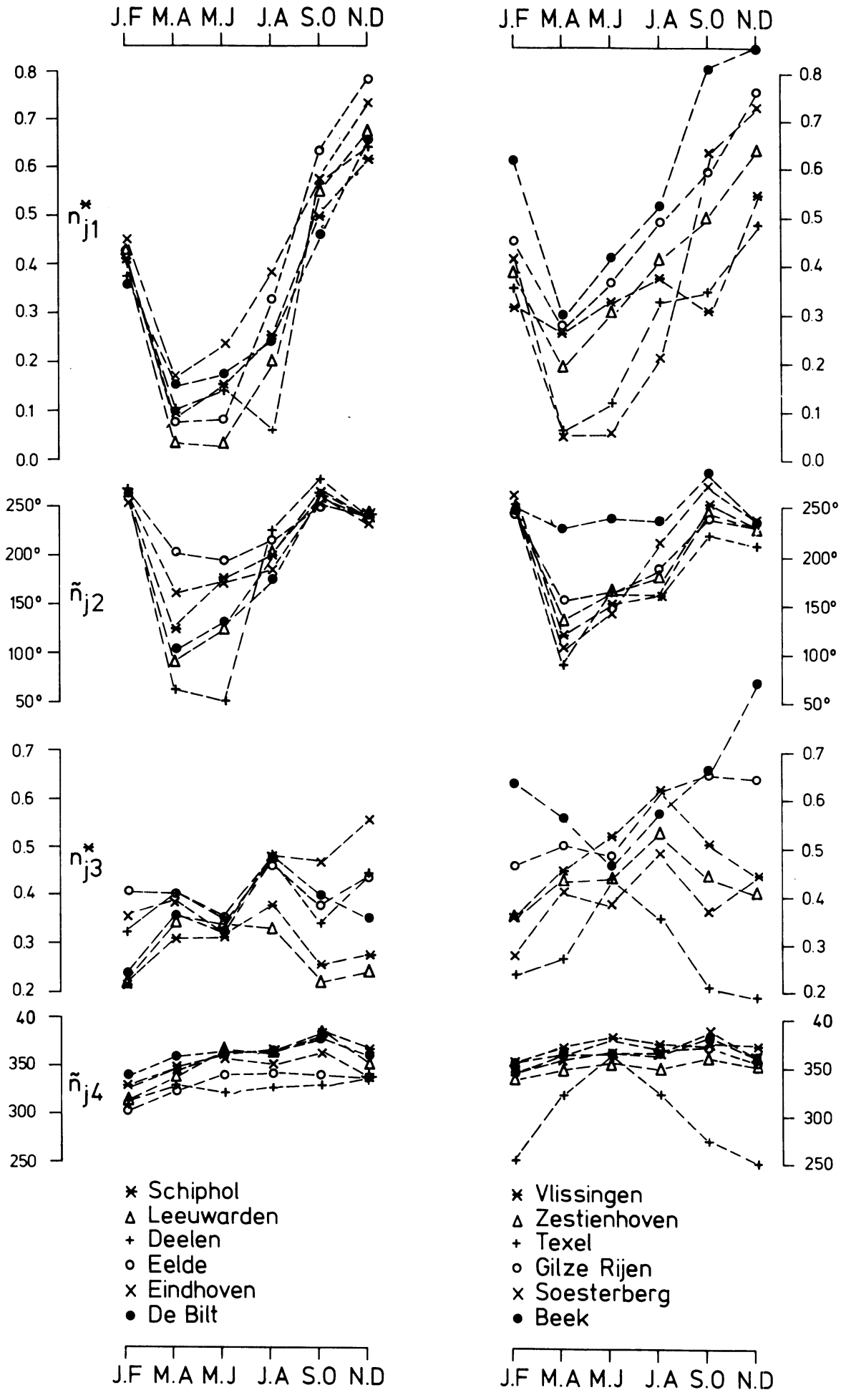


Fig. 6.5 Harmonic analysis parameters for the model parameter n.

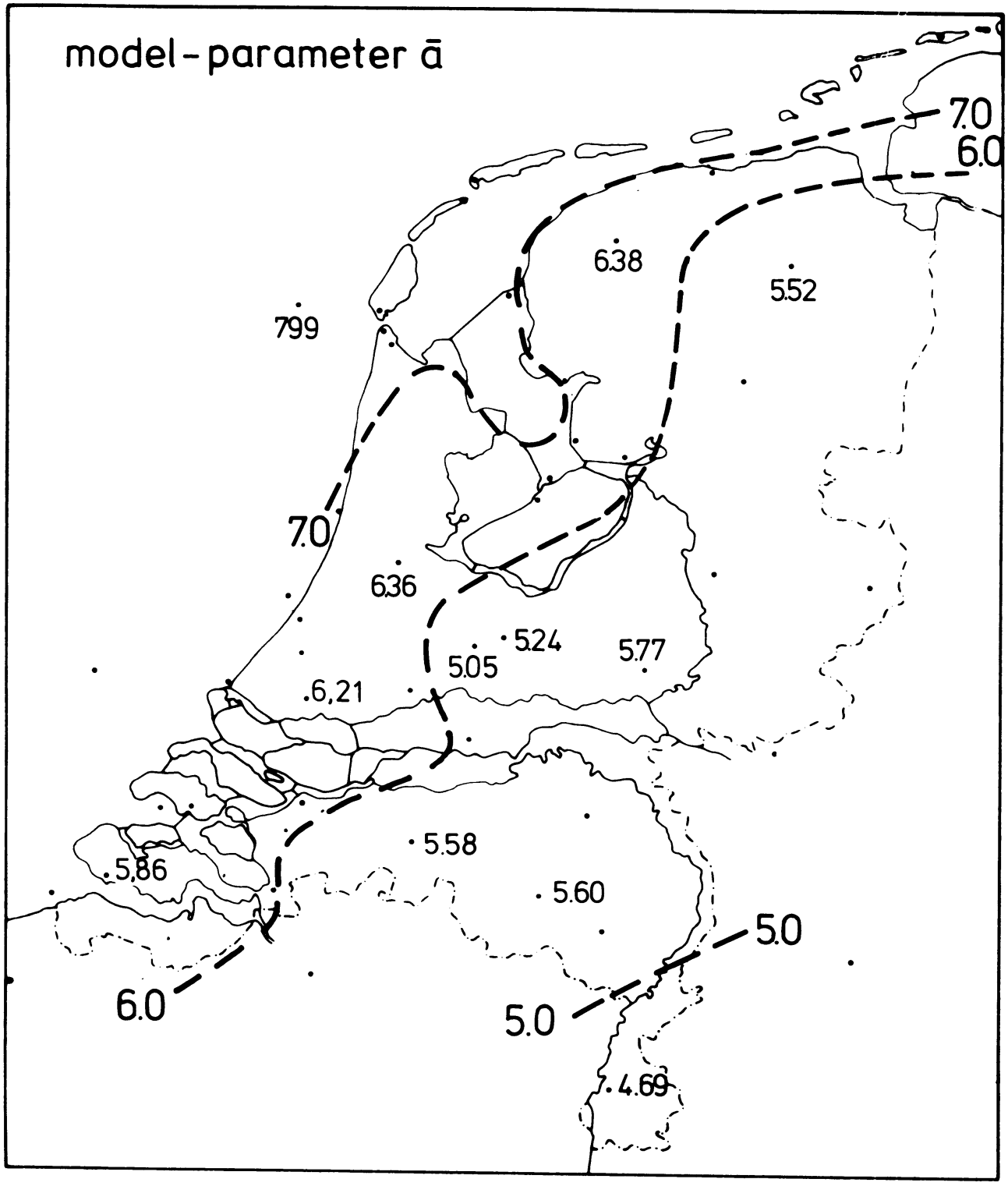


Fig. 7.1 Variation over the Netherlands of model parameter $\bar{a}$ .

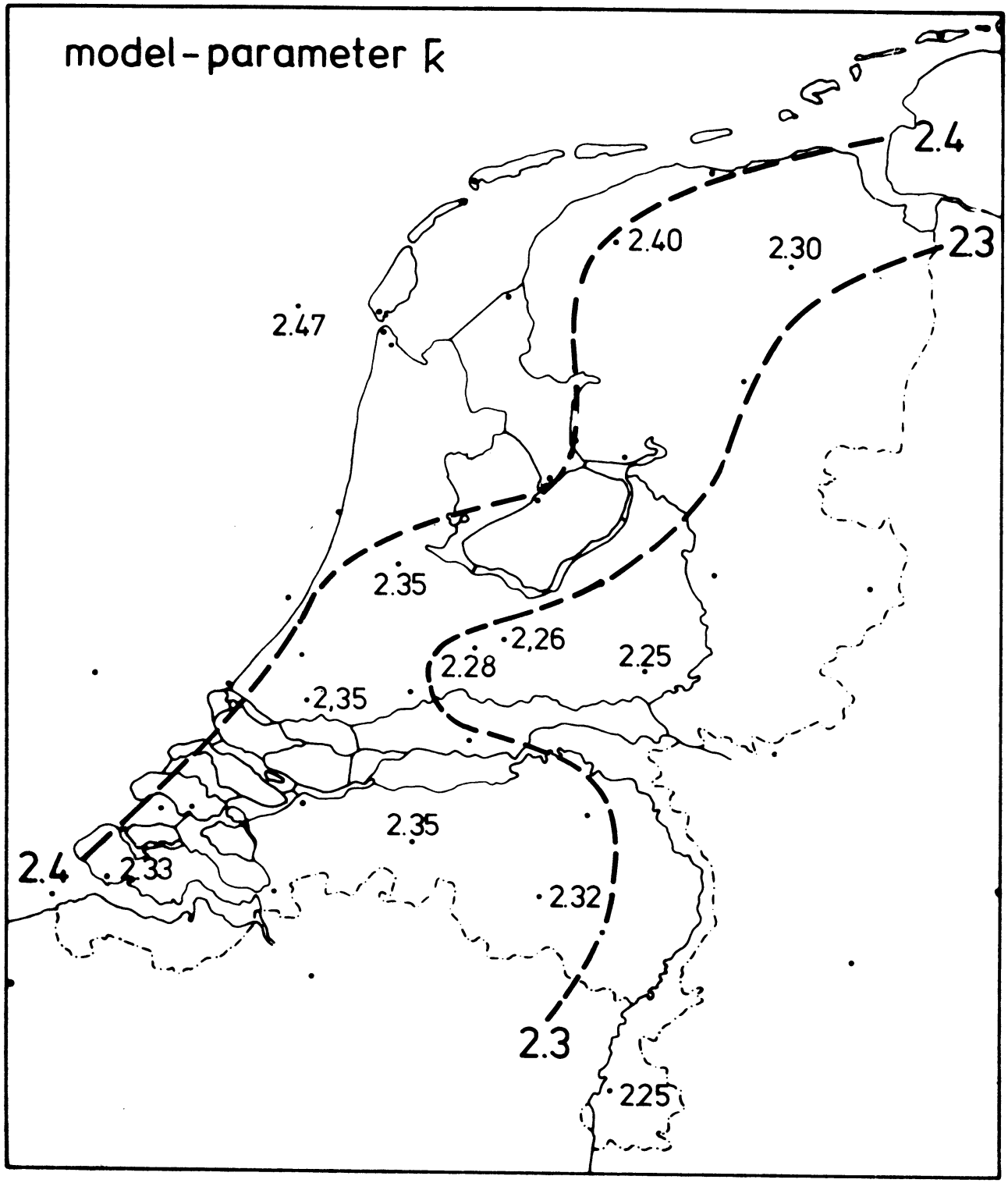


Fig. 7.2 Variation over the Netherlands of model parameter $\overline{k}$ .

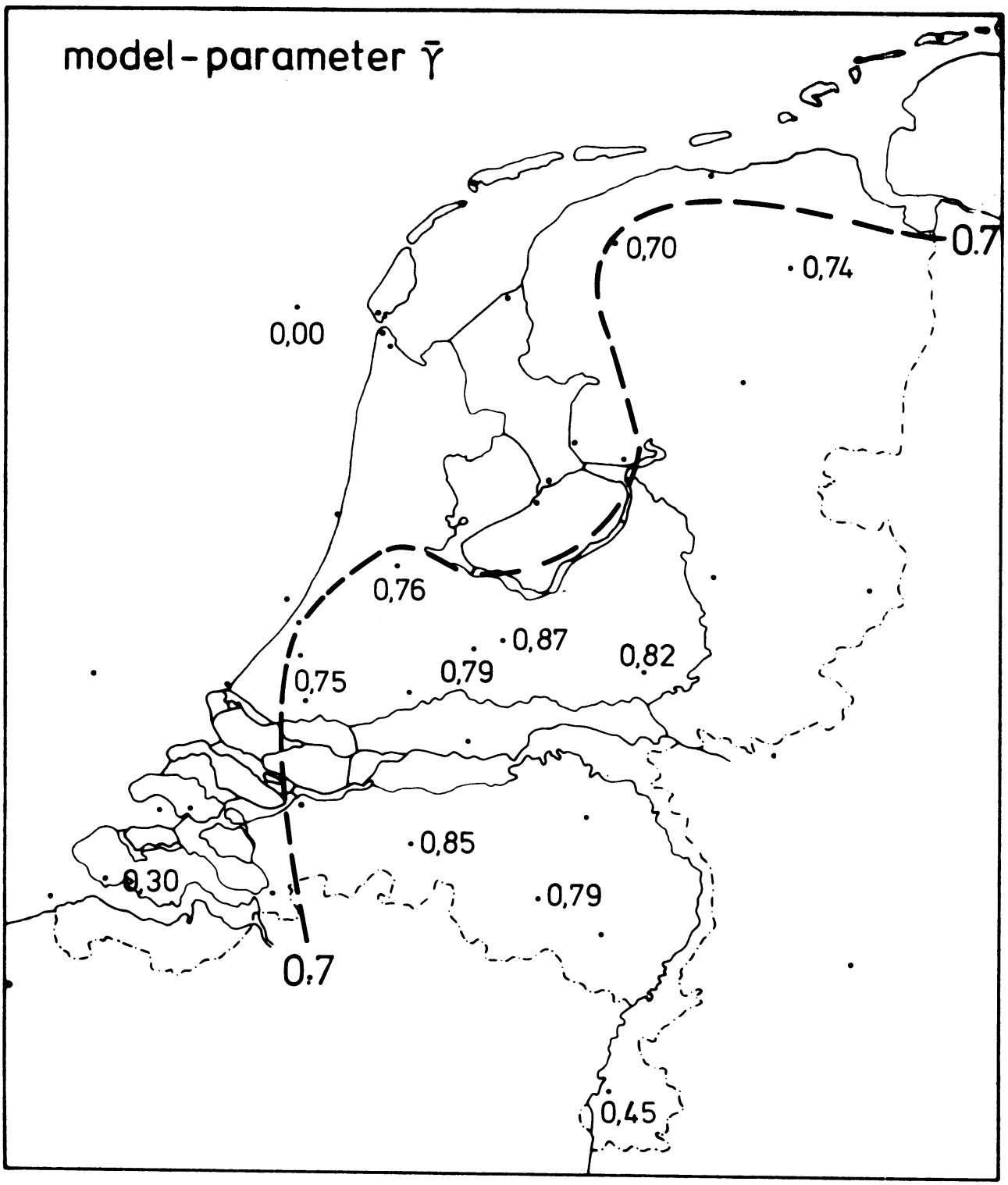


Fig. 7.3 Variation over the Netherlands of model parameter $\bar{\gamma}$ .

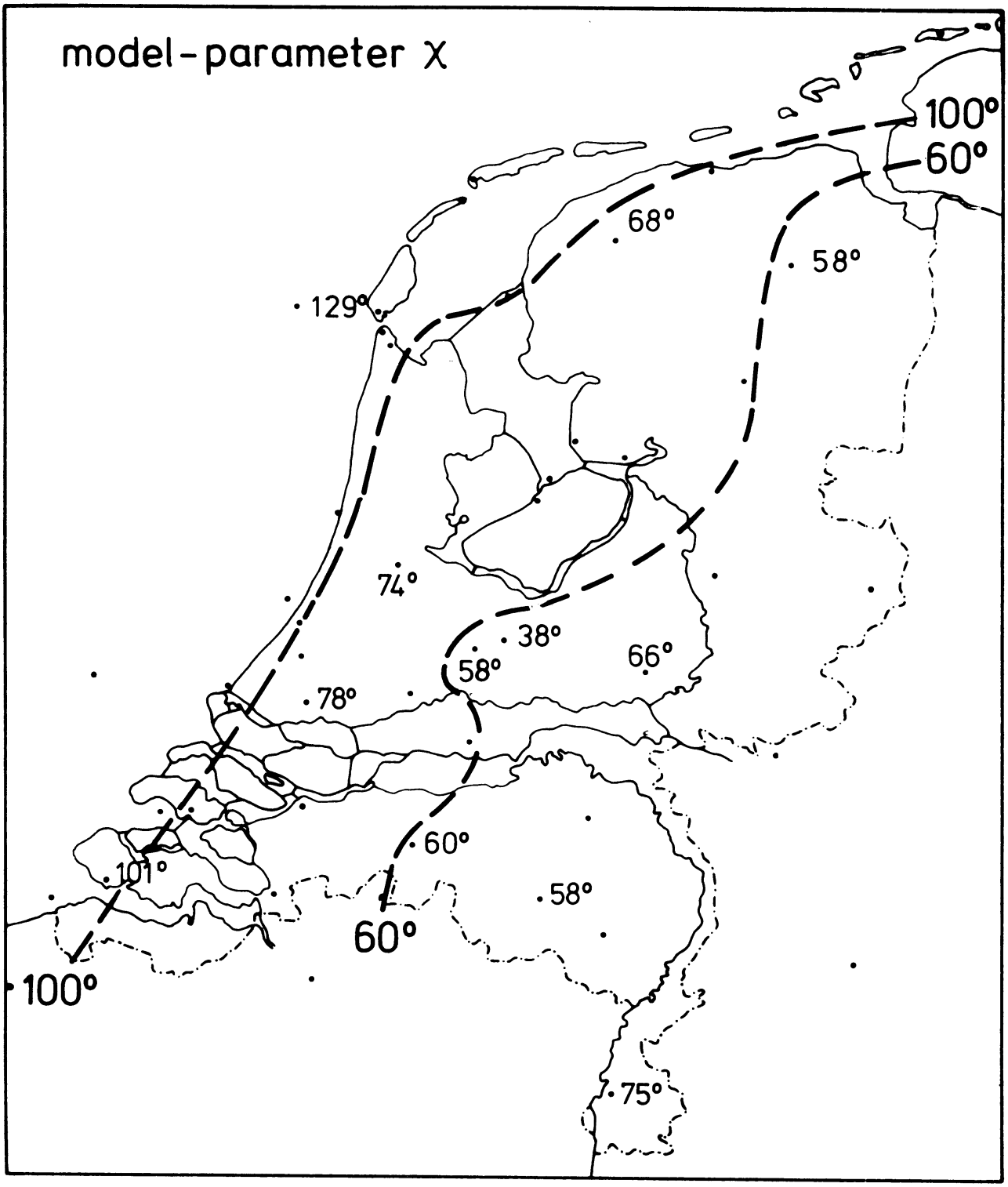


Fig. 7.4 Variation over the Netherlands of model parameter $\chi$ .

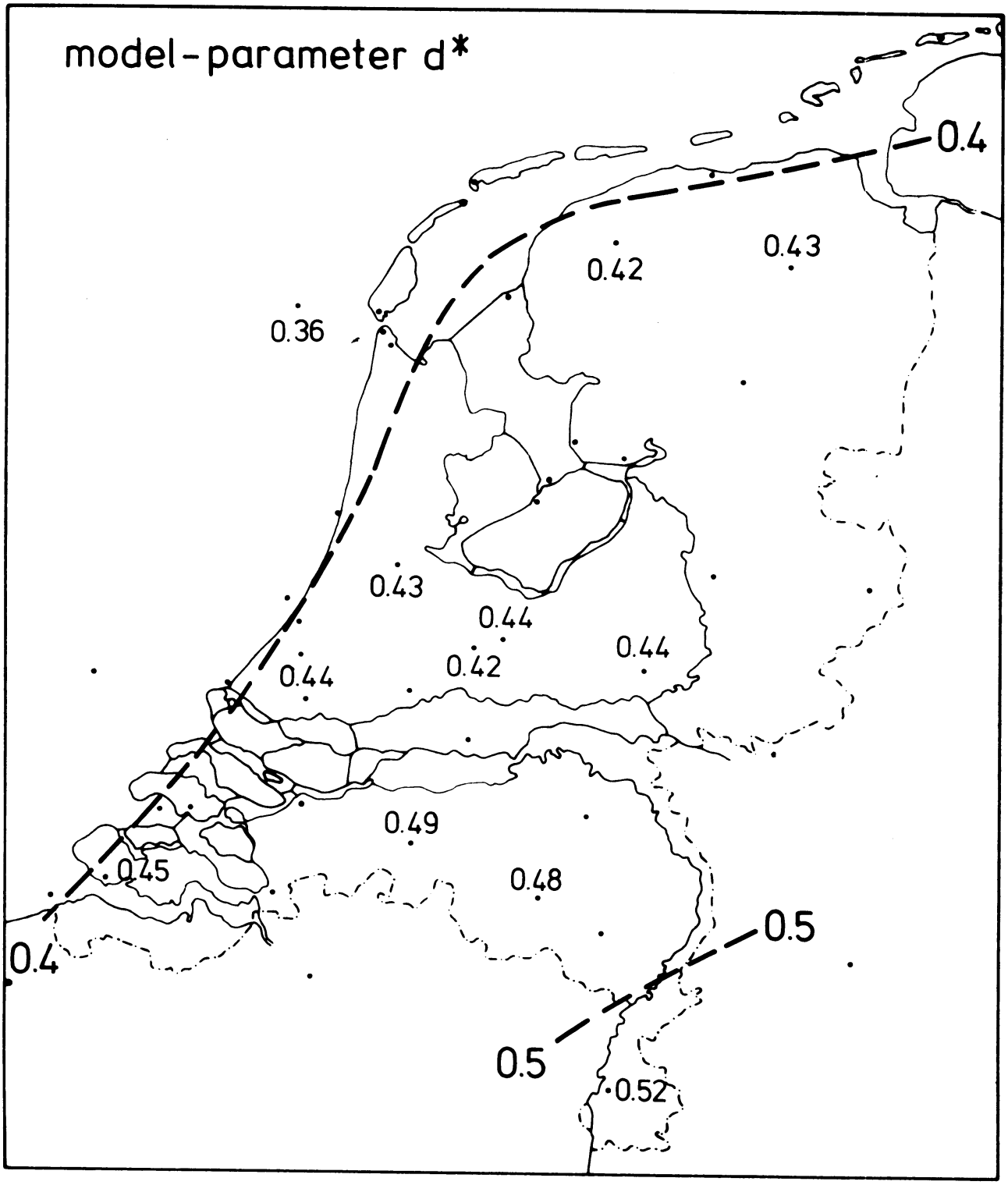


Fig. 7.5 Variation over the Netherlands of model parameter $d^*$ .

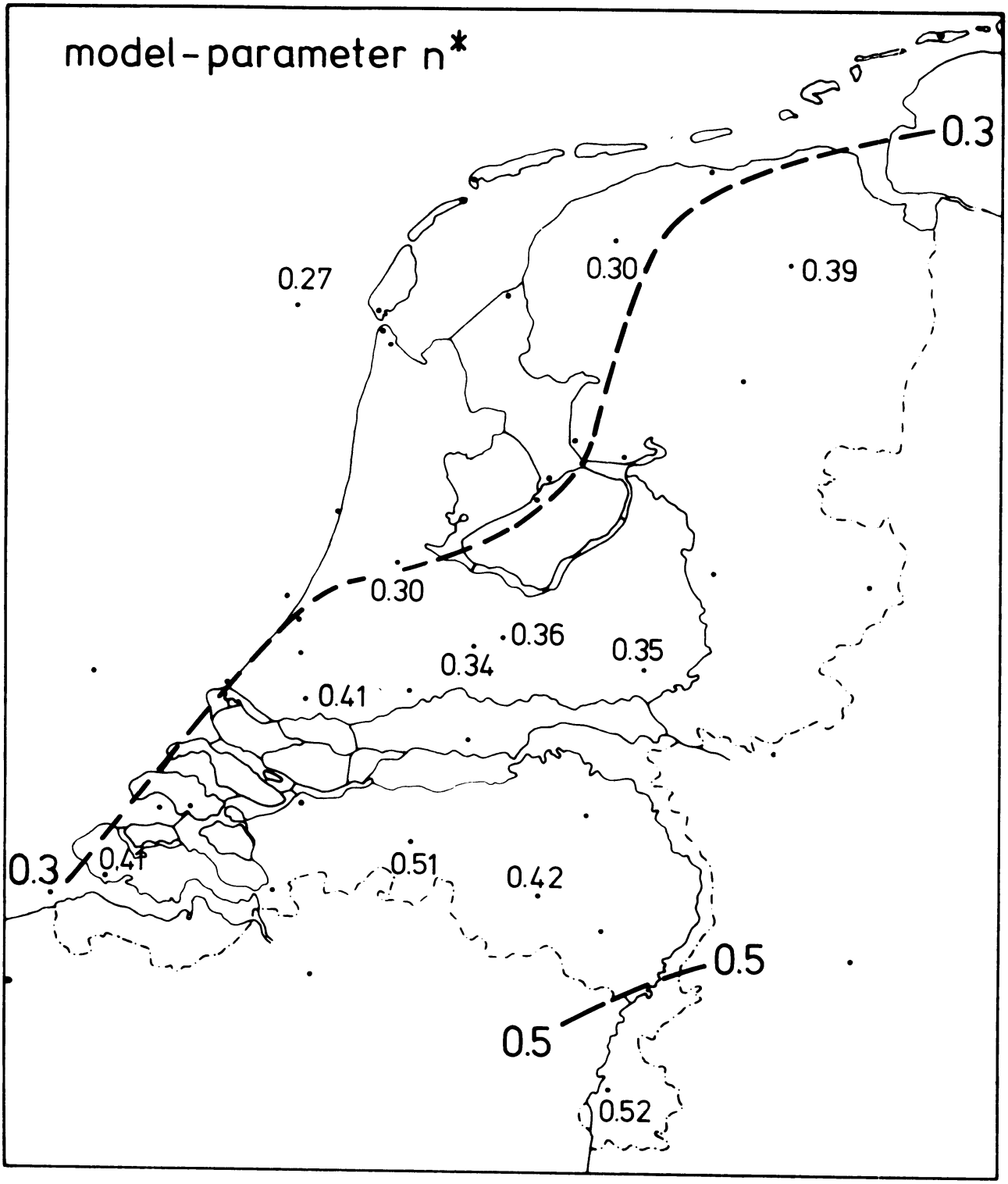


Fig. 7.6 Variation over the Netherlands of model parameter $n^*$ .

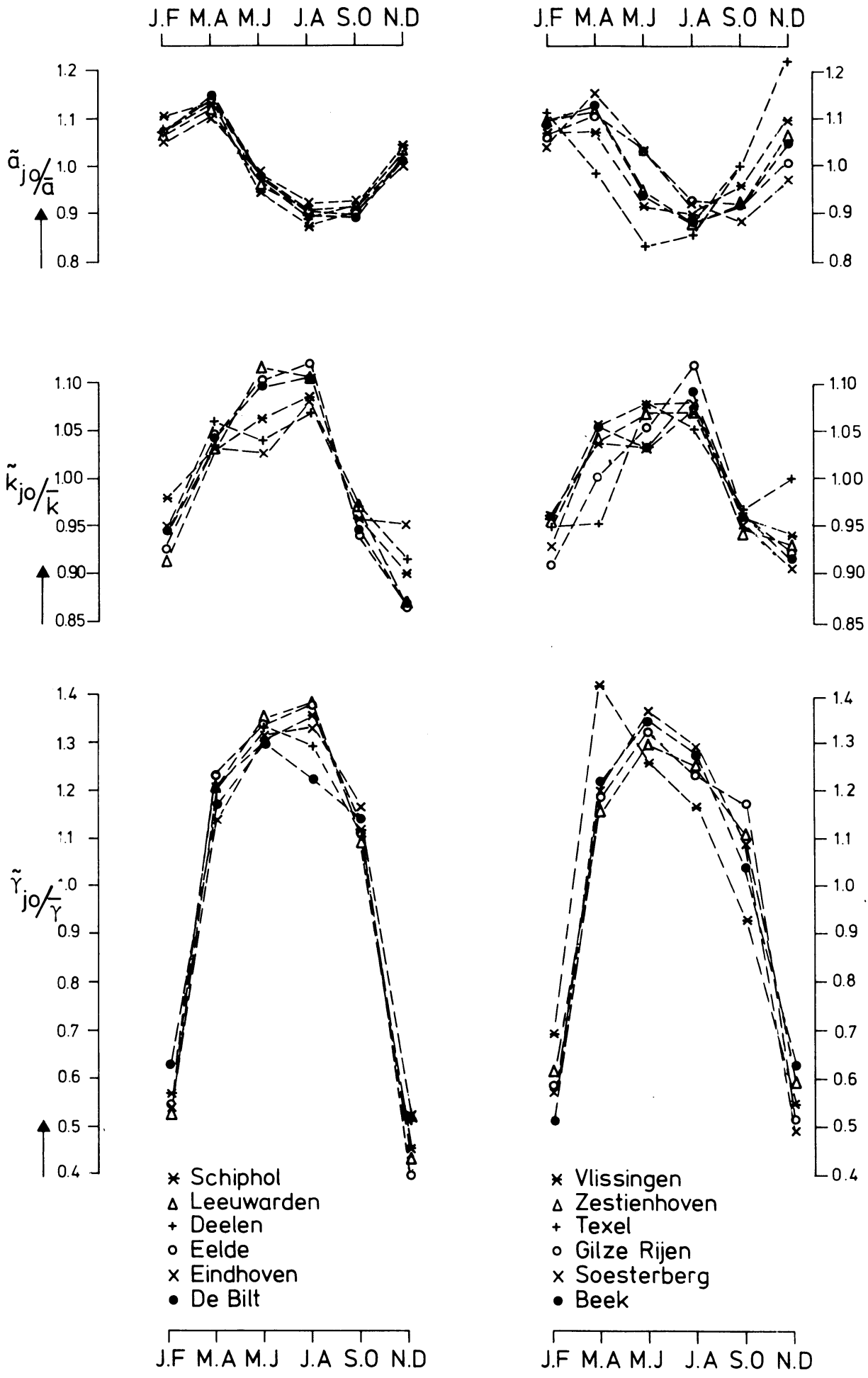


Fig. 8 Variations of the ratios $\hat{a}_{j0}/\bar{a}$, $\hat{k}_{j0}/\bar{k}$ and $\hat{\gamma}_{j0}/\bar{\gamma}$.

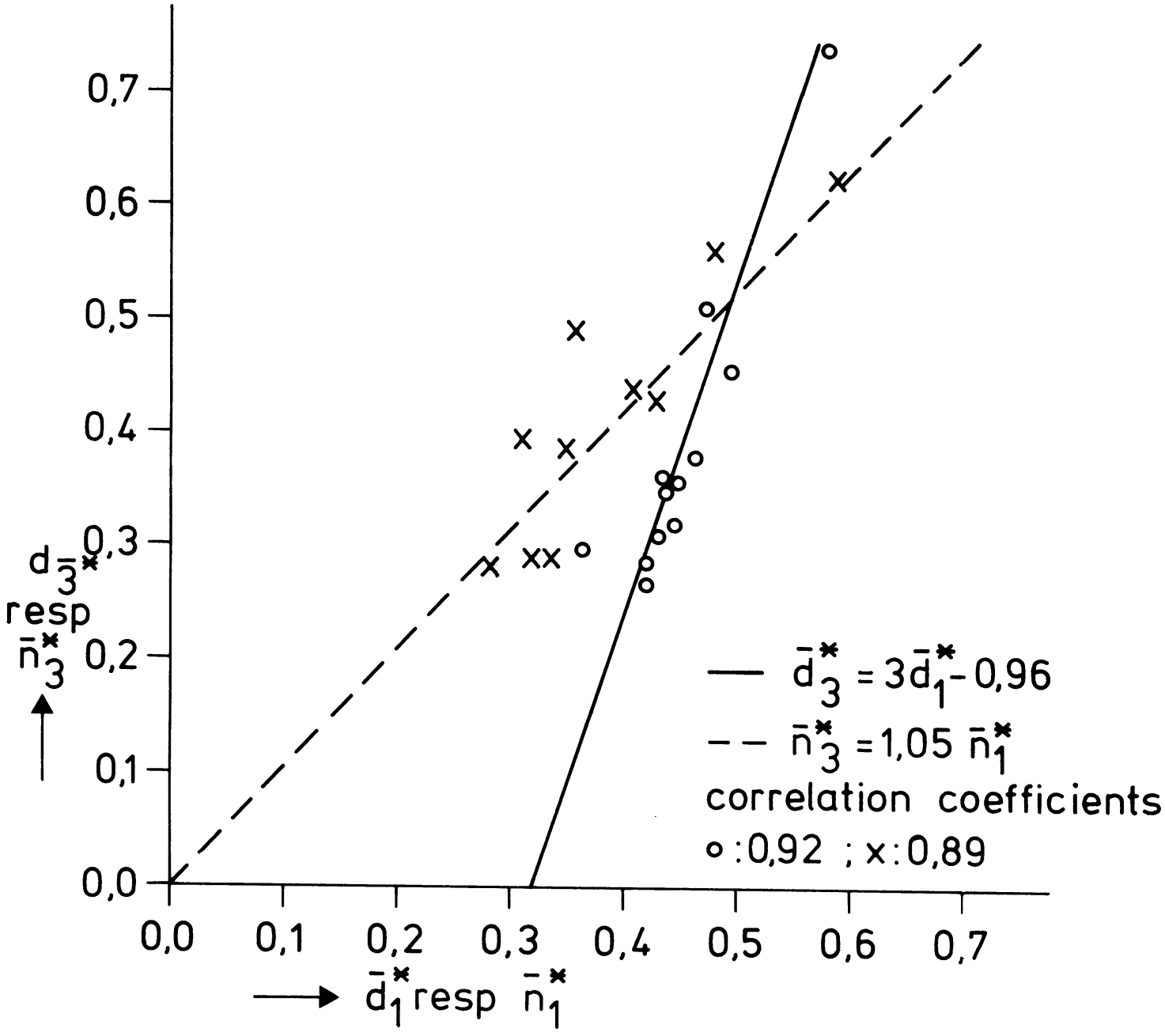


Fig. 9 Relation between the amplitude of first and second harmonic from harmonic analysis of the daytime and nighttime wind direction frequencies.

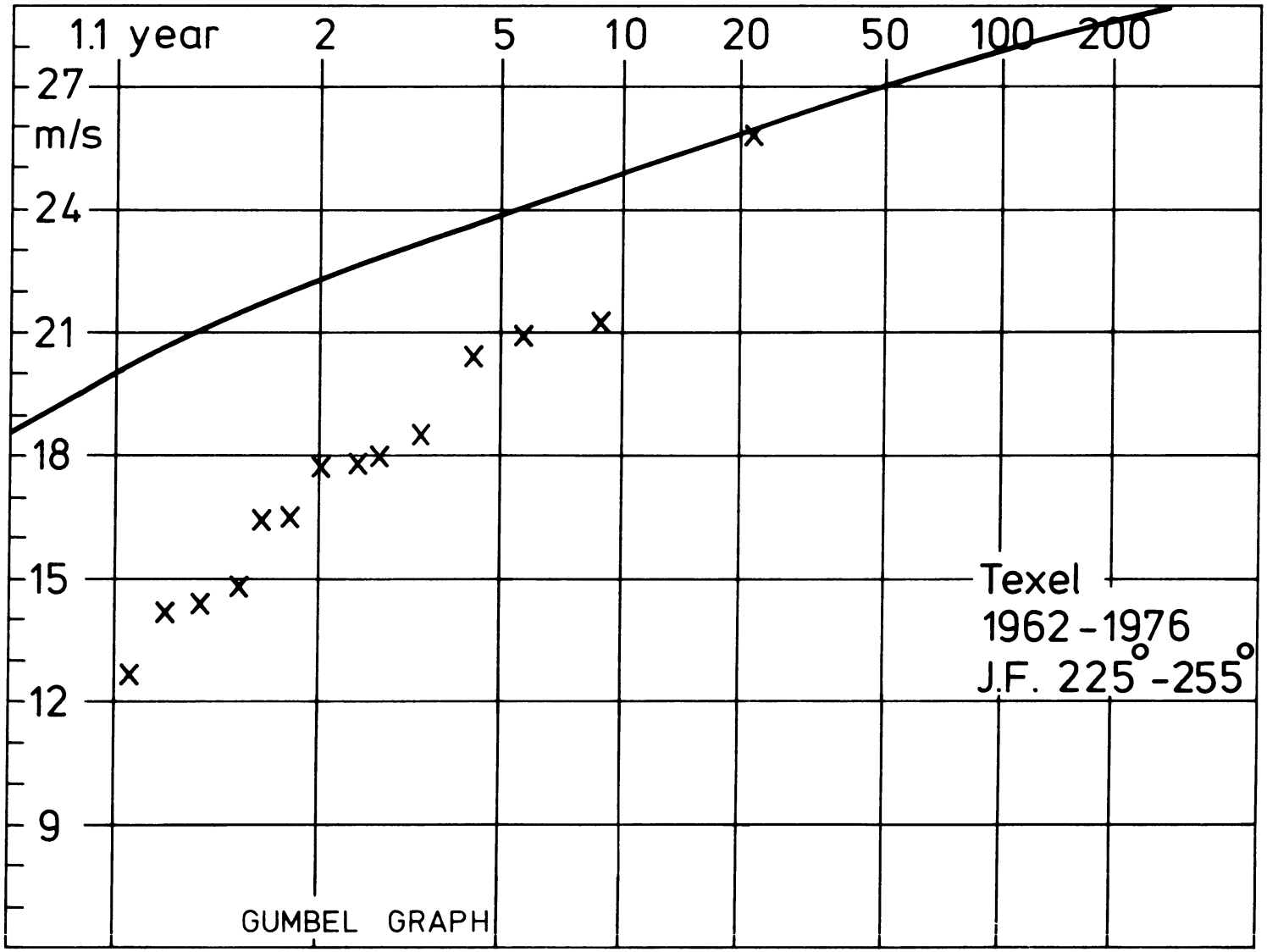


Fig. 10.1 Annual maximum hour-averaged wind speeds for Southwesterly winds at Texel, and extreme value curve obtained from the model without persistence (q = 1).

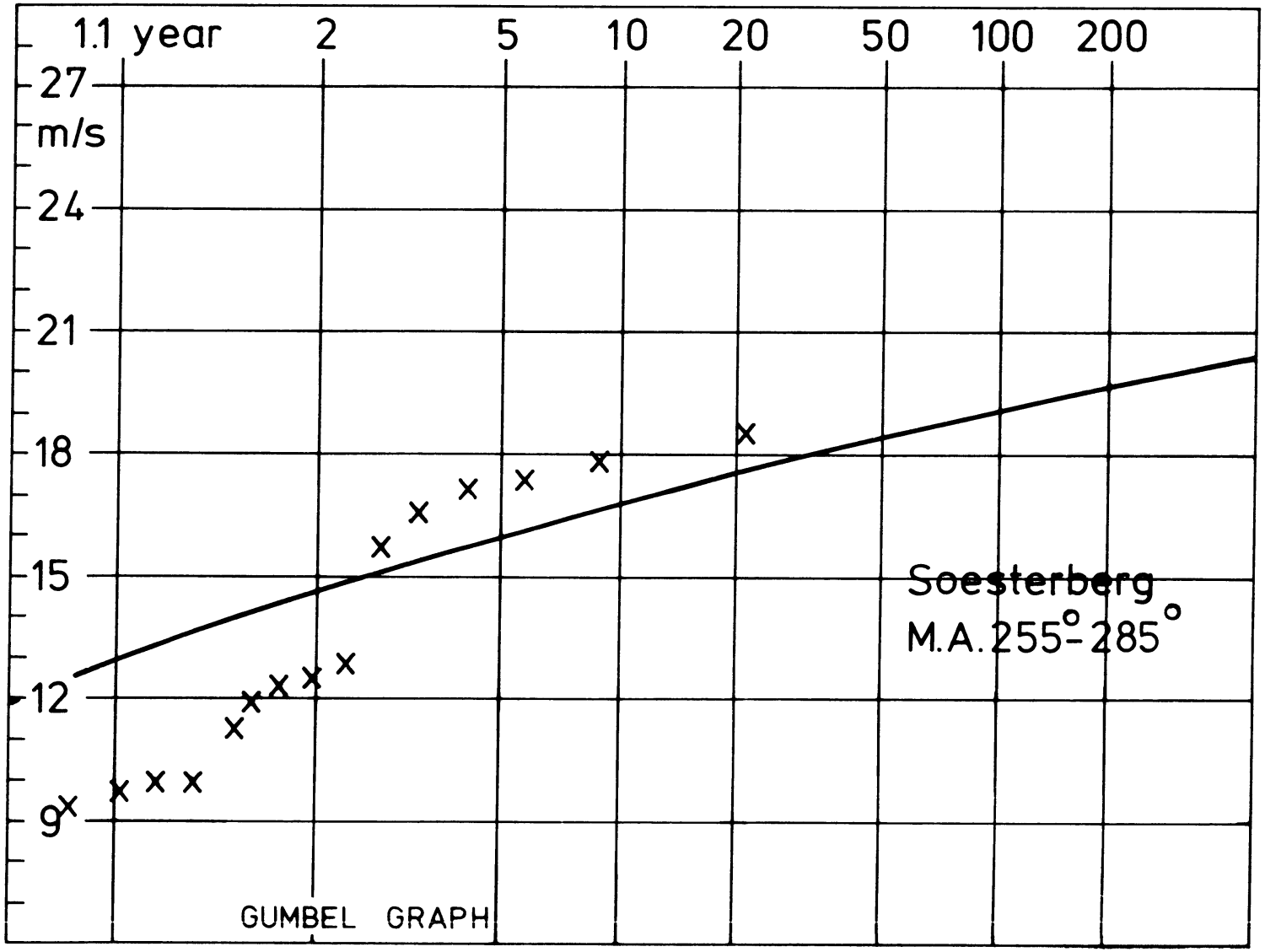


Fig. 10.2 Annual maximum hour-averaged wind speeds for Westerly winds at Soesterberg, and extreme value curve obtained from the model without persistence (q = 1).

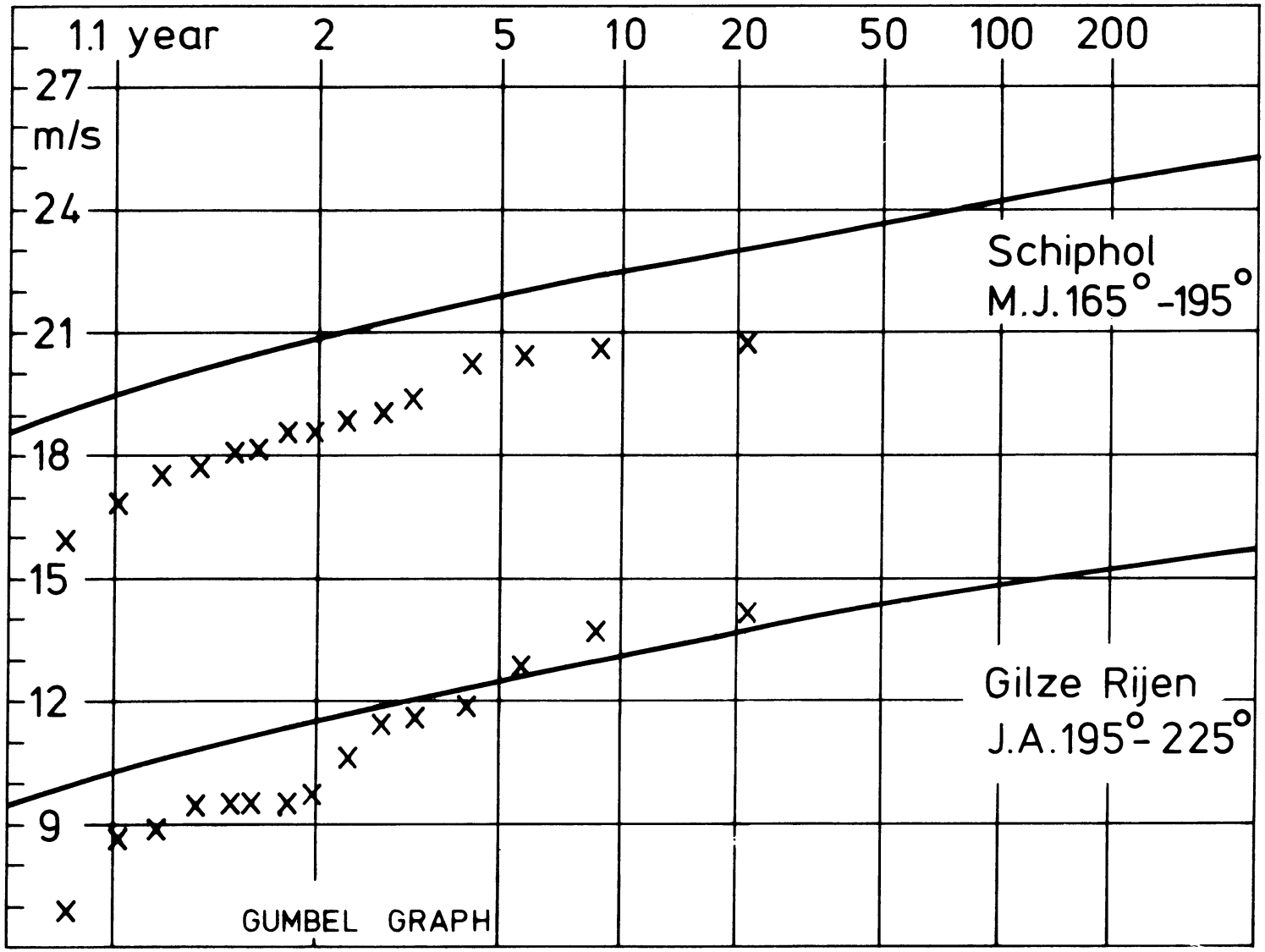


Fig. 10.3 Annual maximum hour-averaged wind speeds for Southerly winds at Schiphol and for Southwesterly winds at Gilze Rijen, and extreme value curves obtained from the model without persistence (q = 1).

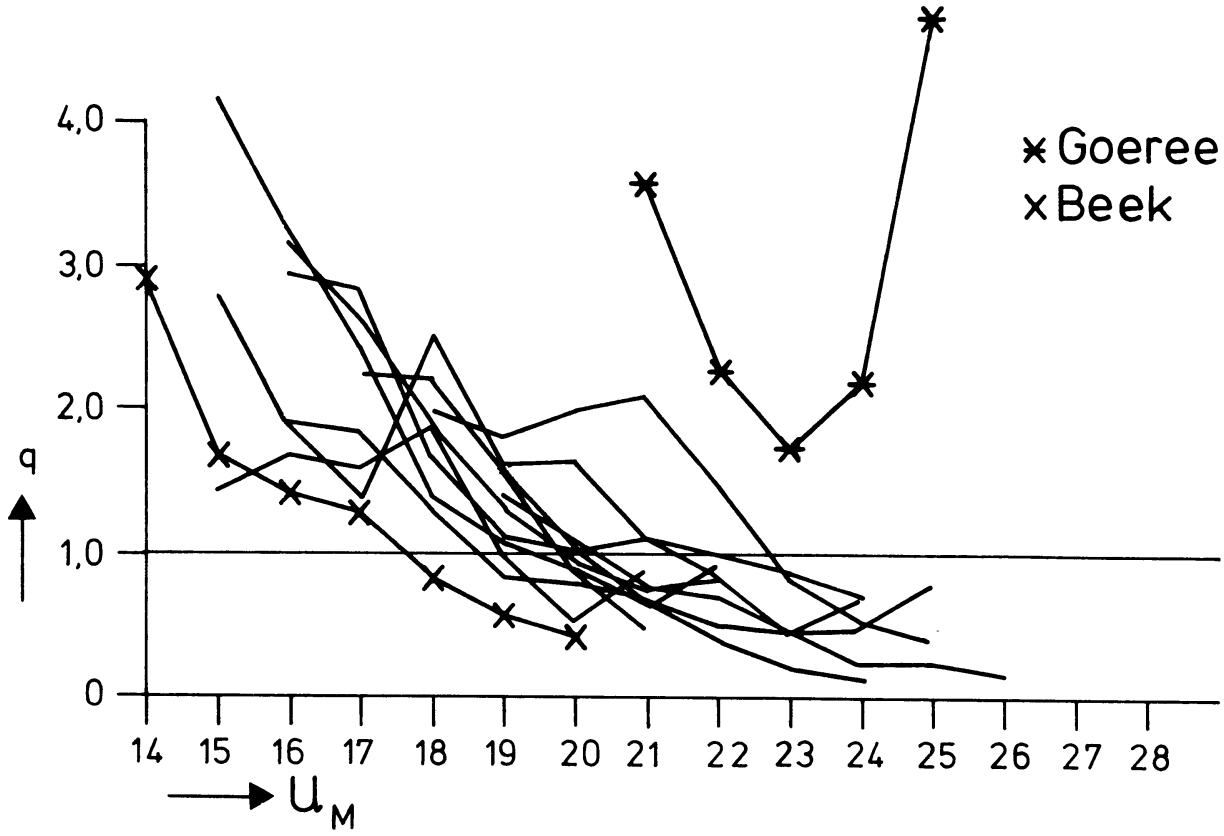


Fig. 11.1 Persistence correction factor q as a function of $U_M$.

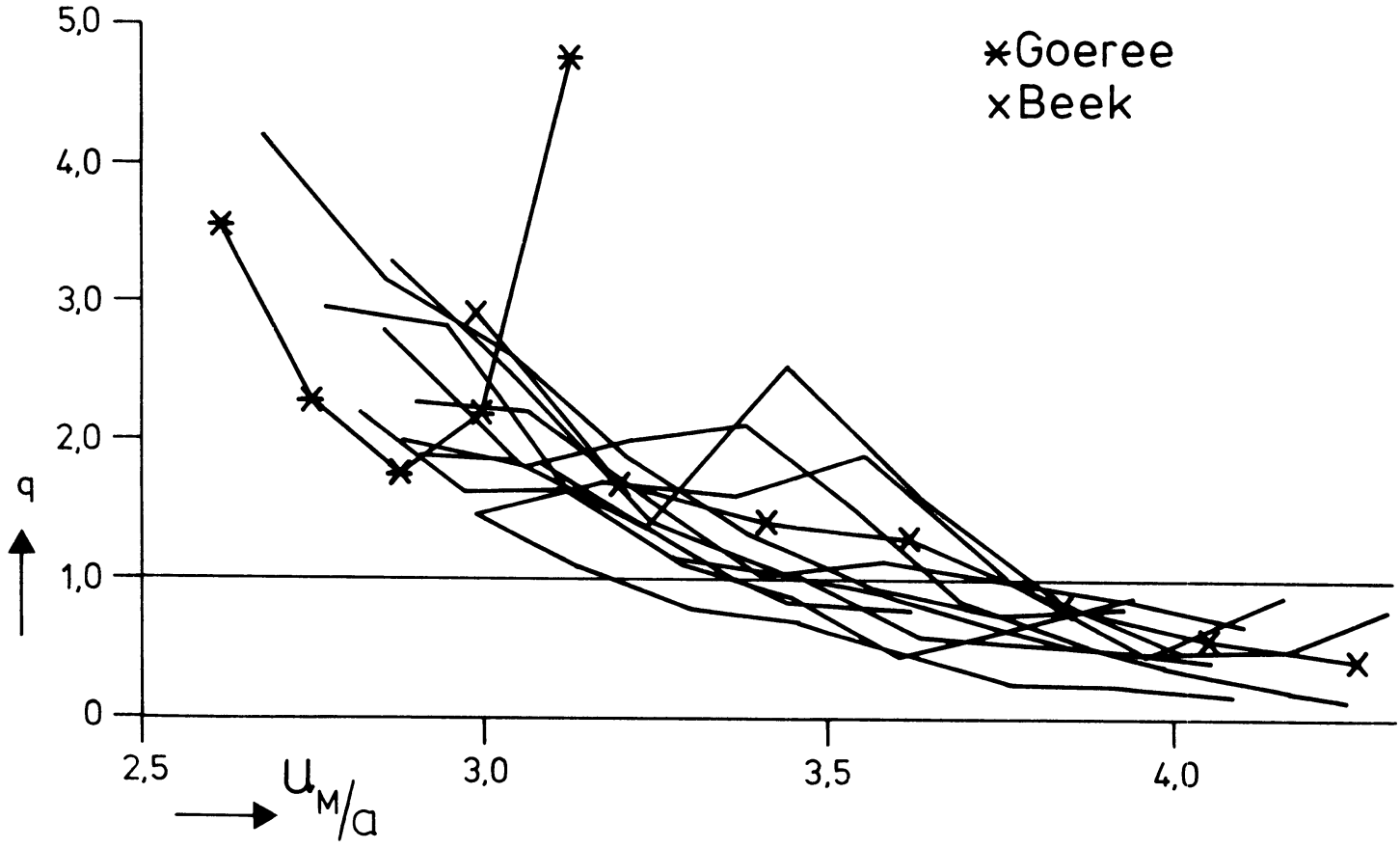


Fig. 11.2 Persistence correction factor q as a function of $U_M/a$.

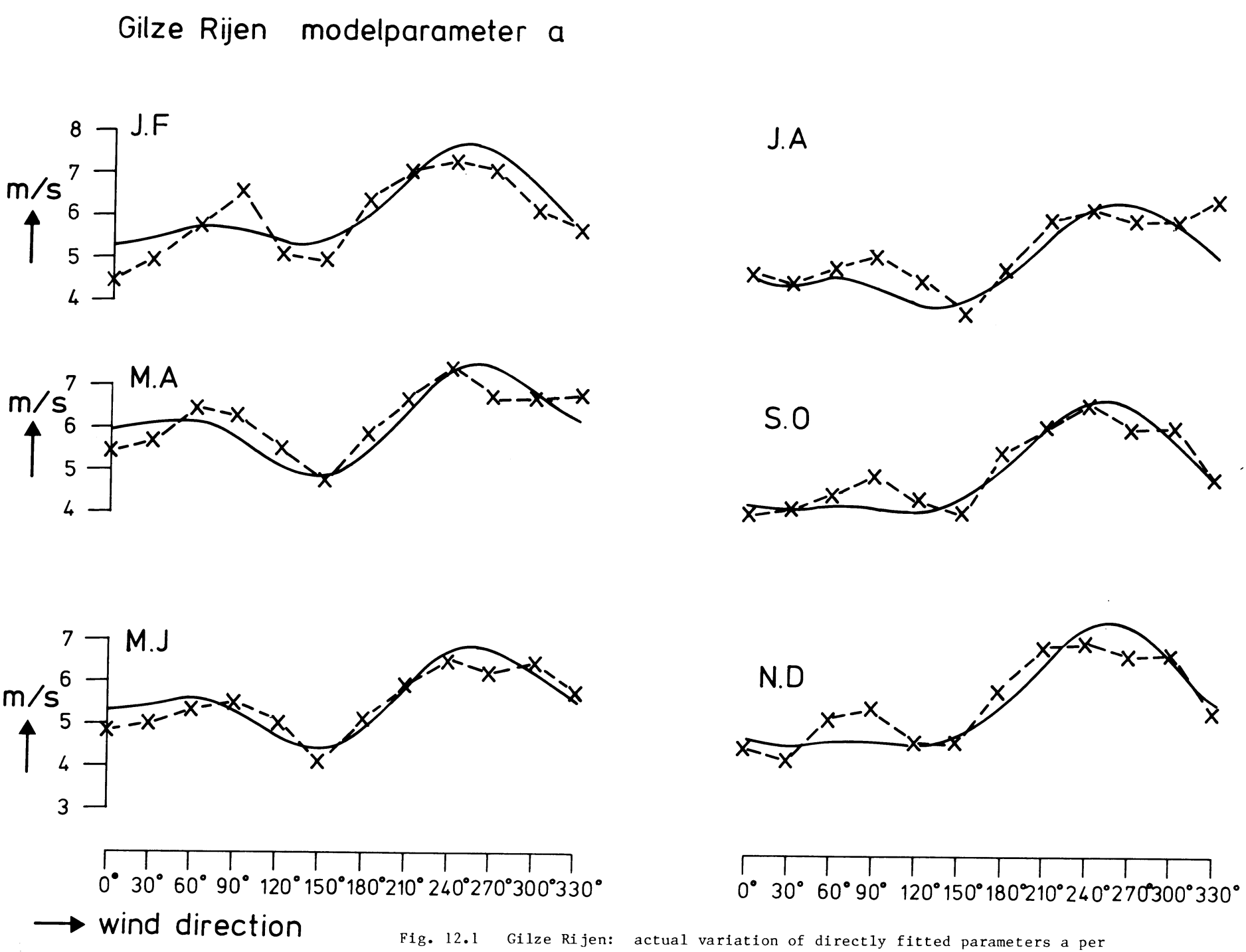


Fig. 12.1 Gilze Rijen: actual variation of directly fitted parameters a per season, compared with the parameter curve obtained from the model after smoothing by harmonic analysis.

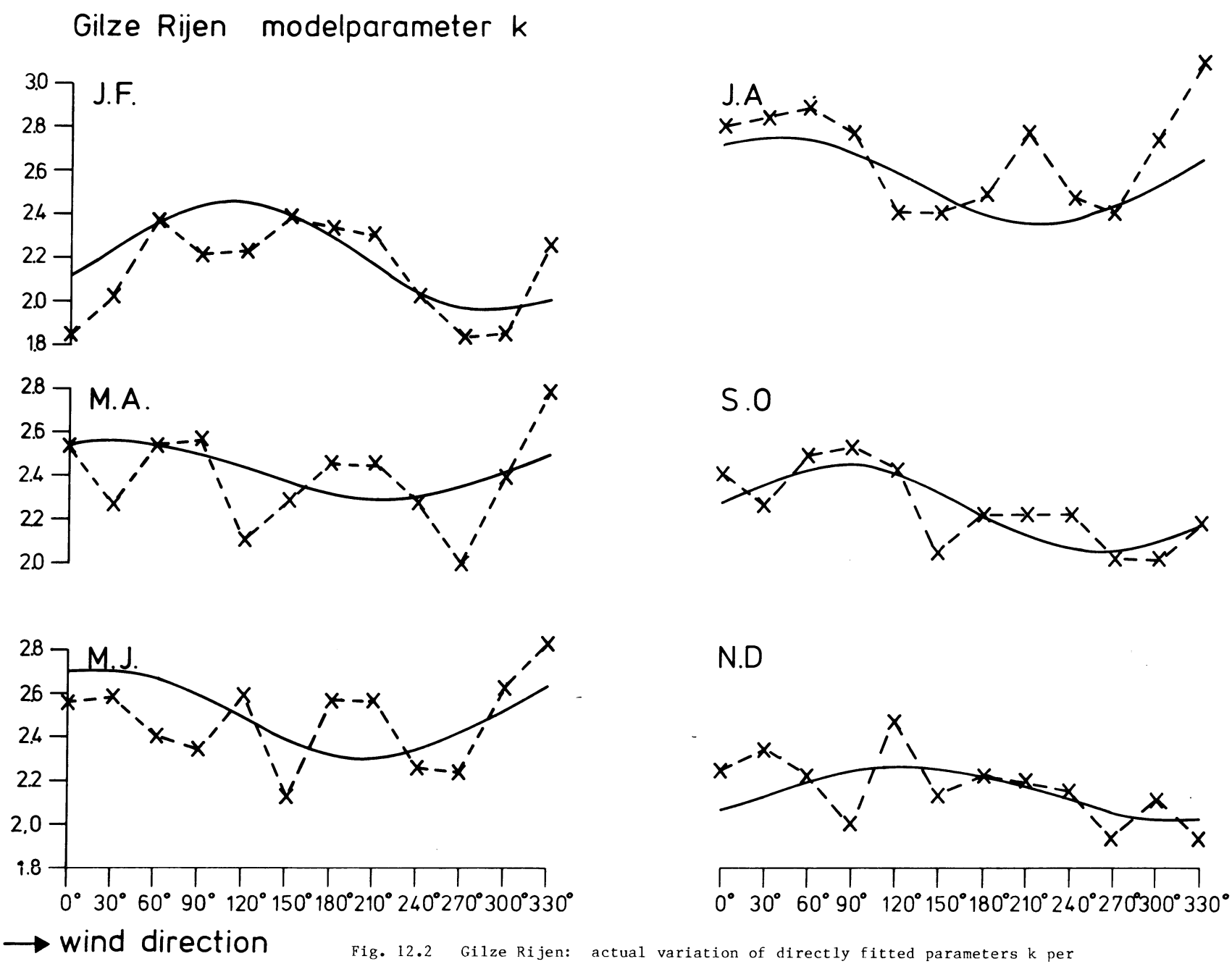


Fig. 12.2 Gilze Rijen: actual variation of directly fitted parameters k per season, compared with the parameter curve obtained from the model after smoothing by harmonic analysis.

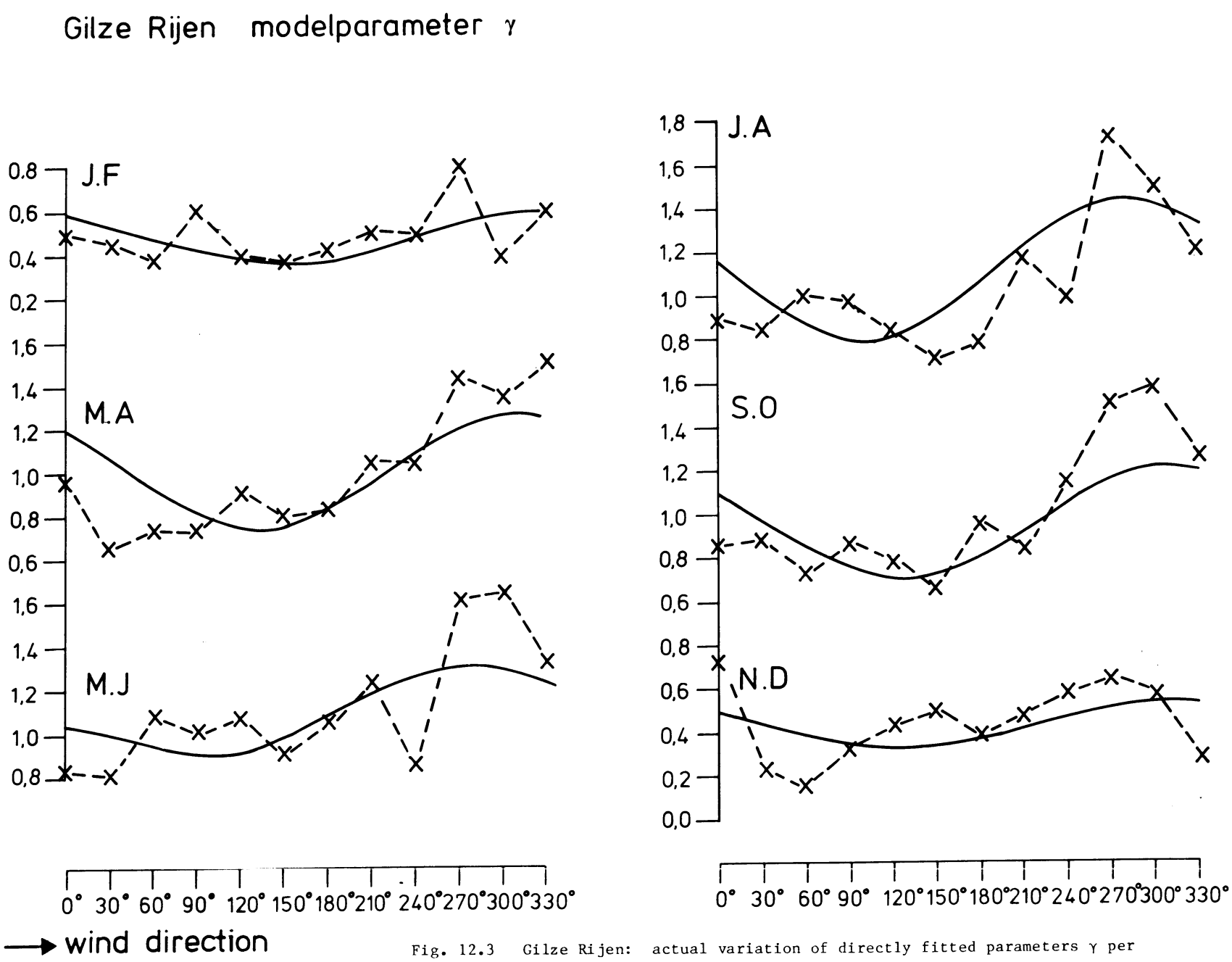


Fig. 12.3 Gilze Rijen: actual variation of directly fitted parameters γ per season, compared with the parameter curve obtained from the model after smoothing by harmonic analysis.

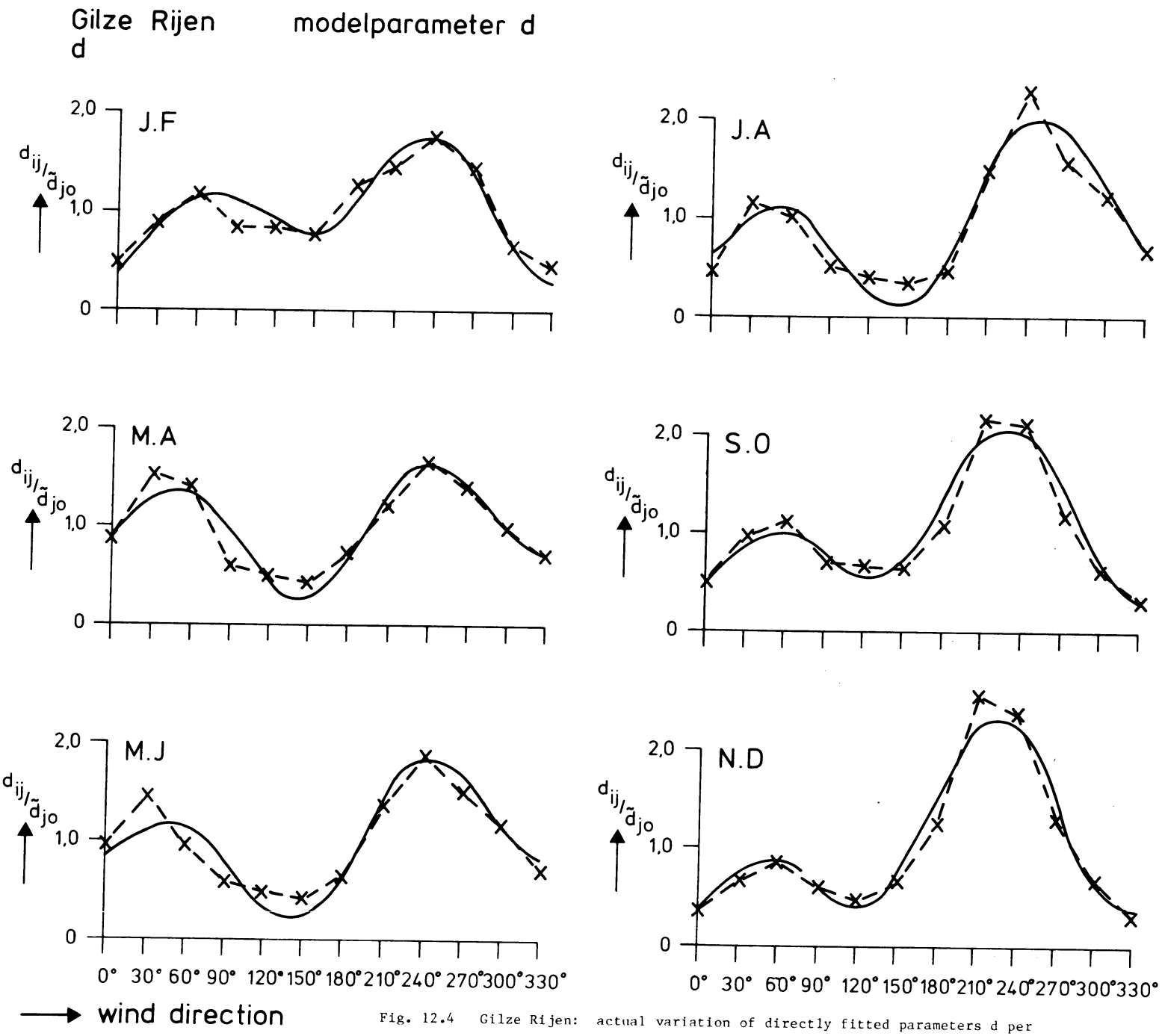


Fig. 12.4 Gilze Rijen: actual variation of directly fitted parameters d per season, compared with the parameter curve obtained from the model after smoothing by harmonic analysis.

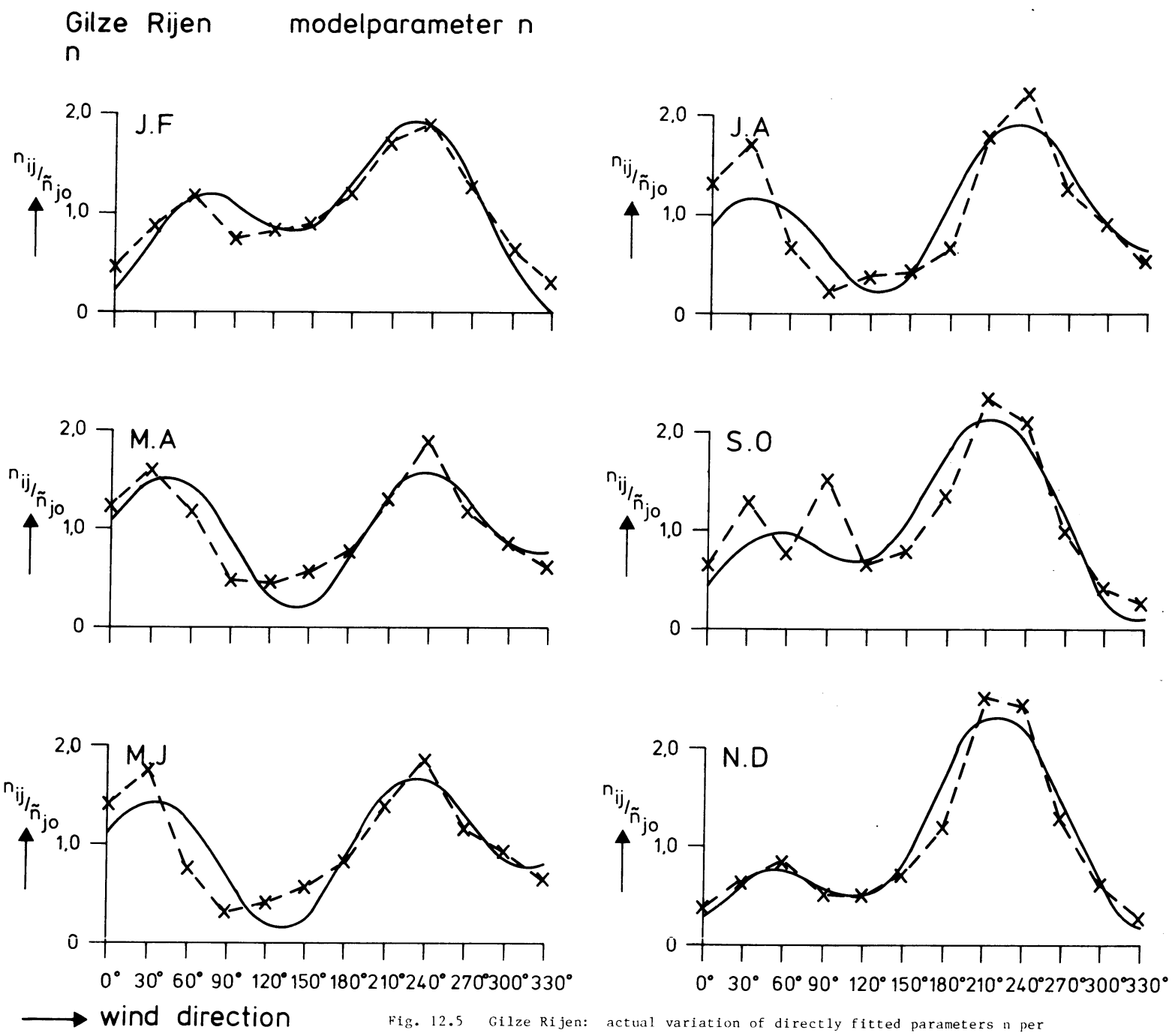


Fig. 12.5 Gilze Rijen: actual variation of directly fitted parameters n per season, compared with the parameter curve obtained from the model after smoothing by harmonic analysis.

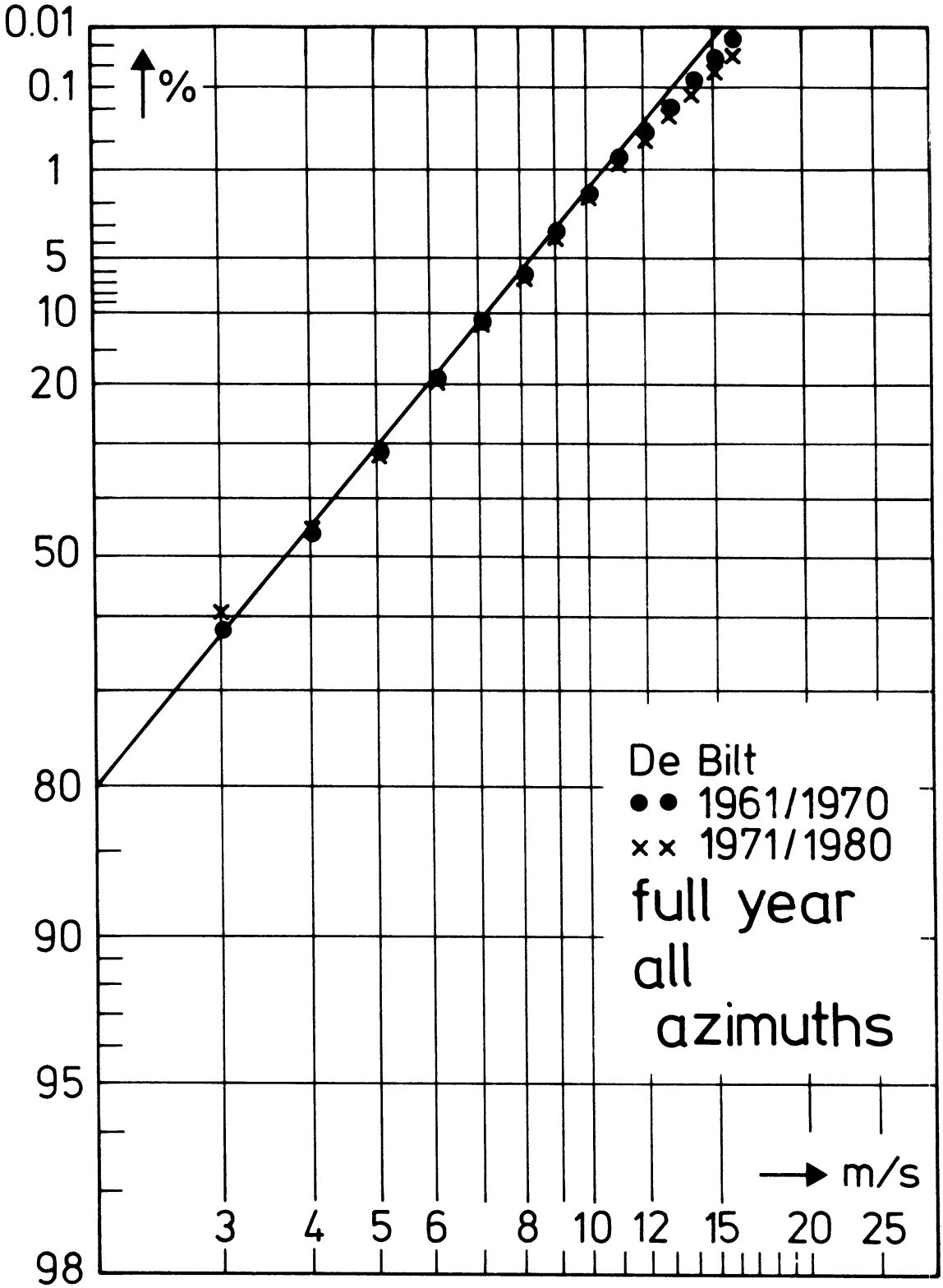


Fig. 13.1 Wind speed distribution of De Bilt from two succesive 10-year periods (full year).

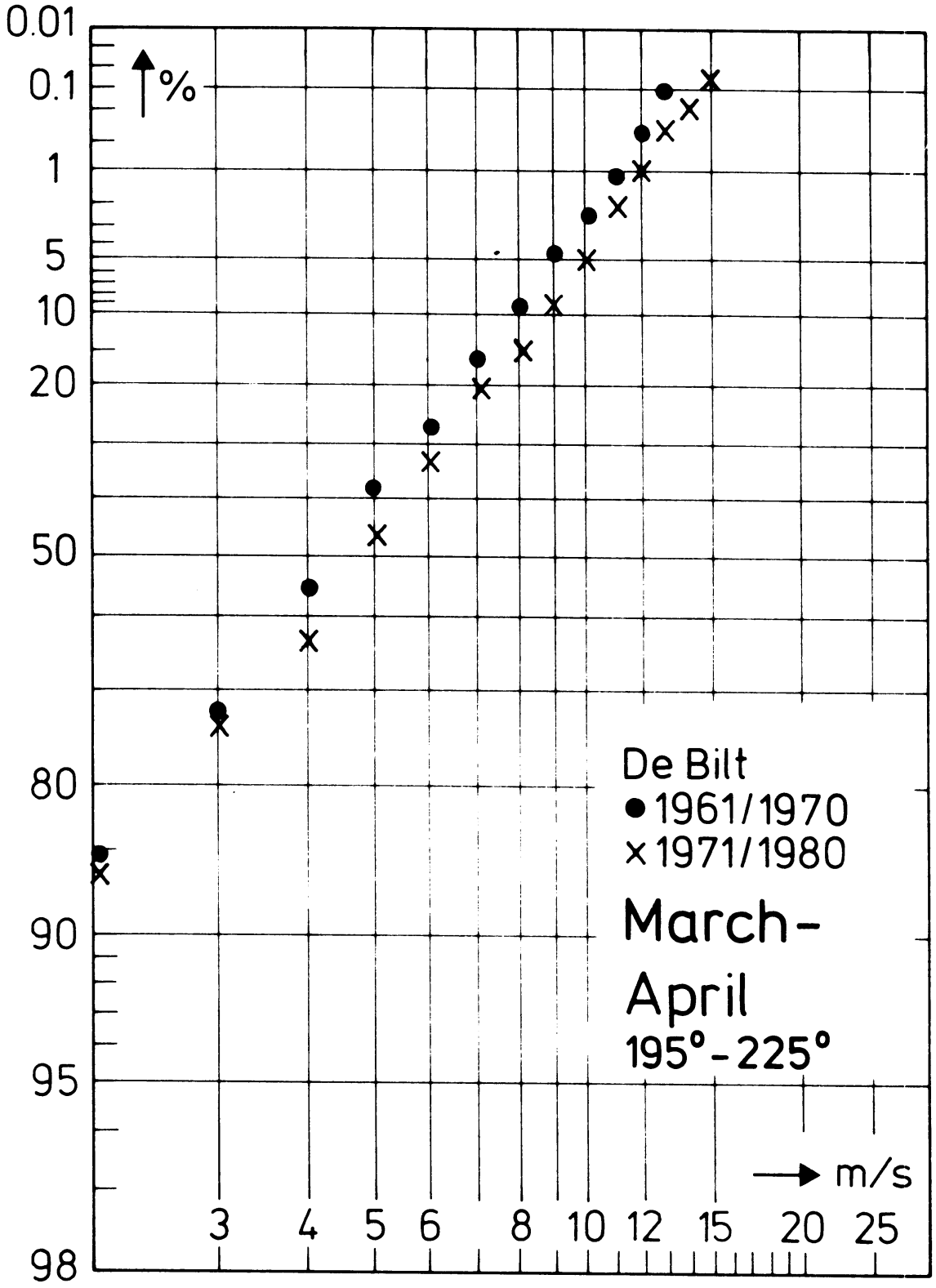


Fig. 13.2 Wind speed distribution of De Bilt from two succesive 10-year periods (March-April, 195°-225°).

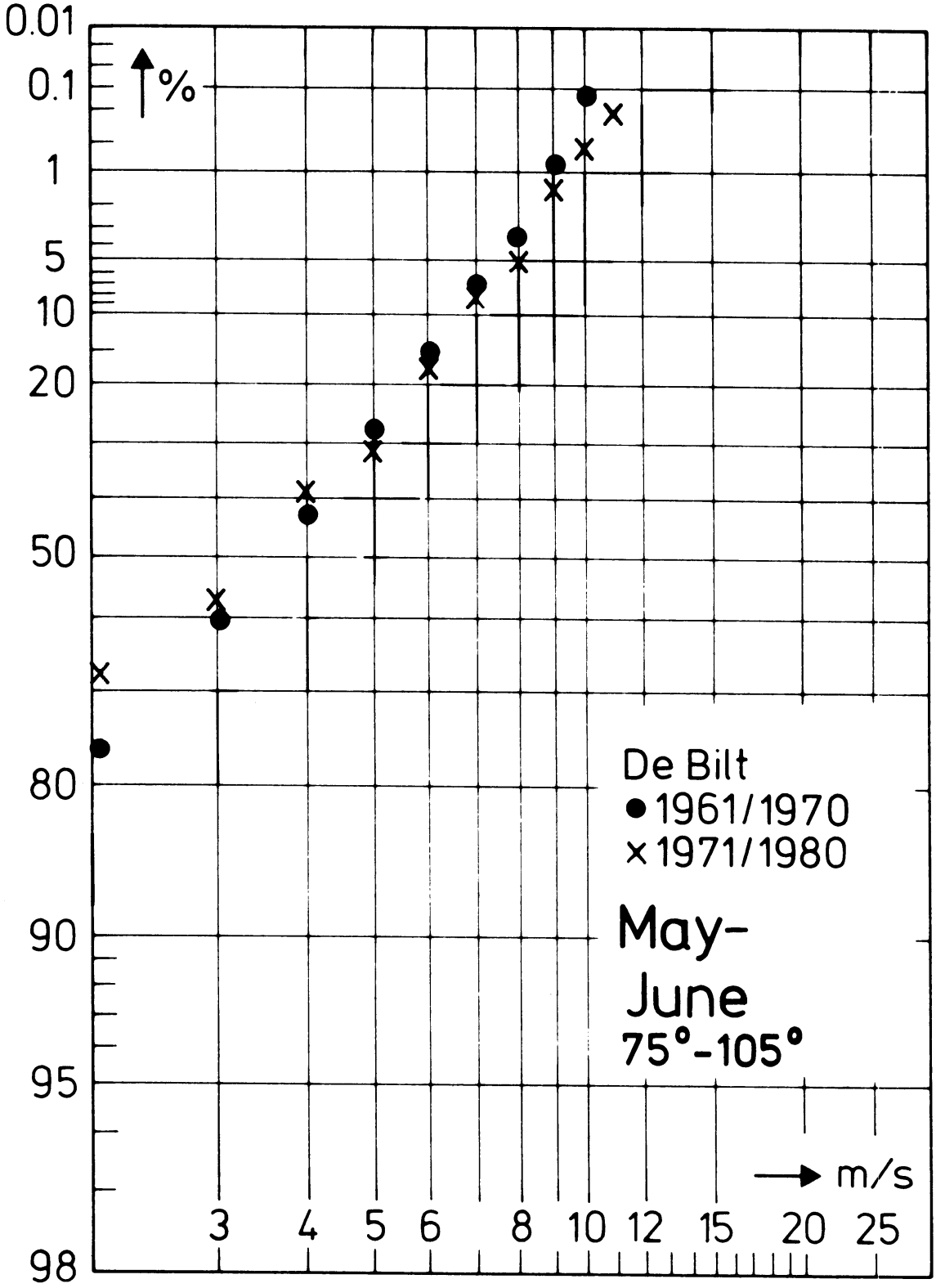


Fig. 13.3 Wind speed distribution of De Bilt from two succesive 10-year periods (May-June, 75°-105°).

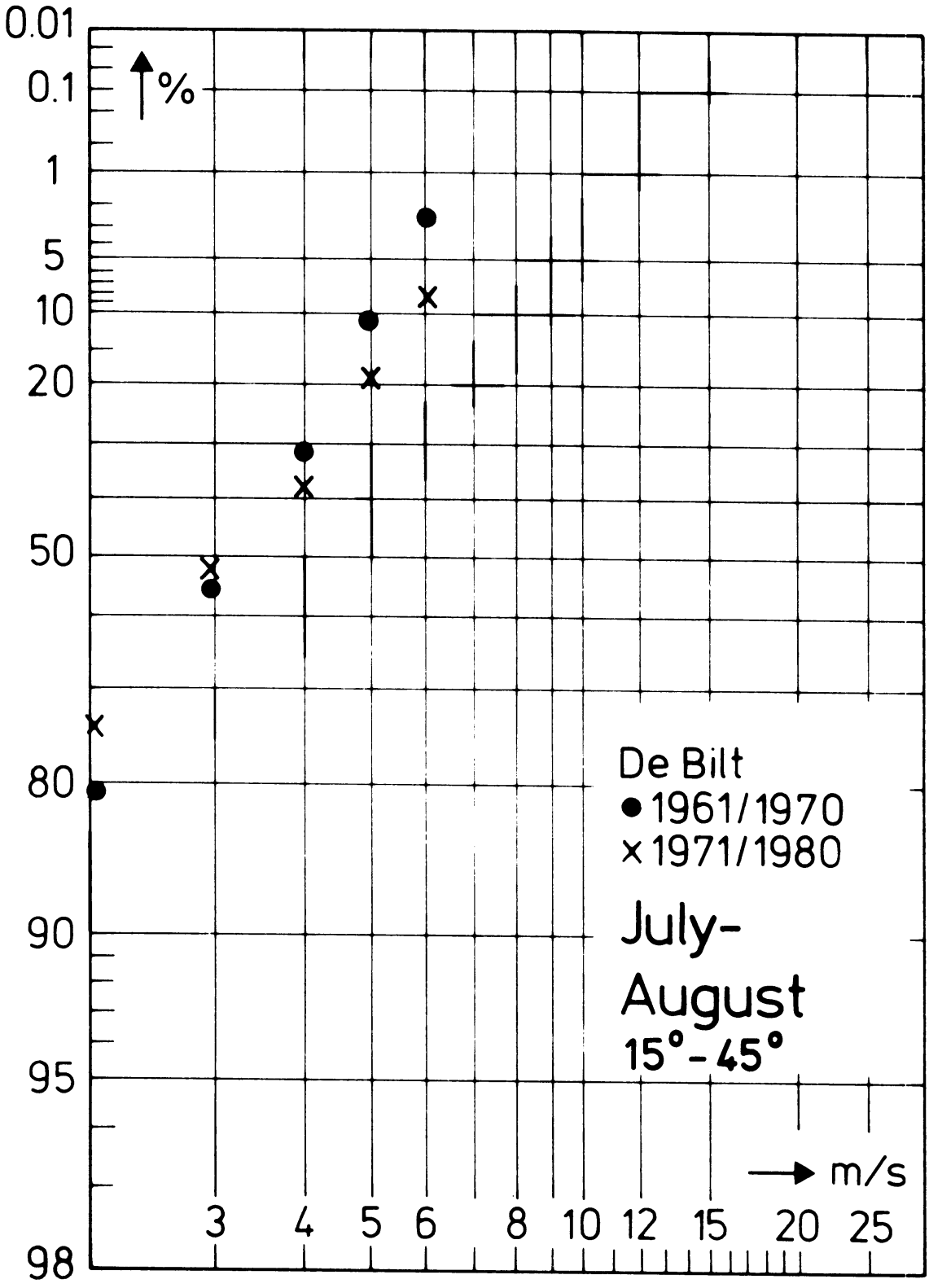


Fig. 13.4 Wind speed distribution of De Bilt from two succesive 10-year periods (July-August, 15°-45°).

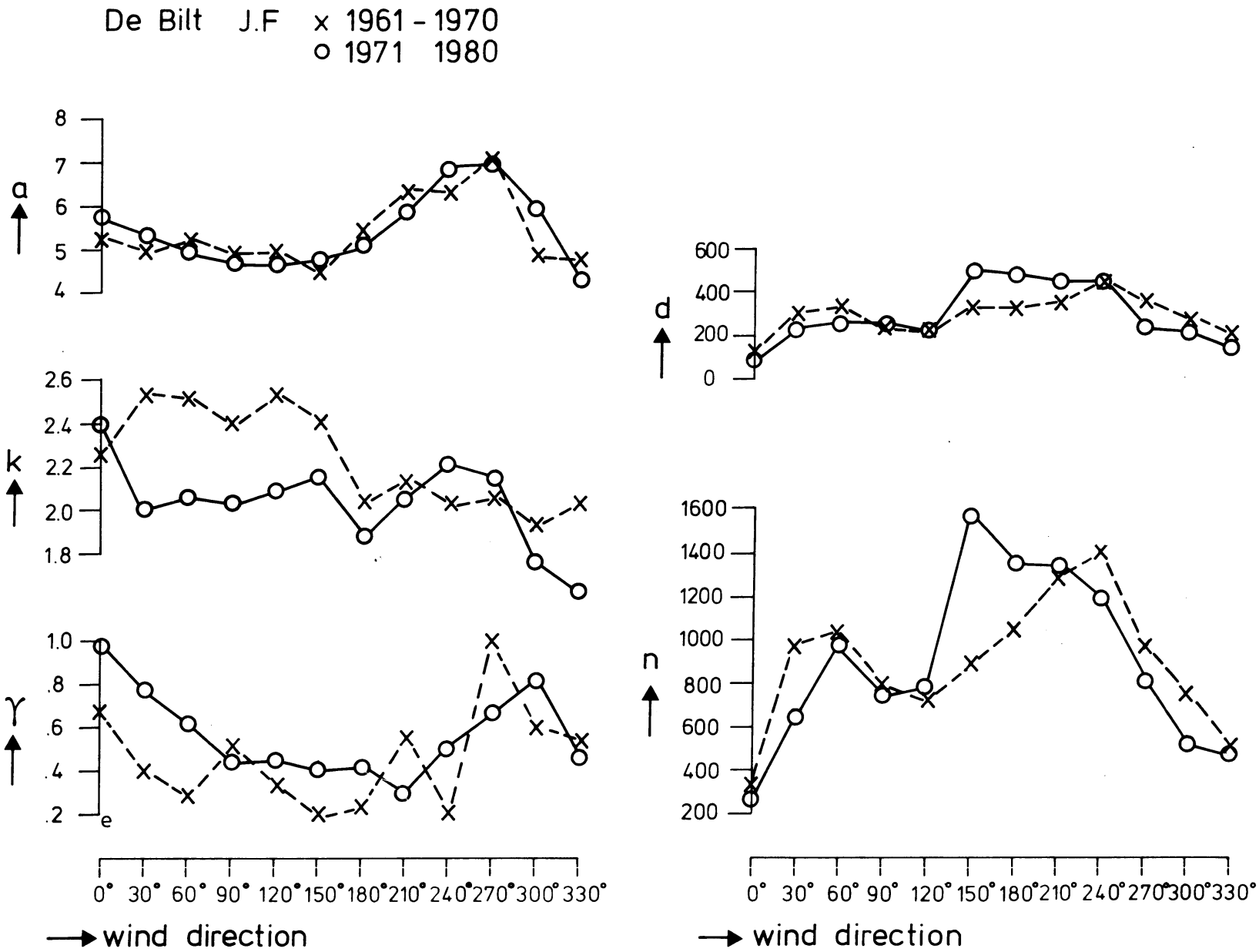


Fig. 13.5 Variation of model parameters a, k, γ, d and n at De Bilt (January-February) for two succesive 10-year periods.

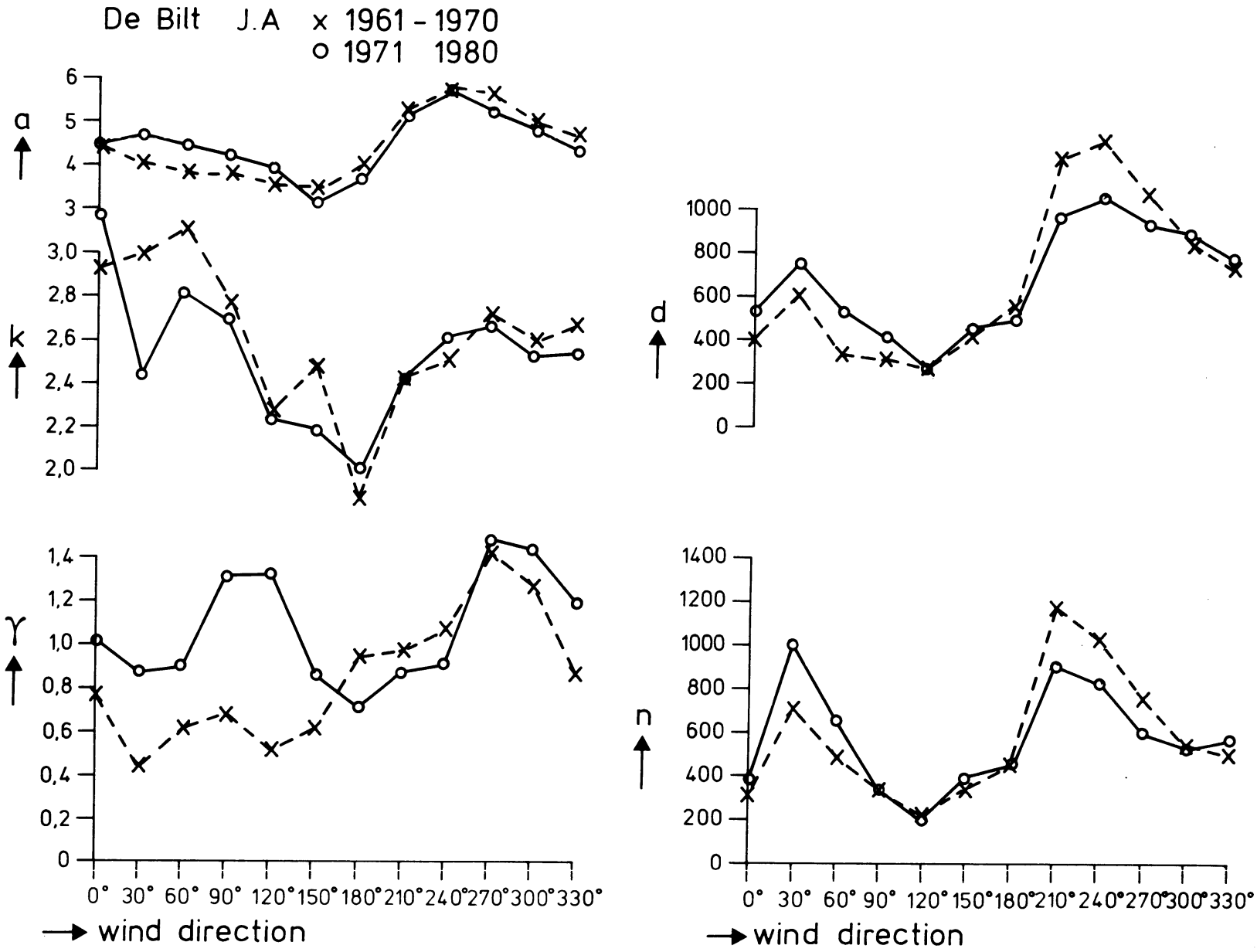


Fig. 13.6 Variation of model parameters a, k, γ, d and n at De Bilt (July-August) for two succesive 10-year periods.

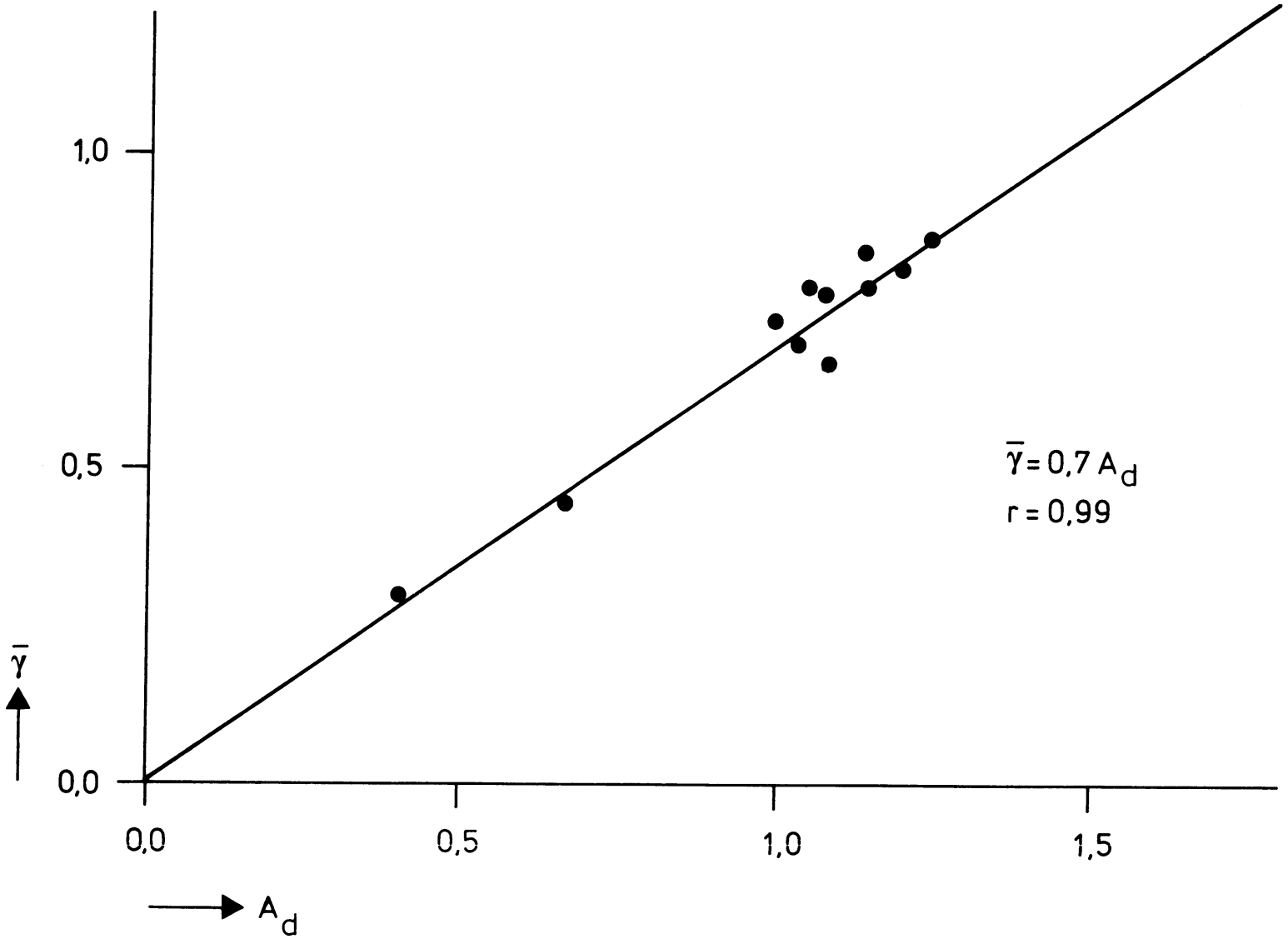


Fig. 14 Relation between the stability parameter $\gamma$ and the amplitude $A_d$ of a sinusoidal fit to the diurnal variation of wind speed.

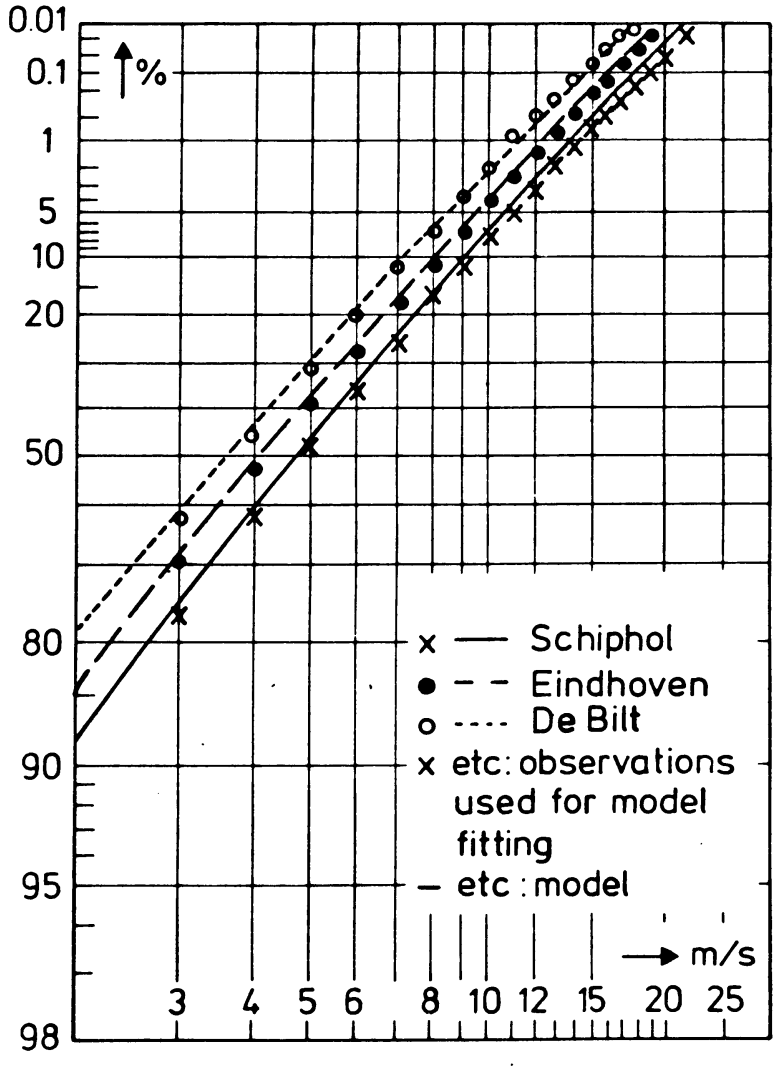


Fig. 15.1 Annual cumulative wind speed frequency distributions of Schiphol, Eindhoven and De Bilt as observed and as a result of model fitting.

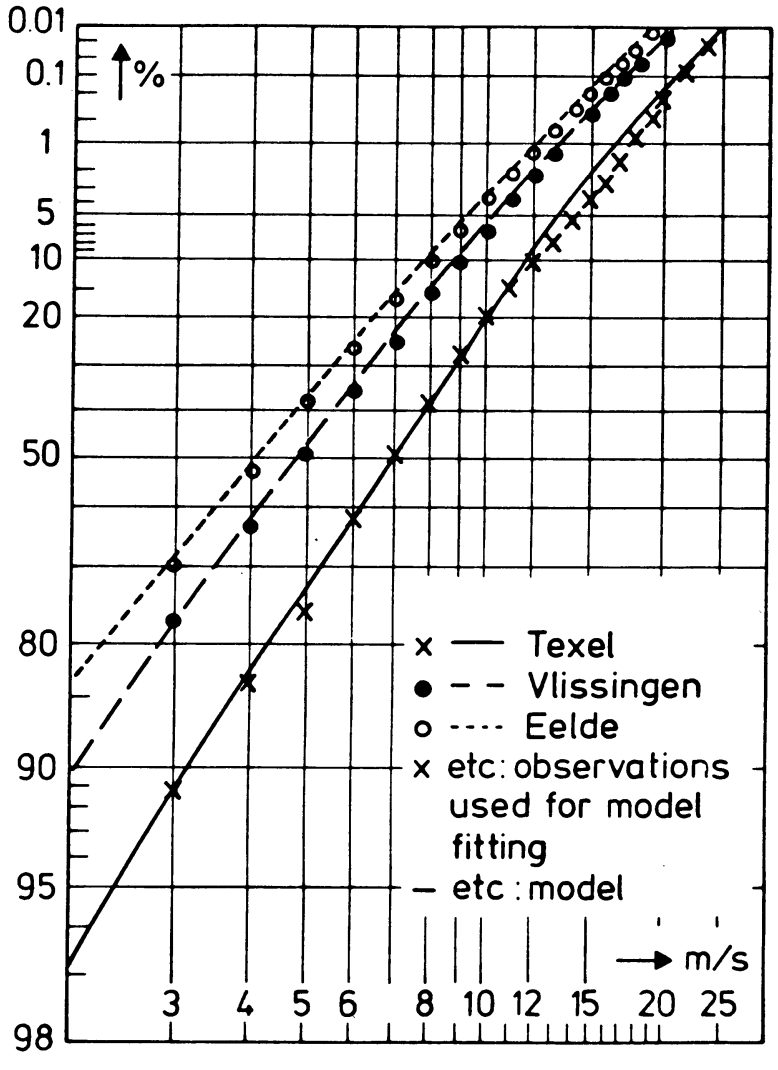


Fig. 15.2 Annual cumulative wind speed frequency distributions of Lightvessel Texel, Vlissingen and Eelde as observed and as a result of model fitting.

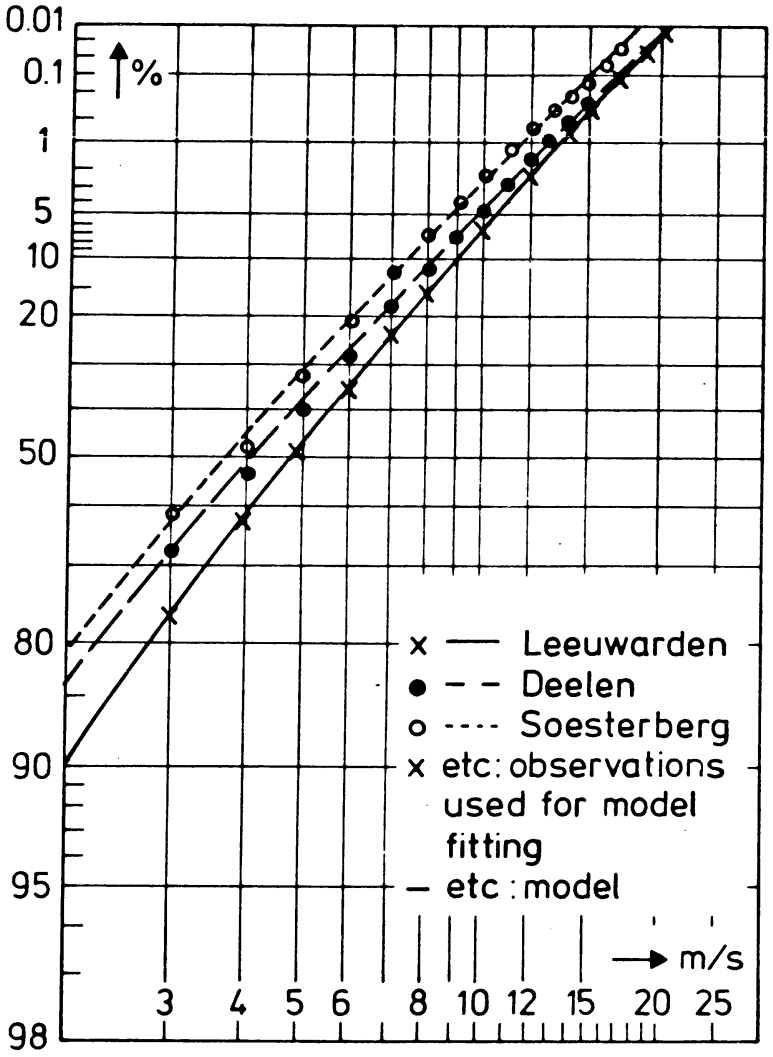


Fig. 15.3 Annual cumulative wind speed frequency distributions of Leeuwarden, Deelen and Soesterberg as observed and as a result of model fitting.

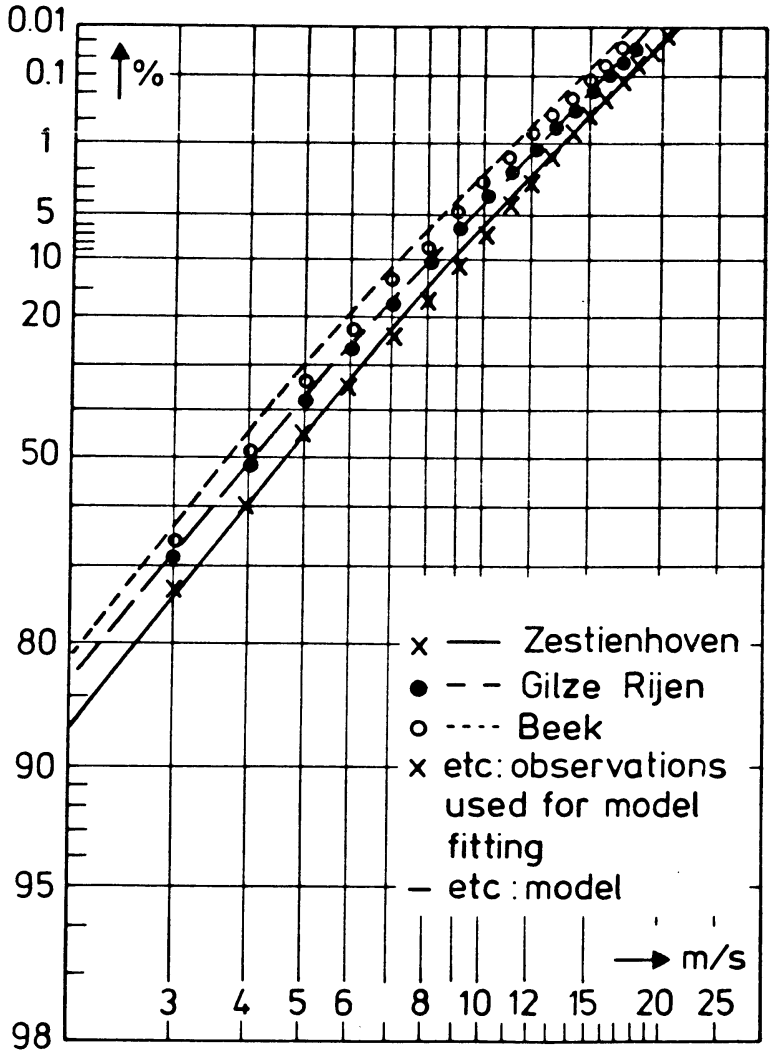


Fig. 15.4 Annual cumulative wind speed frequency distributions of Zestienhoven, Gilze Rijen and Beek as observed and as a result of model fitting.

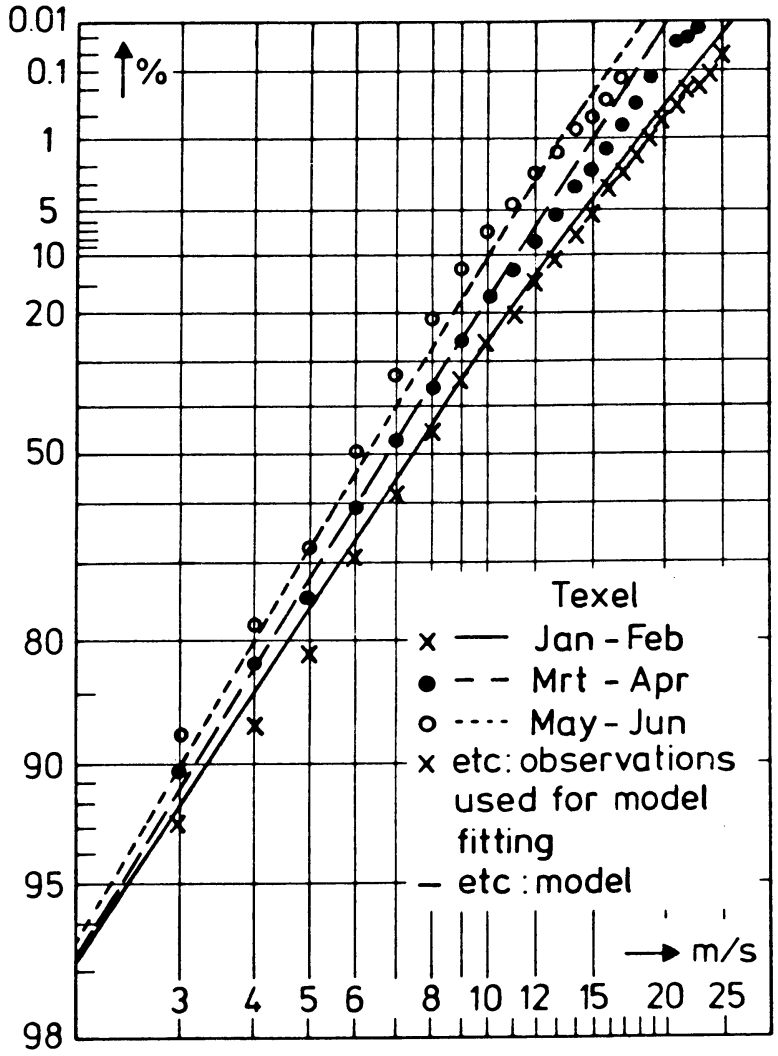


Fig. 15.5 Three seasonal cumulative wind speed frequency distributions of Lightvessel Texel as observed and as a result of model fitting.

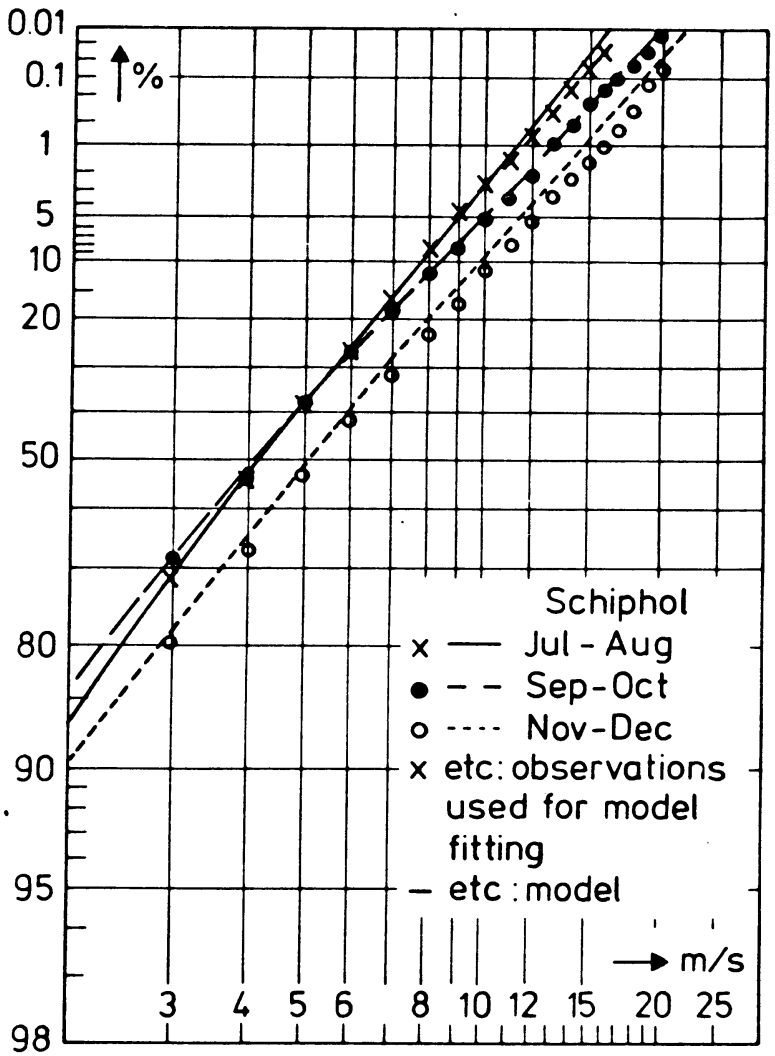


Fig. 15.6 Three seasonal cumulative wind speed frequency distributions of Schiphol as observed and as a result of model fitting.

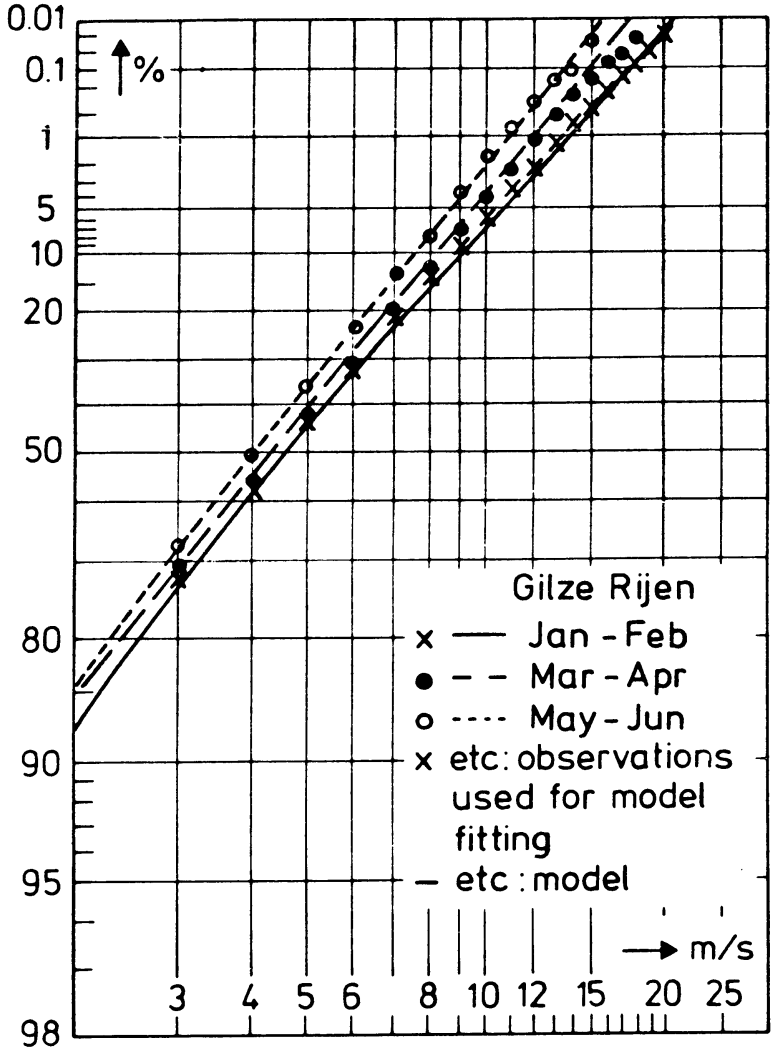


Fig. 15.7 Three seasonal cumulative wind speed frequency distributions of Gilze Rijen as observed and as a result of model fitting.

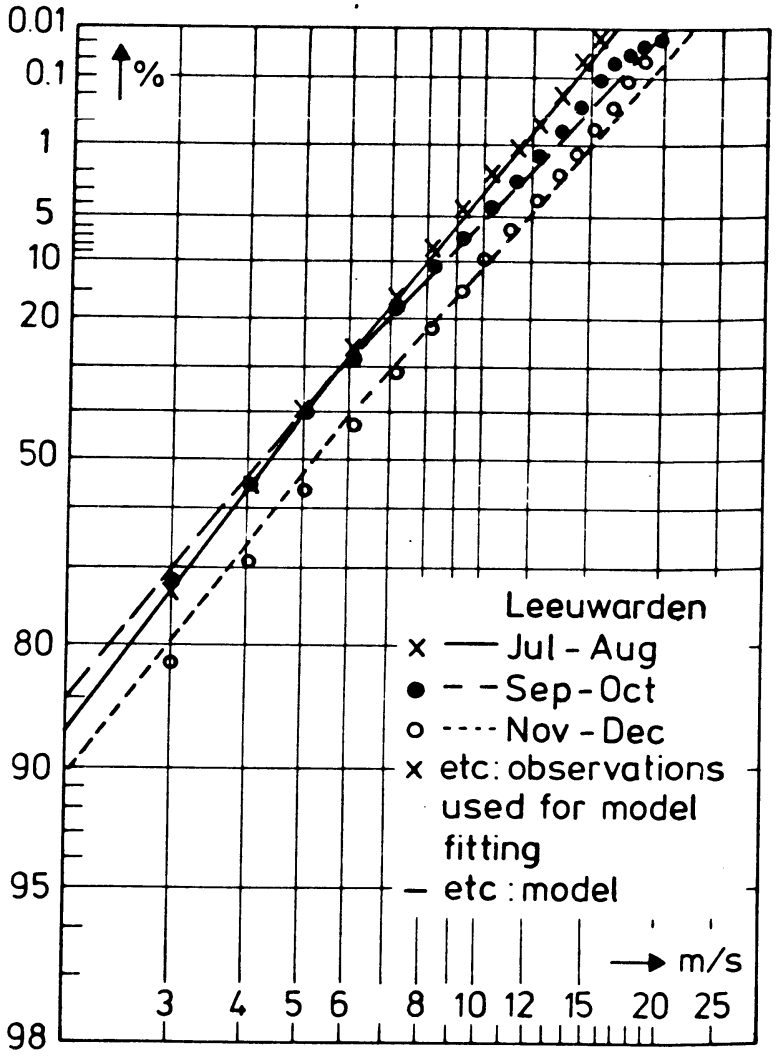


Fig. 15.8 Three seasonal cumulative wind speed frequency distributions of Leeuwarden as observed and as a result of model fitting.

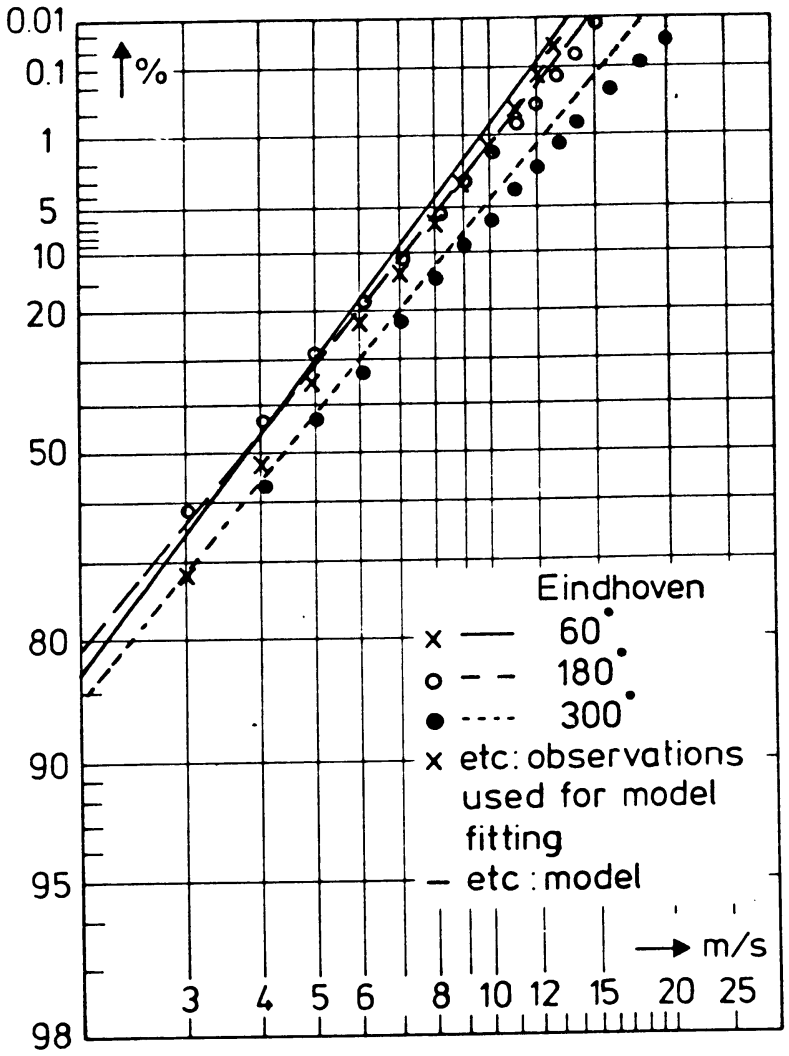


Fig. 15.9 Three azimuth-sector cumulative wind speed frequency distributions of Eindhoven as observed and as a result of model fitting.

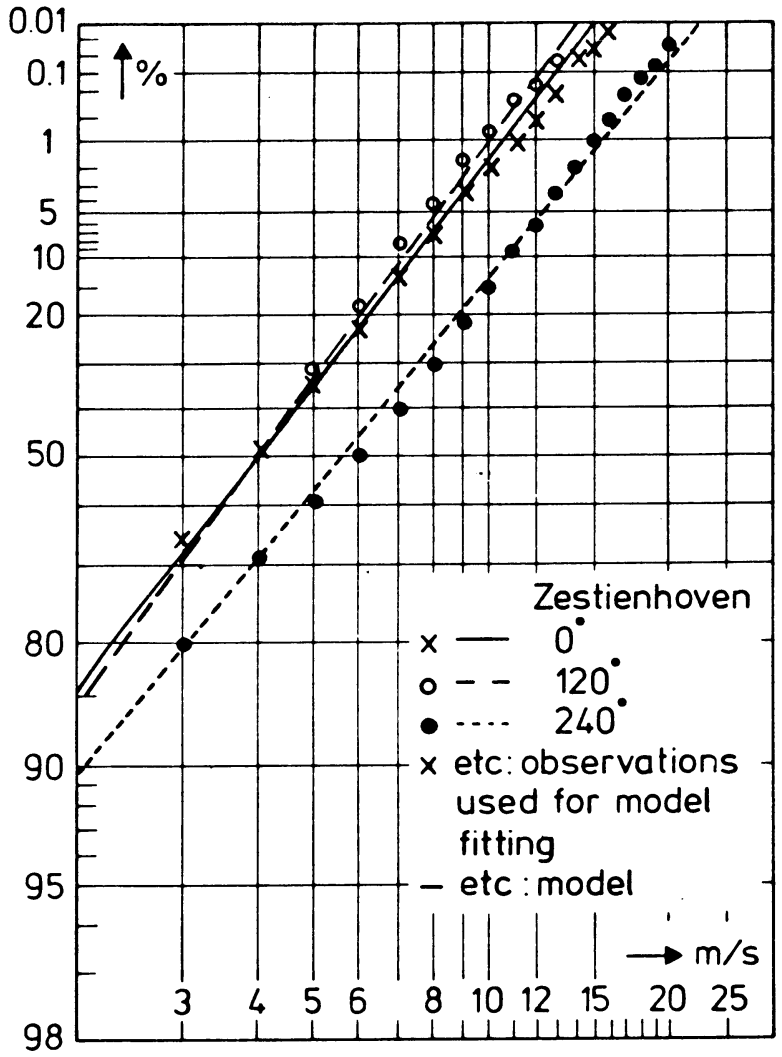


Fig. 15.10 Three azimuth-sector cumulative wind speed frequency distributions of Zestienhoven as observed and as a result of model fitting.

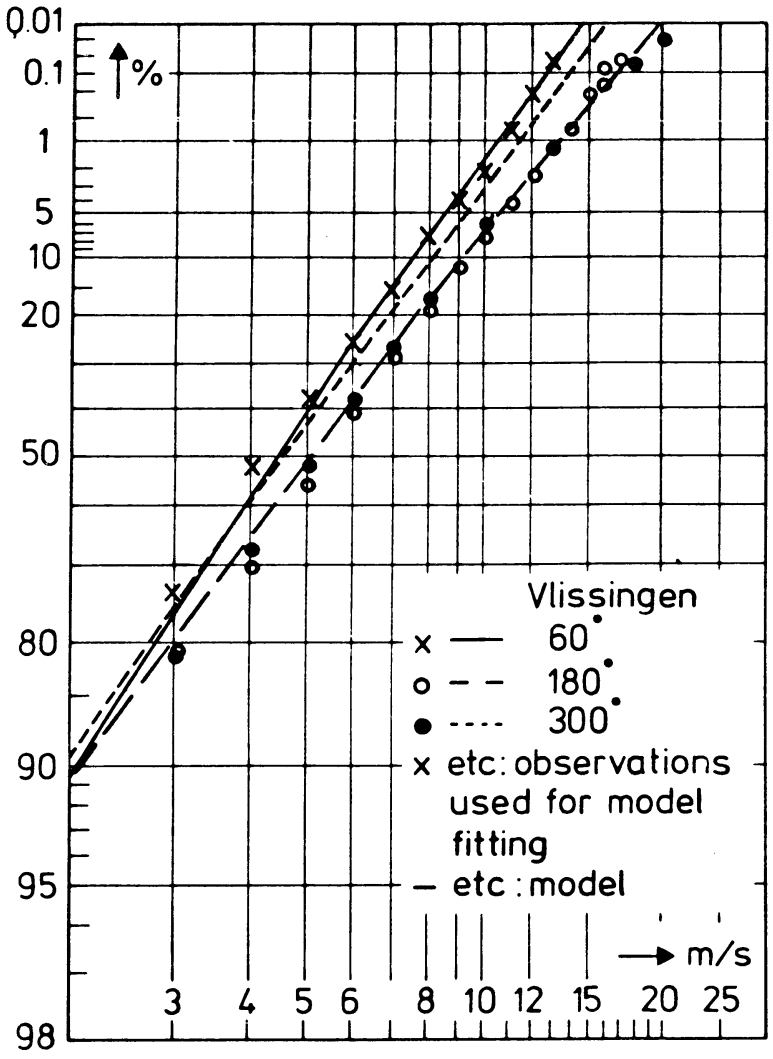


Fig. 15.11 Three azimuth-sector cumulative wind speed frequency distributions of Vlissingen as observed and as a result of model fitting.

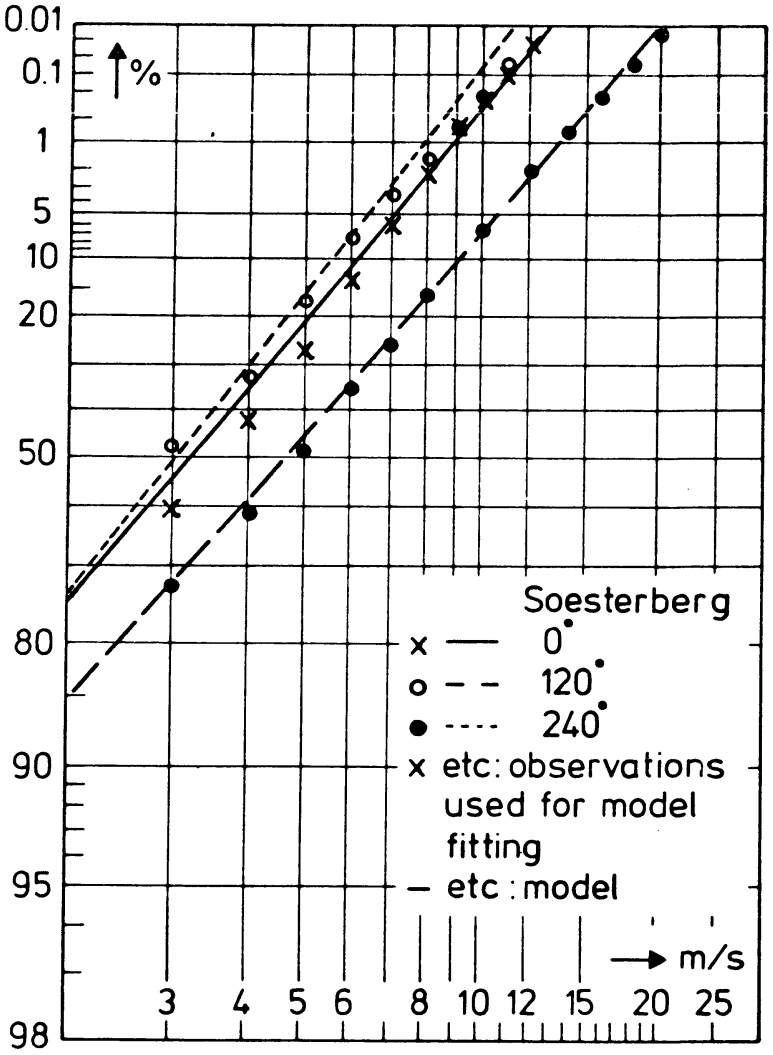


Fig. 15.12 Three azimuth-sector cumulative wind speed frequency distributions of Soesterberg as observed and as a result of model fitting.

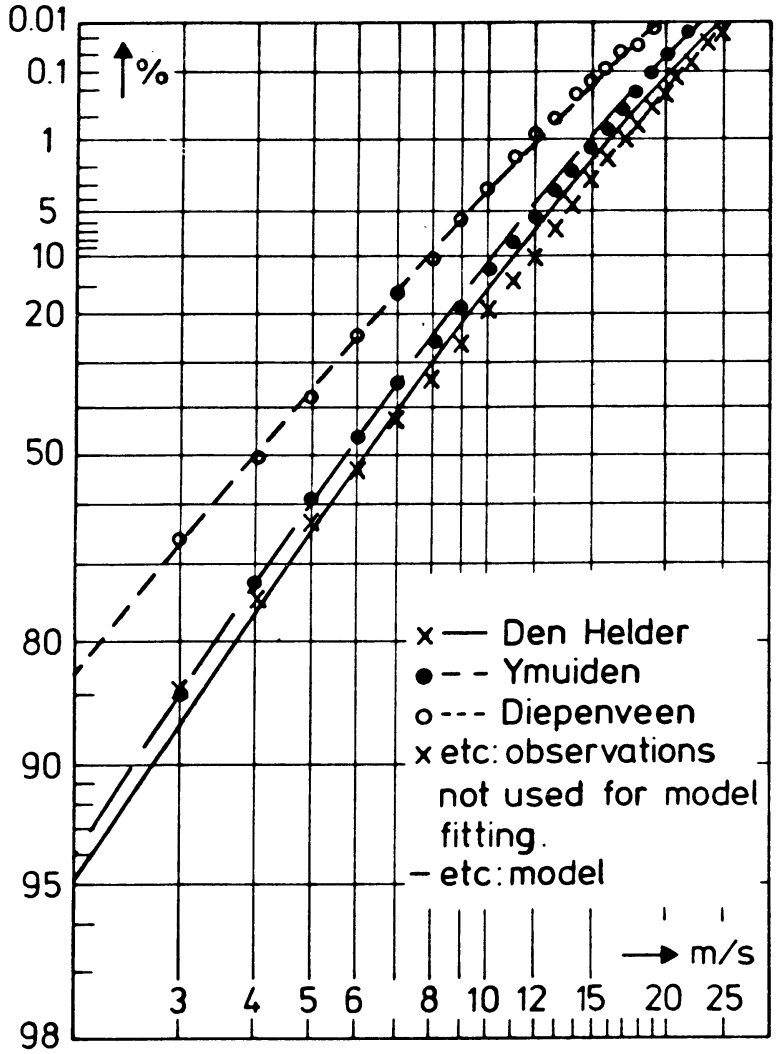


Fig. 16.1 Annual cumulative wind speed frequency distributions of Den Helder, IJmuiden and Diepenveen as observed and as computed from the model independent of the observations.

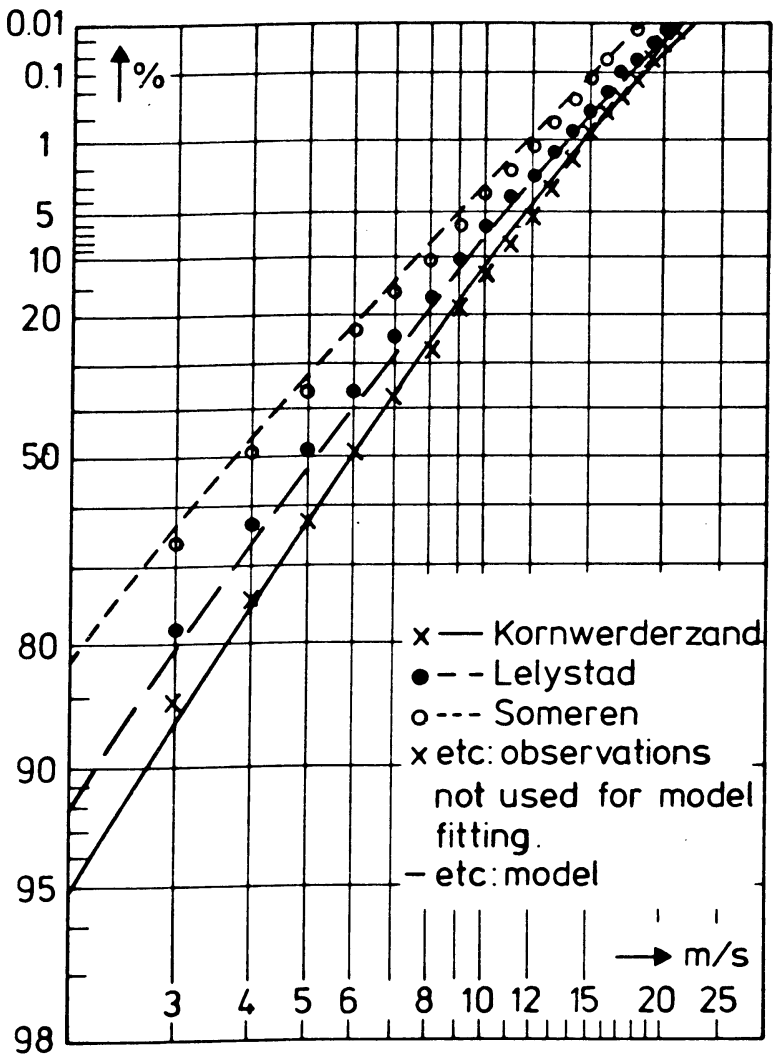


Fig. 16.2 Annual cumulative wind speed frequency distributions of Kornwerderzand, Lelystad and Someren as observed and as computed from the model independent of the observations.

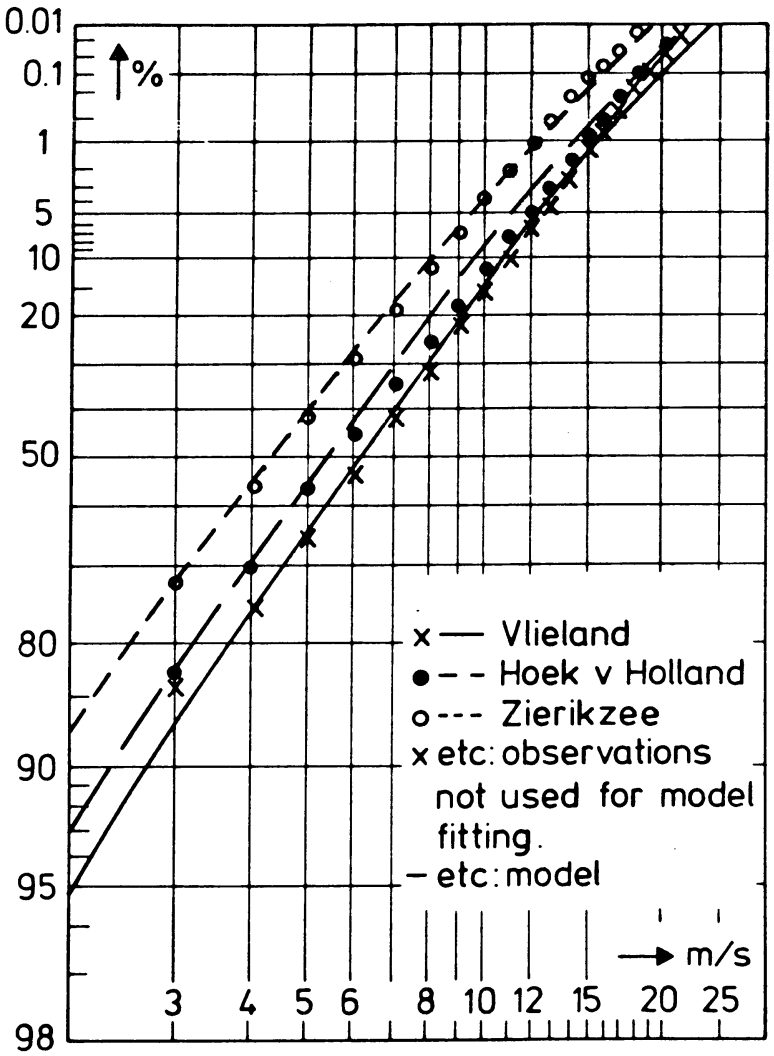


Fig. 16.3 Annual cumulative wind speed frequency distributions of Vlieland, Hoek van Holland and Zierikzee as observed and as computed from the model independent of the observations.

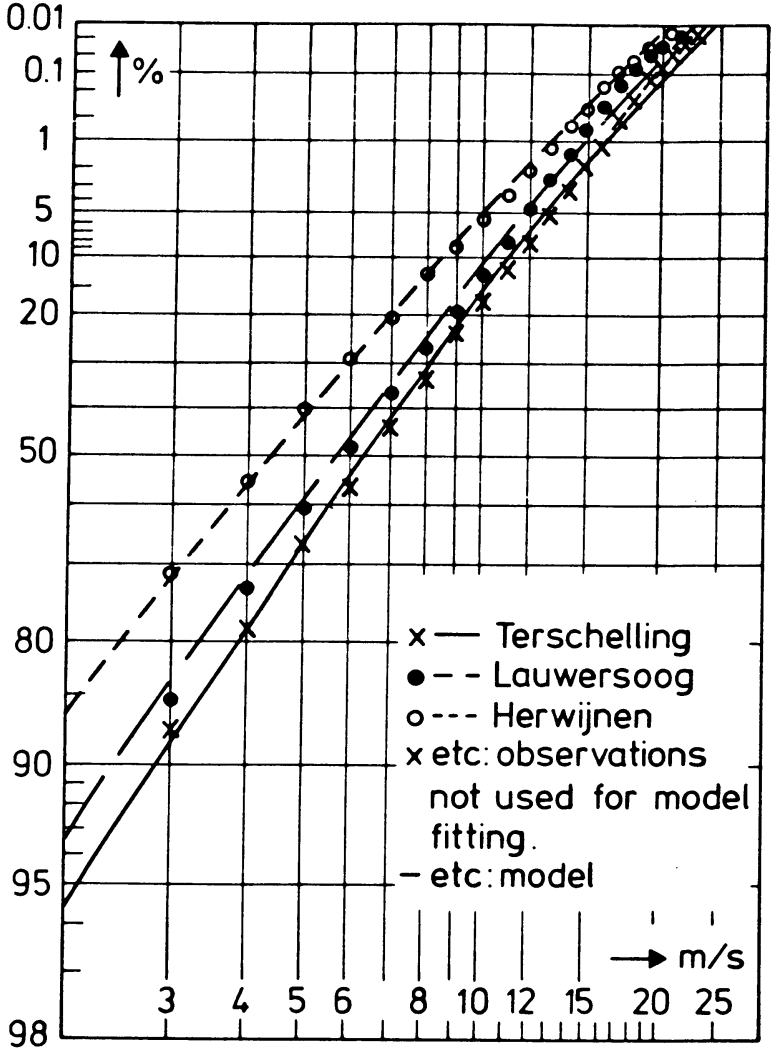


Fig. 16.4 Annual cumulative wind speed frequency distributions of Terschelling, Lauwersoog and Herwijnen as observed and as computed from the model independent of the observations.

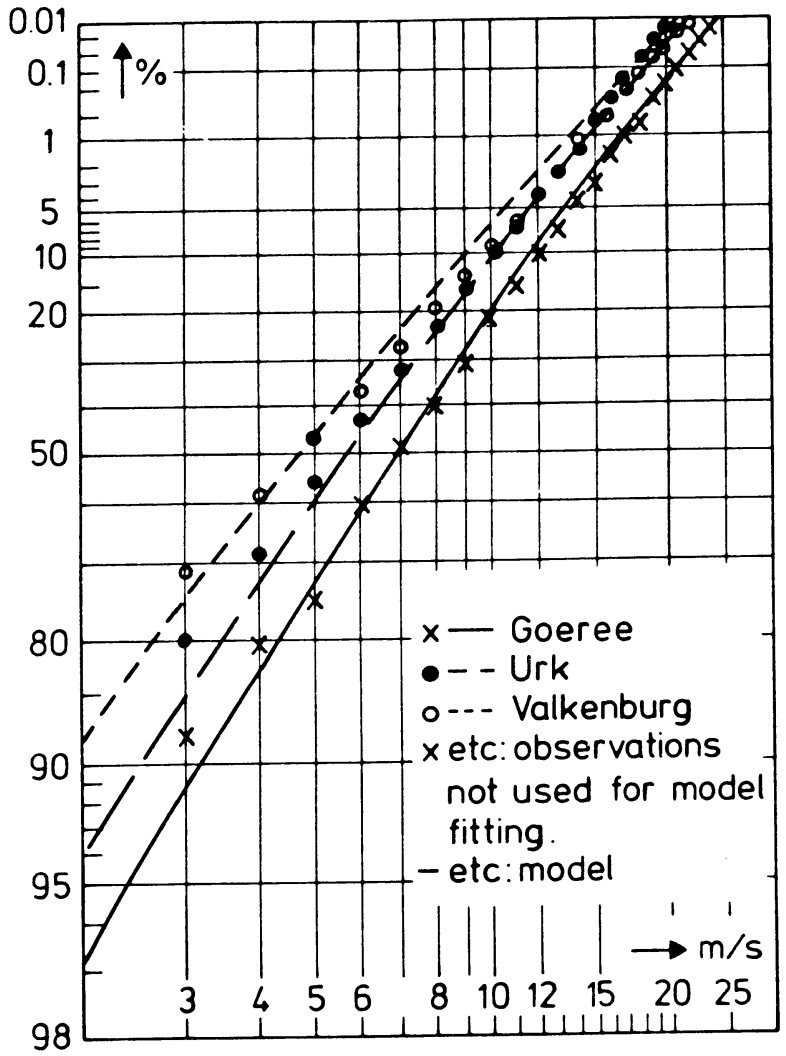


Fig. 16.5 Annual cumulative wind speed frequency distributions of Lightvessel Goeree, Urk and Valkenburg as observed and as computed from the model independent of the observations.

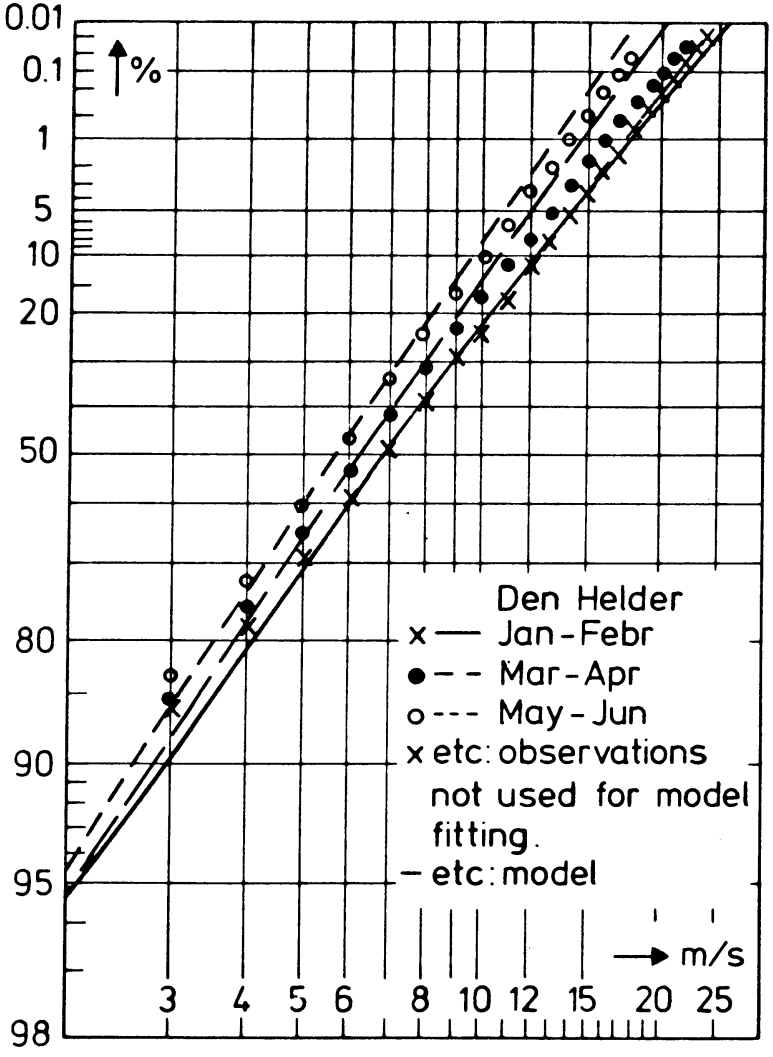


Fig. 16.6 Three seasonal cumulative wind speed frequency distributions of Den Helder as observed and as computed from the model independent of the observations.

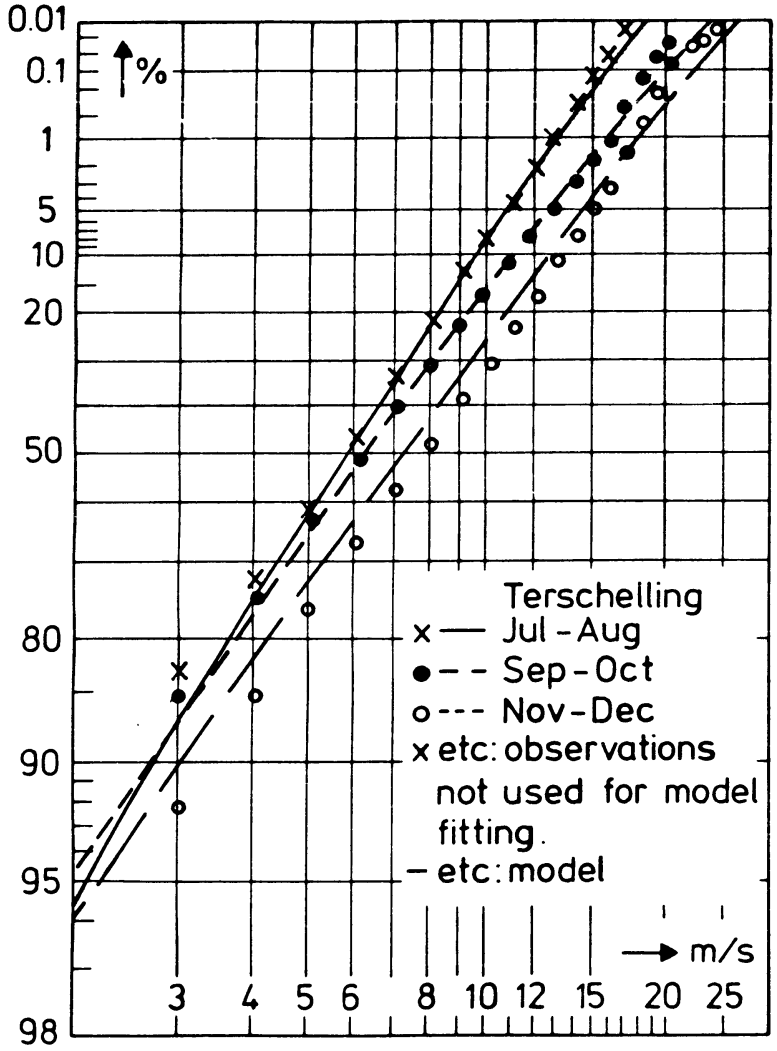


Fig. 16.7 Three seasonal cumulative wind speed frequency distributions of Terschelling as observed and as computed from the model independent of the observations.

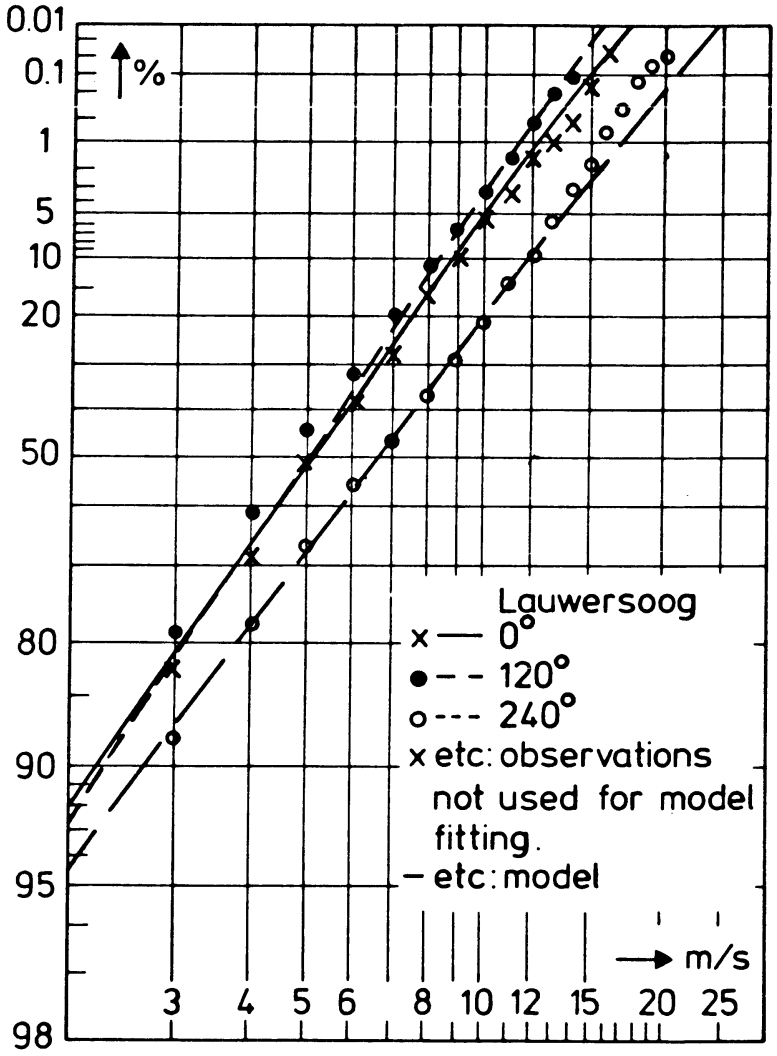


Fig. 16.8 Three seasonal cumulative wind speed frequency distributions of Lauwersoog as observed and as computed from the model independent of the observations.

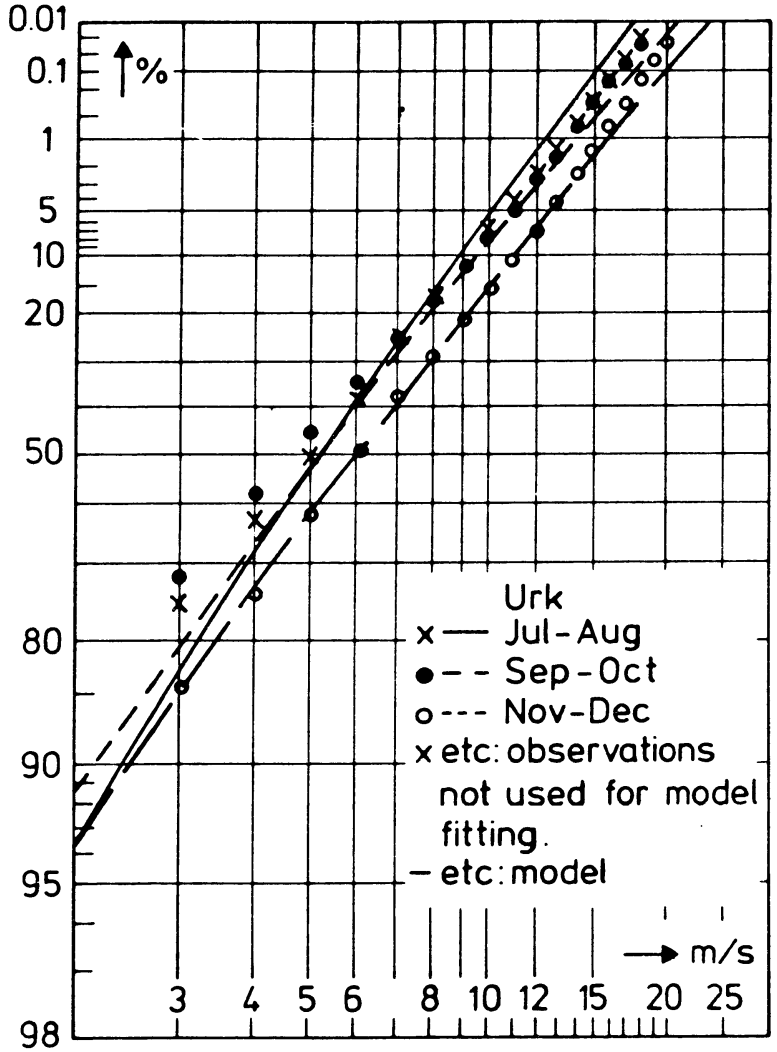


Fig. 16.9 Three seasonal cumulative wind speed frequency distributions of Urk as observed and as computed from the model independent of the observations.

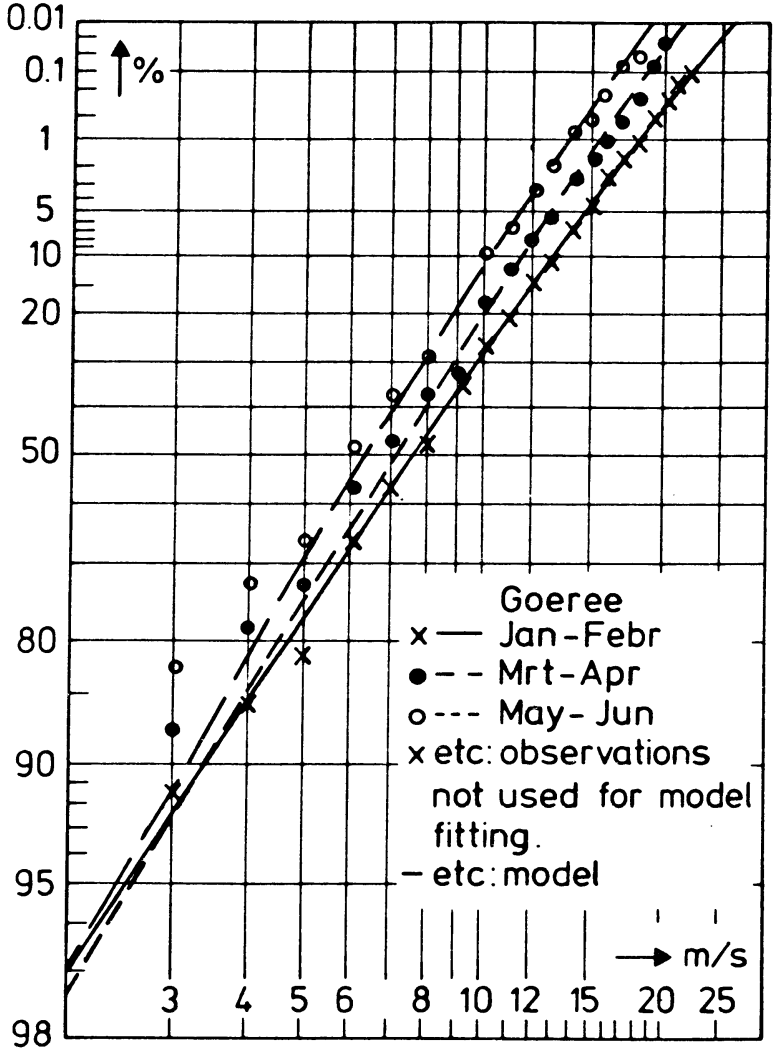


Fig. 16.10 Three seasonal cumulative wind speed frequency distributions of Lightvessel Goeree as observed and as computed from the model independent of the observations.

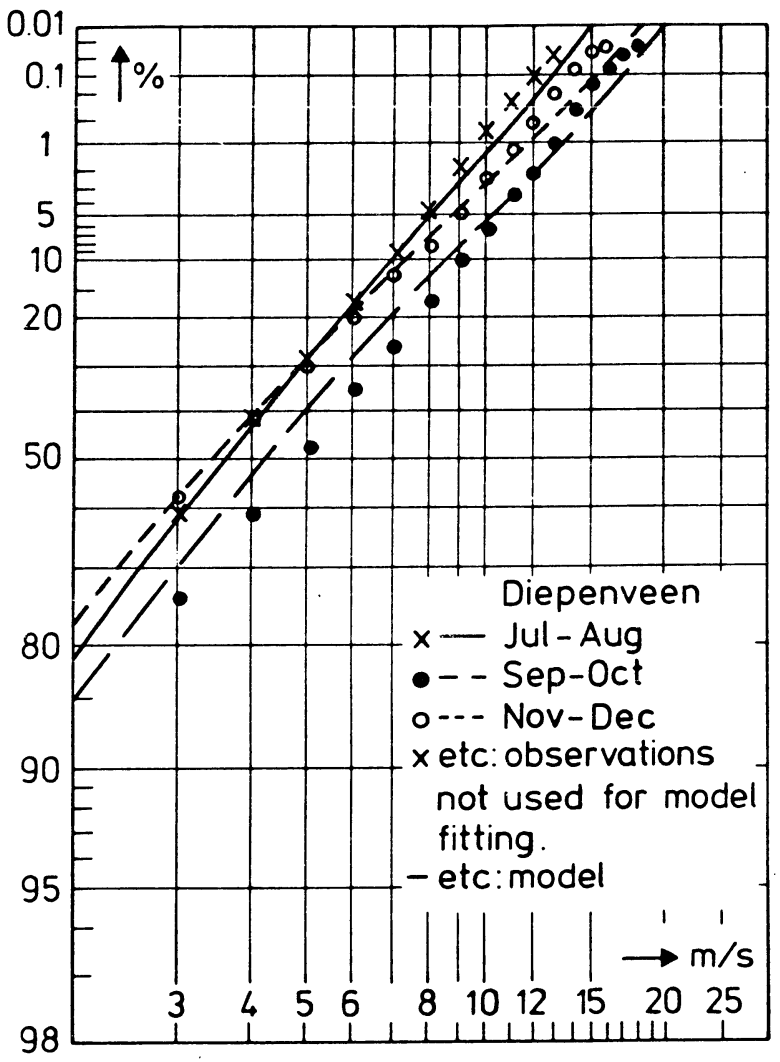


Fig. 16.11 Three seasonal cumulative wind speed frequency distributions of Diepenveen as observed and as computed from the model independent of the observations.

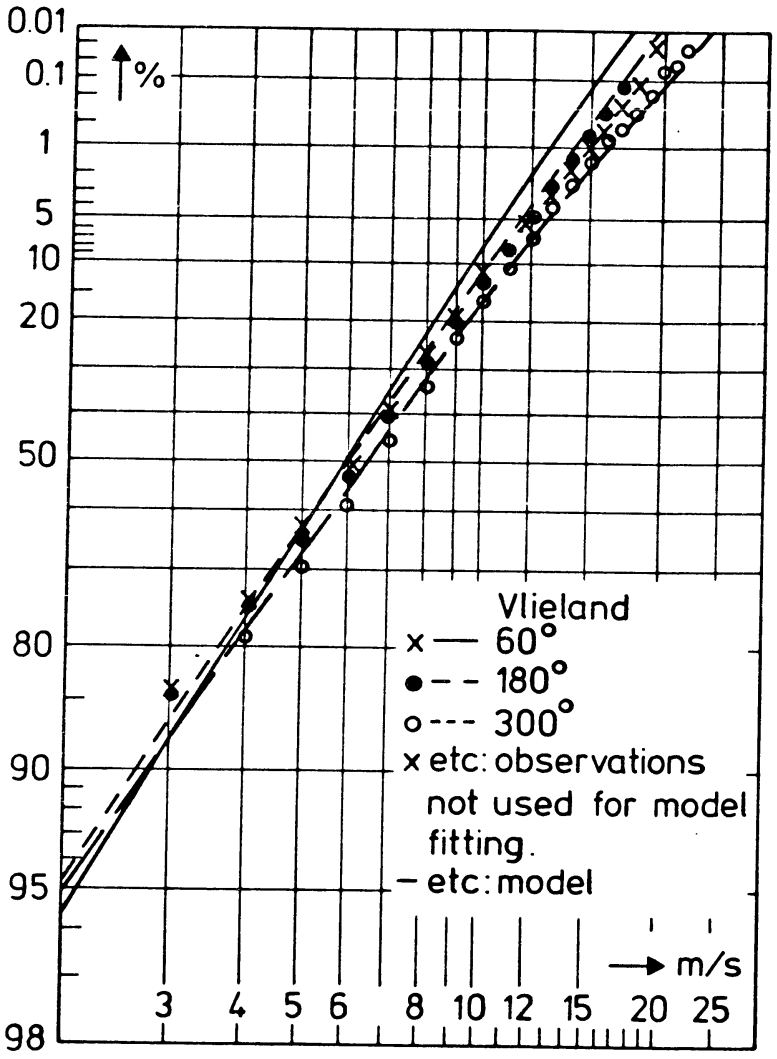


Fig. 16.12 Three azimuth-sector cumulative wind speed frequency distributions of Vlieland as observed and as computed from the model independent of the observations.

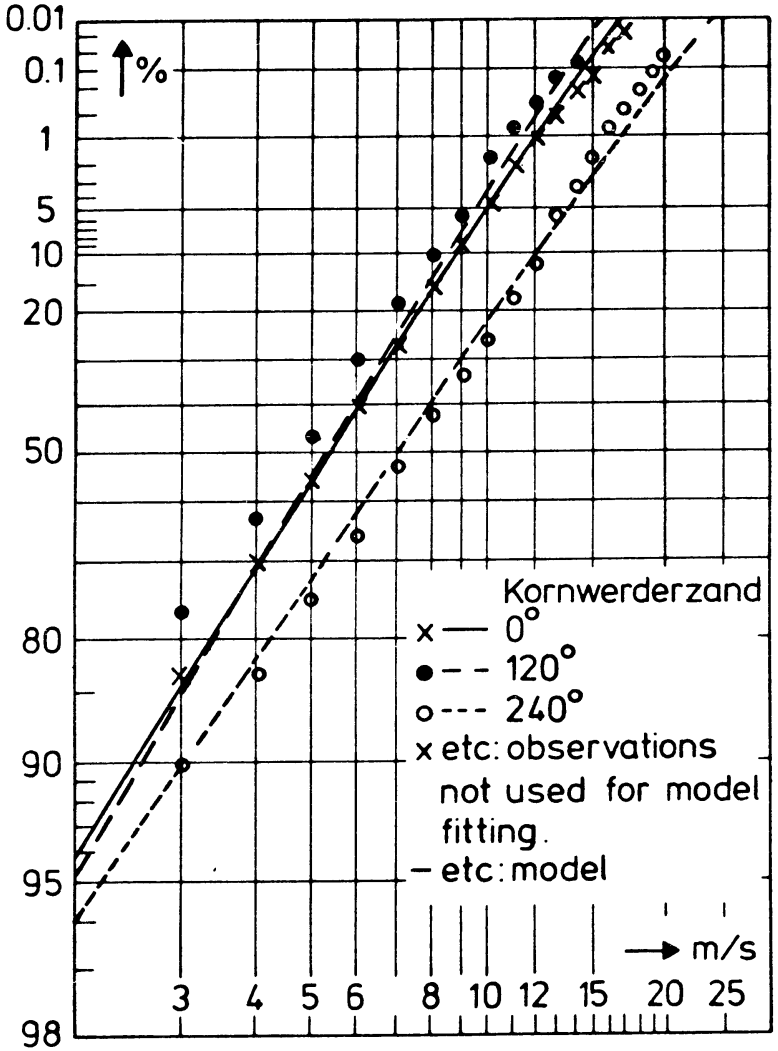


Fig. 16.13 Three azimuth-sector cumulative wind speed frequency distributions of Kornwerderzand as observed and as computed from the model independent of the observations.

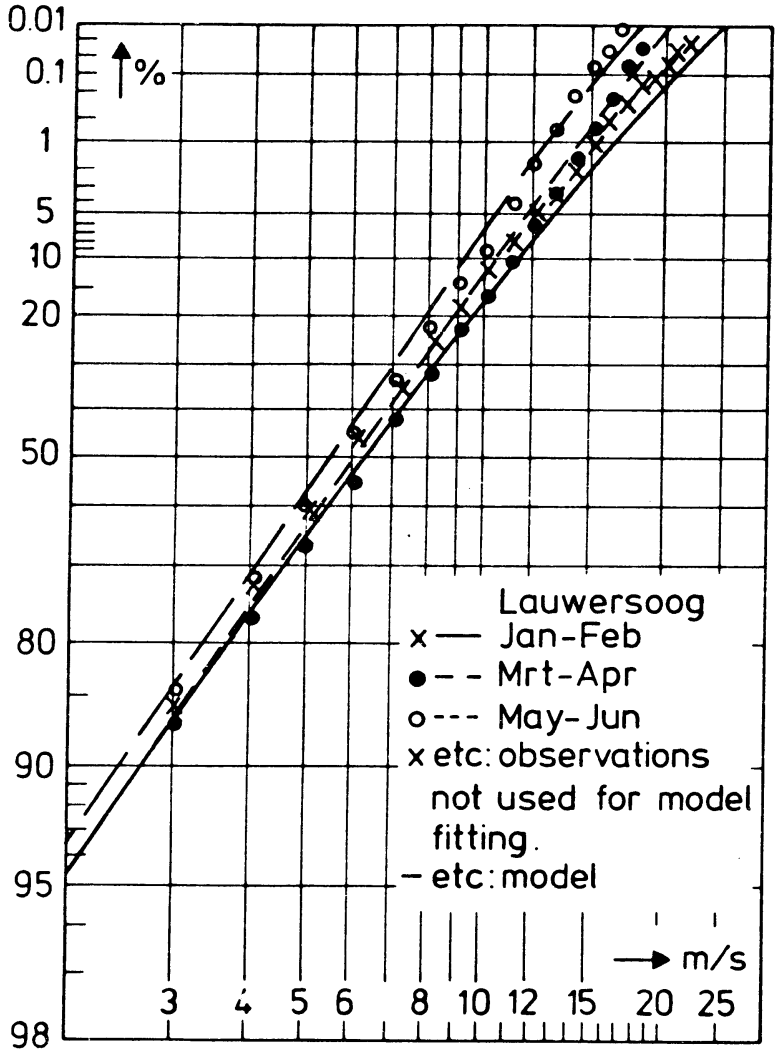


Fig. 16.14 Three azimuth-sector cumulative wind speed frequency distributions of Lauwersoog as observed and as computed from the model independent of the observations.

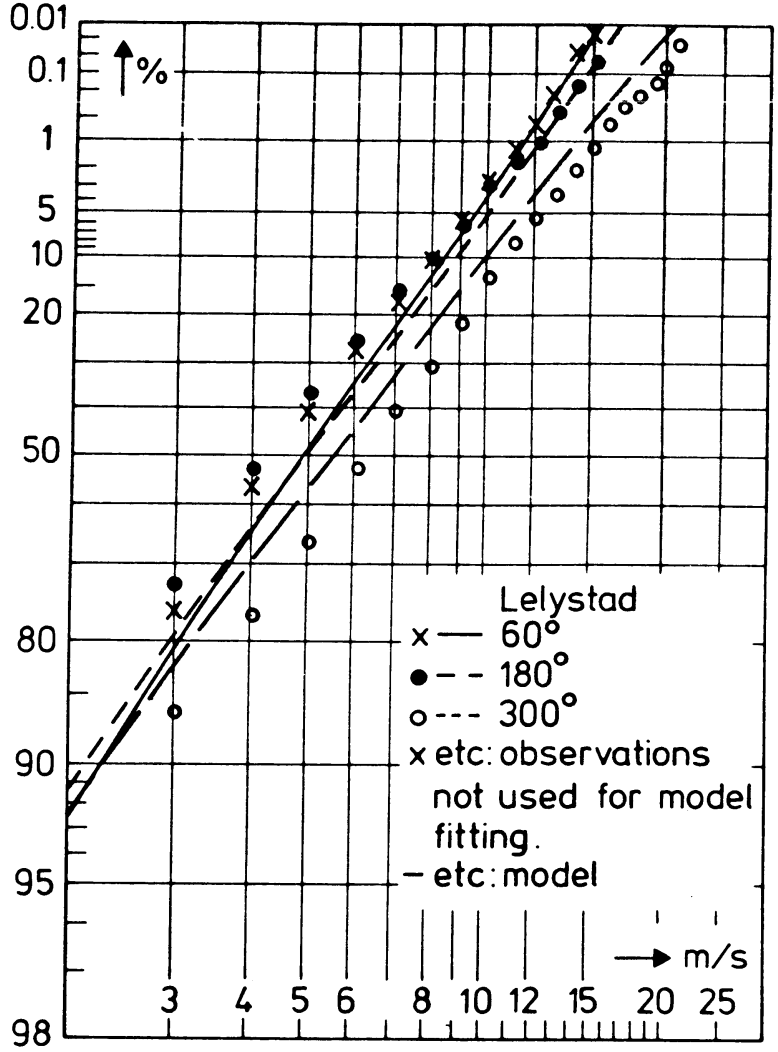


Fig. 16.15 Three azimuth-sector cumulative wind speed frequency distributions of Lelystad as observed and as computed from the model independent of the observations.

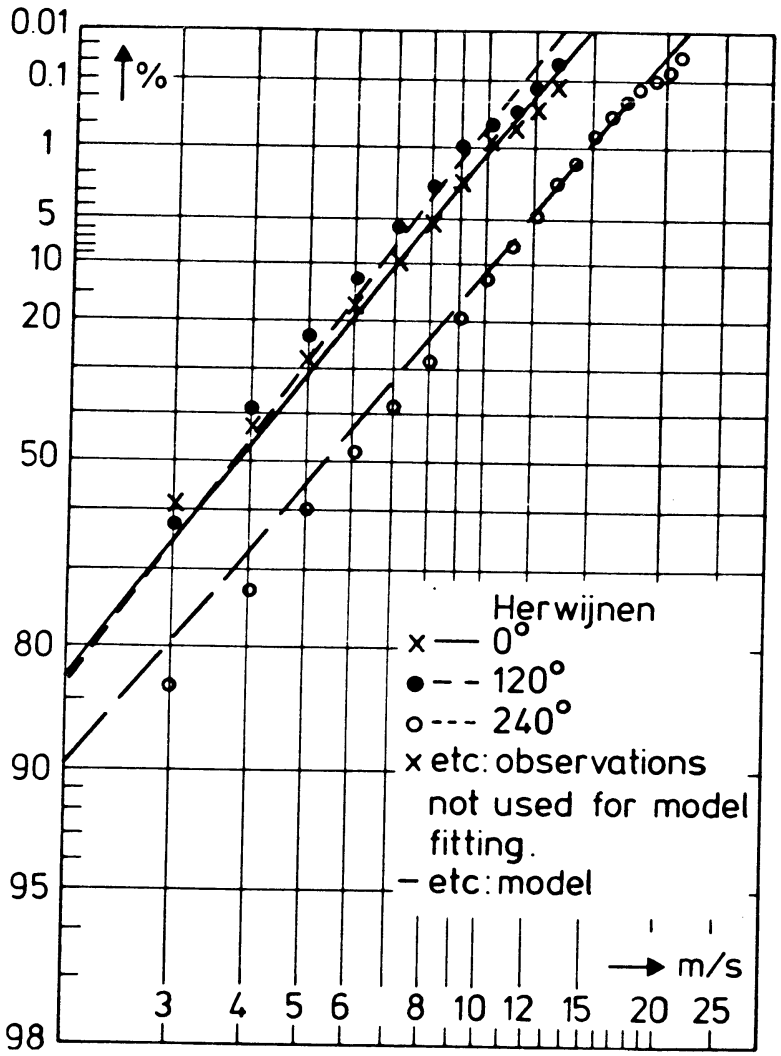


Fig. 16.16 Three azimuth-sector cumulative wind speed frequency distributions of Herwijnen as observed and as computed from the model independent of the observations.

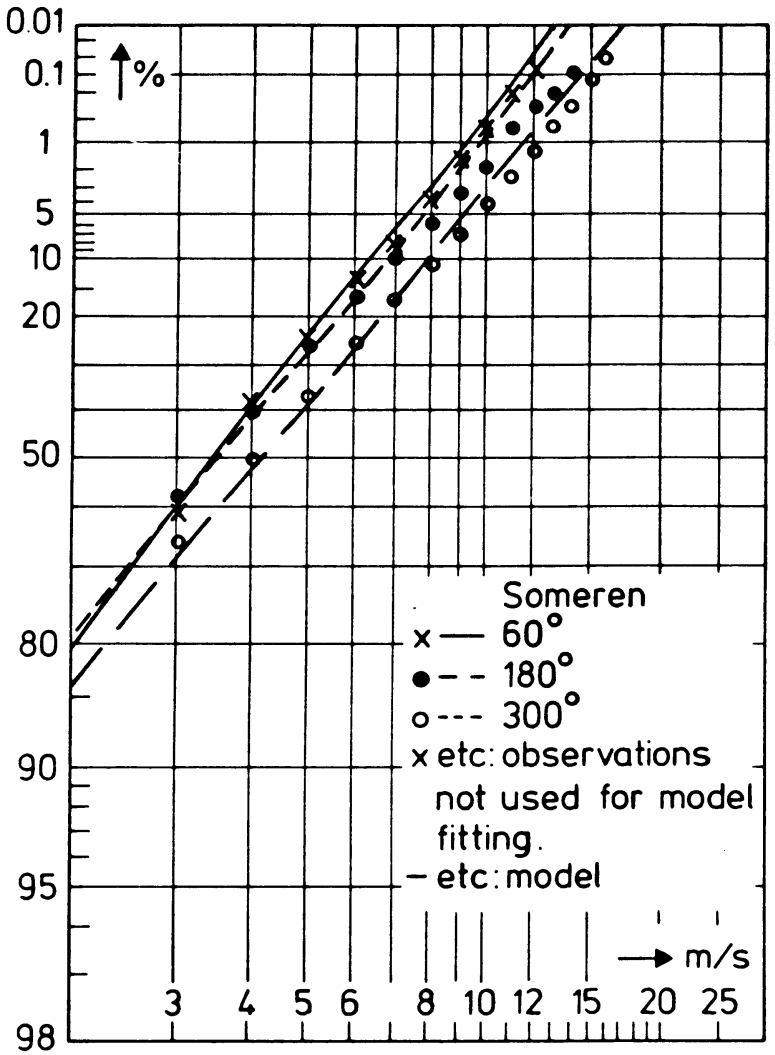


Fig. 16.17 Three azimuth-sector cumulative wind speed frequency distributions of Someren as observed and as computed from the model independent of the observations.

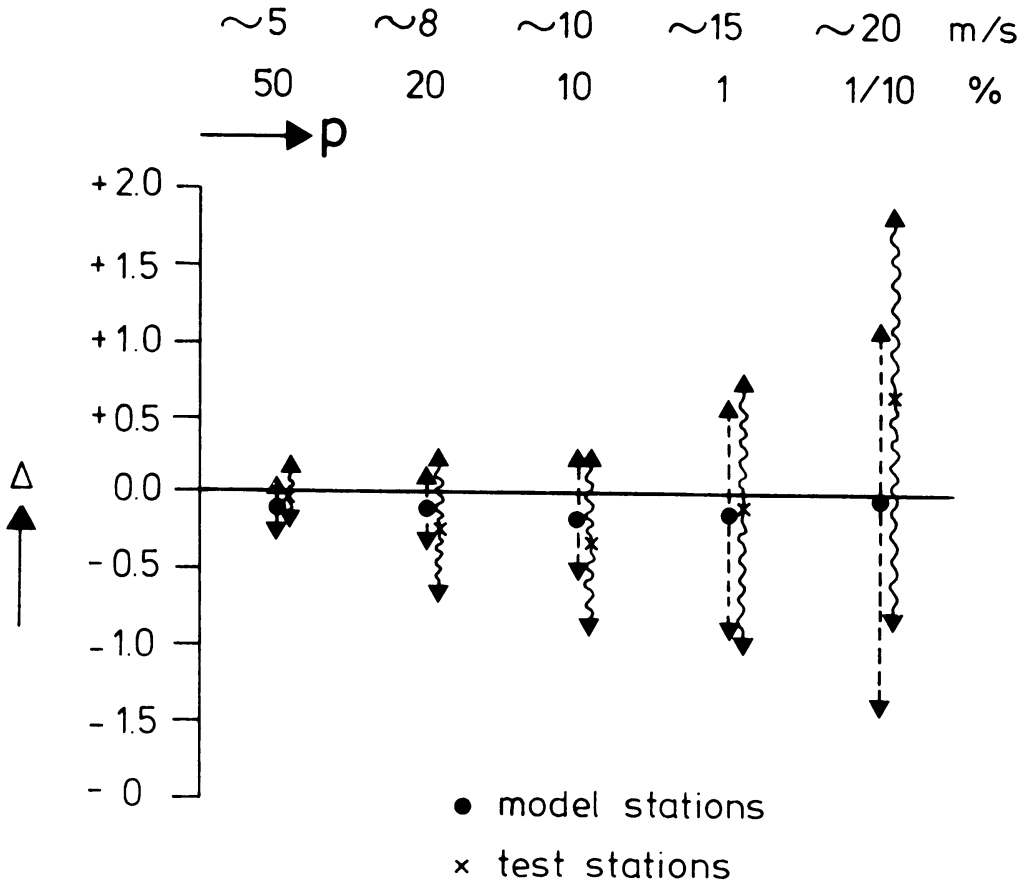


Fig. 17.1 Average values and 95%-ranges for the difference between observations and model at various percentiles of the cumulative distribution.

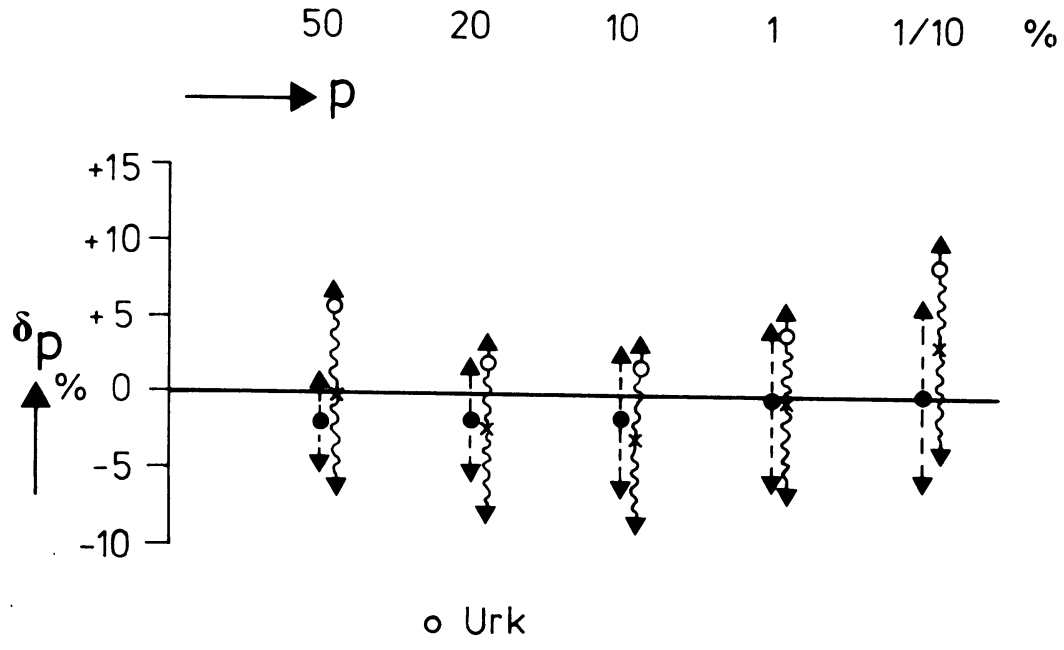


Fig. 17.2 As figure 17.1, but normalized with the average wind speed.

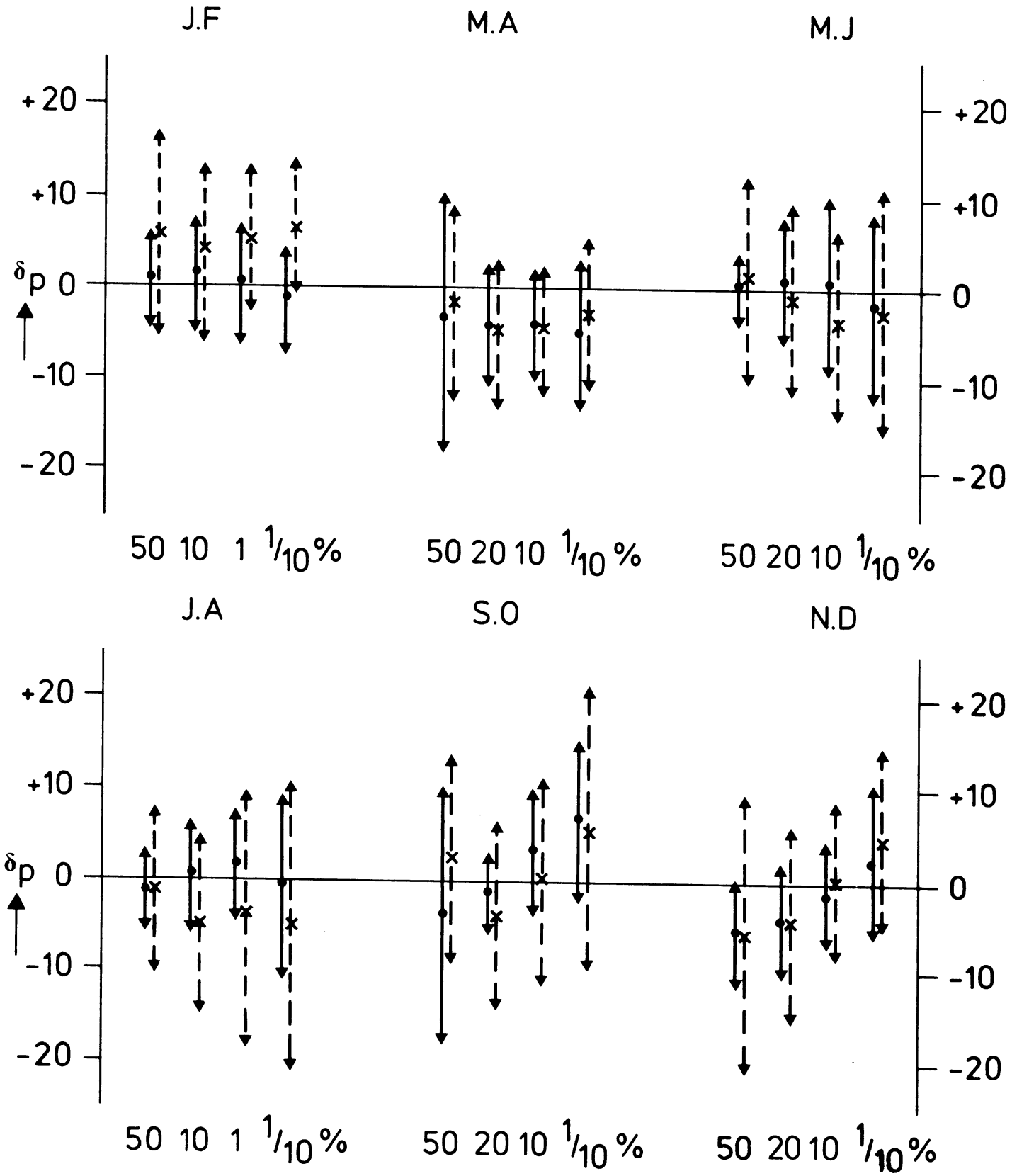


Fig. 17.3 As figure 17.1, but separate for each two-month season.

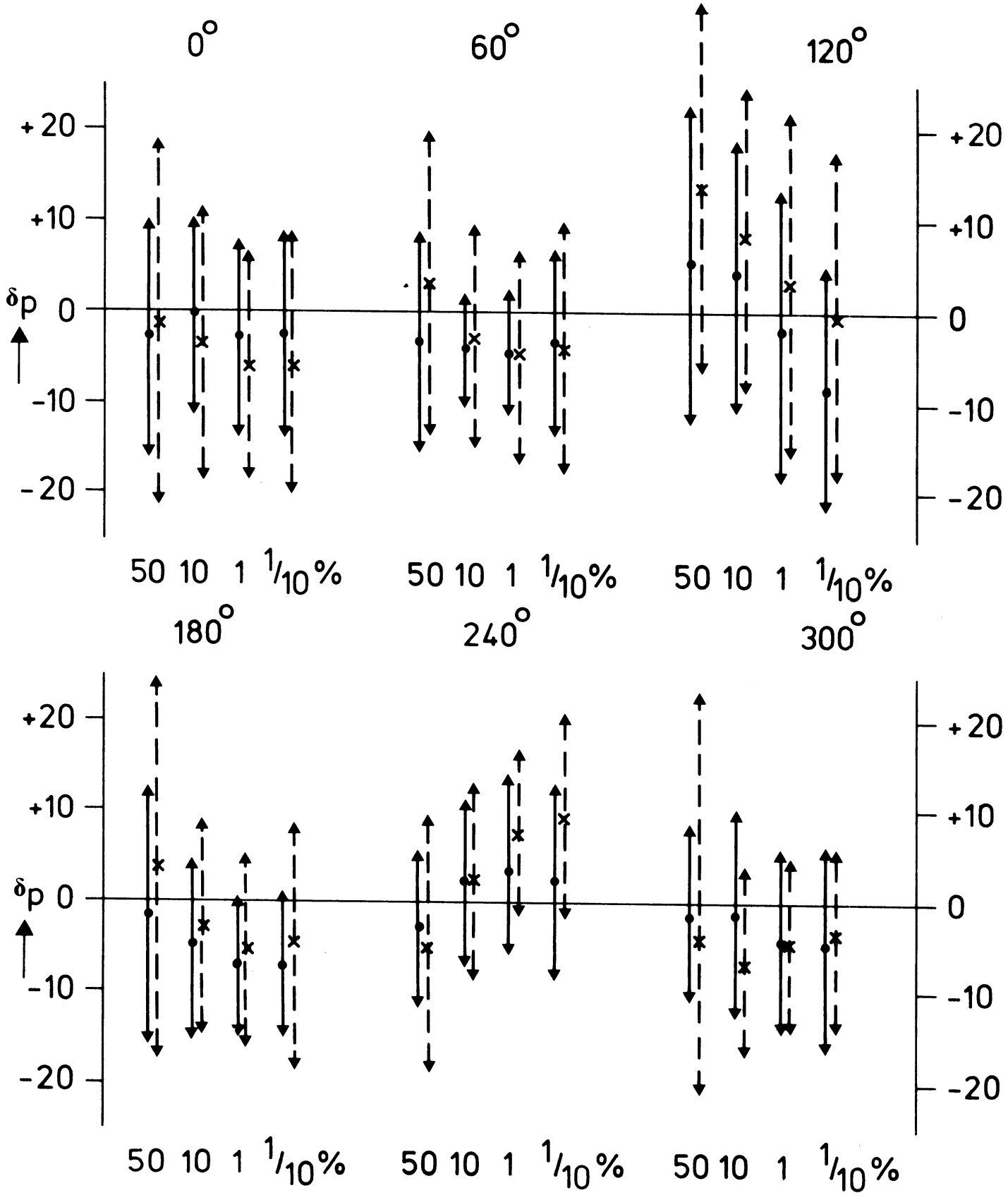


Fig. 17.4 As figure 17.1, but separate for each 30° azimuth sector.

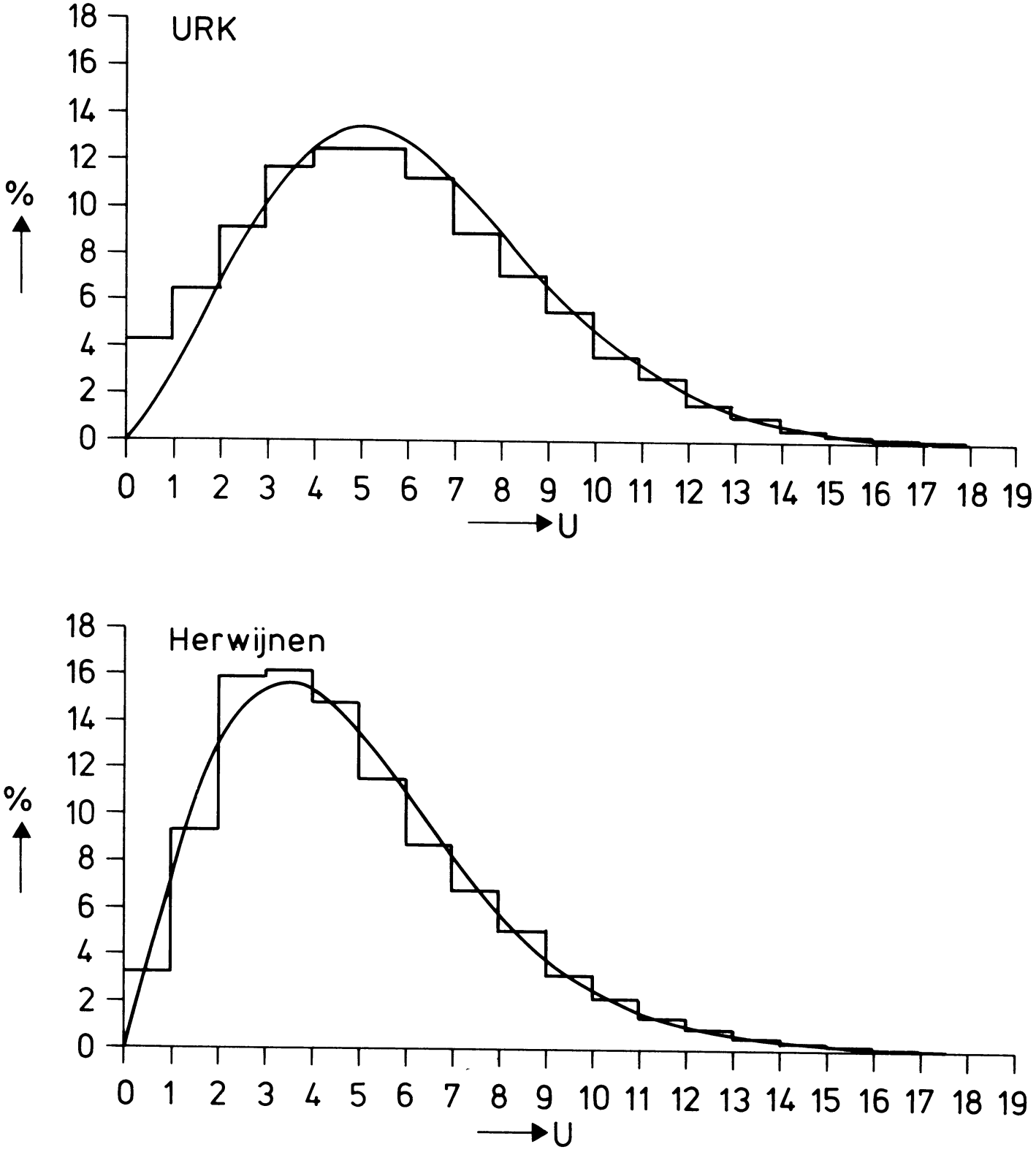


Fig. 18.1 Annual wind speed distribution functions as observed and as independently computed from the model at Urk and Herwijnen.

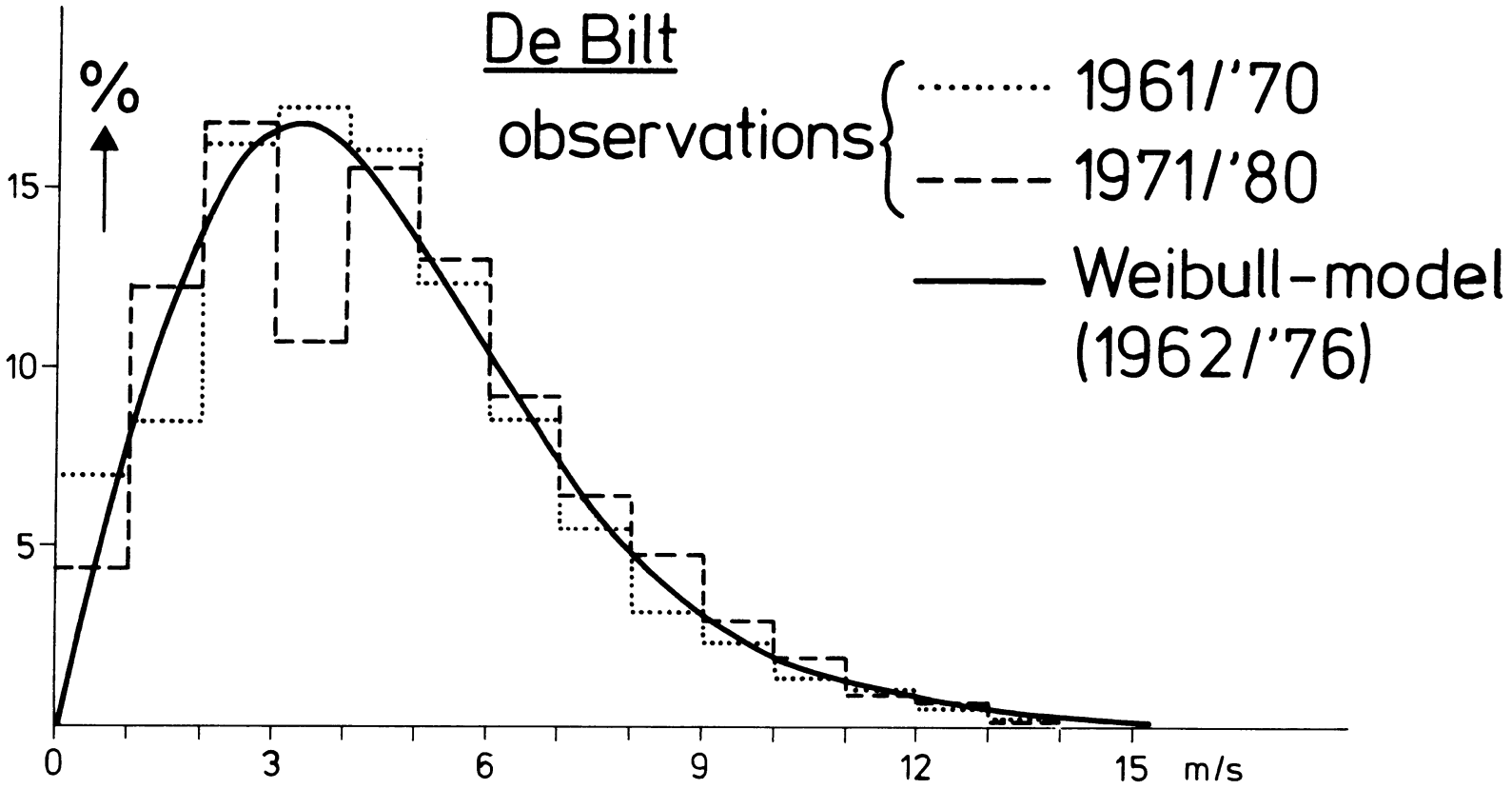


Fig. 18.2 Annual wind speed distribution functions as observed at De Bilt for two 10-year periods, and as independently computed from the model.

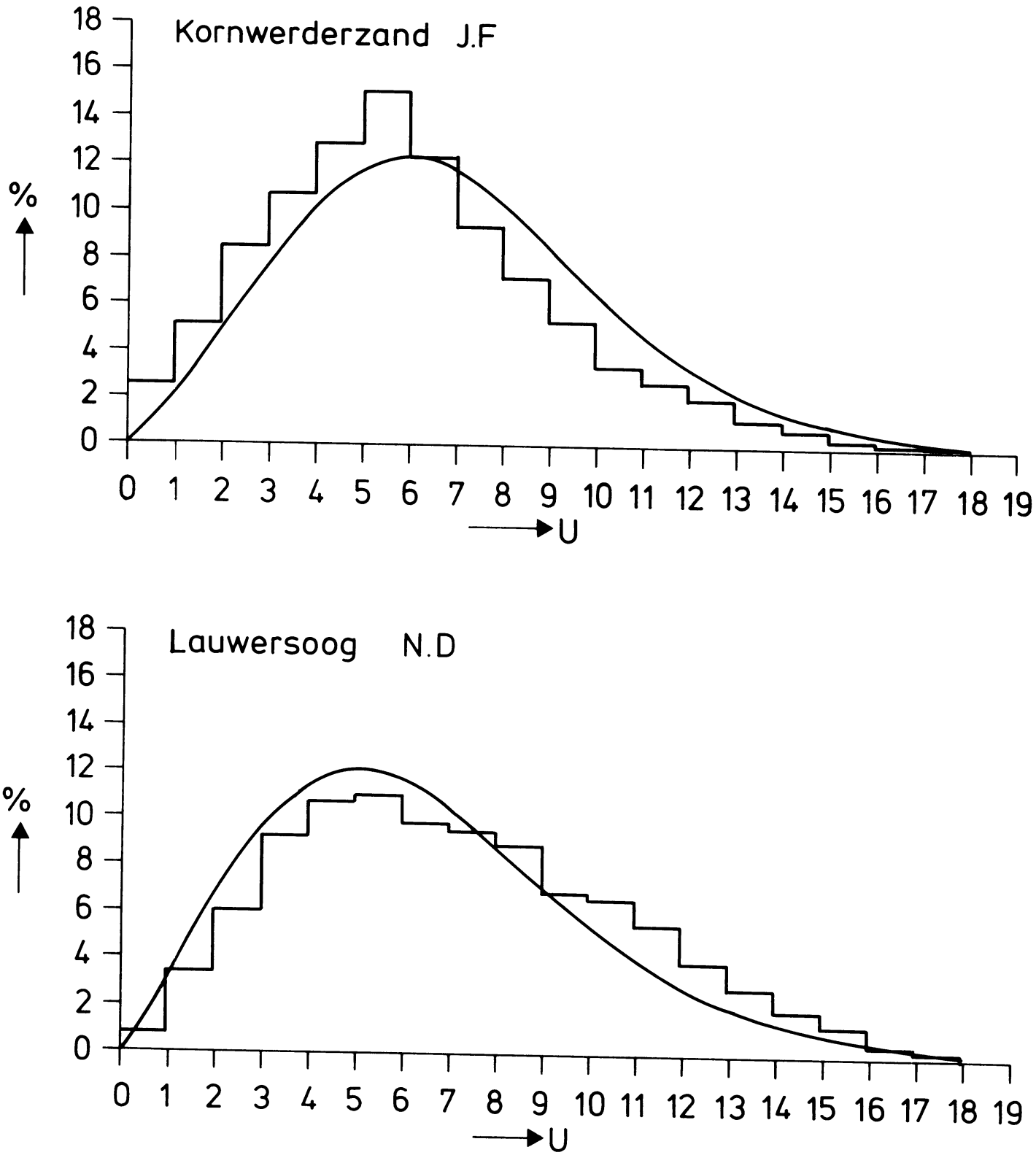


Fig. 18.3 Seasonal wind speed distribution functions as observed and as independently computed from the model at Kornwerderzand and Lauwersoog.

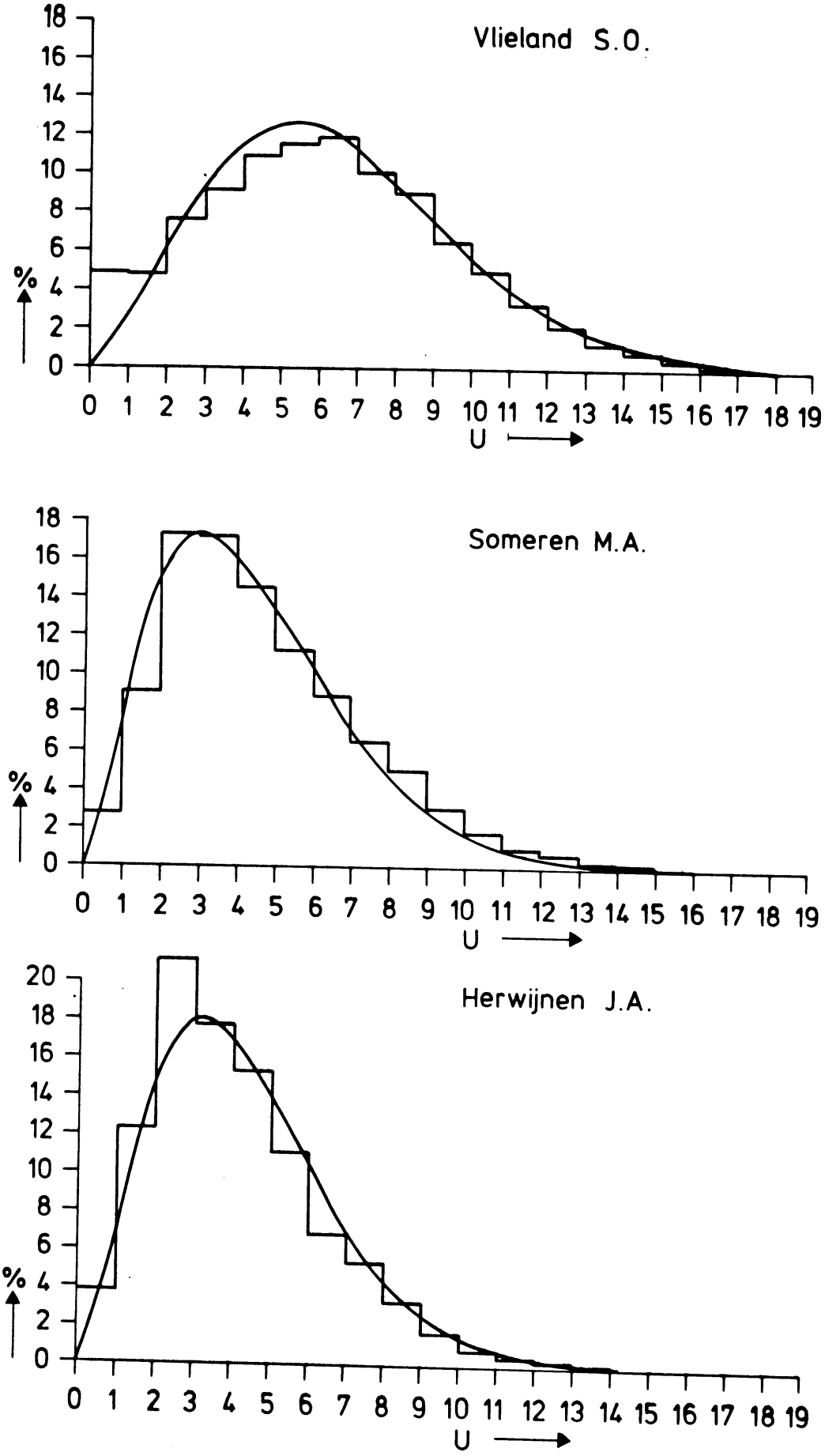


Fig. 18.4 Seasonal wind speed distribution functions as observed and as independently computed from the model at Vlieland, Someren and Herwijnen.

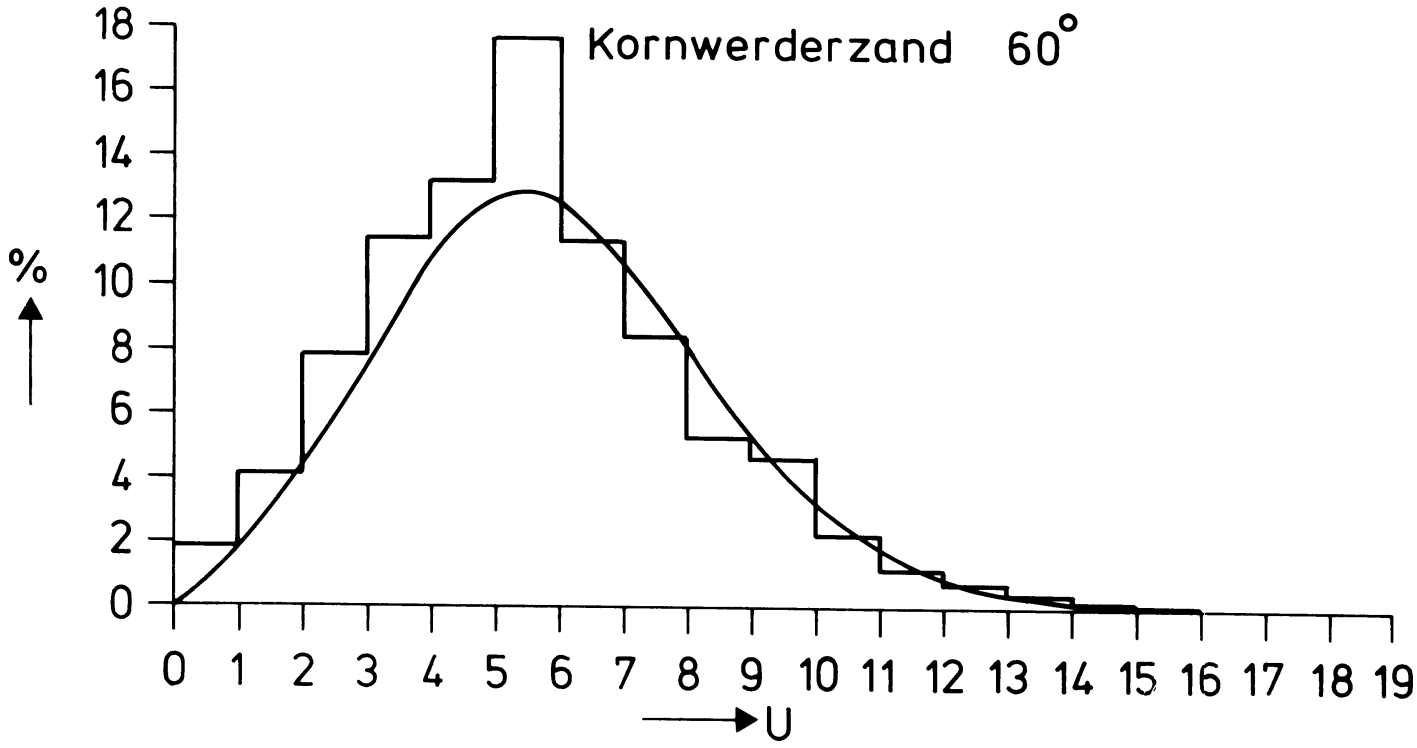


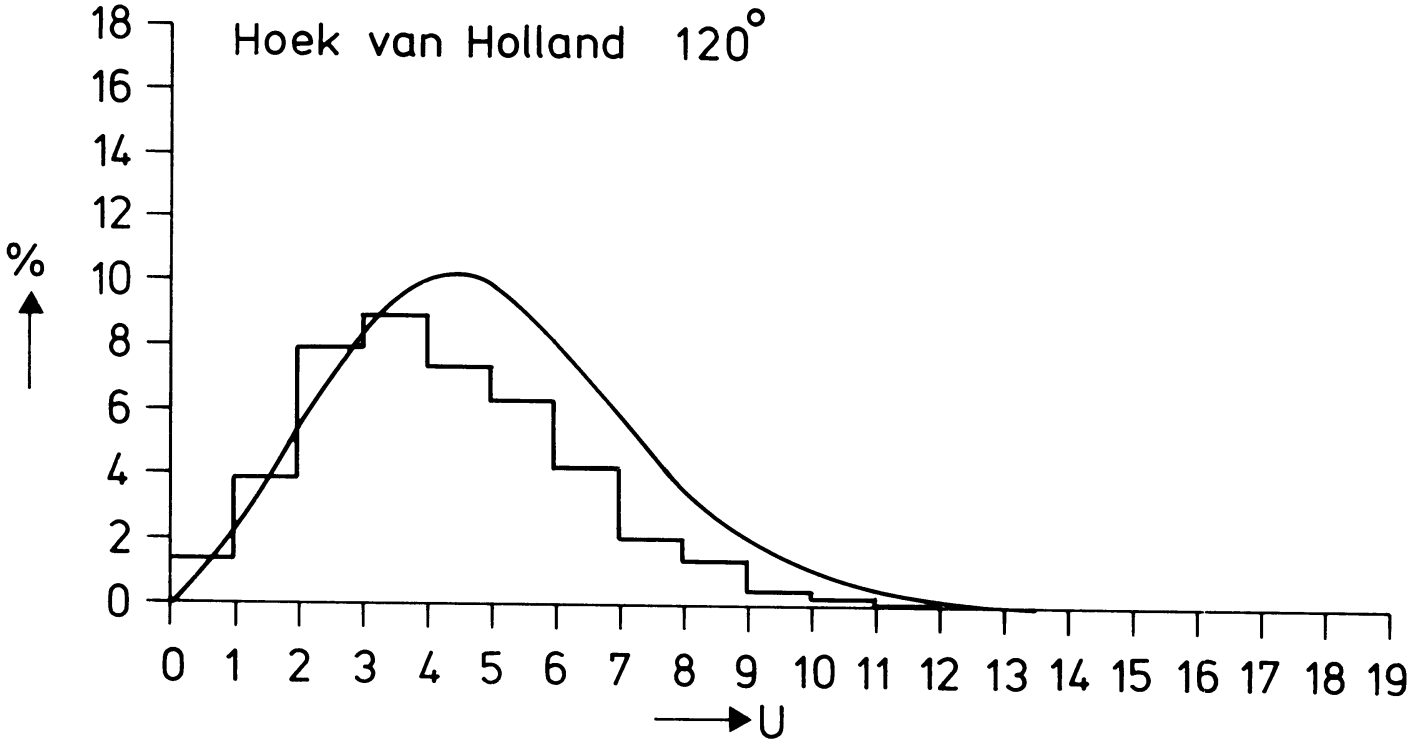


Fig. 18.5 Azimuth-sector wind speed distribution functions as observed and as independently computed from the model at Kornwerderzand and Hoek van Holland.

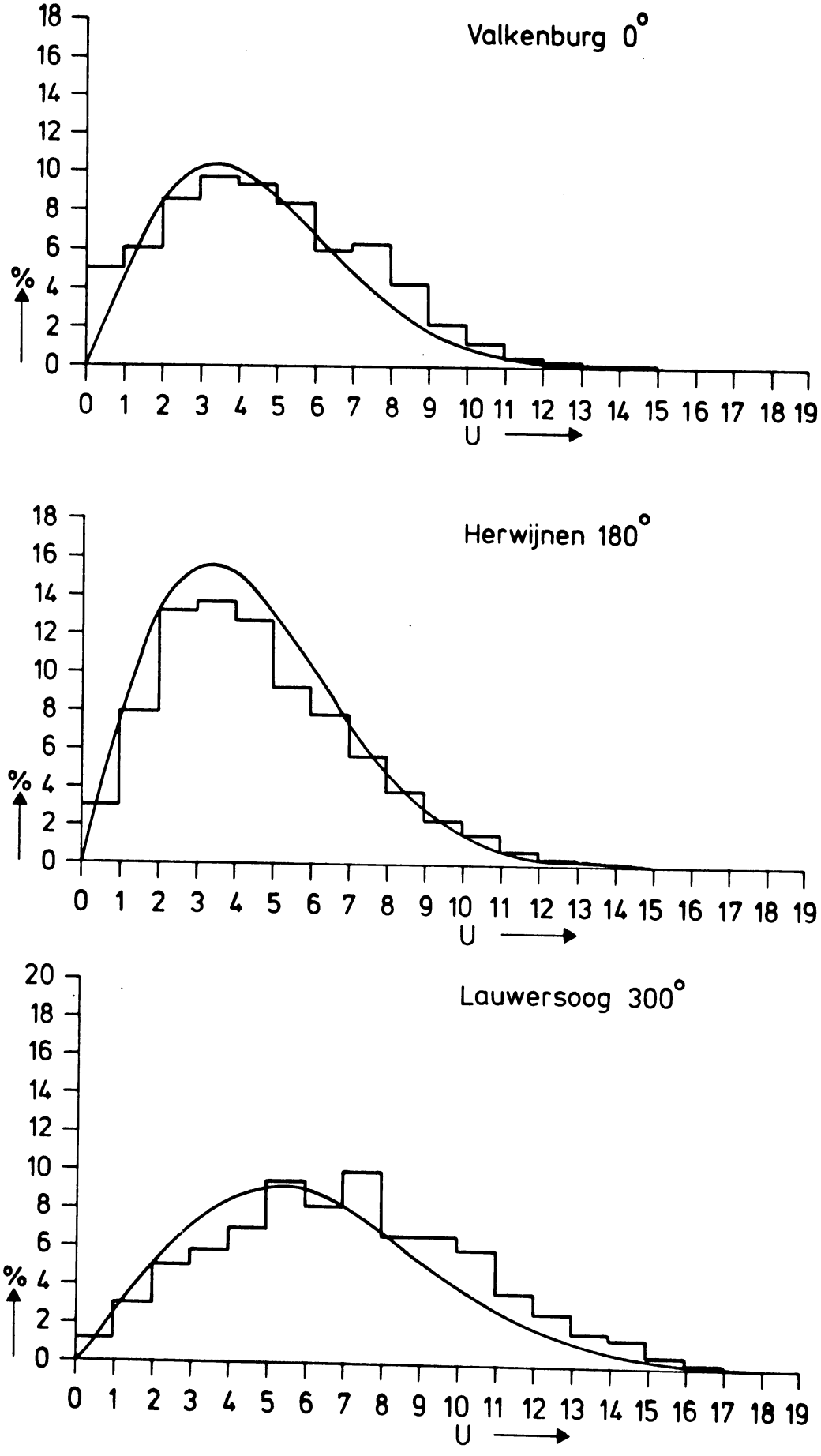


Fig. 18.6 Azimuth-sector wind speed distribution functions as observed and as independently computed from the model at Valkenburg, Herwijnen and Lauwersoog.

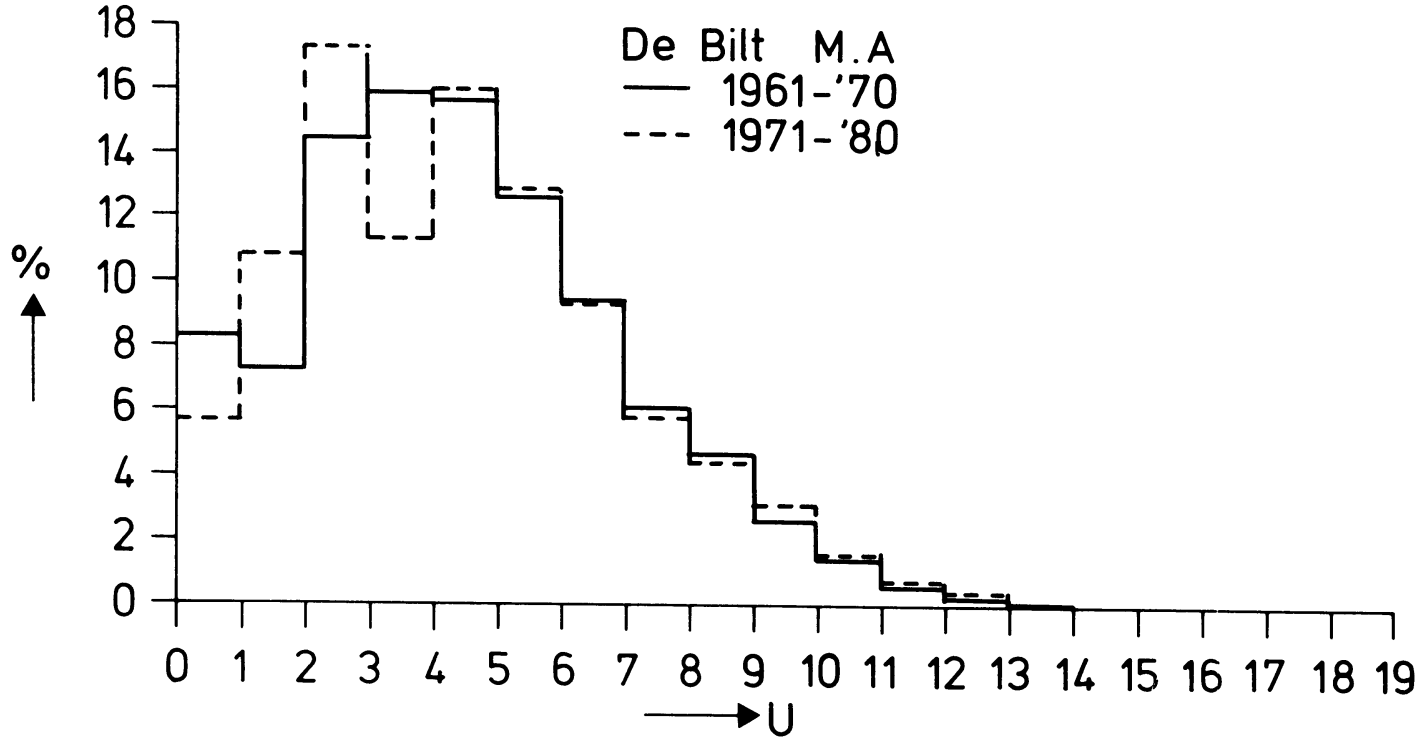


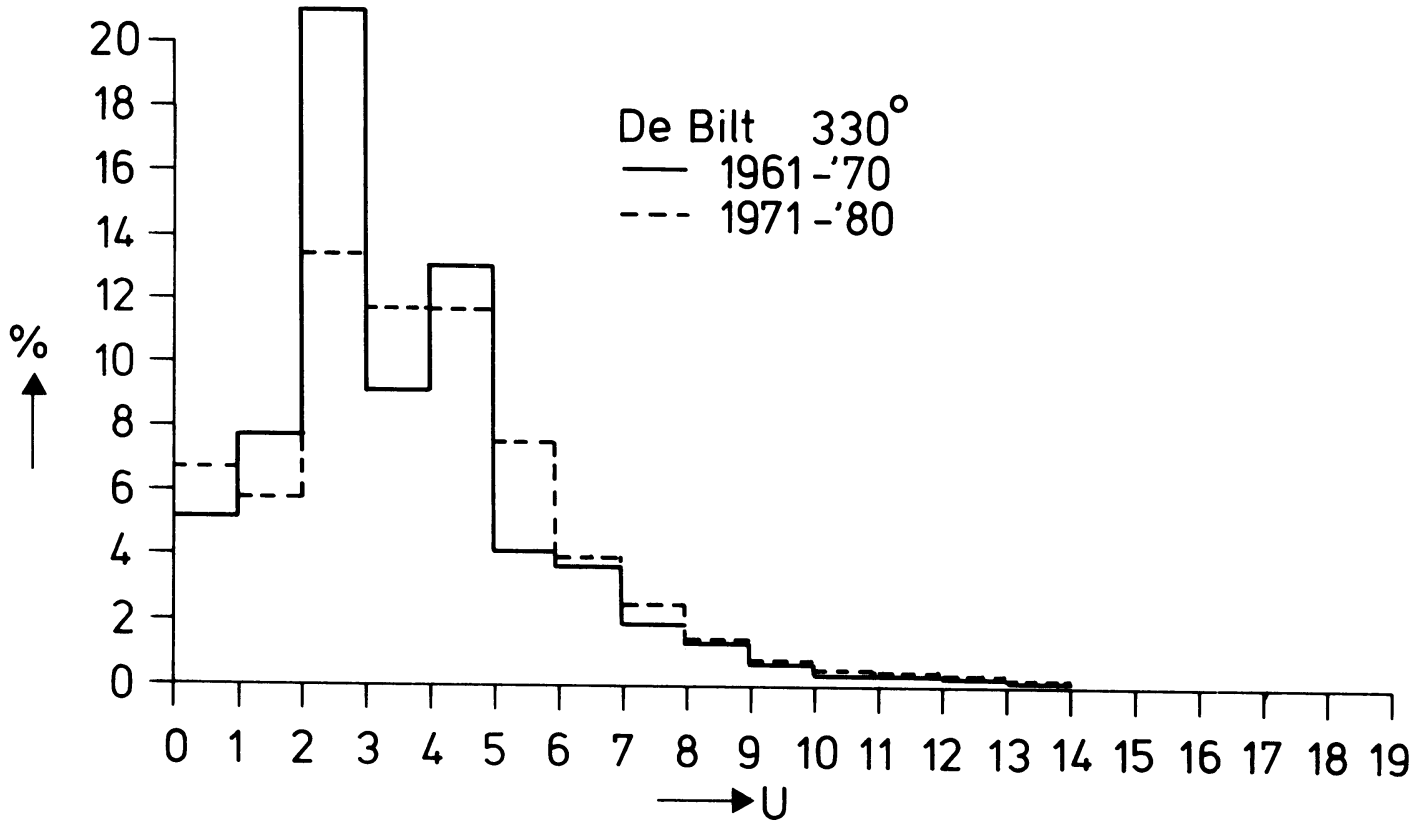


Fig. 18.7 Spring-seasonal and NW-azimuth-sector wind speed distribution functions as observed at De Bilt in two 10-year periods.

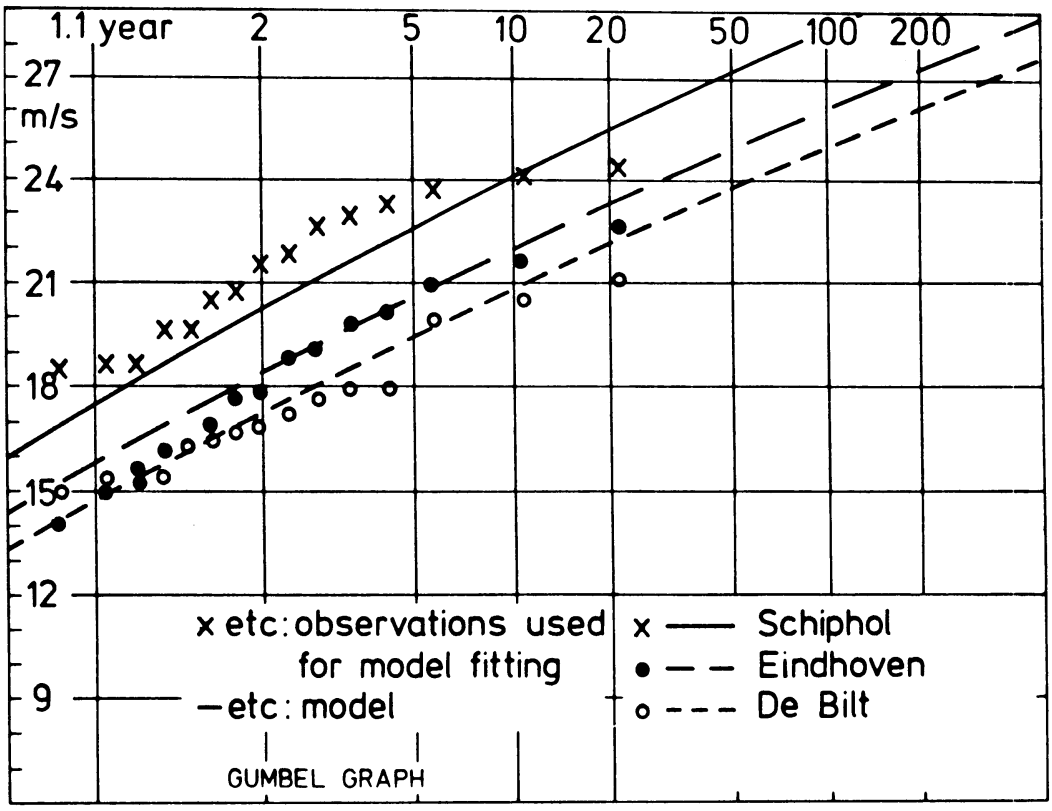


Fig. 19.1 Annual maximum hourly wind speed as observed and as obtained from the fitted model for Schiphol, Eindhoven and De Bilt.

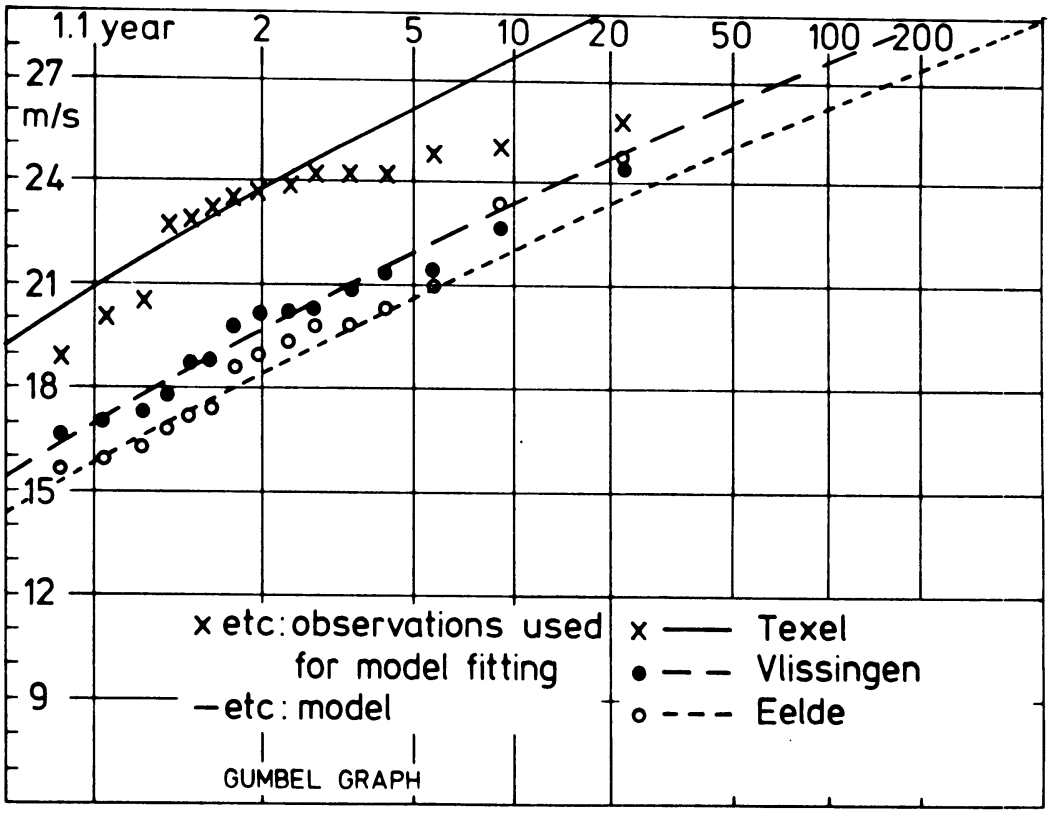


Fig. 19.2 Annual maximum hourly wind speed as observed and as obtained from the fitted model for Lightvessel Texel, Vlissingen and Eelde.

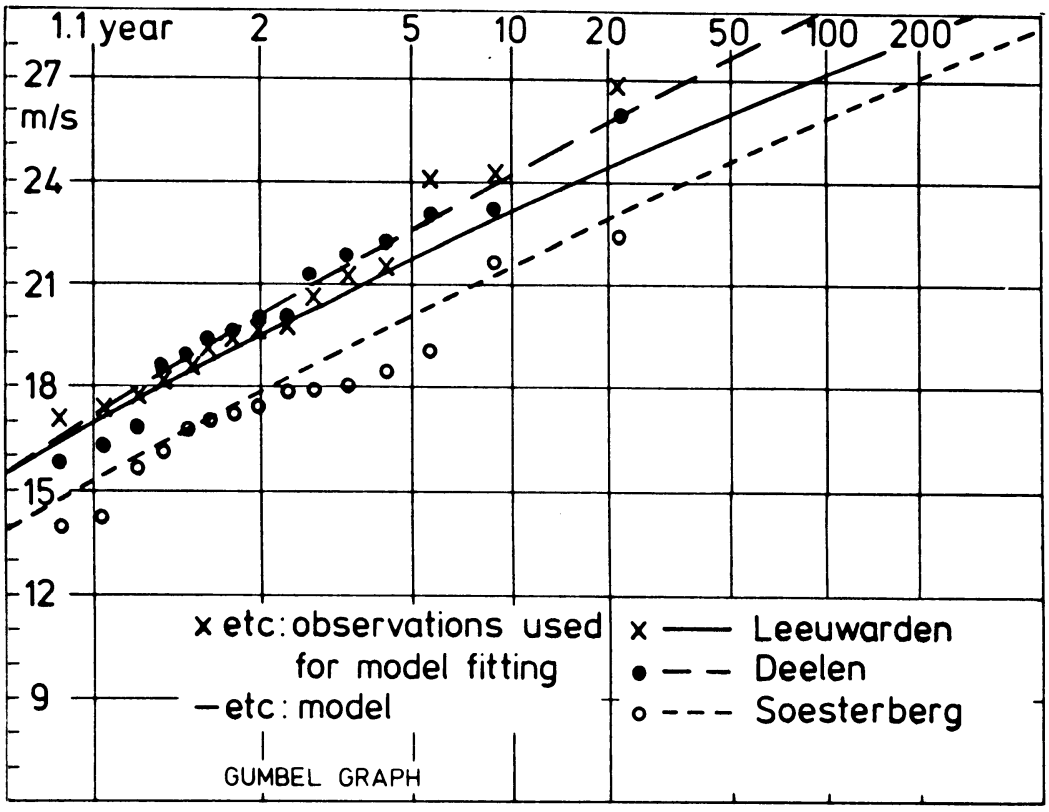


Fig. 19.3 Annual maximum hourly wind speed as observed and as obtained from the fitted model for Leeuwarden, Deelen and Soesterberg.

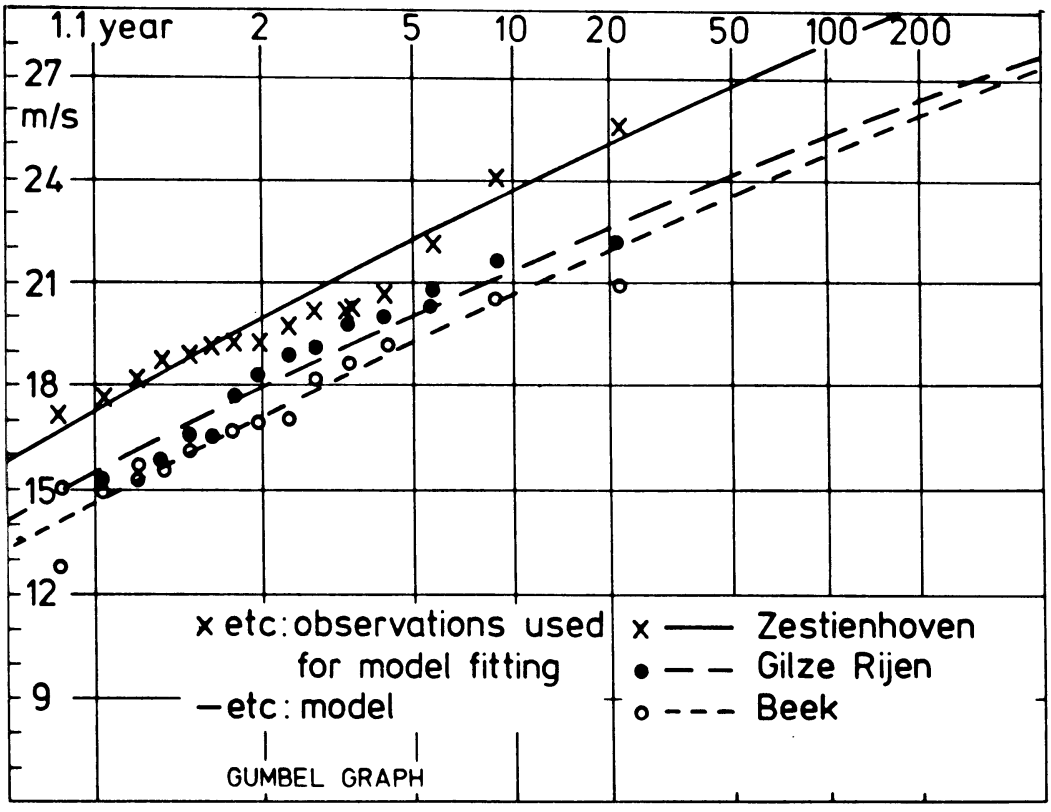


Fig. 19.4 Annual maximum hourly wind speed as observed and as obtained from the fitted model for Zestienhoven, Gilze Rijen and Beek.

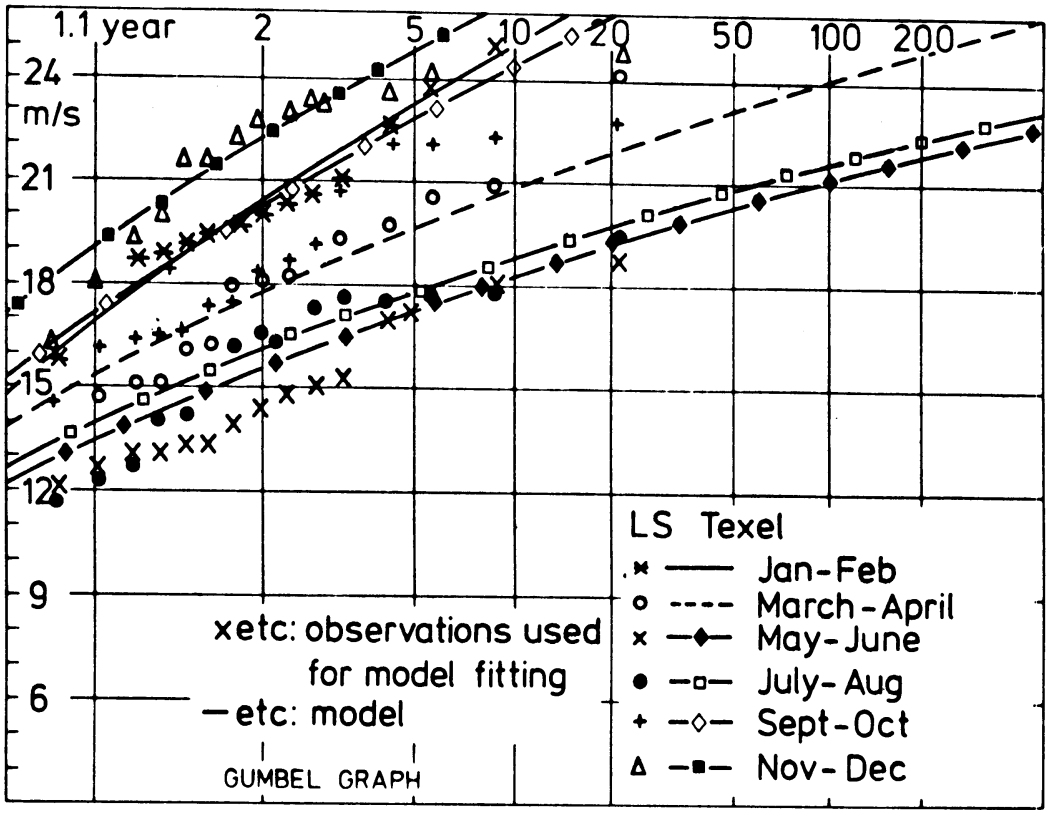


Fig. 19.5 Seasonal maximum hourly wind speed for successive years as observed and as obtained from the fitted model for Lightvessel Texel.

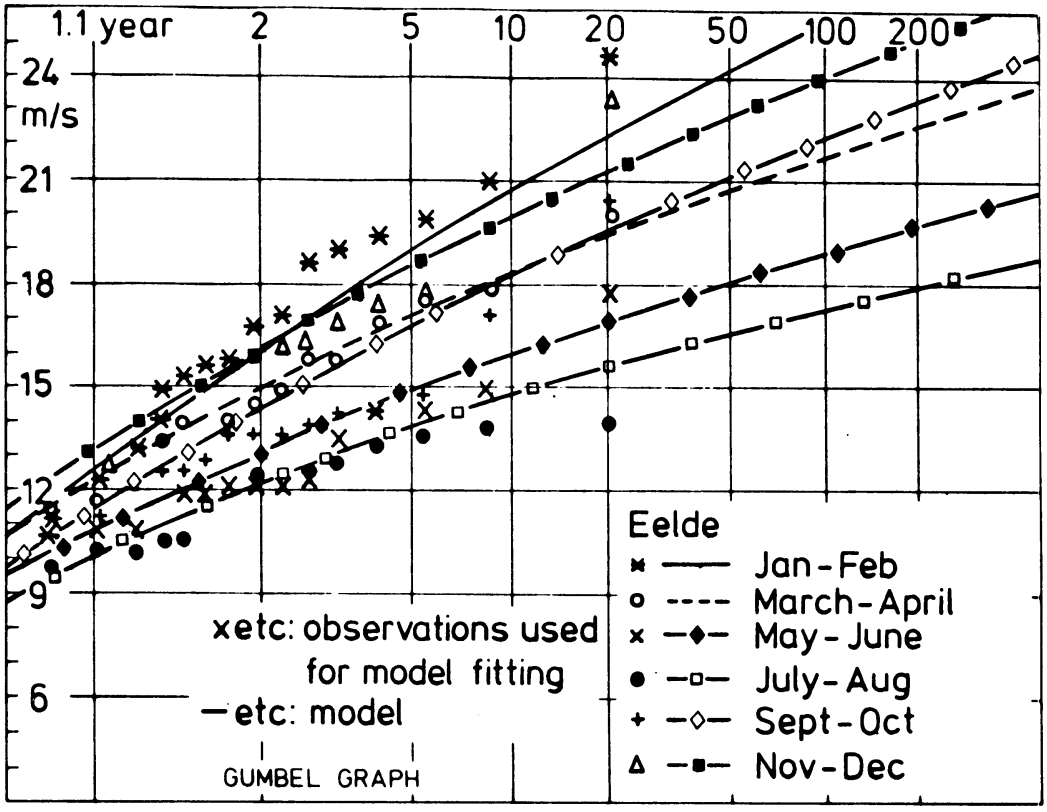


Fig. 19.6 Seasonal maximum hourly wind speed for successive years as observed and as obtained from the fitted model for Eelde.

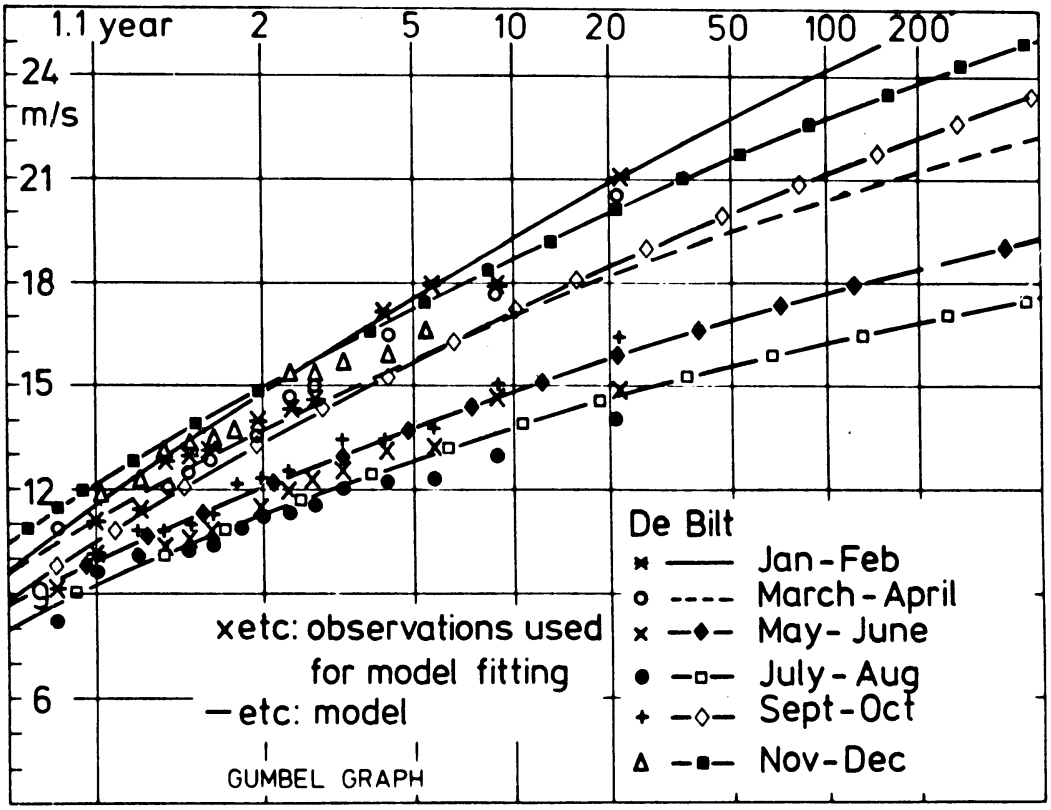


Fig. 19.7 Seasonal maximum hourly wind speed for successive years as observed and as obtained from the fitted model for De Bilt.

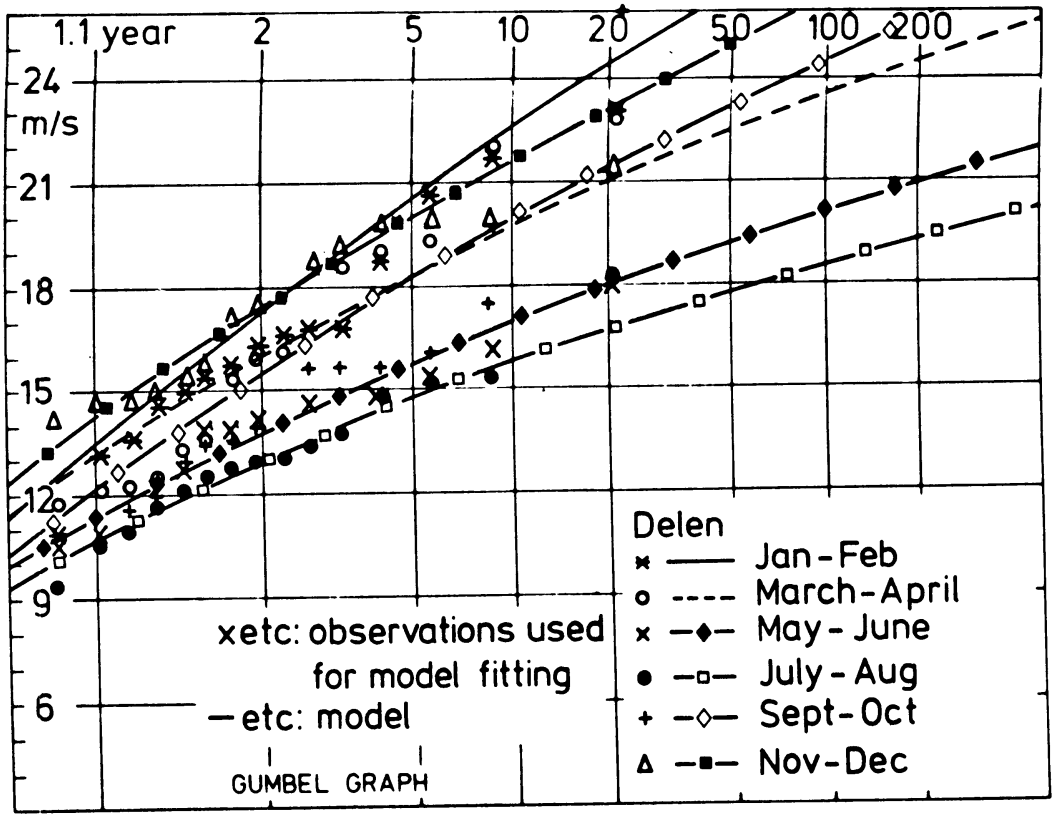


Fig. 19.8 Seasonal maximum hourly wind speed for successive years as observed and as obtained from the fitted model for Deelen.

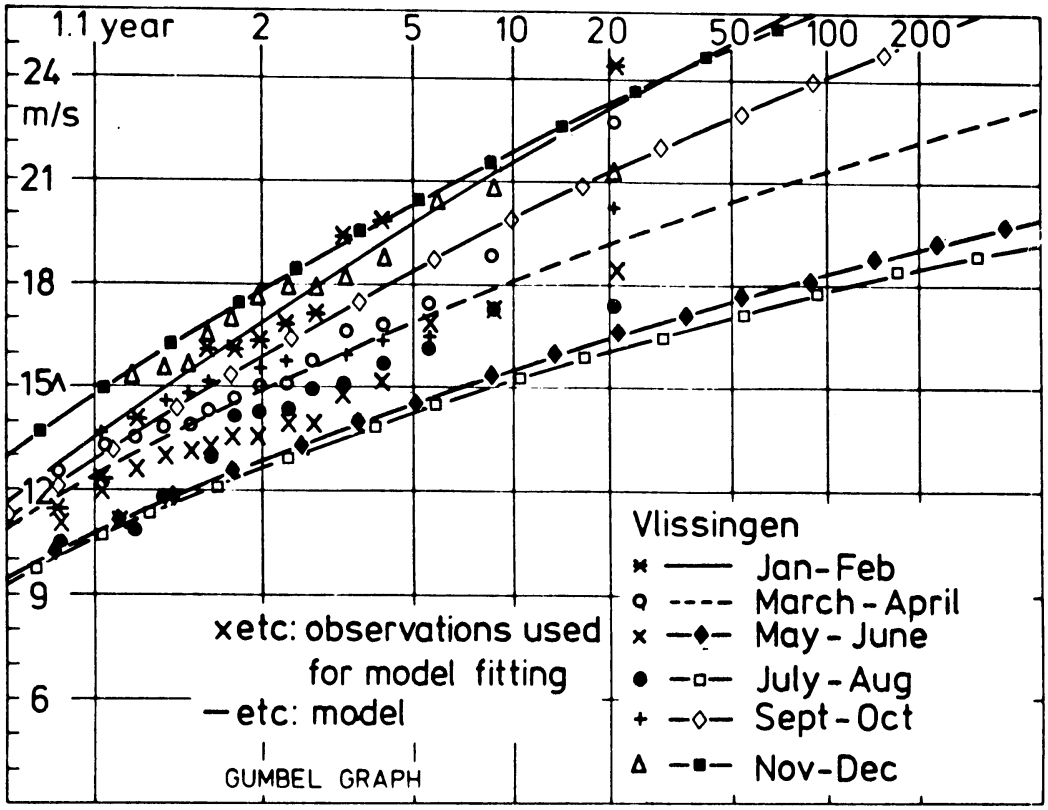


Fig. 19.9 Seasonal maximum hourly wind speed for successive years as observed and as obtained from the fitted model for Vlissingen.

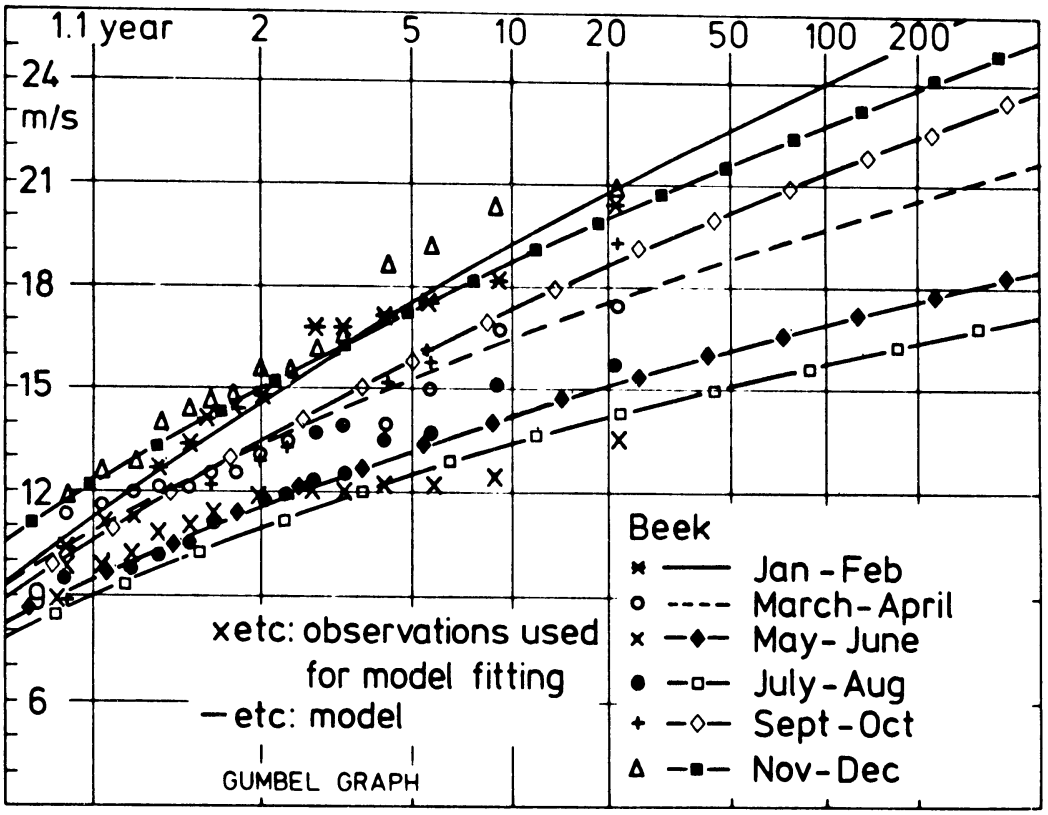


Fig. 19.10 Seasonal maximum hourly wind speed for successive years as observed and as obtained from the fitted model for Beek.

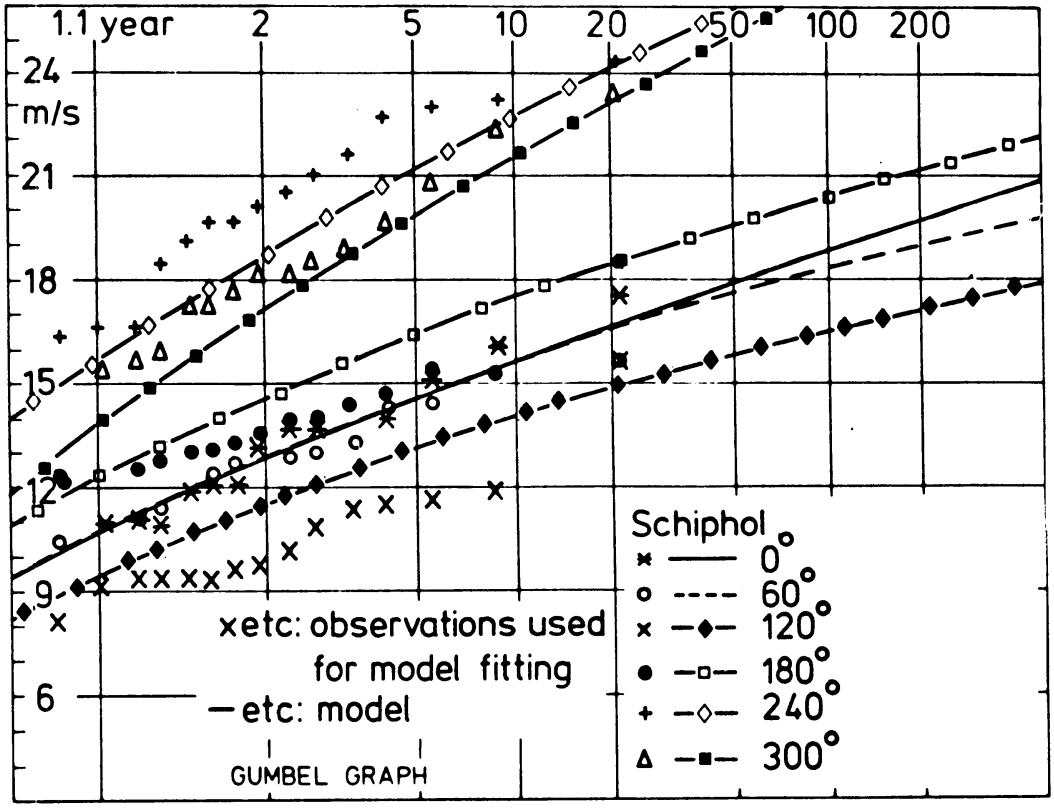


Fig. 19.11 Annual azimuth-sector maximum hourly wind speed as observed and as obtained from the fitted model for Schiphol.

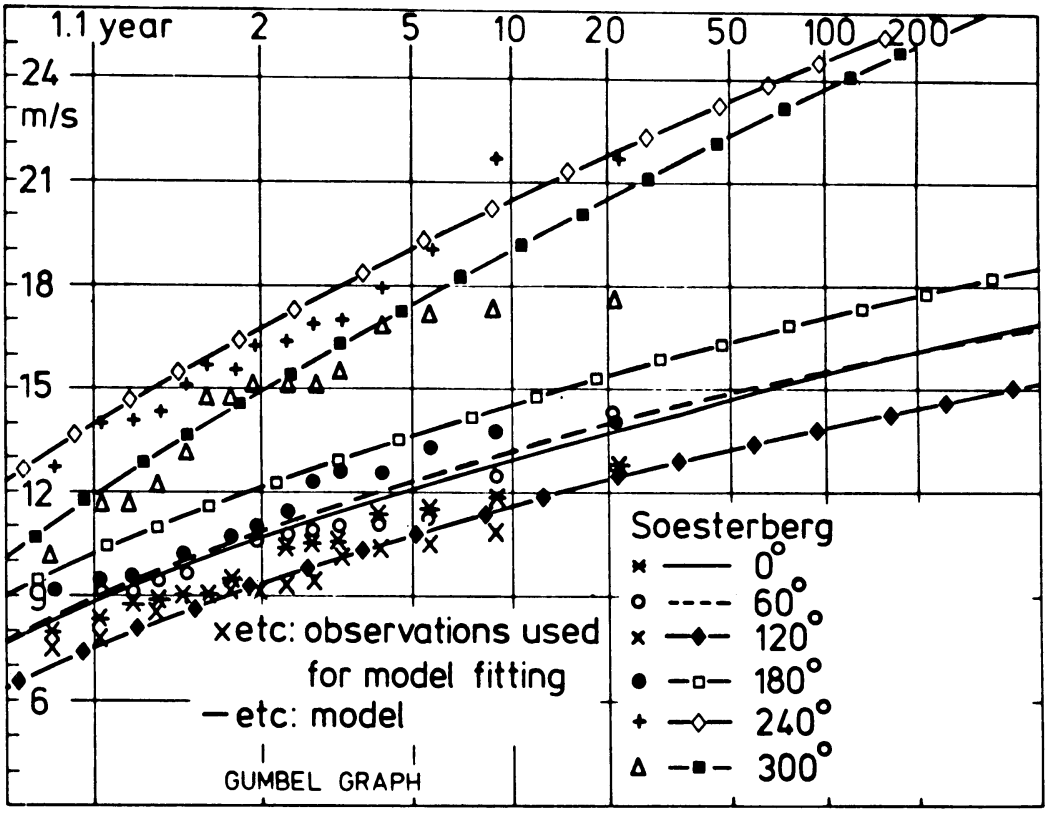


Fig. 19.12 Annual azimuth-sector maximum hourly wind speed as observed and as obtained from the fitted model for Soesterberg.

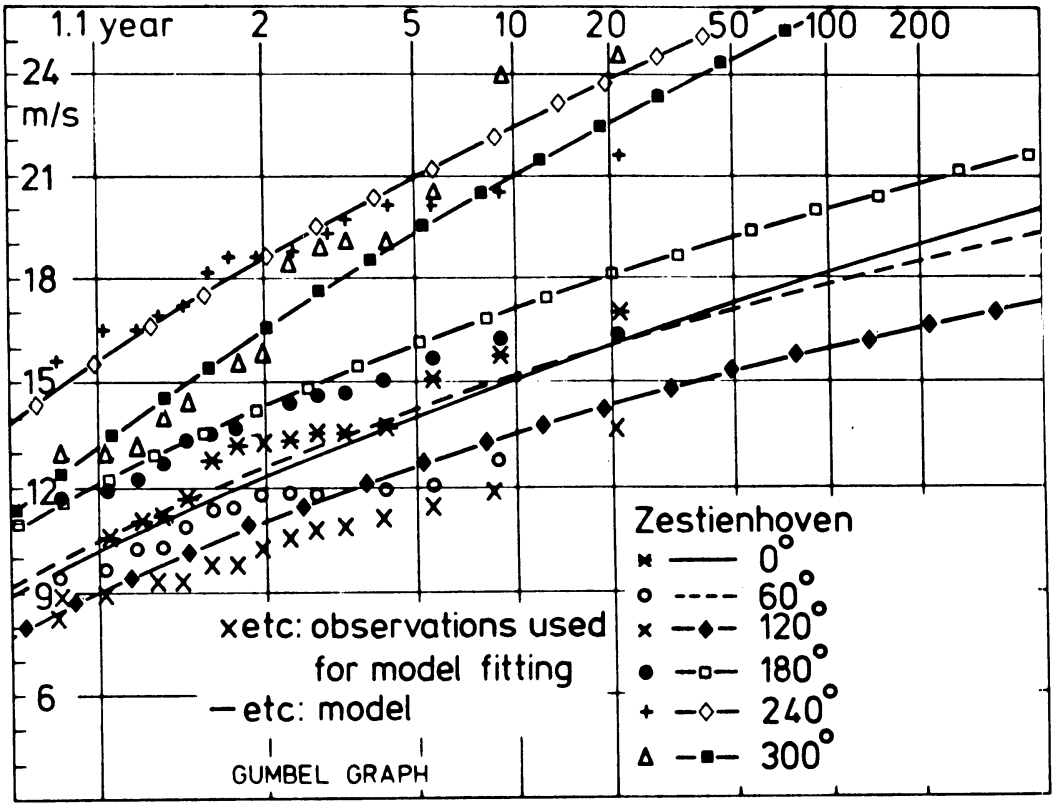


Fig. 19.13 Annual azimuth-sector maximum hourly wind speed as observed and as obtained from the fitted model for Zestienhoven.

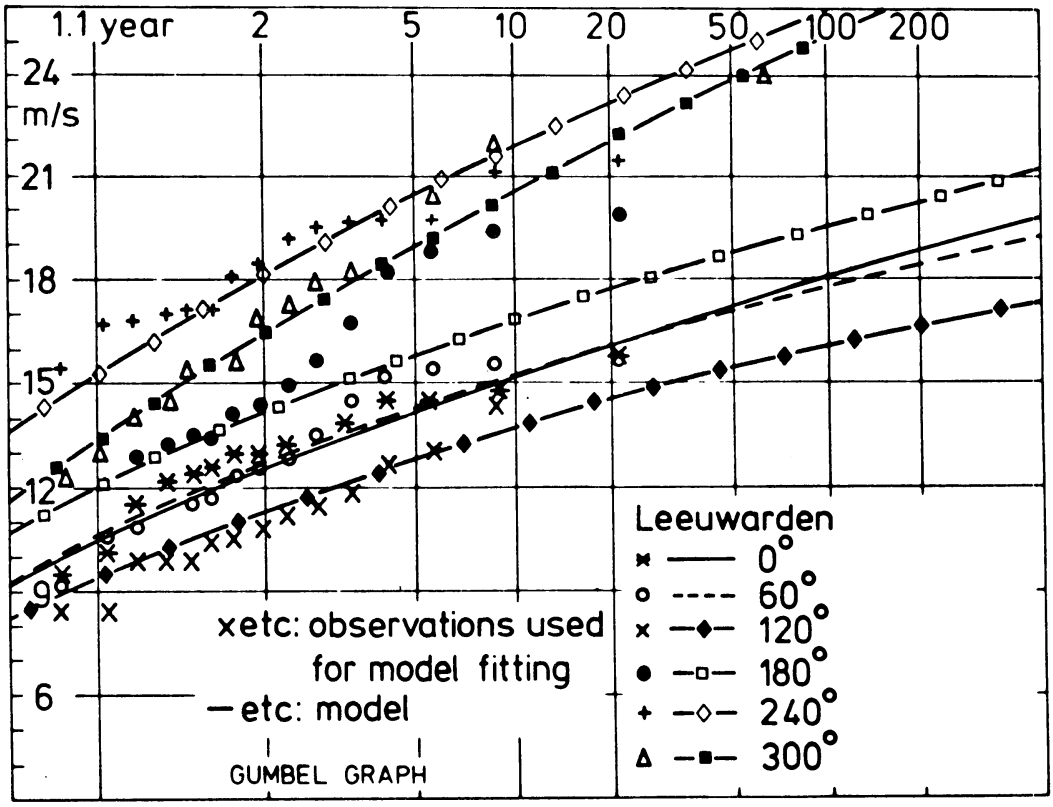


Fig. 19.14 Annual azimuth-sector maximum hourly wind speed as observed and as obtained from the fitted model for Leeuwarden.

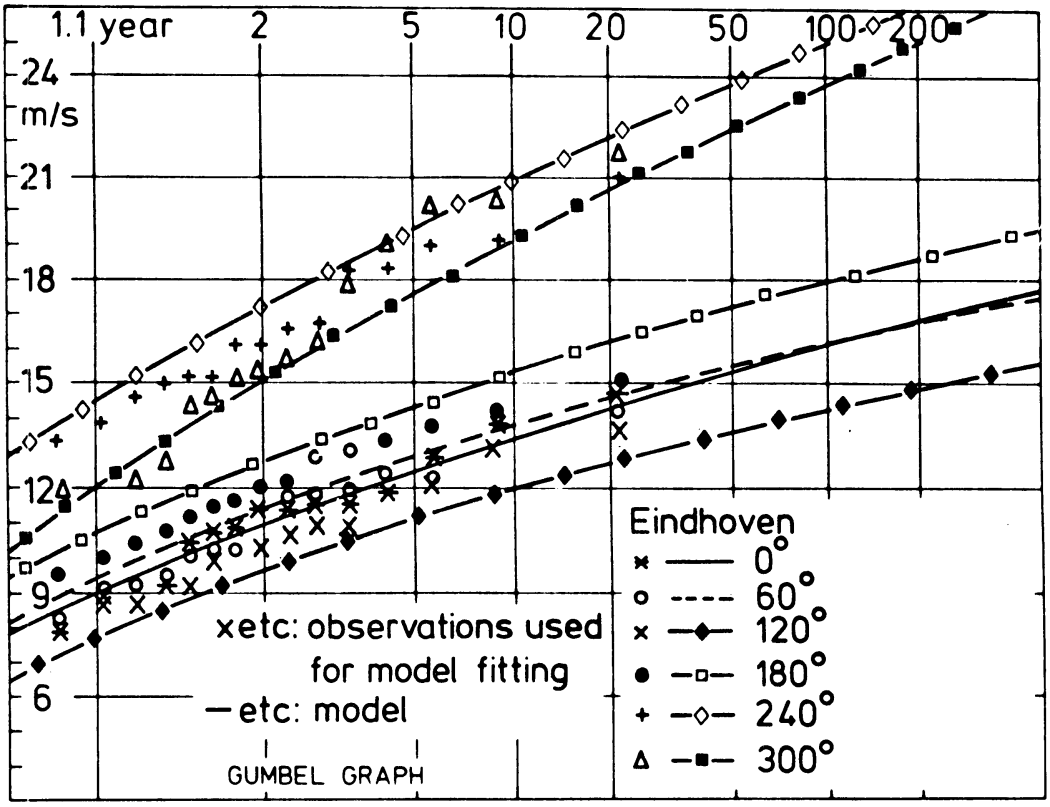


Fig. 19.15 Annual azimuth-sector maximum hourly wind speed as observed and as obtained from the fitted model for Eindhoven.

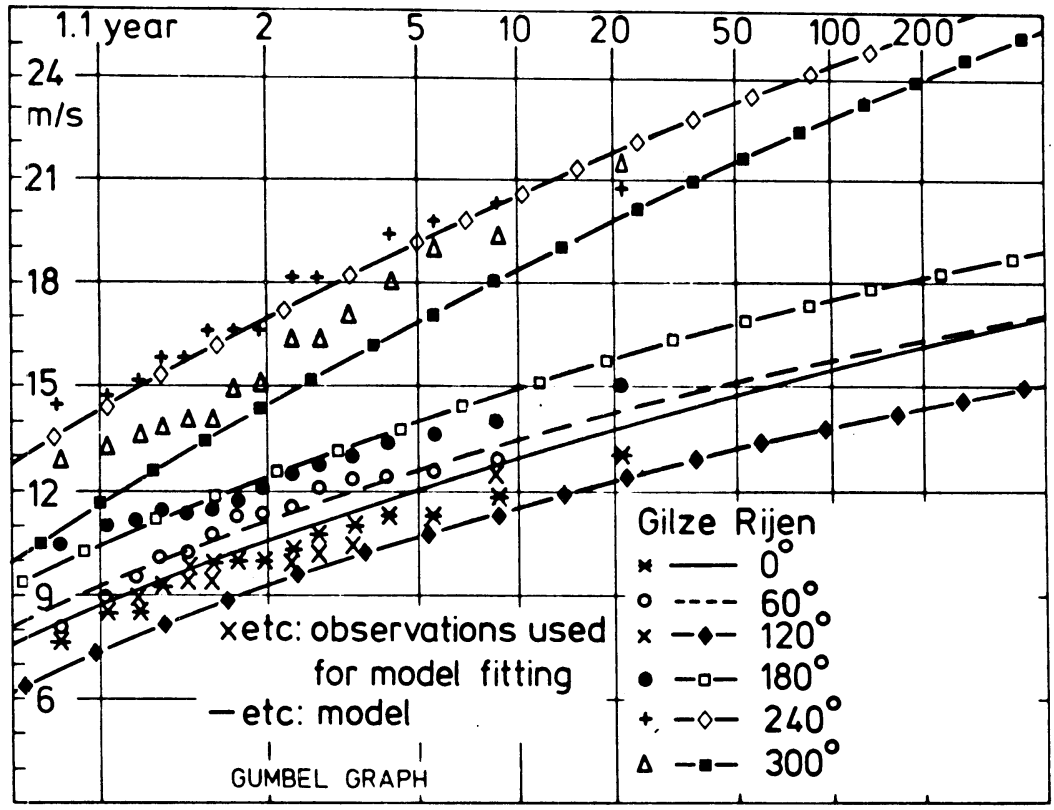


Fig. 19.16 Annual azimuth-sector maximum hourly wind speed as observed and as obtained from the fitted model for Gilze-Rijen.

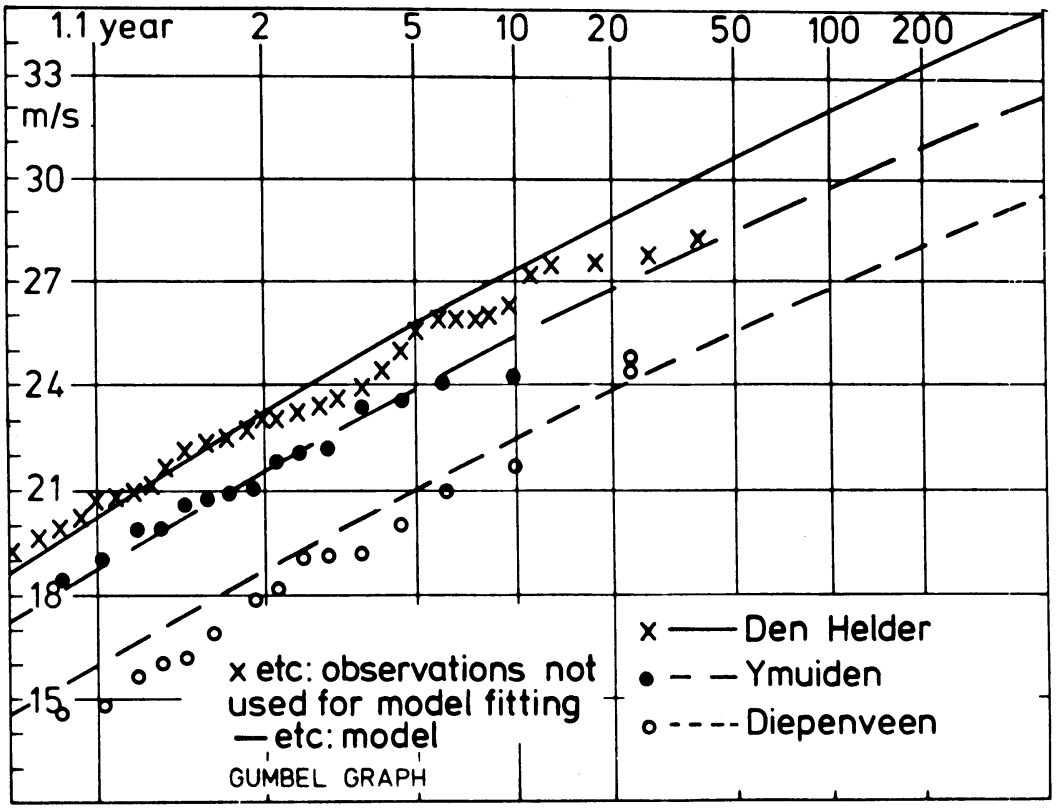


Fig. 20.1 Annual maximum hourly wind speed for Den Helder, IJmuiden and Diepenveen as observed and as computed from the model independent of these observations.

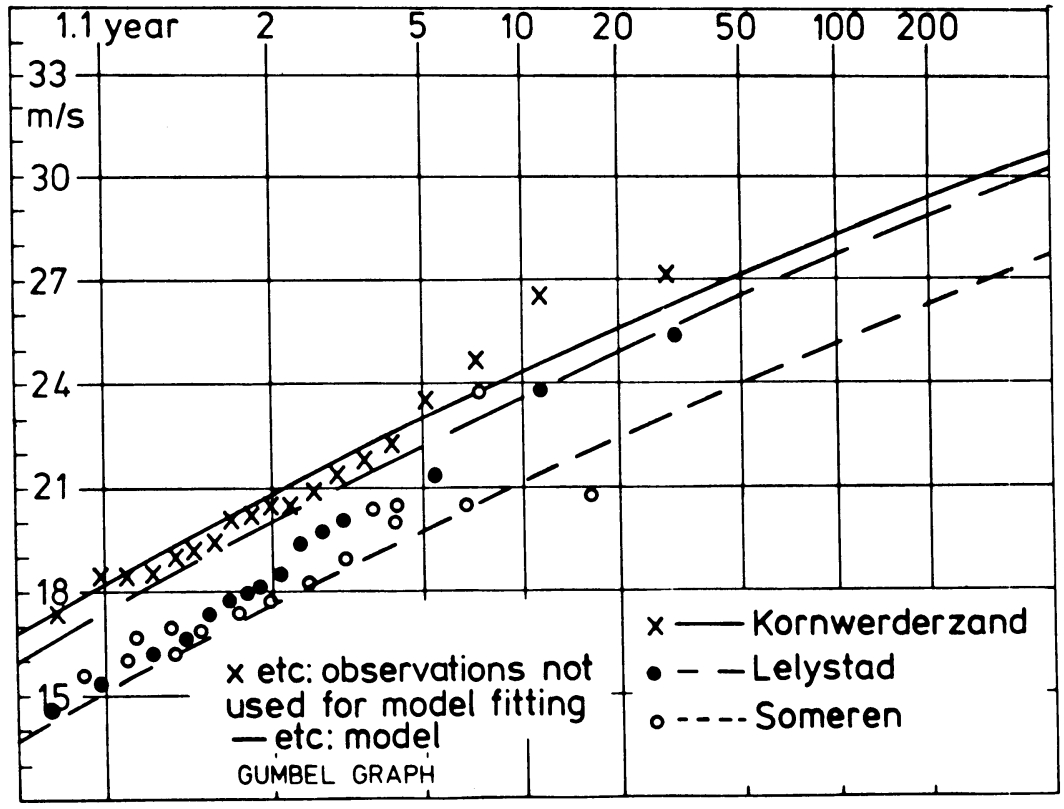


Fig. 20.2 Annual maximum hourly wind speed for Kornwerderzand, Lelystad and Someren as observed and as computed from the model independent of these observations.

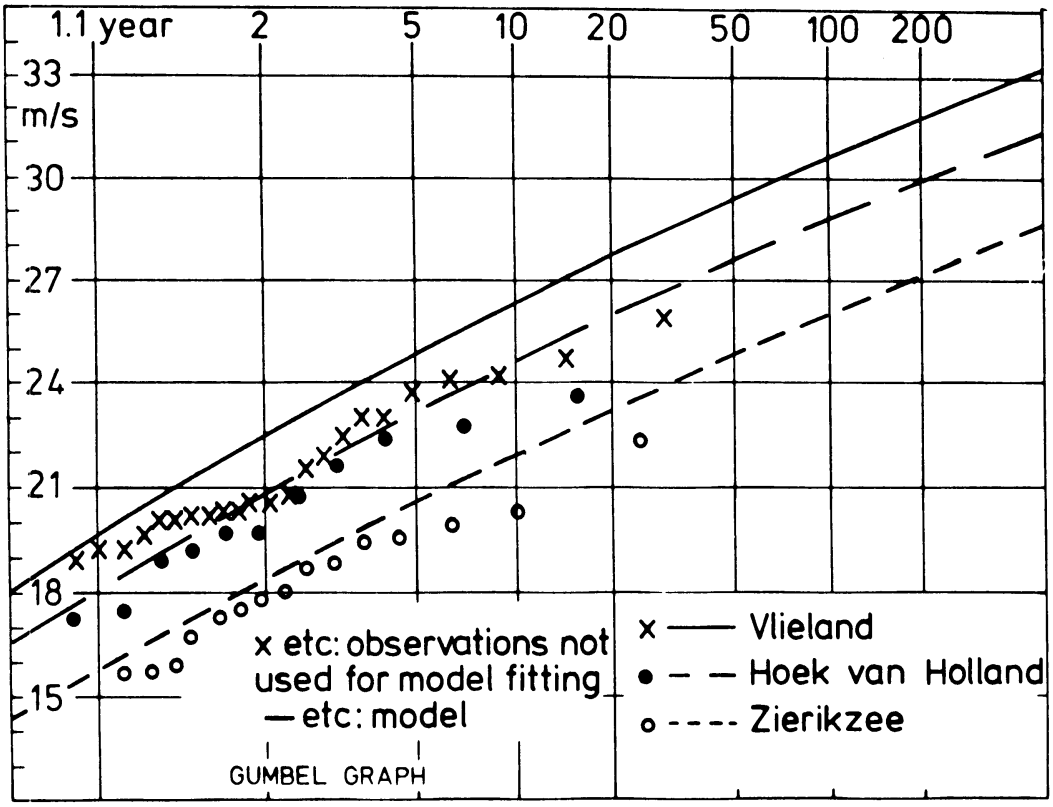


Fig. 20.3 Annual maximum hourly wind speed for Vlieland, Hoek van Holland and Zierikzee as observed and as computed from the model independent of these observations.

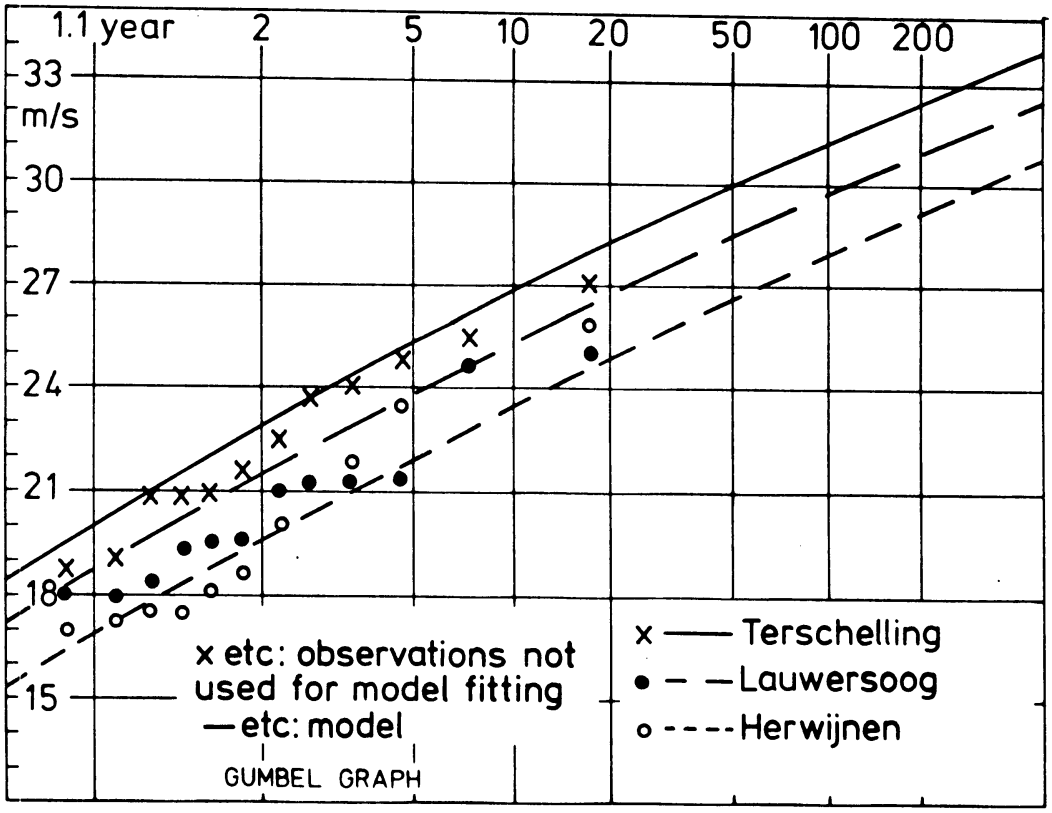


Fig. 20.4 Annual maximum hourly wind speed for Terschelling, Lauwersoog and Herwijnen as observed and as computed from the model independent of these observations.

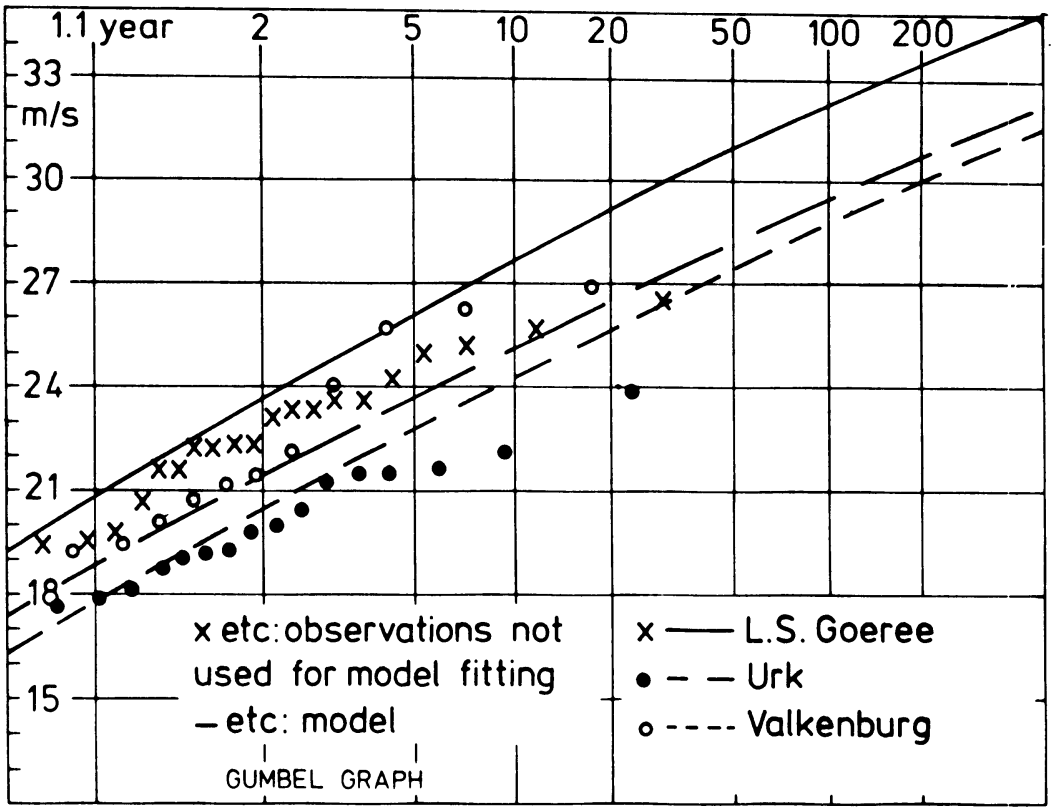


Fig. 20.5 Annual maximum hourly wind speed for Lightvessel Goeree, Urk and Valkenburg as observed and as computed from the model independent of these observations.

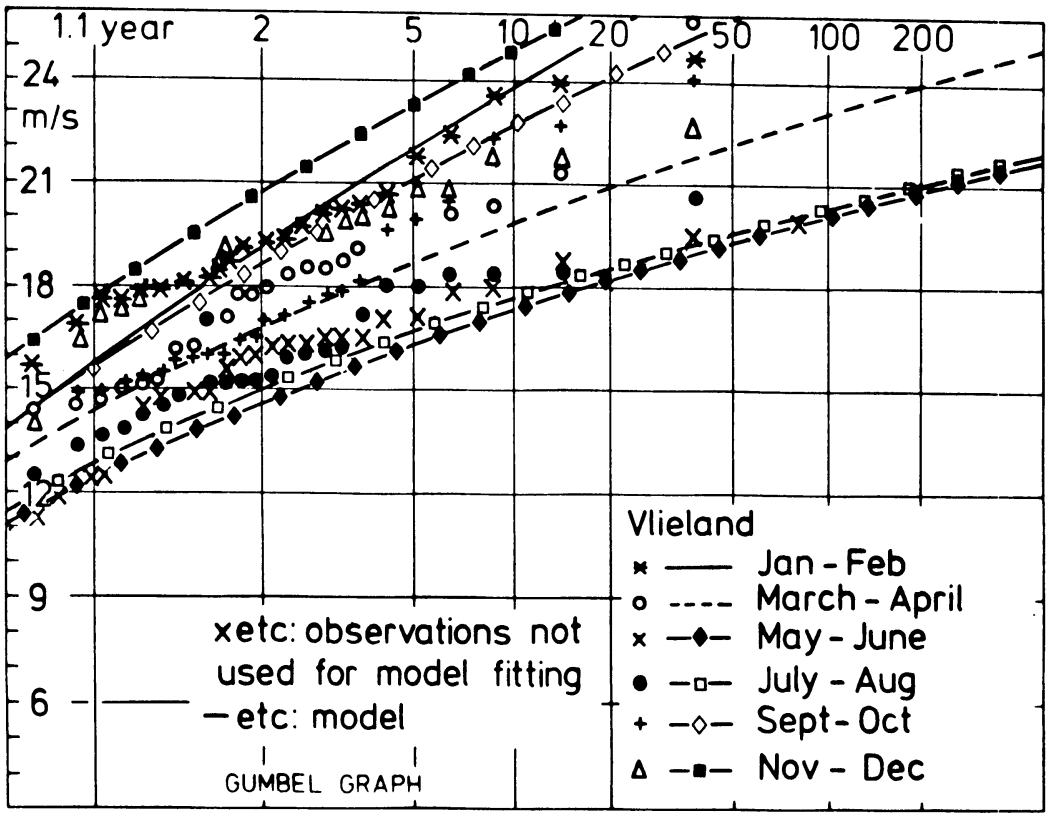


Fig. 20.6 Seasonal maximum hourly wind speed in successive years for Vlieland as observed and as computed from the model independent of these observations.

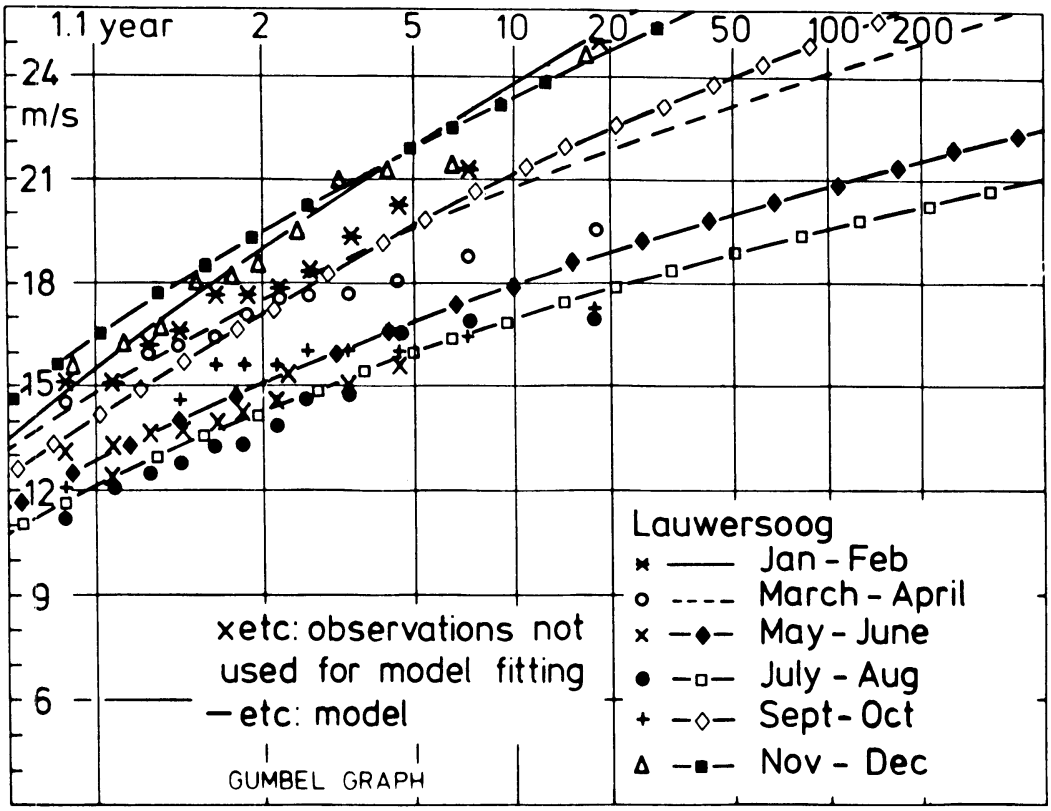


Fig. 20.7 Seasonal maximum hourly wind speed in successive years for Lauwersoog as observed and as computed from the model independent of these observations.

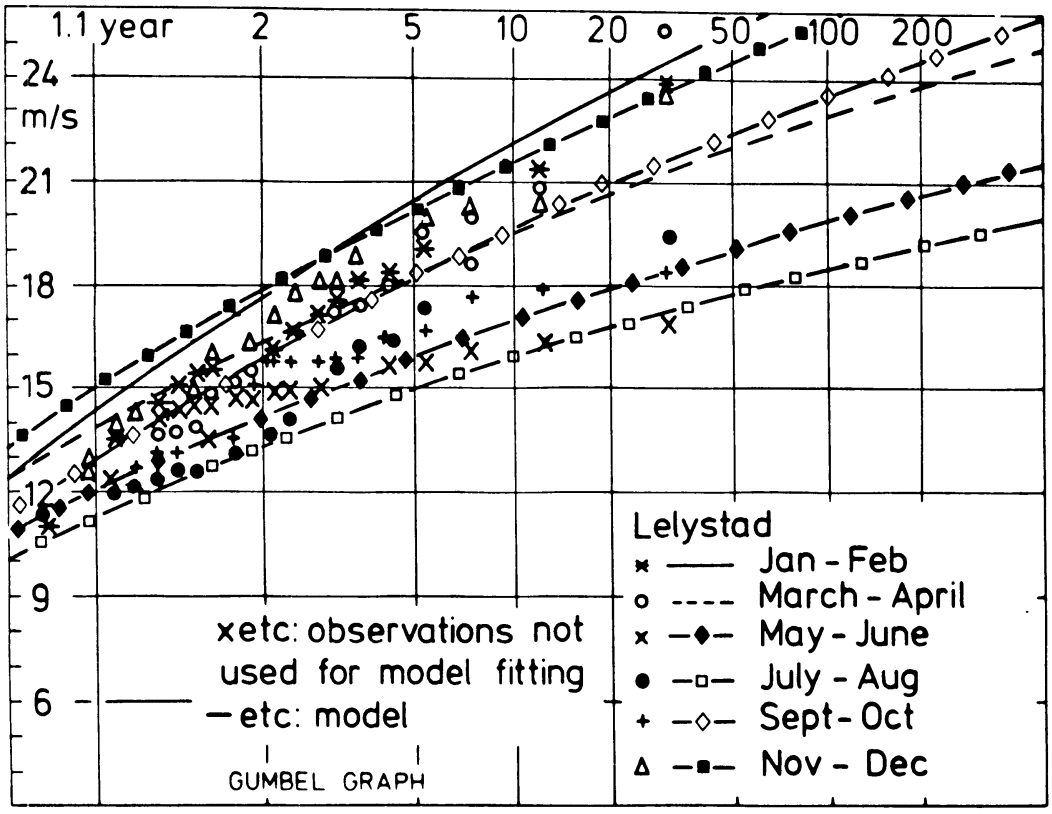


Fig. 20.8 Seasonal maximum hourly wind speed in successive years for Lelystad as observed and as computed from the model independent of these observations.

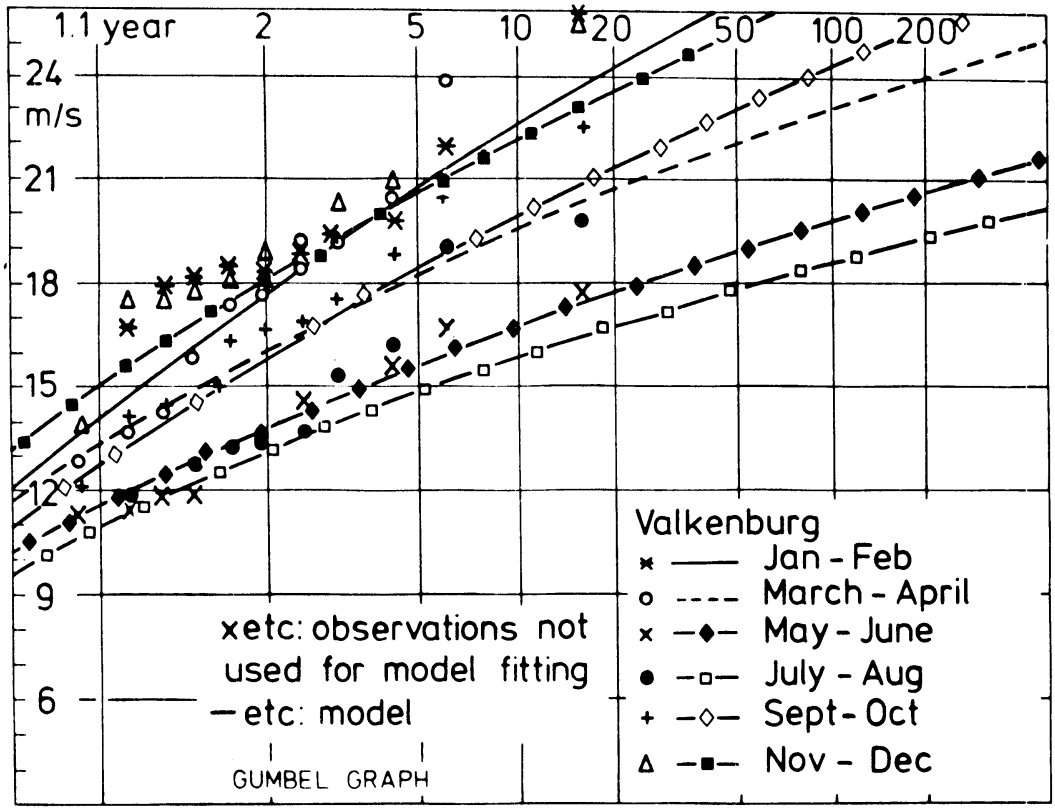


Fig. 20.9 Seasonal maximum hourly wind speed in successive years for Valkenburg as observed and as computed from the model independent of these observations.

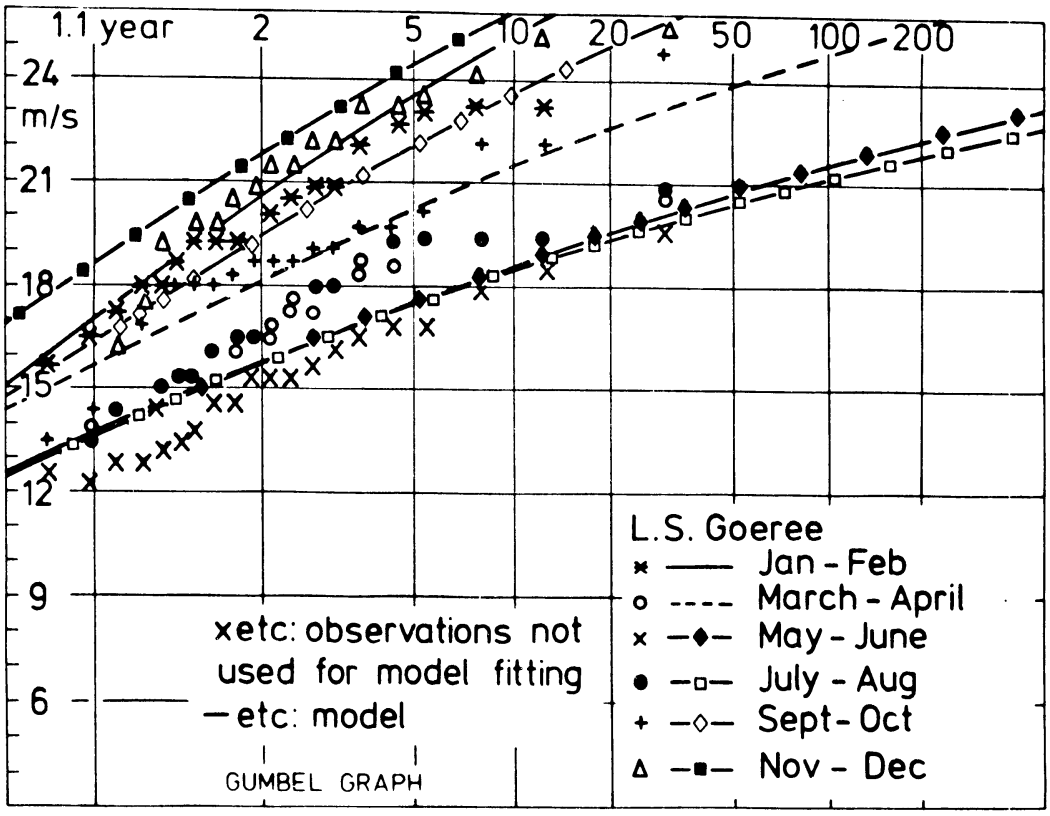


Fig. 20.10 Seasonal maximum hourly wind speed in successive years for Lightvessel Goeree as observed and as computed from the model independent of these observations.

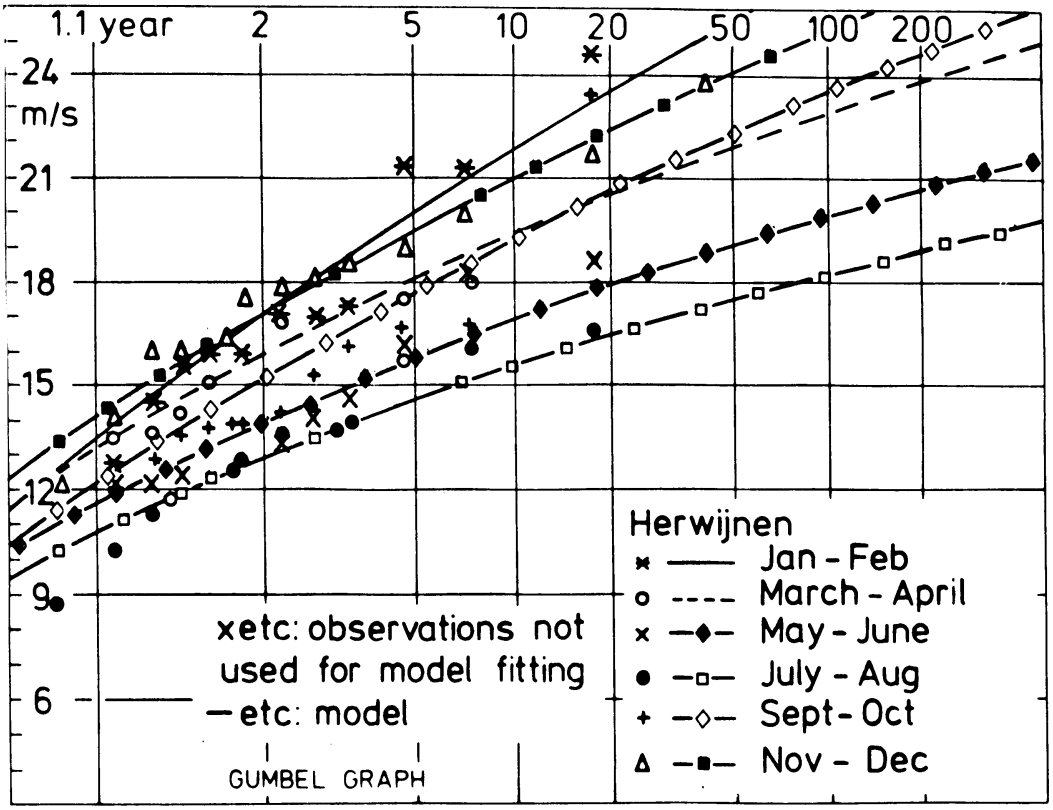


Fig. 20.11 Seasonal maximum hourly wind speed in successive years for Herwijnen as observed and as computed from the model independent of these observations.

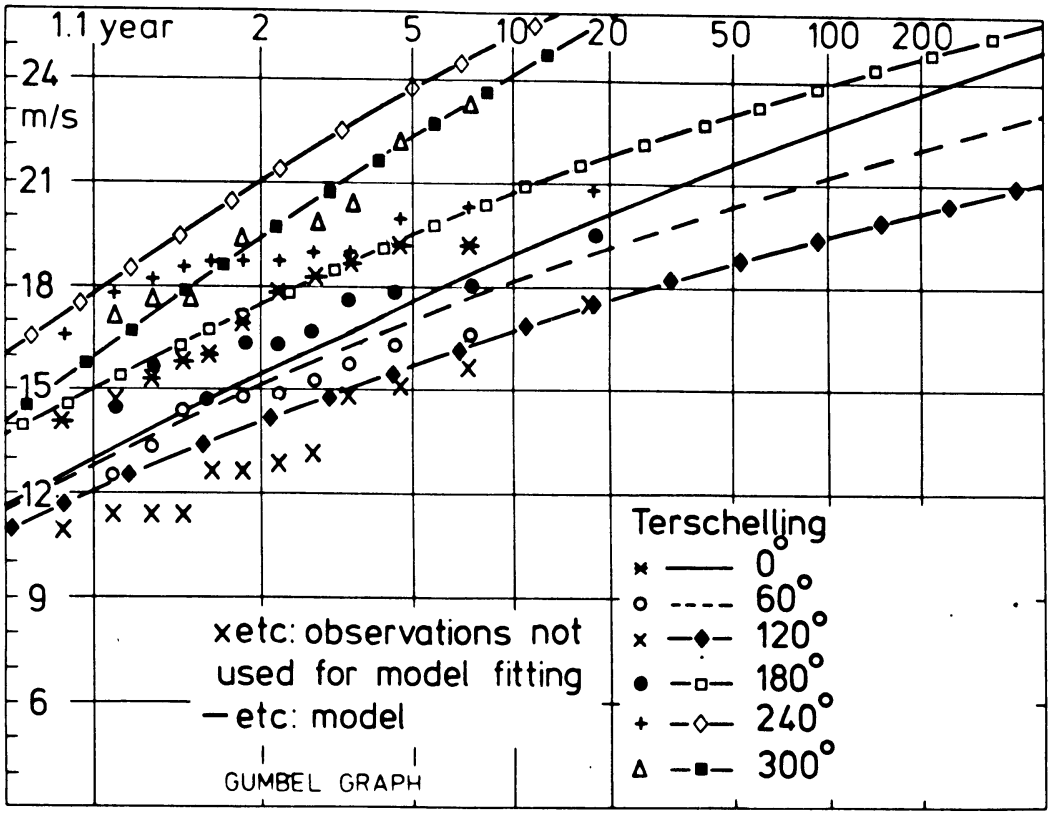


Fig. 20.12 Annual azimuth-sector maximum hourly wind speed for Terschelling as observed and as computed from the model independent of these observations.

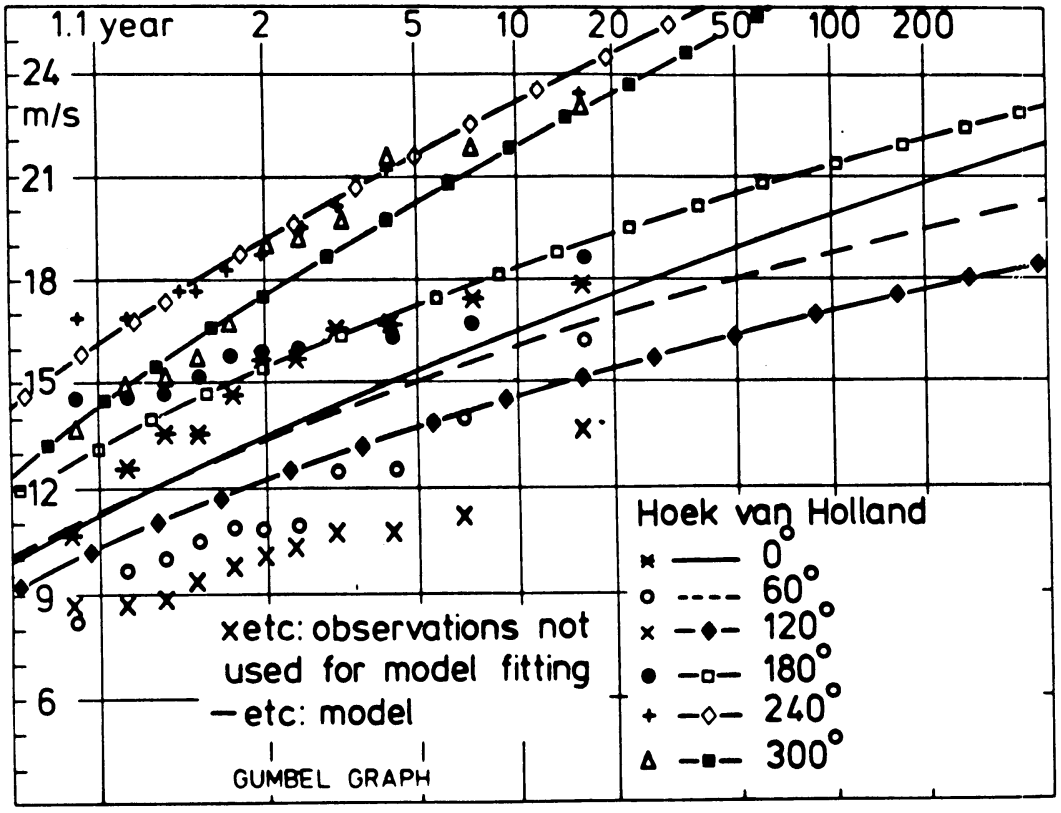


Fig. 20.13 Annual azimuth-sector maximum hourly wind speed for Hoek van Holland as observed and as computed from the model independent of these observations.

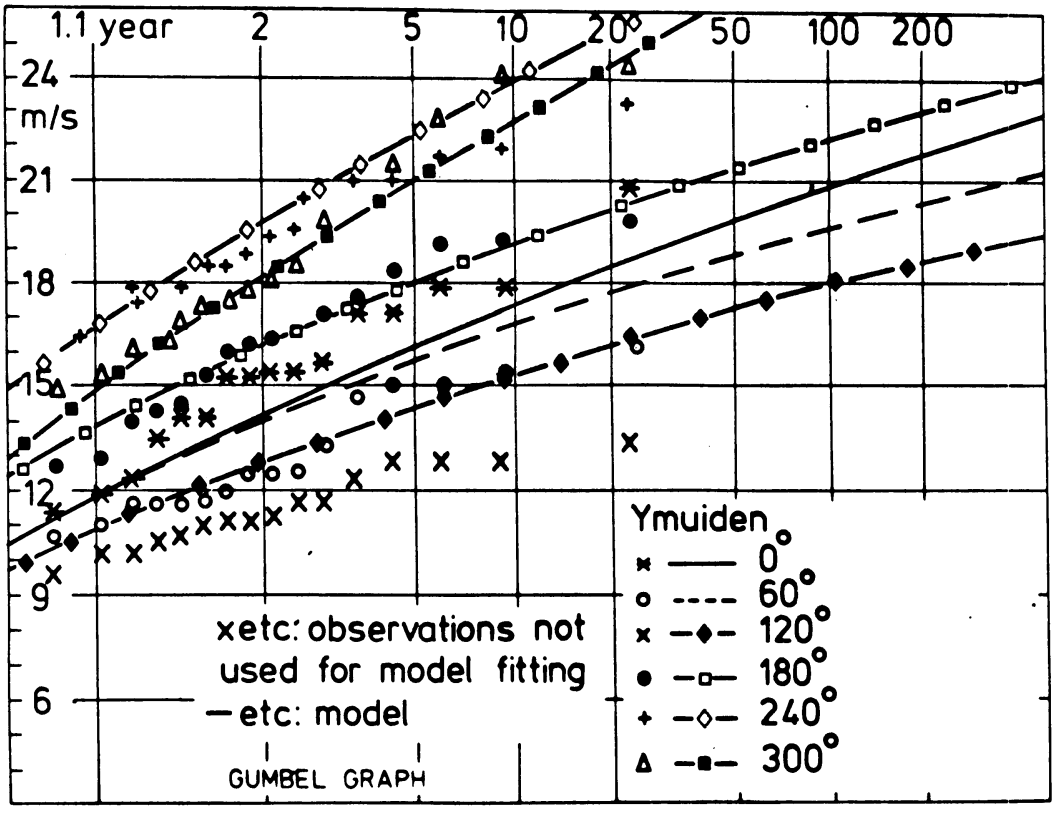


Fig. 20.14 Annual azimuth-sector maximum hourly wind speed for IJmuiden as observed and as computed from the model independent of these observations.

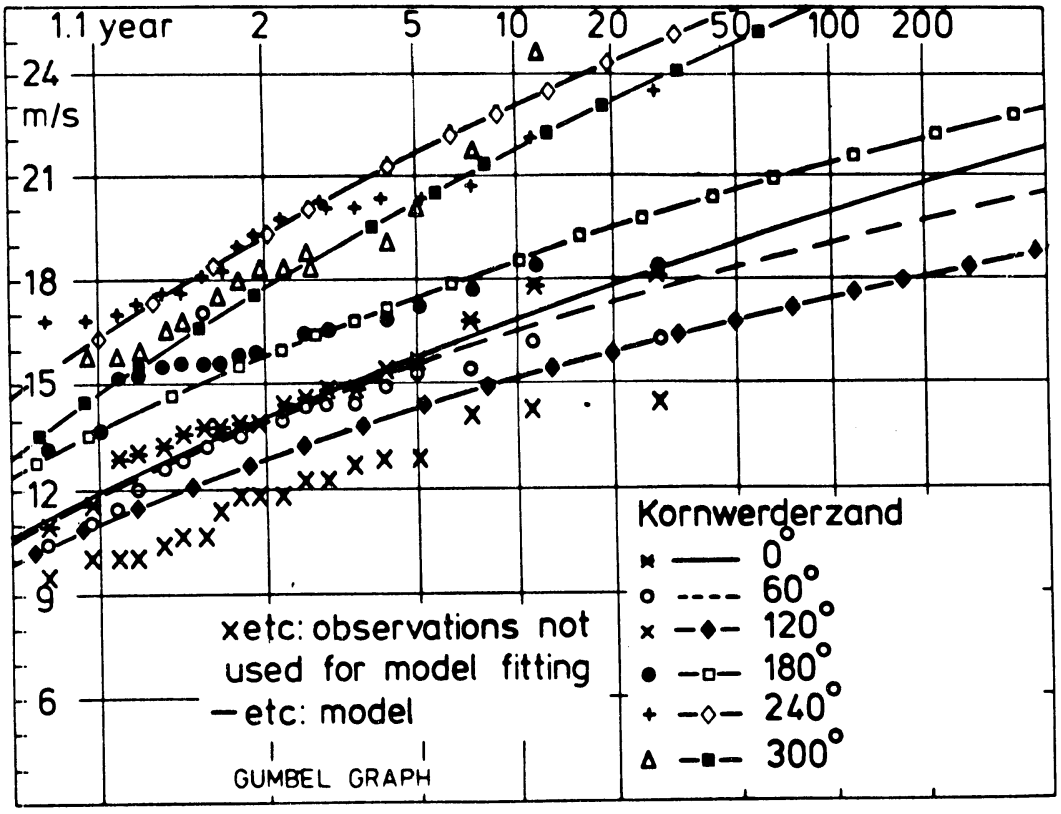


Fig. 20.15 Annual azimuth-sector maximum hourly wind speed for Kornwerderzand as observed and as computed from the model independent of these observations.

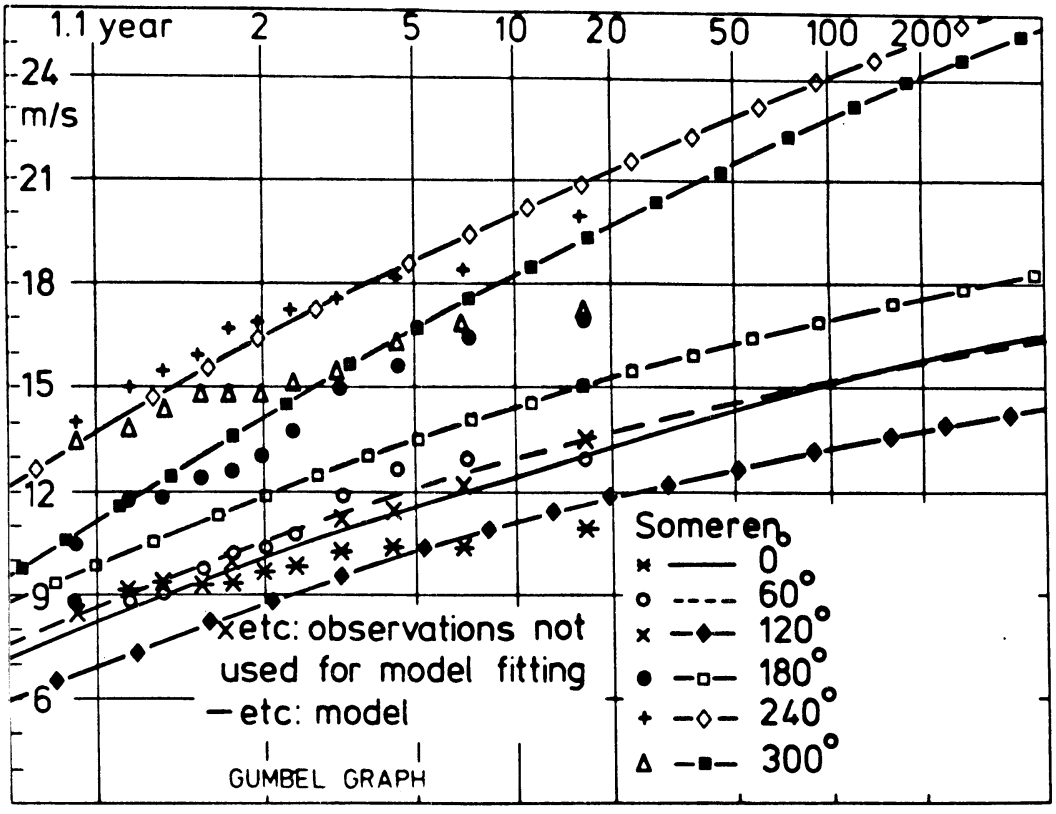


Fig. 20.16 Annual azimuth-sector maximum hourly wind speed for Someren as observed and as computed from the model independent of these observations.

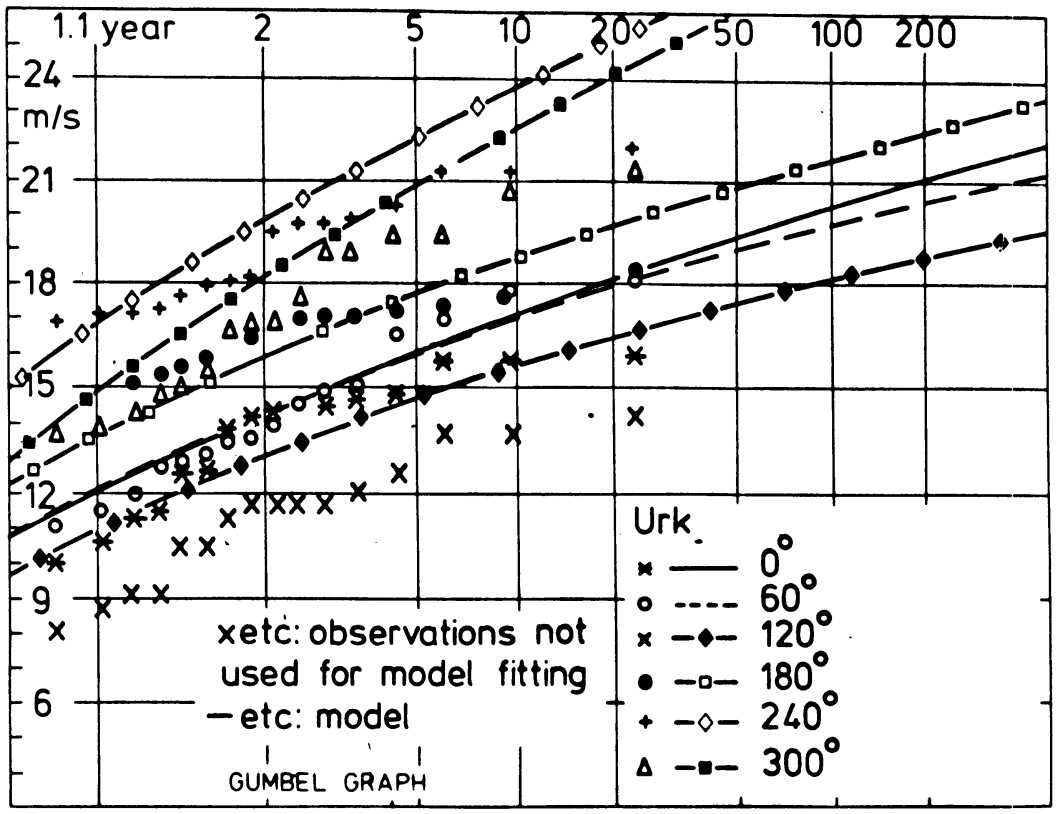


Fig. 20.17 Annual azimuth-sector maximum hourly wind speed for Urk as observed and as computed from the model independent of these observations.

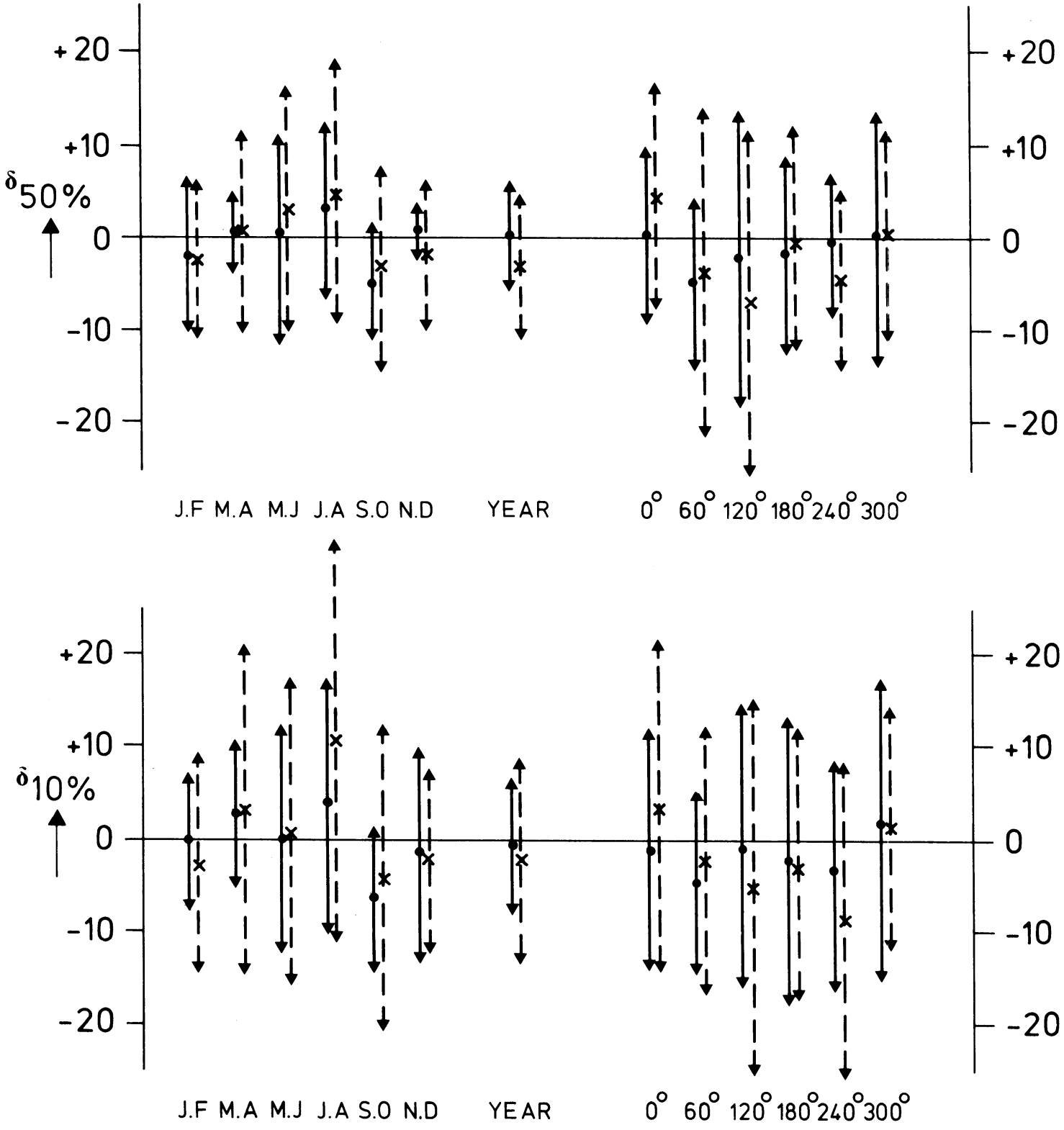


Fig. 21 Average values, and 95%-ranges in percents of the average, for the difference between observations and model at the 50% and 10% percentiles of the extreme value distribution.

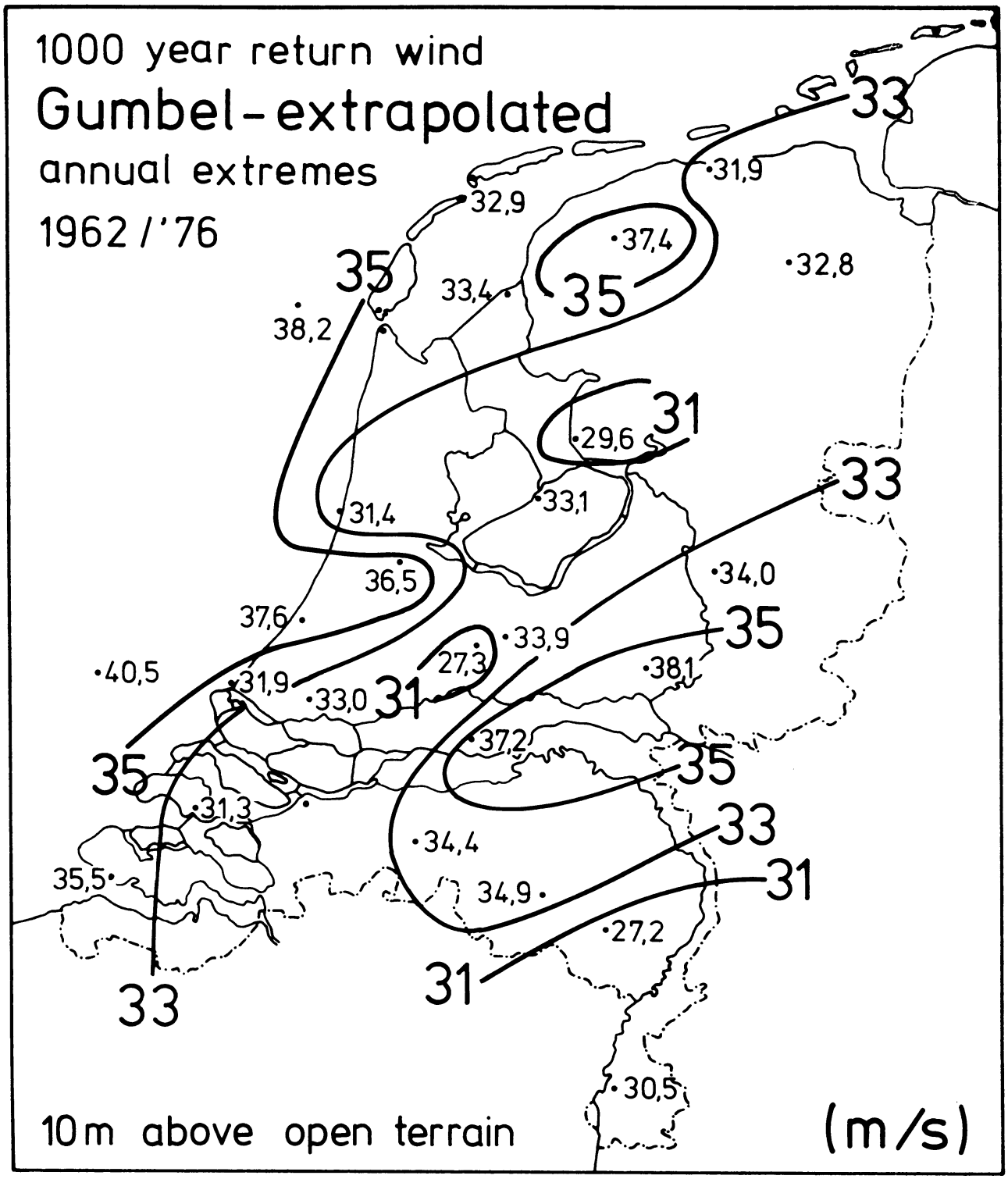


Fig. 22.1 Extreme values of hourly average wind with mean recurrence time of 1000 years computed for all stations from observed annual extremes according to the Gumbel(-Lieblein) method.

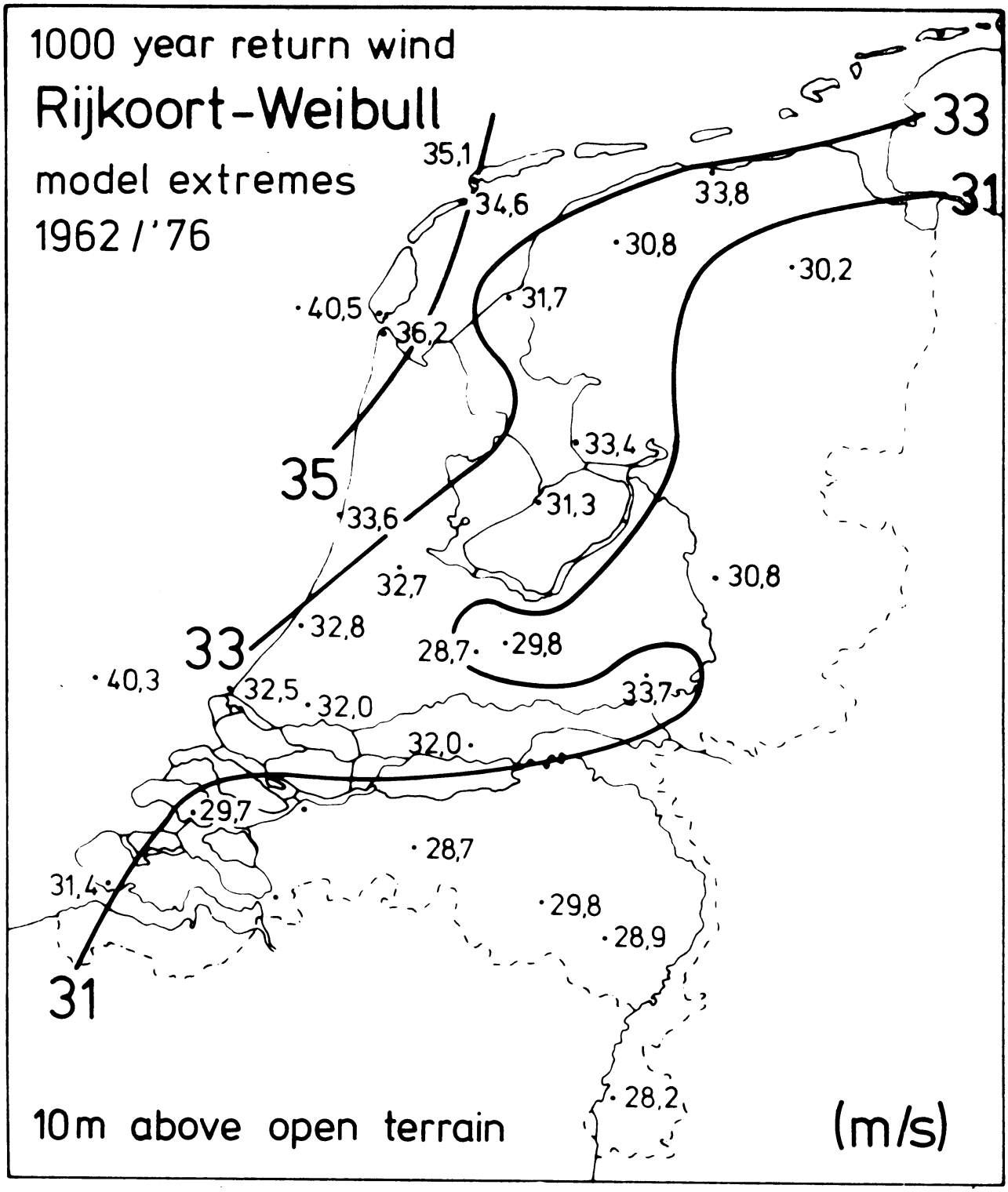


Fig. 22.2 Extreme values of hourly average wind with mean recurrence time of 1000 years computed for all stations from the compound-Weibull extreme value model.

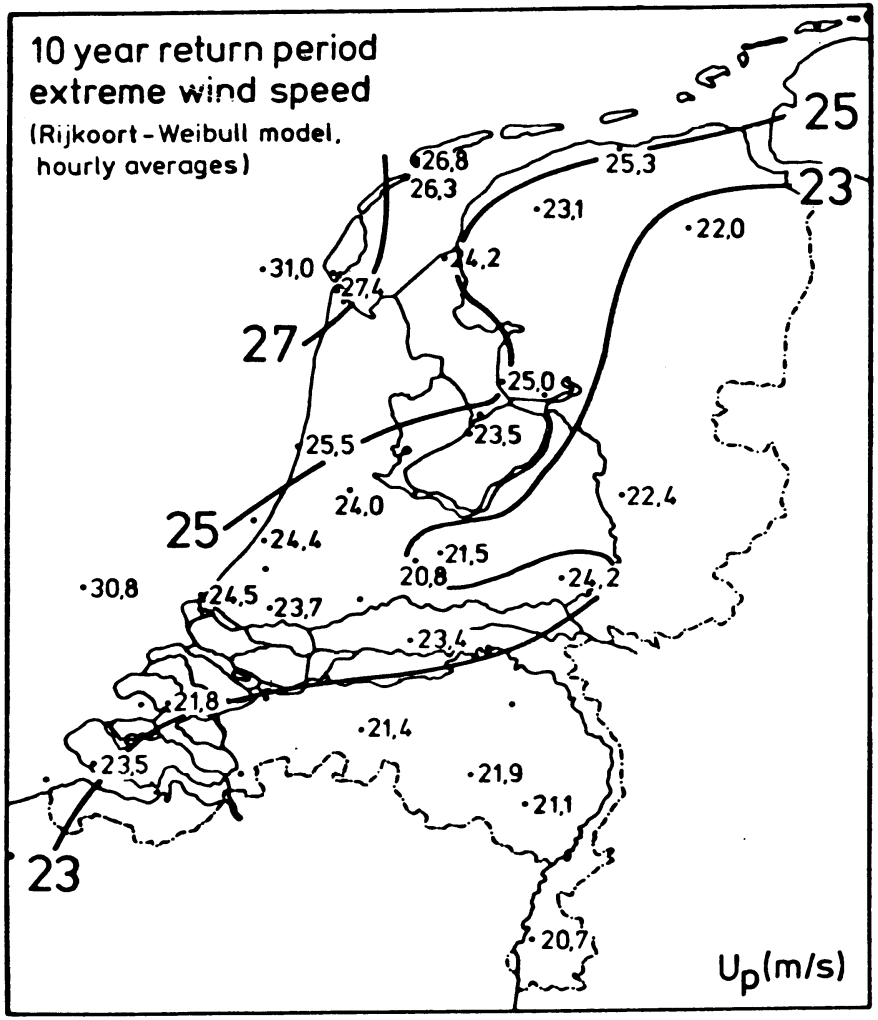


Fig. 22.3 Extreme values of hourly average wind with mean recurrence time of 10 years computed for all stations from the compound model.

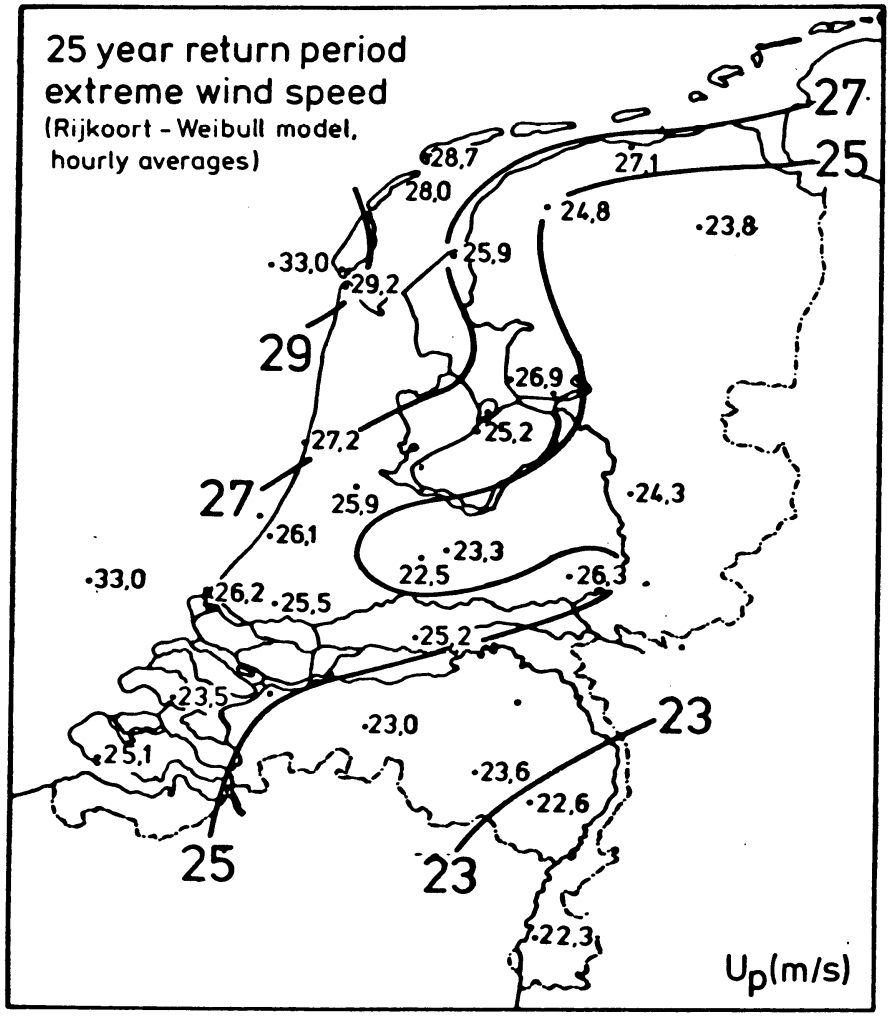


Fig. 22.4 Extreme values of hourly average wind with mean recurrence time of 25 years computed for all stations from the compound model.

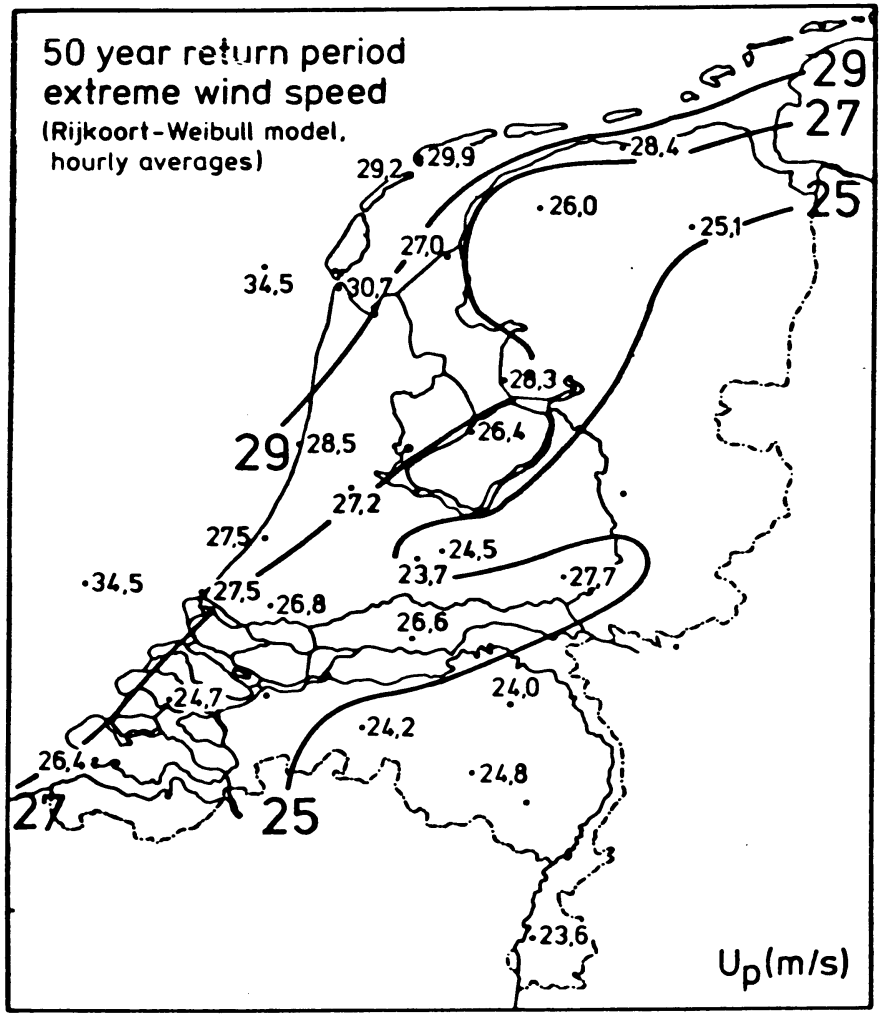


Fig. 22.5 Extreme values of hourly average wind with mean recurrence time of 50 years computed for all stations from the compound model.

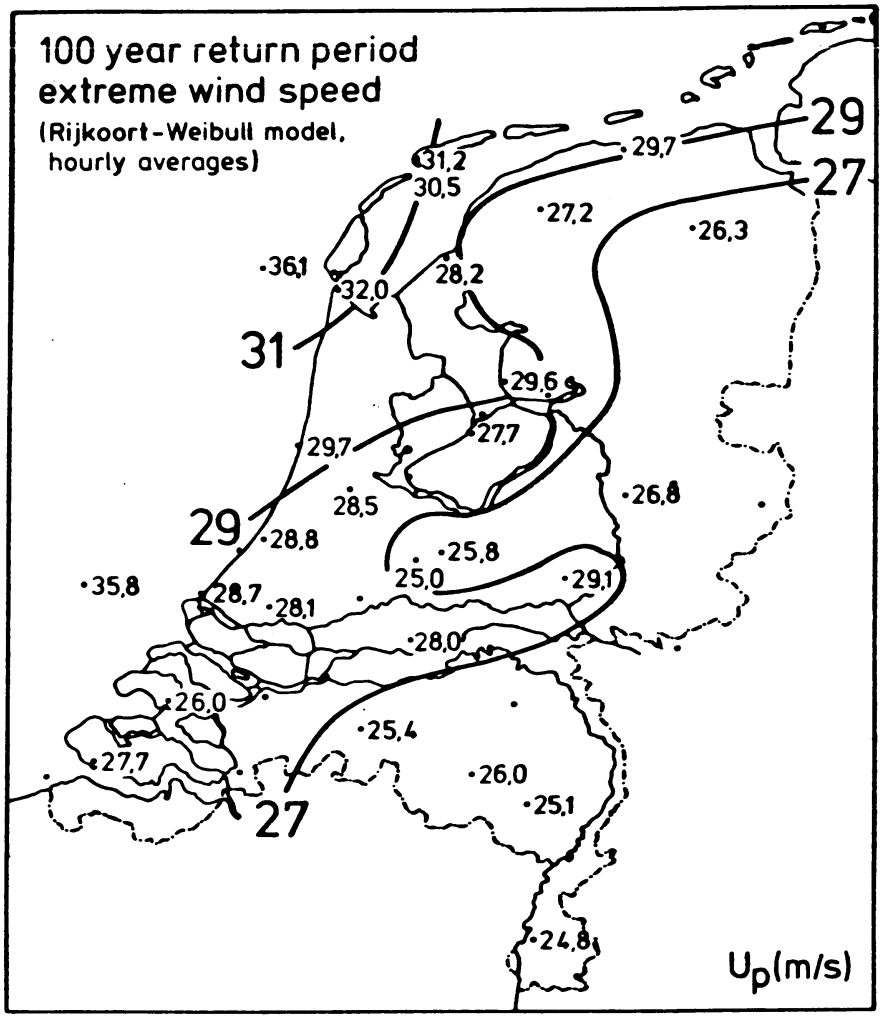


Fig. 22.6 Extreme values of hourly average wind with mean recurrence time of 100 years computed for all stations from the compound model.

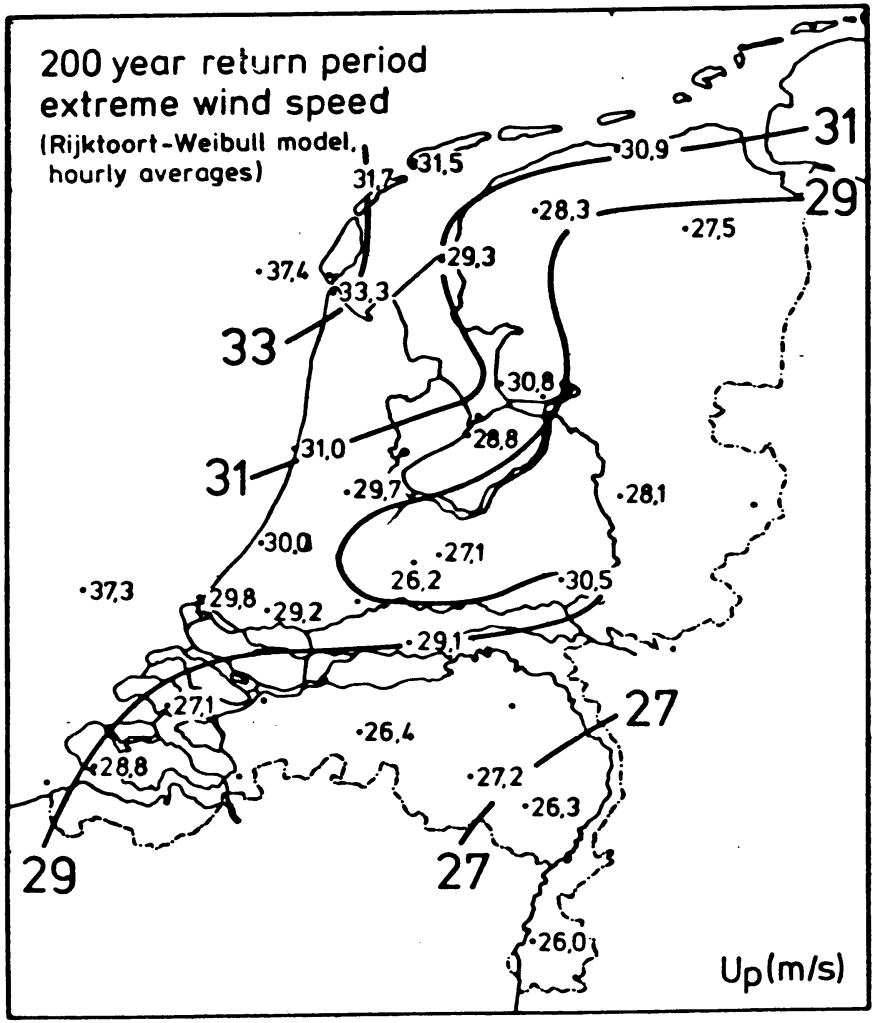


Fig. 22.7 Extreme values of hourly average wind with mean recurrence time of 200 years computed for all stations from the compound model.

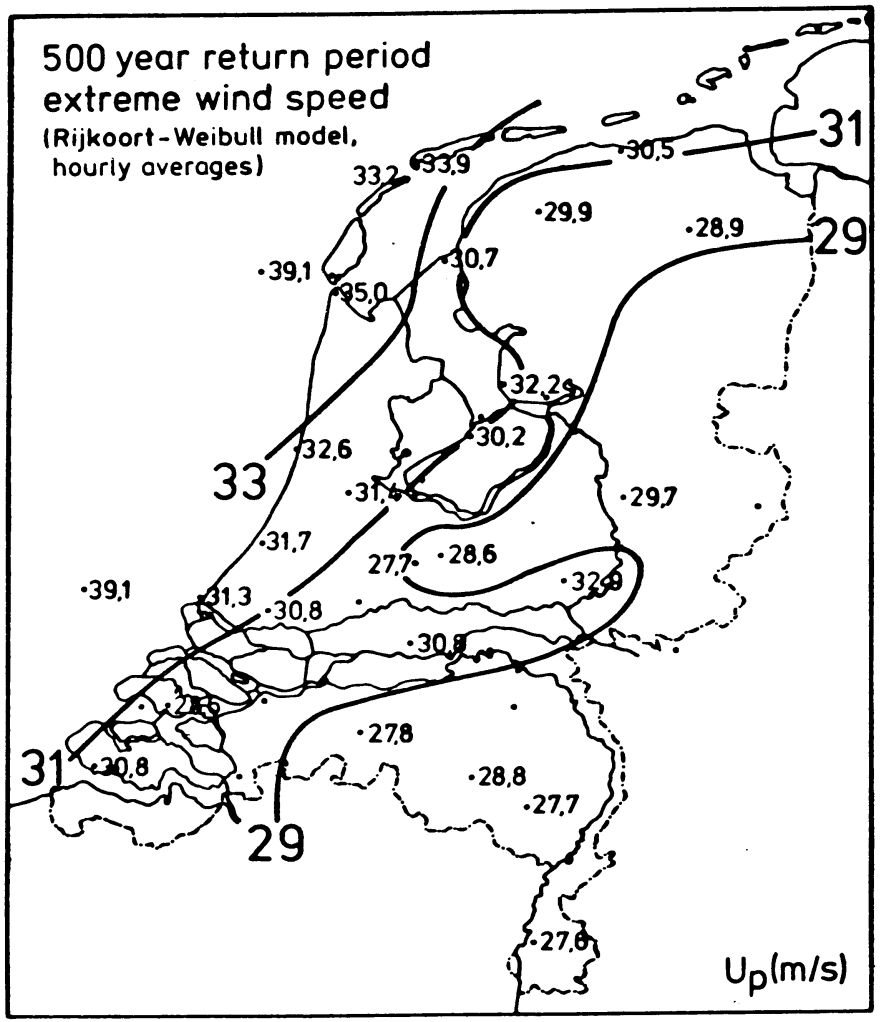


Fig. 22.8 Extreme values of hourly average wind with mean recurrence time of 500 years computed for all stations from the compound model.

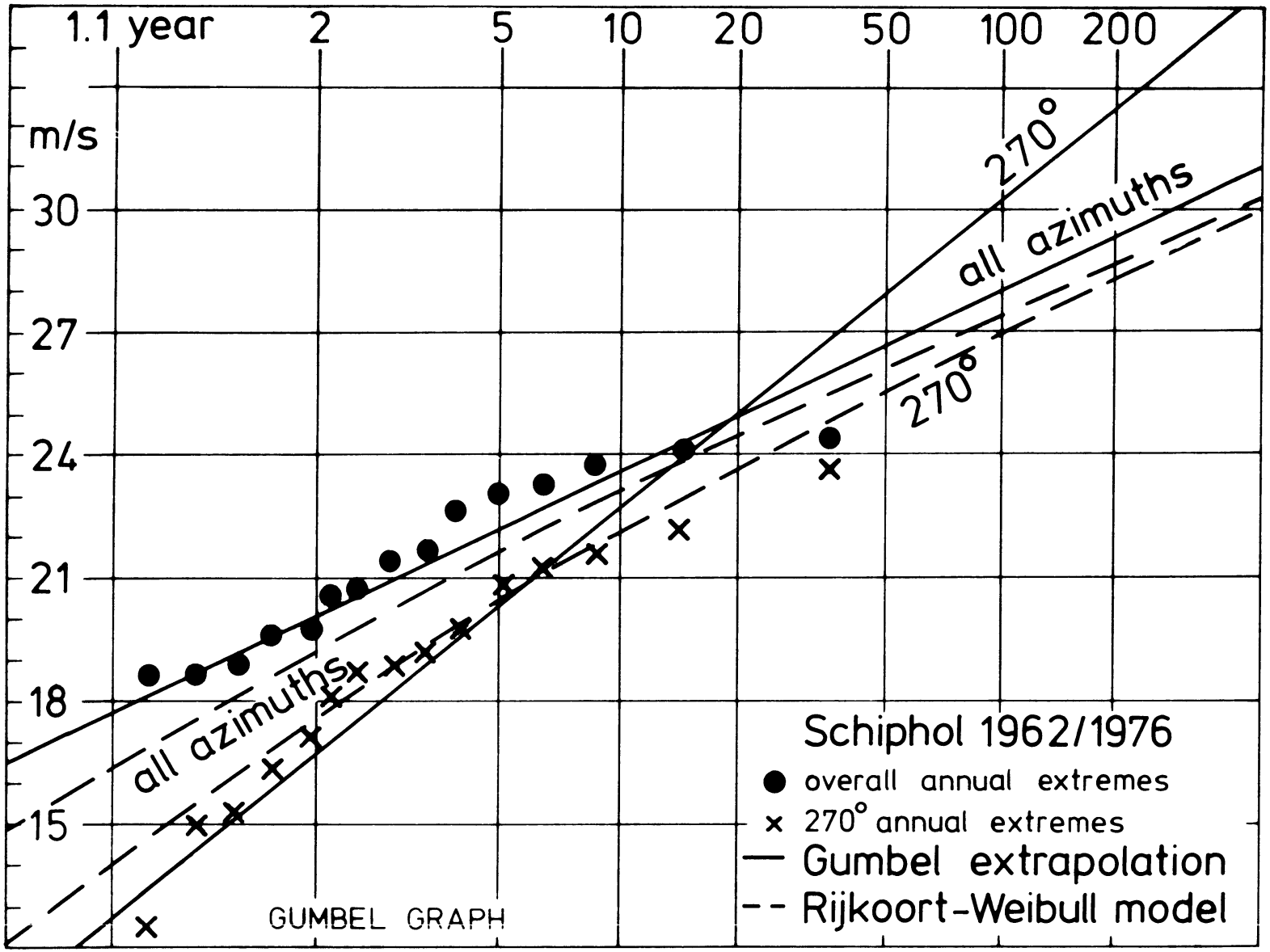


Fig. 23 Annual extreme values of hourly average wind observed at Schiphol, both for all azimuth and only for azimuth sector 255°-285°, with fitted Gumbel-Lieblein lines and computed model curves.

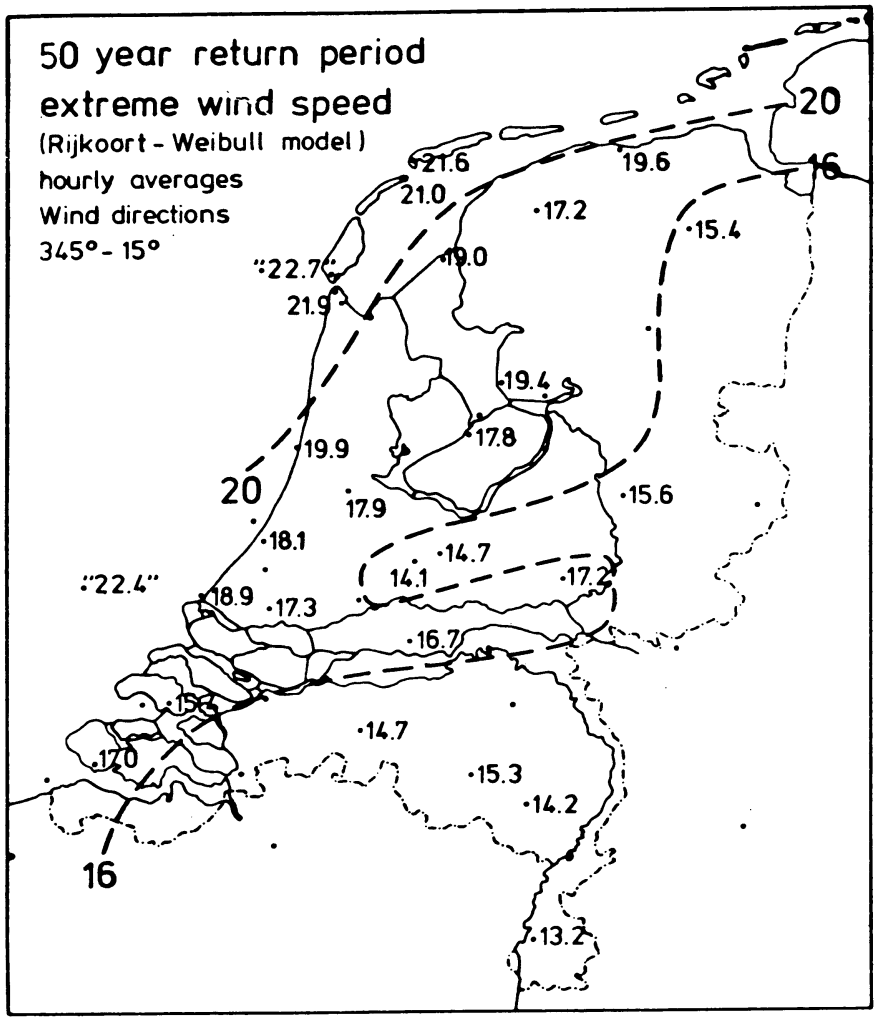


Fig. 24.1 Extreme values of hourly average wind from the 0° azimuth sector with mean recurrence time of 50 years, computed for all stations from the compound model.

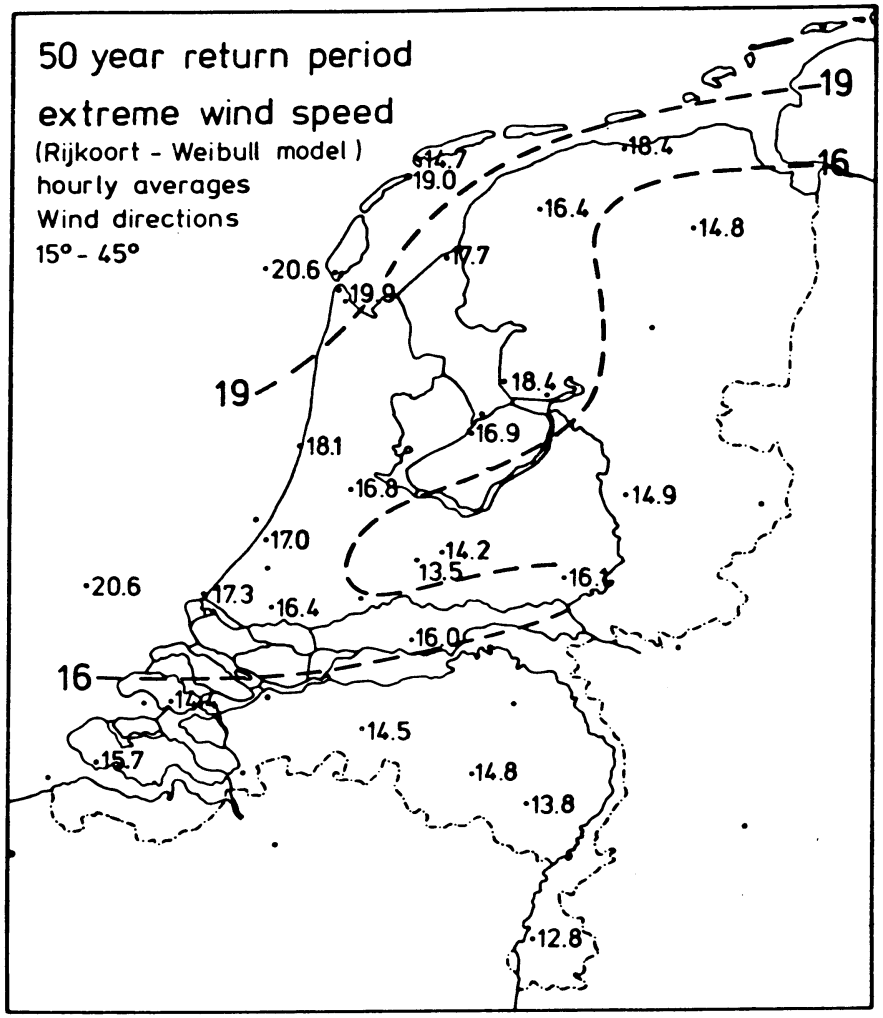


Fig. 24.2 Extreme values of hourly average wind from the 30° azimuth sector with mean recurrence time of 50 years, computed for all stations from the compound model.

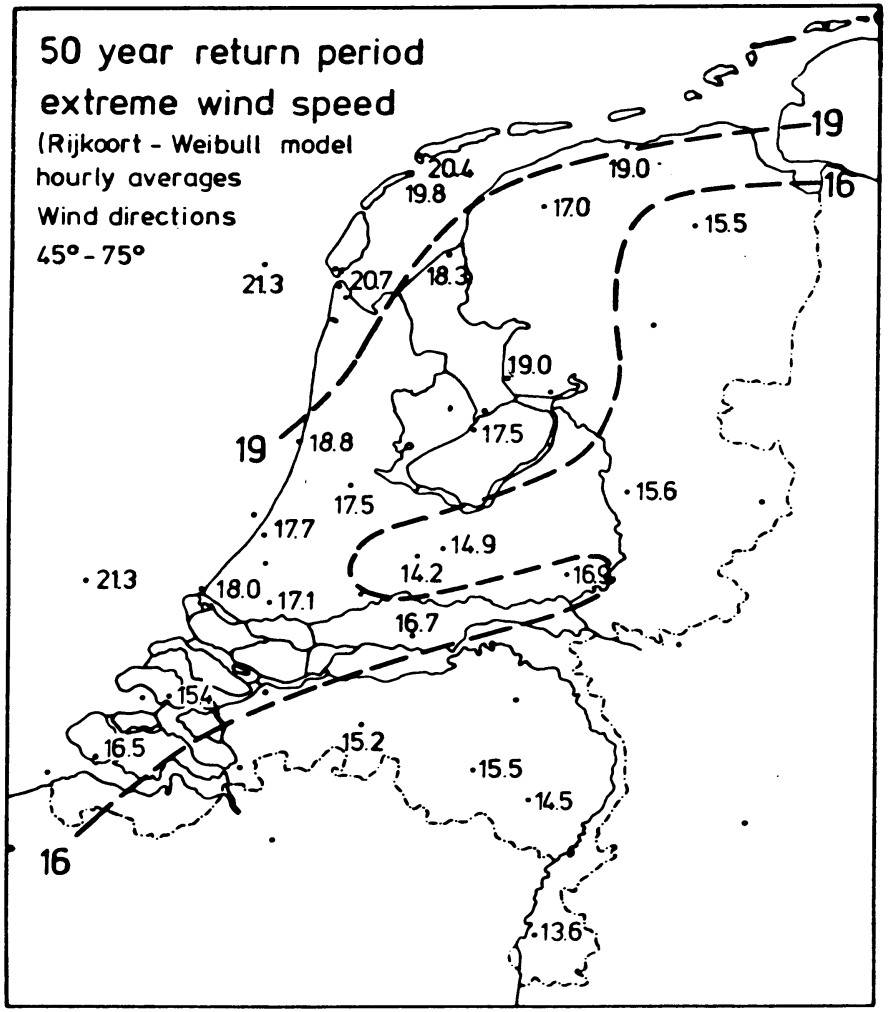


Fig. 24.3 Extreme values of hourly average wind from the 60° azimuth sector with mean recurrence time of 50 years, computed for all stations from the compound model.

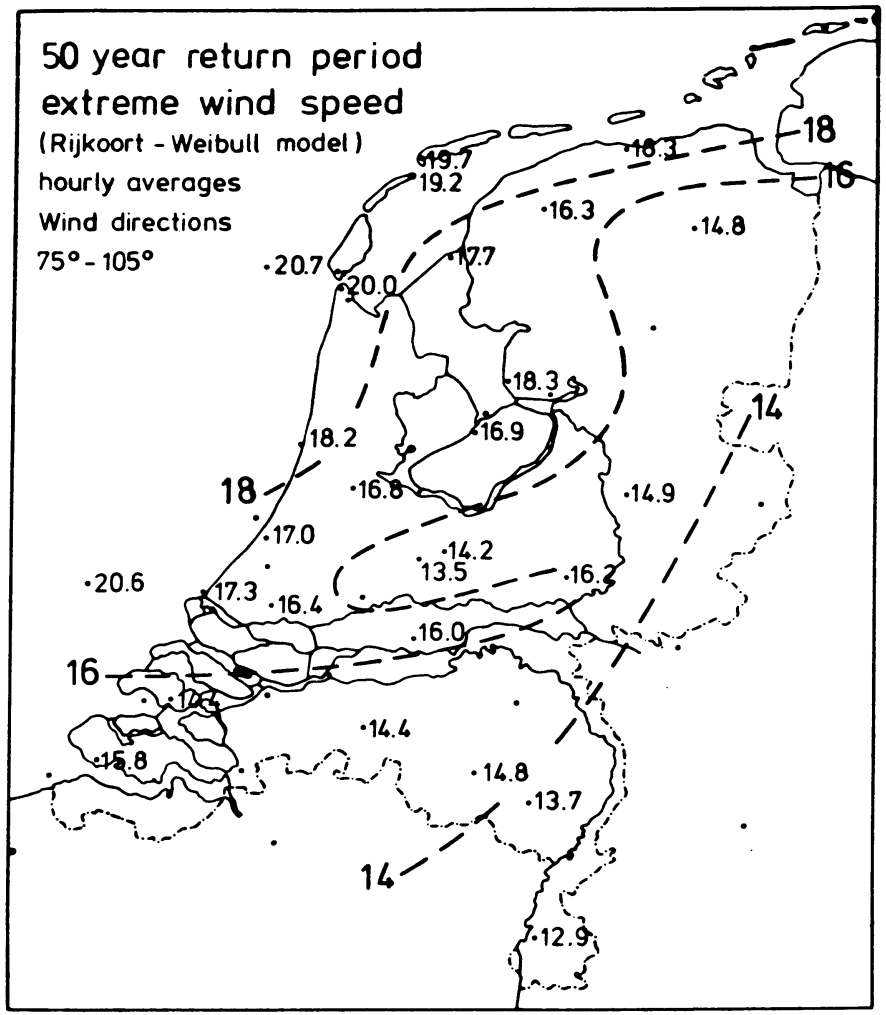


Fig. 24.4 Extreme values of hourly average wind from the 90° azimuth sector with mean recurrence time of 50 years, computed for all stations from the compound model.

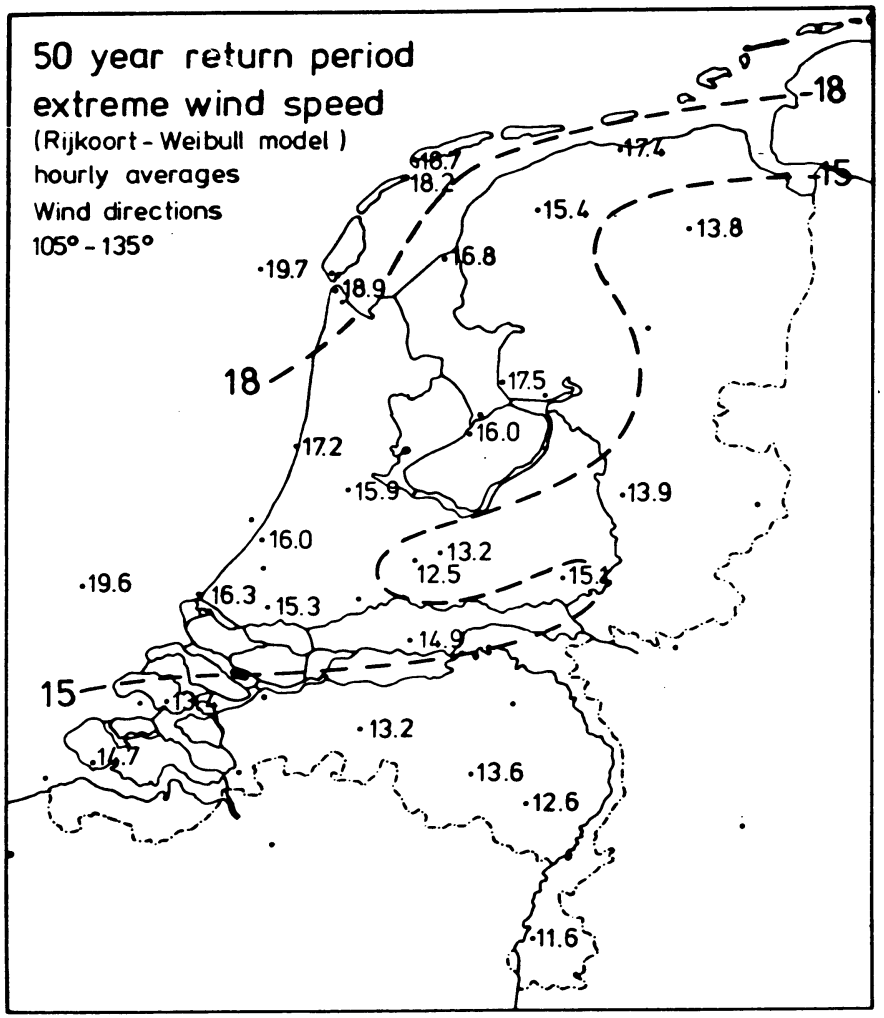


Fig. 24.5 Extreme values of hourly average wind from the 120° azimuth sector with mean recurrence time of 50 years, computed for all stations from the compound model.

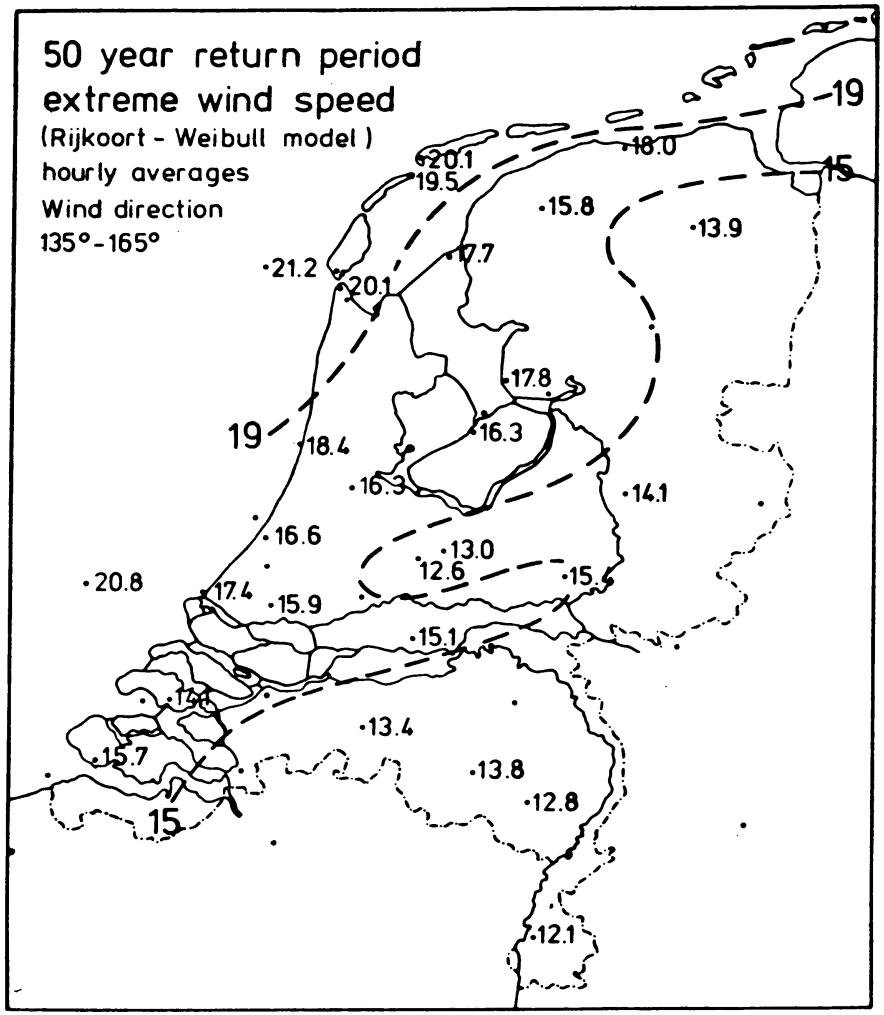


Fig. 24.6 Extreme values of hourly average wind from the 150° azimuth sector with mean recurrence time of 50 years, computed for all stations from the compound model.

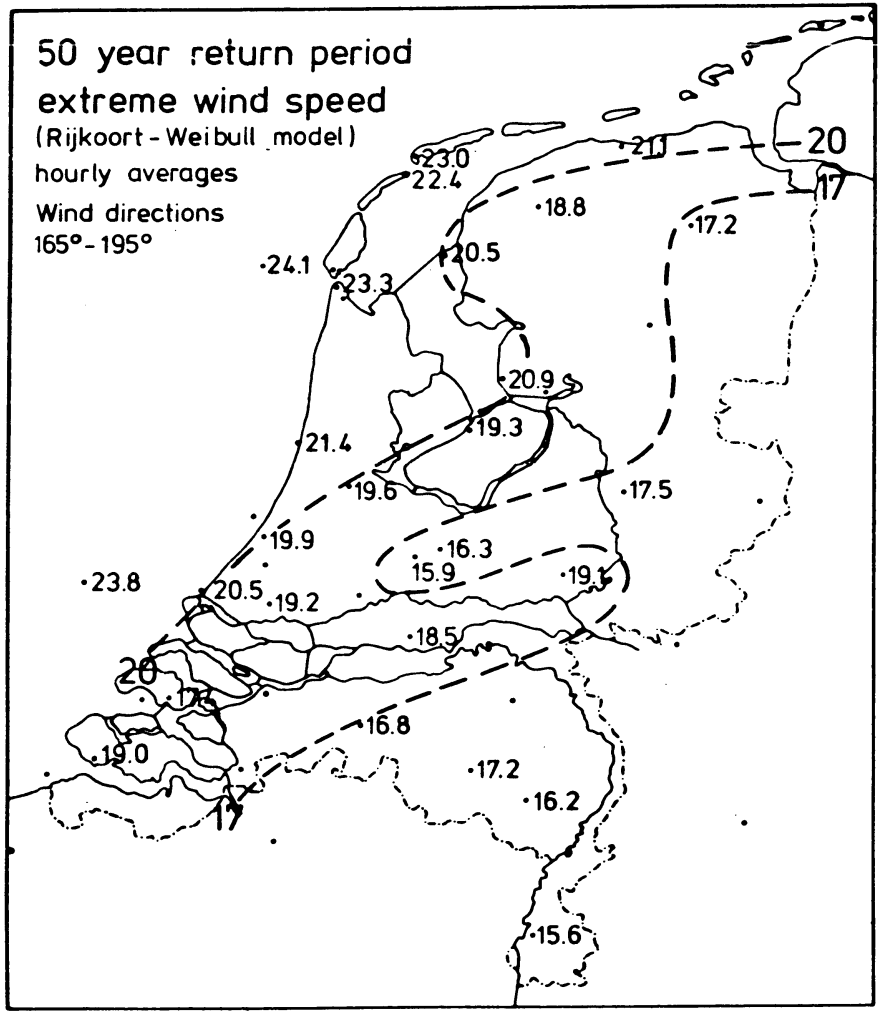


Fig. 24.7 Extreme values of hourly average wind from the 180° azimuth sector with mean recurrence time of 50 years, computed for all stations from the compound model.

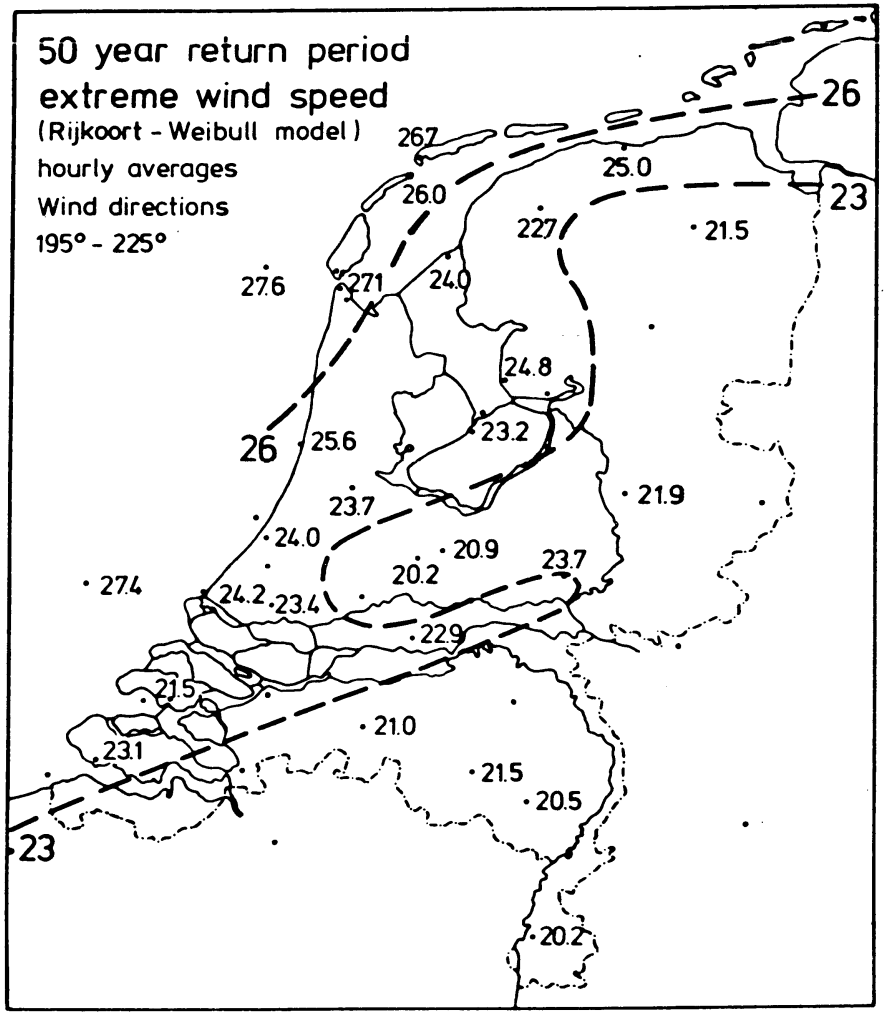


Fig. 24.8 Extreme values of hourly average wind from the 210° azimuth sector with mean recurrence time of 50 years, computed for all stations from the compound model.

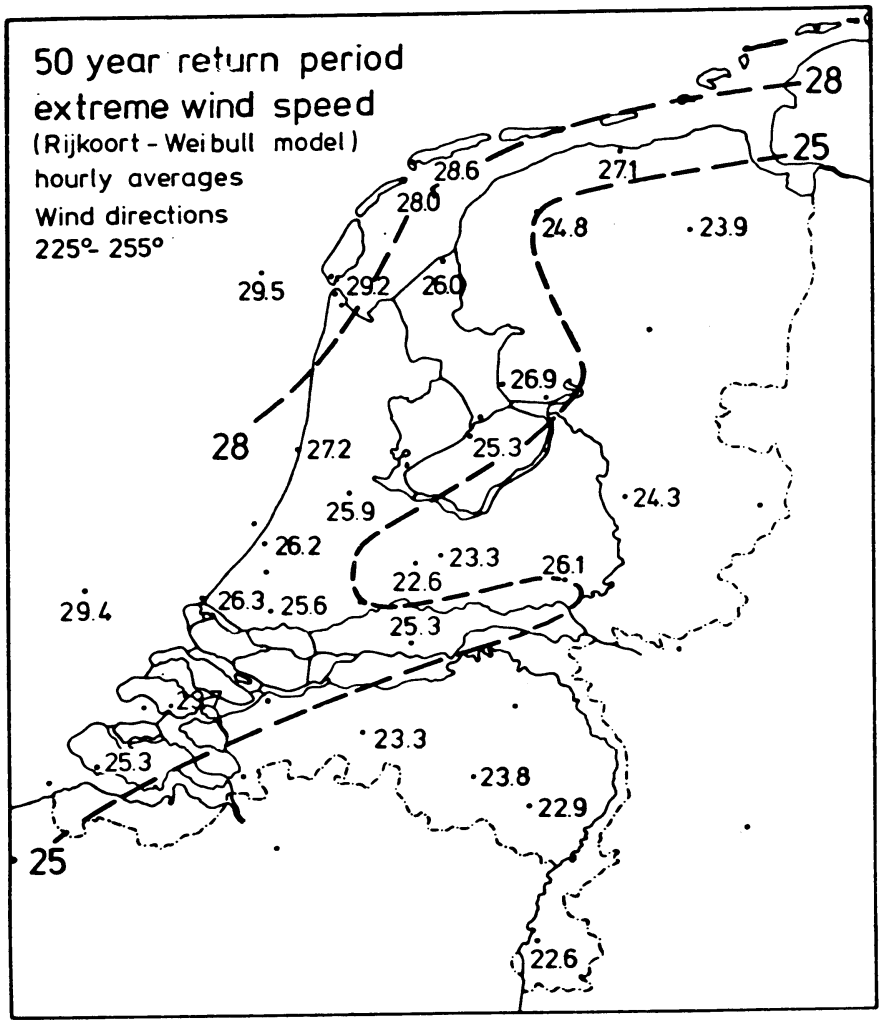


Fig. 24.9 Extreme values of hourly average wind from the 240° azimuth sector with mean recurrence time of 50 years, computed for all stations from the compound model.

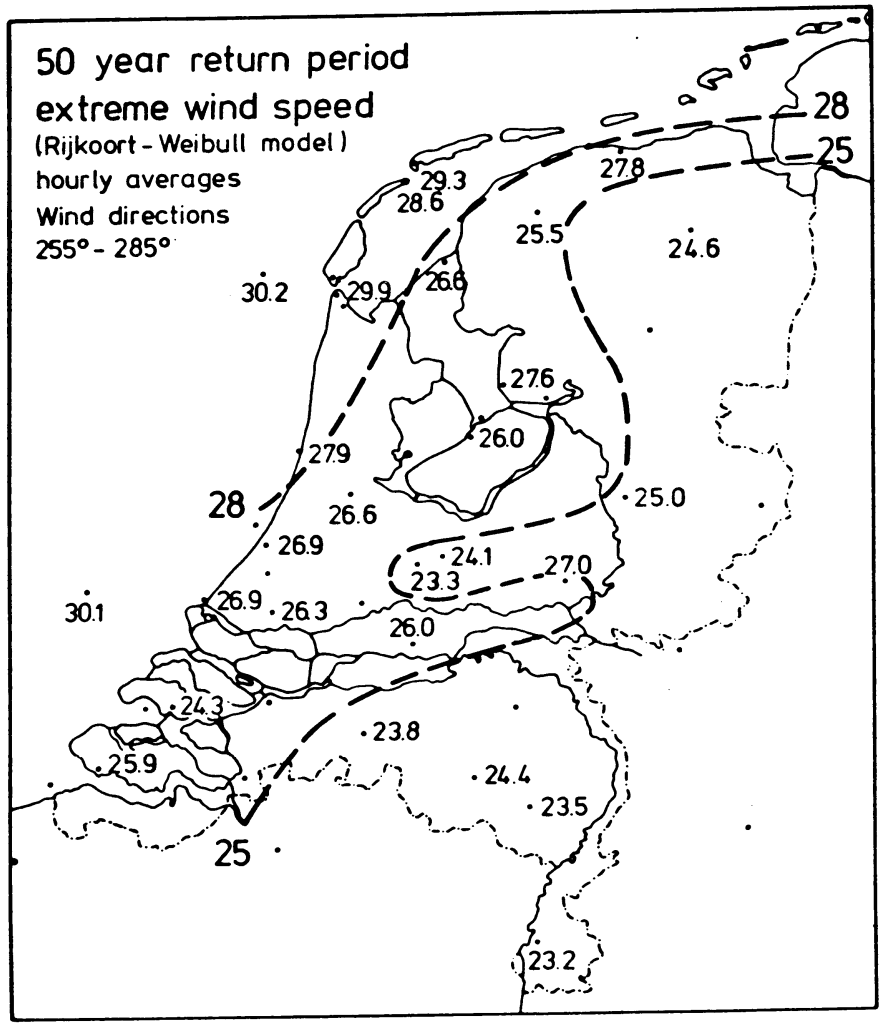


Fig. 24.10 Extreme values of hourly average wind from the 270° azimuth sector with mean recurrence time of 50 years, computed for all stations from the compound model.

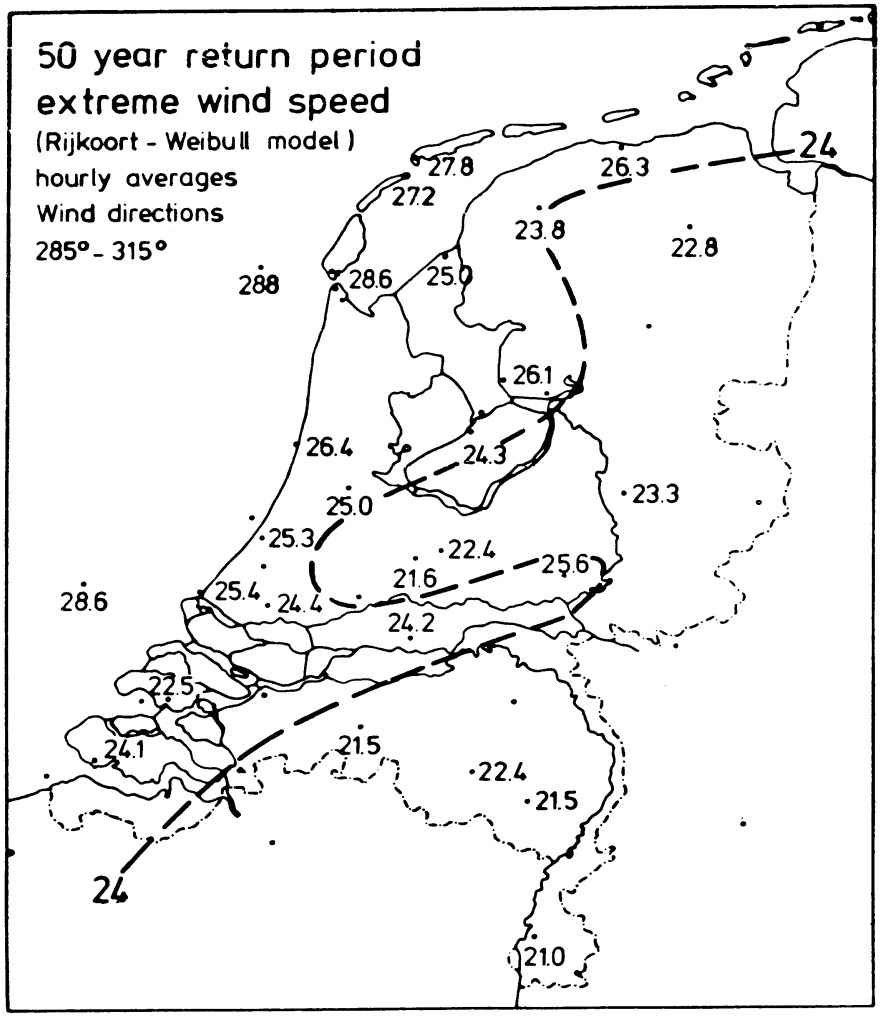


Fig. 24.11 Extreme values of hourly average wind from the 300° azimuth sector with mean recurrence time of 50 years, computed for all stations from the compound model.

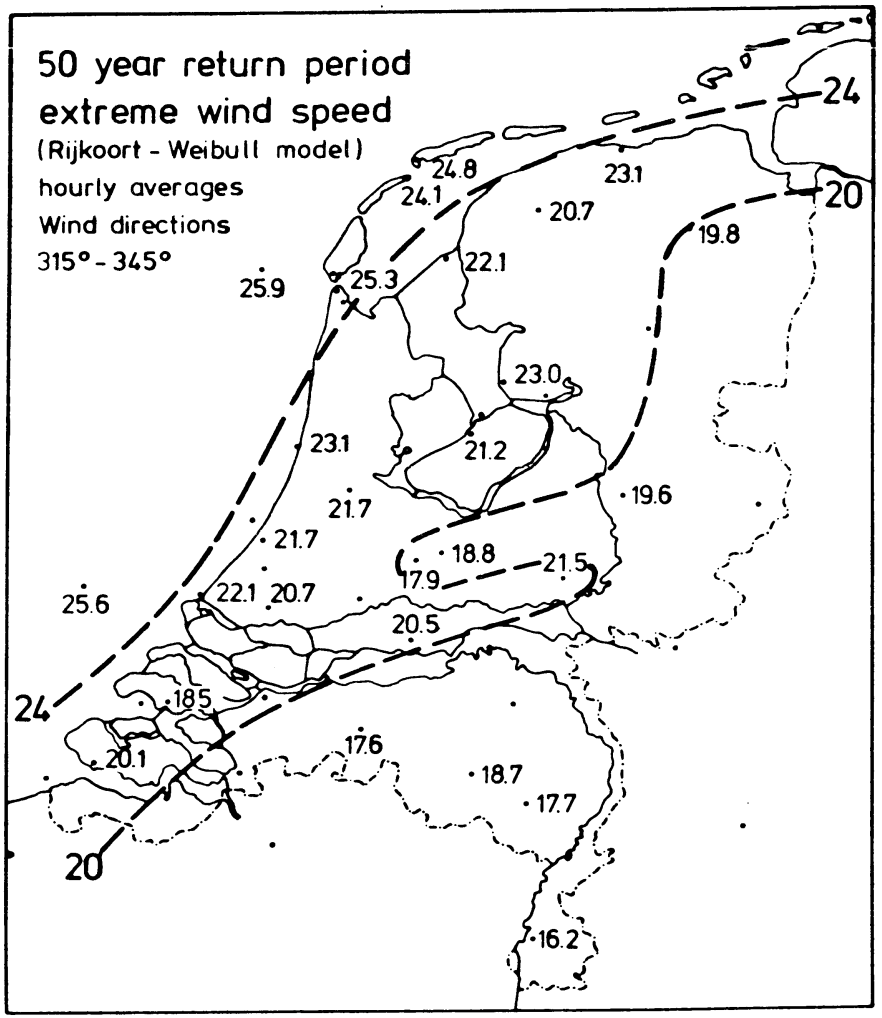


Fig. 24.12 Extreme values of hourly average wind from the 330° azimuth sector with mean recurrence time of 50 years, computed for all stations from the compound model.